Rovibronic Ground-State Molecules near Quantum Degeneracy

Dissertation

zur Erlangung des akademischen Grades
eines Doktors der Naturwissenschaften

eingereicht an der
Fakultät für Mathematik, Informatik und Physik
der Universität Innsbruck

von

Dr. med. univ., Mag. rer. nat.
Johann Georg Danzl

unter der Betreuung von
a. Univ.-Prof. Dr. Hanns-Christoph Nägerl

Institut für Experimentalphysik
der Leopold-Franzens-Universität Innsbruck

Innsbruck, im März 2010

Abstract

Control over all internal and external degrees of freedom of molecules at the level of single quantum states will enable a series of fundamental studies in physics and chemistry. In particular, samples of ground-state molecules at ultralow temperatures and high number densities will allow novel quantum-gas studies and future applications in quantum-information science. However, high phase-space densities for molecular samples are not readily attainable as efficient cooling techniques such as laser cooling are lacking.

This work presents a series of experiments on the production of samples of deeply bound molecules in the near quantum degenerate regime with full control over the internal degrees of freedom. We exploit the fact that high phase-space densities are readily achievable for atoms and that atoms can efficiently and state-selectively be associated on a Feshbach resonance to weakly bound molecules, while maintaining the quantum gas character of the sample. We then transfer the molecules from the weakly bound level to specific deeply bound rovibrational levels of the singlet $X^1\Sigma_g^+$ electronic ground-state potential, most notably to the lowest vibrational and rotational level of the electronic ground state, i. e. to the rovibronic ground state $X^1\Sigma_g^+$ $|v = 0, J = 0>$. Here, v and J are the vibrational and rotational quantum numbers, respectively. Population transfer is mediated by a total of four laser transitions, linking the initial weakly bound level to the rovibronic ground state via two intermediate levels in electronically excited states and one intermediate ground-state level. We employ the Stimulated Raman Adiabatic Passage (STIRAP) technique for coherent population transfer. This four-photon scheme is preferred for the cesium dimer, the molecule used in the present work, because of prohibitively low Franck-Condon factors in homonuclear molecules for a single two-photon Λ-type transition for the electronic potentials used here.

In a first set of experiments, we transfer, with over 80 % efficiency, the molecular population to the intermediate ground-state rovibrational level $|v = 73, J = 2>$ with a binding energy of $>\mathrm{h\,c} \times 1000\ \mathrm{cm}^{-1}$ or $\mathrm{h} \times 30$ THz in a single two-photon step, where h and c are Planck's constant and the speed of light, respectively. This transforms the initial loose long-range bond mediated by van der Waals interaction to a tight chemical bond. We performed two important tests on the sample. In a Ramsey-type experiment we could show that the transfer is indeed coherent. In an expansion measurement, we could demonstrate that the sample is not heated and that the quantum-gas character of the molecular sample is maintained during transfer to deeply bound levels. This latter point is particularly significant because the coherent population transfer takes away an energy of $\sim \mathrm{k_B} \times 1500$ K whereas the molecular sample has an energy on the order of $\mathrm{k_B} \times 10$ nK. Here, $\mathrm{k_B}$ is Boltzmann's constant.

A second set of experiments takes these results a significant step further. We here transfer the population to a particular hyperfine sublevel of the rovibronic ground state while each molecule is trapped at an individual site of an optical lattice. In this case, coherent population transfer removes $\sim \mathrm{k_B} \times 5200$ K of binding energy. Each molecule resides in the motional ground state of an individual well of the optical lattice potential.

We first load a Bose-Einstein condensate of Cs atoms into an optical lattice and drive the superfluid-to-Mott-insulator transition under conditions that maximize the number of lattice sites that are occupied by exactly two atoms. Feshbach association in the optical lattice takes place with near-unit efficiency. We then transfer the population in either a single four-photon transition or with two consecutive two-photon transitions with >50% efficiency to the rovibronic ground state. We achieve motional state control by operating the lattice near a magic wavelength, giving matched trapping potentials for the initial Feshbach level and for the $|v=0>$-molecules. We observe a lifetime of 8 s for the rovibronic ground-state molecules in the optical lattice.

In addition, this work presents the high-resolution molecular spectroscopy both on the electronically excited states and, in the form of two-photon dark resonance spectroscopy, on the electronic ground state necessary for coherent population transfer in the quantum gas regime.

Our results present a crucial step towards Bose-Einstein condensation of ground-state molecules and, when suitably generalized to polar heteronuclear molecules, the realization of dipolar quantum-gas phases in optical lattices.

Zusammenfassung

Die Kontrolle über alle inneren und äußeren Freiheitsgrade von Molekülen auf dem Niveau einzelner Quantenzustände wird eine Reihe von grundlegenden Untersuchungen in Physik und Chemie ermöglichen. Molekülensembles, die ultratiefe Temperaturen und hohe Teilchendichten vereinigen, werden neuartige Quantengasuntersuchungen und zukünftige Anwendungen in der Quanteninformation erlauben. Allerdings sind hohe Phasenraumdichten für Moleküle schwierig zu erreichen, weil hocheffiziente Kühlmethoden, insbesondere die Laserkühlung, für Moleküle bisher nicht verfügbar sind.

Diese Arbeit diskutiert eine Reihe von Experimenten zur Produktion von Ensembles tief gebundener Moleküle nahe der Quantenentartung mit vollständiger Kontrolle über die inneren molekularen Freiheitsgrade. Wir machen uns die Tatsache zu Nutze, dass hohe Phasenraumdichten routinemäßig für Atome erreichbar sind und dass Atome auf sehr effiziente und vollkommen zustandsselektive Weise an einer Feshbach Resonanz zu schwach gebundenen Molekülen assoziiert werden können, wobei der Quantengascharakter des Ensembles erhalten bleibt. In weiterer Folge transferieren wir die molekulare Population vom ursprünglichen, schwach gebundenen Zustand in spezifische tief gebundene Rotations-Schwingungszustände des Singulett $X^1\Sigma_g^+$ elektronischen Grundzustandes, im Besonderen in den niedrigsten Rotations-Schwingungszustand des elektronischen Grundzustandes $X^1\Sigma_g^+$ $|v = 0, J = 0>$. Hierbei ist v die Vibrationsquantenzahl und J die Rotationsquantenzahl. Der Populationstransfer umfasst insgesamt vier Laserübergänge, wobei der schwach gebundene Ausgangszustand über zwei Zwischenzustände in elektronisch angeregten Potentialen und ein intermediäres Niveau des elektronischen Grundzustandspotentials mit dem Rotations-Schwingungs-Grundzustand verbunden wird. Der Zustandstransfer wird in einem kohärenten Prozess mit der Stimulated Raman Adiabatic Passage (STIRAP)-Technik durchgeführt. In dieser Arbeit kommt Cs_2 zum Einsatz, ein homonukleares Molekül. Das Vier-Photonen Schema ist, für die hier verwendeten elektronisch angeregten Potentiale, einem direkten Zwei-Photonen Λ-Schema überlegen, weil es erlaubt, die dabei auftretenden, zu geringen Franck-Condon Faktoren zu umgehen.

In einer ersten Serie von Experimenten transferieren wir mit über 80 % Effizienz die molekulare Population in das intermediäre Grundzustandsniveau $|v = 73, J = 2>$ mit einer Bindungsenergie von $>h\,c \times 1000\ cm^{-1}$ oder $h \times 30$ THz, wobei h und c die Planck-Konstante bzw. die Lichtgeschwindigkeit sind. Dabei wird die anfängliche, lose van der Waals Bindung in eine feste chemische Bindung transformiert. Wir führten zwei wichtige Tests mit dem Molekülensemble durch. In einem Ramsey-Experiment konnten wir zeigen, dass der Transfer tatsächlich kohärent ist. In einer Expansionsmessung gelang es uns nachzuweisen, dass das Ensembe nicht geheizt wird und dass der Quantengascharakter des Ensembles durch den Transfer erhalten bleibt. Dieser letztere Punkt ist besonders signifikant, da der Populationstransfer eine Bindungsenergie von $\sim k_B \times 1500$ K abführt, während das molekulare Ensemble durch Energien in der Größenordnung von $k_B \times 10$ nK charakterisiert ist, wobei k_B die

Boltzmann-Konstante ist.

Eine zweite Serie von Experimenten führt diese Untersuchungen um einen wichtigen Schritt weiter. Hierbei transferieren wir die Population in ein bestimmtes Hyperfeinniveau des Rotations-Schwingungs-Grundzustandes, wobei jedes Molekül an einem individuellen Gitterplatz eines optischen Gitters gefangen ist. In diesem Fall führt der kohärente Populationstransfer $\sim k_B \times 5200$ K an Bindungsenergie ab. Die Moleküle befinden sich dabei im Bewegungsgrundzustand des entsprechenden Gitterplatzes. Wir laden zunächst ein Bose-Einstein Kondensat von Cäsium Atomen in ein optisches Gitter und treiben den Suprafluid-zu-Mott-Isolator Phasenübergang unter Bedingungen, die die Anzahl der Gitterplätze, die mit exakt zwei Atomen besetzt sind, maximieren. Feshbach-Assoziation im optischen Gitter erfolgt mit einer Effizienz nahe eins. Entweder in einem einzigen Vier-Photonen Schritt oder in zwei aufeinanderfolgenden Zwei-Photonen Schritten transferieren wir dann die Population in den Grundzustand mit über 50% Effizienz. Dabei erreichen wir Kontrolle über den externen Bewegungszustand, indem wir das optische Gitter nahe einer magischen Wellenlänge betreiben, die idente Fallenpotentiale für das ursprüngliche Feshbachniveau und für die $|v = 0>$-Moleküle ergibt. Die Lebensdauer der Grundzustandsmoleküle im optischen Gitter beträgt 8 s.

Darüber hinaus werden in dieser Arbeit die hochauflösenden molekülspektroskopischen Messungen, die für kohärenten Transfer im Quantengasregime notwendig sind, sowohl an elektronisch angeregten Zuständen als auch, in der Form von Zwei-Photonen-Dunkelresonanz-Spektroskopie, am elektronischen Grundzustand diskutiert.

Unsere Ergebnisse stellen einen wichtigen Schritt zur Bose-Einstein-Kondensation von Grundzustandsmolekülen und, wenn sie entsprechend auf polare heteronukleare Moleküle erweitert werden, zur Realisierung von dipolaren Quantengas-Phasen in optischen Gittern dar.

Contents

Chapter 1

Introduction

High density samples of ultracold molecules are ideally suited for a series of fundamental studies in physics and chemistry. The advent of ultracold atoms has revolutionized the field of atomic physics. Exquisite control over the entire parameter space for ultracold matter has enabled ground-breaking experiments, including the realization of Bose-Einstein condensation [And95, Dav95] in dilute atomic vapors. Atoms have been loaded into optical lattice potentials [Mor06], allowing the realization of model systems from condensed matter physics with amazing experimental control over all degrees of freedom and near perfect decoupling from the environment [Blo08]. Ultracold atoms have been used to study strongly interacting fermionic systems that lie at the heart of high-temperature superconductivity [Ing08]. On the applied side, ultracold atoms have led to the development of greatly improved atomic clocks [Did04]. Now, optical atomic clocks based on single ions [Ros08] have reached uncertainties of 10^{-17} and ensembles of ultracold atoms trapped in an optical lattice have shown great potential as future frequency standards [Tak05]. Accordingly, ultracold atoms have attracted a lot of interest from a variety of fields traditionally disjunct from atomic physics.

Molecules are characterized by additional degrees of freedom not present in atoms and therefore constitute more complex and richer model systems. They promise exciting new insights from future experiments in the ultracold domain. It can be expected that the impact of ultracold molecules on physics and chemistry will be as profound as the revolution set forth by ultracold atoms. It has been a long standing aim to fully control all internal and external quantum degrees of freedom of molecules. For many of the proposed experiments, the molecules will have to be prepared in the respective lowest energy ground state of each degree of freedom. The internal degrees of freedom of molecules include the electronic structure, molecular vibration and rotation and molecular hyperfine structure. Only in the lowest energy internal state is stability against inelastic two-body collisions and against radiative decay assured.

Most experiments with ultracold molecules either rely on or benefit from ultralow temperatures in combination with high number densities, i. e. from high phase-space densities [Ket99, Car09]. Phase-space density is defined in free space as $D = n\lambda_{dB}^3$, where n is the number density and λ_{dB} is the thermal deBroglie wavelength, which increases with decreasing temperature. The phase transition to a Bose-Einstein condensate (BEC) takes place when a macroscopic number of particles occupy the same quantum state and form a coherent macroscopic matter wave. For a uniform Bose gas in a three-dimensional box, this takes place at a phase-space density of $D \simeq 2.612$

[Pet02].

Control over the external quantum degrees of freedom implies that the molecules are prepared in the "quantum gas regime", i. e. near quantum degeneracy and, ultimately, that they all occupy a defined motional state. As a starting point for the realization of novel quantum phases, the molecular ensemble should ideally be in the ground state of the many-body system. For a trapped molecular ensemble, this is a Bose-Einstein condensate of molecules or, in the case of fermions, a degenerate Fermi gas. For an ensemble of molecules in a deep optical lattice potential, the many-body ground state is the Mott-insulator state [Gre02, Blo08].

However, such state control has been a tantalizing goal since highly efficient direct cooling methods, most importantly laser cooling, are lacking in the case of molecules [Bah96, Dul09a]. There has been tremendous progress in the development of versatile, non-optical direct cooling methods for molecules [van08, Sch09, Fri09] and in photoassociation [Jon06, Car09] of atoms in magneto-optical traps. Nevertheless, the achievable phase-space densities are many orders of magnitude short of quantum degeneracy with these methods. In contrast, Feshbach association from a high phase-space-density atomic gas leads to high-density samples of extremely weakly bound molecules [Köh06, Hut06, Chi10] at temperatures in the nK-range. From a molecular point of view, the molecules produced on a Feshbach resonance, commonly called "Feshbach molecules", correspond to the least bound, most highly excited vibrational levels. As a spectacular achievement, molecular Bose-Einstein condensation has been realized for molecules made up of two fermionic atoms in the limit of vanishing binding energy [Joc03, Gre03, Zwi03, Bou04].

This thesis presents a series of experiments that lead to the production of a sample of alkali dimer molecules in a defined hyperfine sublevel of the rovibronic ground state, i. e. of the lowest vibrational and rotational level of the electronic ground state potential, with each molecule trapped in the motional ground state of an individual well of an optical lattice. We make use of the fact that atoms can readily be brought to quantum degeneracy by a combination of laser cooling and evaporative cooling and that atoms can be efficiently associated on Feshbach resonances [Chi10] with minimal loss of phase-space density when an optical lattice is present. Subsequently, the molecules are coherently transferred by Stimulated Raman Adiabatic Passage (STIRAP) [Ber98] to a specific hyperfine sublevel of the rovibronic ground state in a stimulated multi-photon process while maintaining control over the motional wave function. This procedure results in a long lived sample with high lattice filling factor and full control over all degrees of freedom. Our scheme for the production of a quantum gas of rovibronic ground-state molecules is summarized in figure 1.1.

We will now give a brief overview of the potential applications of cold and ultracold molecules in section 1.1. Then the current status of the field in terms of experimental realization of cold and ultracold molecular systems is discussed in section 1.2.

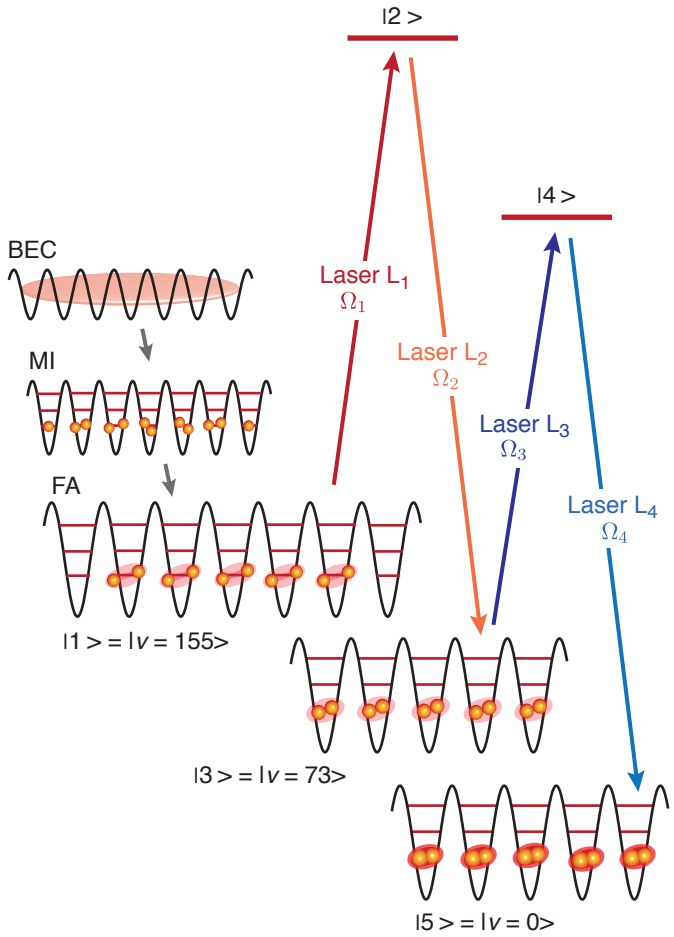

Figure 1.1: **Production of an ultracold high-density sample of rovibronic ground-state molecules in an optical lattice:** A BEC of Cs atoms is loaded into an optical lattice. By increasing the lattice depth, a Mott-insulator state (MI) with preferentially two atoms per site is created. Feshbach association (FA) subsequently converts atom pairs into weakly-bound molecules in state $|1>$. These are then transferred in the presence of the lattice to a specific hyperfine level $|I = 6, M_I = 6>$ of the rovibronic ground state $|5> = X^1\Sigma_g^+ \; |v = 0, J = 0>$ by a stimulated four-photon process (STIRAP) involving lasers L_i with Rabi frequencies Ω_i $i = 1, 2, 3, 4$, and two intermediate excited state levels $|2>$ and $|4>$ and one intermediate ground state level $|3>$. Here, I and M_I are the total molecular nuclear spin and its projection on the magnetic field axis, and v and J are the vibrational and rotational quantum numbers, respectively.

1.1 Fundamental studies with cold and ultracold molecules

The vibrant activity in the field of cold molecules stems from the promise that cold molecules hold for a variety of fundamental studies in physics and chemistry and a series of potential future applications. It is convenient to distinguish cold (1 mK - 1K) from ultracold (below 1 mK) molecules [Dul09a, Car09] and, within the realm of ultracold molecules, to further set apart the near quantum-degenerate regime that is characterized by values of the phase-space density close to unity. While practically all experiments profit from high phase-space density, a lot of insight can also be gained from experiments at higher temperatures in the cold regime.

A number of review articles [Dul09a, Car09, Fri09, Chi10, Sch09, Cha09, van08, Fer09b, Hut06, Dul06, Doy04] and three recent focus issues dedicated to cold and ultracold molecules [Far09, New09, Eur04], containing a series of original research articles, give an excellent overview of the current status of the field and future directions. Some of the most important applications are highlighted in the following, including novel quantum gas studies, collisional studies, cold controlled chemistry, quantum information science, quantum simulation, and precision tests.

Three main features of ultracold molecules make them interesting for a variety of applications once the experimental challenges in controlling all molecular degrees of freedom are mastered. First, heteronuclear molecules in deeply bound vibrational levels exhibit a large electric dipole moment in the presence of an external electric field. The dipole-dipole interaction between the molecules is both long-range and anisotropic [Bar08, Lah09] in contrast to the usual short-range contact interaction between ultracold atoms. The dipole-dipole interaction falls off as $1/R^3$, where R is the separation between the particles. This nature of the dipole-dipole interactions gives rise to exotic novel quantum phases [Gór02] and makes ultracold molecules attractive candidates as a platform for quantum computation [DeM02] and quantum simulation [Pup09]. Second, the complex energy structure of molecules, albeit posing some experimental challenges, can be harnessed for a series of tasks, such as tailoring the interaction potential between molecules by radiofrequency-dressing fields [Büc07a, Gor08] and engineering desired Hamiltonians [Mic06]. Well established experimental tools, such as microwave and laser radiation, can be used to manipulate the internal molecular state and optical dipole, electric or magnetic forces can be used to trap the molecules. Third, the molecular energy structure depends on fundamental physical constants in a way that makes ultracold molecules an attractive platform for precision measurements [Chi09]. In search of a violation of fundamental symmetries, research involving ultracold molecules may be able to make important contributions. For example, the energy shifts caused by a possible electron electric dipole moment are greatly amplified by the strong internal electric fields in molecules [Tar09].

1.1.1 Quantum gas studies

For molecular Bose-Einstein condensation, stability of the molecules against inelastic dimer-dimer collisions must be assured. At the high particle densities in near quantum-degenerate gases, inelastic collisions would otherwise quickly destroy the sample. They would inevitably lead to a conversion of binding energy to kinetic energy and the particles would either leave the trap or, if the gain in kinetic energy is insufficient for the particles to leave the trap, lead to heating of the sample. It is illustrative to compare energy scales in this context. The binding energy of an alkali dimer is on the order of 0.5 electron volt or $k_B \times 6000$ K, where k_B is Boltzmann's constant. In contrast, ultracold samples of molecules near quantum degeneracy feature temperatures of a few nK and typical trap depths for optical dipole traps commonly employed in quantum gas experiments, are on the order of μK. Two basic mechanisms can lead to a release of binding energy in a dimer-dimer collision, first, quenching of the internal state of one or both of the molecules to an energetically lower lying internal state and second, a chemical reaction with an exchange of atoms between the colliding molecules. The most notable example for the first mechanism is vibrational relaxation, but also the much smaller energy scale associated with molecular rotation is far greater than the trap depth of typical optical traps. Even a release of the energy associated with the weak hyperfine splitting of the rovibronic ground state in alkali dimers [Ald09, Ald08] can potentially lead to molecular loss. In the case of dimer molecules that are made up of two fermionic atoms, in the limit of extremely weak binding, the so-called universal regime, collisional relaxation is suppressed as a consequence of a Pauli-blocking effect. As a major accomplishment, molecular Bose-Einstein condensation has been attained for the special case of bosonic molecules formed from two fermionic atoms in the limit of vanishing binding energy [Joc03, Gre03, Zwi03, Bou04]. Important insights have come from studying the crossover between a molecular BEC and a Bardeen-Cooper-Schrieffer (BCS) superfluid in strongly interacting fermionic systems (for an overview, see Ref. [Ing08]).

Apart from this special situation, stability against inelastic collisions is only assured for molecules prepared in the lowest-energy internal quantum state, namely the lowest hyperfine sublevel of the rovibronic ground state. However, even molecules in the rovibronic ground state can suffer from loss in dimer-dimer collisions if chemical reactions are energetically allowed. The constituent atoms can be rearranged and either lead to the formation of two dimers of different composition or to the formation of a trimer and an atom. Chemical reactions between rovibronic ground-state molecules have recently been observed in the near quantum-degenerate regime for KRb molecules [Osp10b]. The experiments presented in this thesis deal with Cs_2 molecules in the rovibronic ground state. For these, an open channel for the formation of a trimer and an atom in a dimer-dimer collision would be the most serious loss mechanism and most serious obstacle to the formation of a Bose-Einstein condensate. In the case of Cs_2, this channel is predicted to be energetically closed [Dul09b, Hut09].

For experiments working towards achieving molecular Bose-Einstein condensa-

tion, maximum phase-space density is of paramount importance and hence all molecules in the sample should reside in a single internal quantum state. A distribution over several hyperfine sublevels would dilute the phase-space density.

One attractive route to the formation of a BEC of ground-state molecules is to load a BEC of atoms into an optical lattice and to drive the superfluid-to-Mott-insulator phase transition [Gre02, Blo08] under conditions that maximize the size of the two-atom Mott shell in the center of the lattice. Atoms at doubly occupied sites can be associated to weakly bound molecules on a Feshbach resonance with near unit efficiency and perfect control over the internal quantum state [Tha06, Chi10]. In the central region, essentially every lattice well is occupied by a single Feshbach molecule that resides in the motional ground state of the lattice well [Vol06]. The molecules are then transferred to the rovibronic ground state while assuring that motional state control is maintained and that the rovibronic ground state molecules hence remain trapped in the lowest vibrational lattice level, as realized in the framework of the work presented in this thesis [Dan10b]. During molecule production and transfer to the rovibronic ground state, the molecules are perfectly shielded from collisional loss by the optical lattice. For sufficiently high production and transfer efficiency and suitable choice of parameters, adiabatic release of the molecules into an optical dipole trap should then result in the formation of a molecular Bose-Einstein condensate [Jak02].

Some loss of phase-space density can be tolerated during the production and transfer procedure if the collisional properties of the ground-state molecules turn out to be sufficiently favorable for a final stage of evaporative cooling or sympathetic cooling with atoms.

Ultracold ground-state molecules constitute a highly attractive platform for a new generation of quantum gas experiments. The long-range and anisotropic nature of the dipole-dipole interaction between heteronuclear ground-state molecules in the presence of an electric field allows the realization of strongly-correlated quantum systems and gives rise to a plethora of novel phenomena, such as dipolar crystals and supersolid phases (for an overview, see Refs. [Bar08, Lah09, Pup09]). Weakly bound molecular levels of heteronuclear molecules do not exhibit an appreciable dipole moment. Therefore, for the realization of dipolar physics, the heteronuclear molecules have to be prepared in deeply bound molecular levels and most notably in the rovibronic ground state where they can easily be polarized by a DC electric field.

For particles interacting through dipole-dipole forces, the stability of the sample and hence the possibility of Bose-Einstein condensation crucially depends on the trapping geometry [San00]. For polar molecules in an optical lattice, the Bose-Hubbard Hamiltonian has to be extended [Gór02]. Góral and coworkers analyze the various quantum phases that arise for dipolar bosons in an optical lattice and find superfluid, supersolid, Mott insulator, checkerboard, and collapse phases [Gór02]. Novel quantum phases in 2-dimensional (2D) and 3-dimensional (3D) optical lattices also include striped supersolid and layered supersolid [Yi07] and a series of metastable states [Men07]. Dipolar BECs have also been theoretically studied in bilayer lattice systems [Tre09] and in double-well potentials [Zam09]. In addition to the on-

site interaction usually present between particles in optical lattices, for long-range interactions also nearest-neighbour and next-nearest-neighbour interactions play an important role. It should be possible to engineer the shape and the strength of the interaction potential between polar molecules through mixing of rotational states by means of static and microwave fields and to modify the elastic and inelastic scattering cross sections [Büc07a, Mic07, Gor08]. Also three-body interactions play an important role [Büc07b]. When confined in reduced dimensions, ultracold polar molecules self-assemble into crystalline structures in the form of chains or lattices [Wan06, Büc07a, Pup08, Ast08].

There are several candidate systems for the realization of dipolar physics. Groundbreaking experiments with chromium atoms [Gri05, Stu05, Lah07, Koc08] have allowed the observation of dipole-dipole interactions in an ultracold atomic gas. Here, the dipole-dipole interaction is mediated by magnetic forces that are large in chromium compared to the alkali metals due to the large magnetic moment of 6 μ_B of chromium, where μ_B is the Bohr magneton. When the magnitude of the contact interaction is reduced by means of a Feshbach resonance, the dipole-dipole interactions become of a magnitude comparable to the contact interaction. However, for many of the theoretical proposals with polar particles, the magnitude of the dipole-dipole interaction in chromium is too small. Rare earth atoms, such as Erbium [McC06, Ber08] or Dysprosium [Lu09], offer even higher magnetic moments in combination with a much higher atomic mass, allowing to reach further into the dipolar regime. The strength of dipolar interactions achievable with ultracold ground-state molecules surpasses that of atoms and will enable the realization of many of the theoretical proposals. Recently, dipole-dipole interactions have been observed for dipolar molecules in the quantum gas regime [Ni10]. It has also been proposed to induce strong dipolar interactions in an atomic gas by laser-coupling the atomic ground state to a highly excited Rydberg state [San00].

1.1.2 Collisional studies and cold controlled chemistry

The ability to control molecules at the level of single quantum states with respect to both the internal as well as external degrees of freedom opens up exciting new possibilities for quantum-state resolved collisional studies and for the control of chemical reactions [Wei99, Kre08, Dul09a, Car09]. The investigation of collisional processes gives important insights into the underlying molecular structure. Striking examples include the magnificent detail of understanding of the molecular structure near the dissociation threshold brought about by Feshbach spectroscopy. Cesium, the atomic species used in the present work, was the first alkali atom that was predicted to show Feshbach resonances [Tie93]. A collaboration between the group of Steve Chu at Stanford and NIST at Gaithersburg later investigated the collisional properties and the underlying molecular structure with amazing accuracy [Vul99, Chi00, Leo00, Chi04]. Detailed measurements of the molecular level structure near threshold were later performed in Innsbruck [Mar07a]. Feshbach resonances in a Bose-Einstein condensate were first ob-

served and characterized in the group of Wolfgang Ketterle at MIT [Ino98]. A detailed account including other atomic species is given in Ref. [Chi10]. An exciting finding from ultracold collisonal experiments is the observation of the Efimov effect, which was predicted more than 30 years ago in the context of nuclear physics [Efi70, Efi71]. Efimov-related resonances have been observed in atomic gases involving universal trimer states [Kra06b, Zac09, Gro09, Pol09] and tetramer states [Fer09a, Pol09] and in atom-dimer collisions [Kno09]. These experiments constitute prime examples for collisional experiments involving either atoms or very weakly bound molecules in precisely controlled quantum states. An illustration of the important role of quantum statistics in ultracold collisions is provided by the stability of fermionic Feshbach molecules against inelastic collisions [Zir08].

Up until very recently, comparable state control has not been possible for more deeply bound molecules. Nevertheless, important insights about scattering cross sections have been obtained from collisional experiments between atoms and molecules formed in a distribution of vibrational levels by photoassociation [Sta06, Zah06]. Both experiments have found inelastic atom-molecule collision rate constants that were largely independent of the vibrational quantum number. Inelastic collisions between heteronuclear molecules formed by photoassociation in a two-species magneto-optical trap have also been observed [Hud08].

Contrary to what one might expect from traditional chemistry thinking, chemical reactions in the ultracold domain are predicted to proceed with large rate constants and, where present, tunneling through reaction barriers plays an important role. Chemical reactions in the form of exchange processes in an ultracold atom-dimer mixture and in a pure dimer sample have recently been observed with precisely defined internal quantum states in two different experiments. In the first experiment with Cs, one atom in a Cs_2 Feshbach molecule was exchanged for an incoming atom, as could be demonstrated by monitoring the population in different spin states [Kno10]. The second experiment involved fermionic KRb molecules in the rovibronic ground state [Osp10b]. Slow dynamics were found for reactions involving tunneling through a p-wave barrier for identical fermions. In contrast, for atom-molecule collisions or collisions involving molecules in two different spin states, i. e. for reactions that proceed without a barrier via s-wave scattering, the rate constants were much higher. The observed rate constants could be explained with a simple quantum defect theory [Idz09] that predicts universal rate constants and is potentially applicable to a wide range of problems.

Rich collisional physics can be expected both for heteronuclear [Tic08] and homonuclear ground-state molecules, both in a harmonic trap and in reduced dimensions [Li08]. In Cs_2, with its extremely high mass, one can expect the density of tetramer states to be very high near the dimer-dimer scattering threshold. For collisions between Cs Feshbach molecules, a Feshbach-like collision resonance caused by a Cs_4 bound state has been observed [Chi05]. Similar scattering resonances might be found with rovibronic ground-state molecules [Jul09]. One can expect to observe inelastic collisions at a near universal rate [Idz09] for an energetically excited hyperfine sublevel of the rovibronic ground state but a stable molecular quantum gas for mole-

cules in the lowest hyperfine sublevel of the rovibronic ground state. Here, scattering resonances would potentially be observable.

1.1.3 Quantum information and quantum simulation

A vast body of literature has been developed dealing with a possible application of ultracold polar molecules as q-bits in quantum computation schemes [DeM02]. The dipole-diole interaction provides for the coupling between q-bits necessary for quantum gates. Entanglement tests [Mil07] and strategies for switching the dipole-dipole interactions have been proposed [Yel06]. Molecular dipolar crystals might be used as quantum memories in future hybrid quantum computation schemes [Rab07] and interfacing of polar molecules with mesoscopic solid-state devices such as quantum dots or Josephson junctions should be possible [And06]. This would allow to exploit the specific strengths of each system for different tasks in quantum computation.

Similarly, ultracold polar molecules hold promise for the simulation of more complex quantum systems, such as solid state systems [Mic06, Pup09, Ort09]. Many of the proposals rely on ground-state molecules in lattice configurations.

1.1.4 Precision measurements

Ultracold molecules offer prospects for posing new limits on e. g. the time variation of fundamental constants and a possible electron electric dipole moment. The molecular energy structure depends both on the value of the fine structure constant α and on the electron-to-proton mass ratio m_e/m_p. High resolution measurements of the time evolution of these constants in a laboratory setting can potentially surpass the precision currently attainable with e. g. astrophysical observations, which profit from extremely long observation times but suffer from systematic error sources, which are hard to control (for an overview, see Ref. [Chi09]).

Promising candidate systems based on diatomic molecules [Fla07, Zel08, DeM08], including Cs_2 molecules [DeM08], have been identified for the determination of the time evolution of m_e/m_p. For these schemes, the molecules need to be prepared at ultralow temperatures in defined rovibrational levels. Ideally, the molecules will be trapped in an optical lattice to allow for long interrogation times and perfect decoupling from the environment [Zel08, Tak05, Ye08]. A different scheme for the determination of a time variation of m_e/m_p rests on resonant scattering near a Feshbach resonance [Chi06].

One important fundamental physics problem where ultracold molecules might be able to make a contribution is the investigation of a possible violation of fundamental symmetries (for an overview, see Ref. [Tar09]). In order to measure the energy shifts associated with a possible electron electric dipole moment, large electric fields are necessary. The internal electric field in a polar molecule can greatly enhance the magnitude of an externally applied field and therefore, this mechanism dramatically

increases the overall sensitivity. A first measurement of the electron electric dipole moment with cold molecules has been demonstrated [Hud02].

1.2 Production of cold and ultracold molecules

Due to the complex energy structure of molecules with optical cycling transitions only being found in very few selected molecules, laser cooling of molecules has not been demonstrated so far and is not an option for most molecules. Two broad categories of techniques for the production of cold and ultracold molecules have been developed, on the one hand direct cooling and slowing of preexisting molecules and on the other hand an indirect route starting with cold atoms that are associated to molecules. In the latter approach, the focus has been on bialkali molecules and either photoassociation or association on a Feshbach resonance are applied. An general overview covering both routes to cold molecules is given in Refs. [Dul09a, Car09].

1.2.1 Direct cooling and slowing of molecules

A variety of non-optical cooling and slowing techniques for molecules have been developed [Fri09, Sch09, Cha09, Car09, Dul09a, van08, Hut06, Dul06, Doy04]. They have the advantage of being applicable to a broad range of molecules. Typically, temperatures in the K to mK regime are reached. These methods are not suitable for quantum gas studies since the phase-space densities attained thus far range below 10^{-12} and are thus many orders of magnitude from the quantum degenerate regime [Car09].

In buffer gas cooling [Wei98], molecules are allowed to thermalize with a cryogenic gas and both external and internal degrees of the molecule are cooled. Molecules can then be trapped in a variety of different configurations, including electrostatic trapping [Bet00, Rie05, Mee05], magnetic trapping [Cam07], magnetic trapping with additional adjustable electric fields [Saw07], trapping in alternating electric fields [Jun04b], or in a ring configuration [Cro01]. From an effusive source, the slow tail of the velocity distribution can further be selected by a bent molecular guide [Jun04a].

In crossed beam experiments, molecules have been brought to rest through the collapse of the energy distribution in a single "billiard like" collision [Eli03]. Stark deceleration [Bet99] applies pulsed electric fields to slow a beam of molecules along a decelerator (for an overview, see Refs. [Sch09, van08]). Recently, a minituarized decelerator on a chip has become available [Mee09]. For particles that cannot be Stark decelerated, slowing by pulsed magnetic fields, i. e. Zeeman deceleration, has been demonstrated both with atoms [Van07, Nar08a] and with molecules [Nar08b].

There have been proposals to apply laser cooling to molecules, either based on broadband simultaneous addressing of a multitude of rovibrational levels [Bah96] or based on the identification of the rare molecules that feature closed optical cycling transitions [Di 04, Stu08]. Similarly, it might be possible to exploit a cycling transition between vibrational levels [Zep09] for cooling. In an effort towards the experimental

realization of laser cooling of molecules, radiative forces from optical cycling have been observed [Shu09].

Starting from Cs_2 molecules formed in a variety of internal rovibrational states, a redistribution of the population towards lower lying vibrational levels and vibrational cooling was realized by shaped broadband light [Vit08]. Strategies for rotational cooling have been proposed [Vog04] and, recently, laser cooling of rotational degrees of freedom of diatomic molecular ions has been demonstrated [Sch10, Sta10].

An interesting set of proposals for cooling of molecules exploits coupling to an optical cavity mode [Hor97, Vul00]. A theoretical analysis of the prospects for cavity cooling of molecules is given in Refs. [Mor07, Kow07, Lev08]. Experimentally, cavity cooling has been demonstrated for atoms [Mau04].

1.2.2 Photoassociation of ultracold atoms

In photoassociation, two colliding atoms absorb a photon and form an excited molecule in a free-to-bound transition [Jon06]. The excited molecular state can then spontaneously emit a photon and decay to a multitude of rovibrational levels governed by optical selection rules and Franck-Condon factors. Consequently, molecules are formed in a range of different internal states. Alternatively, in two-colour photoassociation, a stimulated emission step follows. Early photoassociation experiments include the work on Rb by the Heinzen group [Mil93] and the work on Cs in Orsay [Fio98]. Optical trapping of cold neutral molecules has first been demonstrated by Takekoshi *et al.* [Tak98].

Photoassociation spectroscopy is typically done with a sample of laser cooled atoms, most often in a magneto-optical trap. Therefore, like any approach based on the association of ultracold atoms, it is limited to (diatomic) molecular species whose constituent atoms can be efficiently laser cooled. Typically, temperatures range from mK to somewhat below a hundred μK in such photoassociation experiments. In combination with the low atomic densities typical of magneto-optical traps and the limited conversion efficiency, the phase-space densities of the produced molecules are very low. Similar to the direct cooling methods, the resulting phase-space densities are many orders of magnitude below the quantum degenerate regime. Most photoassociation experiments have focused on weakly bound rovibrational levels of the electronic ground state. A lot of insight on molecular structure has been gained from photoassociation spectroscopy, as reviewed in the article by Jones and coworkers [Jon06]. For example, weakly bound levels of the Cs dimer have been investigated by two-color photoassociation [Van04].

In the past few years, there has been a very active endeavor to produce deeply bound molecules in photoassociation experiments. Nikolov and coworkers reached low-lying vibrational levels of the electronic ground state by two-colour photoassociation [Nik00]. In a pump-dump scheme, Sage *et al.* produced RbCs molecules in a distribution of vibrational and rotational levels, including the rovibronic ground state [Sag05]. More recently, Deiglmayr and colleagues applied a single photoassociation

step followed by spontaneous emission in order to produce LiCs molecules [Dei08b]. Among other rovibrational levels, the rovibronic ground state of the dimer was populated. Deeply bound vibrational levels of the electronic ground state in NaCs have also been populated [Hai09]. Photoassociation rates can be increased by the presence of a nearby Feshbach resonance [Pel08, Cou98, Tol03, Jun08, Dei09] and it has been proposed to use photoassociative STIRAP near a Feshbach resonance [Kuz09]. An exciting perspective is opened up by vibrational cooling of these molecules with broadband light whereby population is accumulated in the vibrational ground state [Vit08]. An additional step of rotational cooling [Vog04] will then be necessary to accumulate the molecules in the rovibronic ground state. However, state control at the level of single quantum states seems at present taunting with this approach. Further propsals for transfering population to deeply bound molecular levels in photoassociation experiments include the exploitation of coherent wave-packet dynamics and optimal control theory [Koc04, Gho09].

1.2.3 Ultracold molecules near quantum degeneracy

The near quantum-degenerate regime is characterized by phase-space densities close to unity. Scattering between particles is restricted to *s*-wave scattering, although tunneling through higher partial wave barriers plays a role for reactions between molecules. The only approach that is currently capable of delivering ultracold ground-state molecules near quantum degeneracy is based on molecule association on a Feshbach resonance from a quantum degenerate or nearly quantum degenerate atomic sample. The molecules are then transferred from the initial weakly bound level to the rovibronic ground state by coherent optical transfer without heating of the molecular ensemble. Two experimental efforts are currently capable of producing rovibronic ground-state molecules in the quantum-gas regime, the experiment on KRb [Ni08] at JILA, Colorado, without the use of an optical lattice, and the experiments presented in this thesis [Dan08, Dan10b]. In a similar effort, also in Innsbruck, the rovibrational ground-state of the shallow lowest triplet potential has been reached with Rb_2 [Lan08b].

The molecules are prepared at high densities and ultralow temperatures. The great advantage of these experiments is that all internal degrees of freedom, i. e. the electronic state, the vibrational and rotational state and the hyperfine state, of the molecules can be controlled at the level of single quantum states and that the internal state can, within certain constraints, be arbitrarily chosen, in contrast to all previous experiments. This makes such systems an ideal platform for many of the proposed experiments with ultracold molecules.

One key ingredient to our experiments is the ability to coherently associate atoms to weakly bound molecules [Her03, Reg03, Xu03, Zwi03, Bou04, Str03, Par05] on a magnetically tunable Feshbach resonance [Köh06, Hut06, Chi10, Fer09b]. Molecules have also been coherently associated in a BEC by optical Raman techniques [Wyn00] and atom-molecule coherence in a BEC has been induced by a time-varying magnetic field near a Feshbach resonance [Don02]. Feshbach association is highly efficient and

perfectly state selective. Accordingly, the molecular sample inherits the high phase-space density of the atomic gas. When two atoms reside at the same site of an optical lattice, these can be associated to molecules with almost unit efficiency [Tha06]. The resulting molecules reside in the least bound vibrational levels with binding energies of h × kHz to h × MHz. In the limit of vanishing binding energy, these molecules constitute a halo dimer with universal properties [Köh06]. The molecules reside in either an s-wave state characterized by $\ell = 0$, where ℓ is the quantum number associated with the mechanical rotation of the nuclei [Chi10] or in other low rotational states. Feshbach molecules with up to $\ell = 8$ have been created [Kno08] by transferring the molecular population via avoided crossings between bound molecular states [Mar07a]. Importantly, association of atoms to Feshbach molecules greatly increases the wave-function overlap for subsequent optical transfer to the rovibronic ground state and hence a high phase-space density sample of Feshbach molecules constitutes an ideal starting point for the production of near quantum degenerate rovibronic ground-state molecules. The strength of the first optical transition in a Λ-type optical transfer scheme to deeply bound molecular levels can be optimized by choosing particular Feshach levels as starting state for the optical transfer [Dan08, Dan09b], as demonstrated in the framework of this thesis. For weakly bound molecular states, transfer between bound molecular levels can in addition to optical methods either be accomplished by slow and fast magnetic field sweeps over avoided crossings [Chi04, Mar07b, Hut08] between bound molecular states [Mar07a] or by means of radio-frequency dressing of molecular states [Lan08a].

Deeply bound molecules near quantum degeneracy

Several schemes have been proposed to produce ultracold ground state molecules near quantum degeneracy. Jaksch and coworkers proposed photoassociation of pairs of atoms in an atomic Mott-insulator state in optical lattice to weakly bound molecular levels followed by a series of two-photon Raman pulses to transfer the population to the rovibrational ground state [Jak02]. Kokkelmans and colleagues propose to combine an optical Raman transition with a magnetic field sweep over a Feshbach resonance to produce a molecular BEC [Kok01] and Stwalley proposed ground-state transfer from Feshbach states via the electronically excited coupled $(A - b)$ states in alkali dimers with stimulated Raman transitions [Stw04]. Gradual accumulation of population in deeply bound ground-state levels has been suggested by piecewise adiabatic transfer with an optical frequency comb [Sha08]. An overview of the quest for rovibronic ground-state molecules, including further proposals, is also given in Ref. [Dul09a].

The experiments presented in this thesis combine two very powerful techniques for the formation of a high-density, ultracold sample of rovibronic ground-state molecules in a defined quantum state, as illustrated in figure 1.1: Feshbach association [Chi10] and coherent optical transfer in the form of Stimulated Raman Adiabatic Passage (STIRAP) [Ber98]. STIRAP relies on the existence of a dark state that has only contributions from the initial molecular level and the target ground-state level with no

contribution from the electronically excited intermediate level, as further discussed in chapter 1.3. In principle, it allows for complete population transfer between quantum states in a very robust manner. Since this is a coherent process, it can be reversed and the absence of any spontaneous emission step further implies perfect state selectivity as long as the target quantum level is selectively addressed. Specific addressing of one quantum state can be achieved either by ensuring a frequency detuning of the STIRAP lasers from other nearby transitions or by relying on optical dipole selection rules. A combination of both approaches is employed in the experiments presented in this thesis.

In a pioneering experiment in Innsbruck, Winkler *et al.* demonstrated high-efficiency transfer of Feshbach molecules from the least bound vibrational level to the next lower vibrational level in Rb_2, bridging a binding energy difference of about $h \times 600$ MHz [Win07b]. A similar experiment was later performed by the JILA group with KRb, transferring population to a molecular level that was bound by about $h \times 10$ GHz [Osp08]. These experiments were operating in a regime where both the initial and the final molecular levels were very weakly bound and of highly mixed singlet and triplet character. Therefore, it was straight forward to identify excited state intermediate levels that offered good Franck-Condon overlap with both the initial and the final ground-state level and hence adequate transition strengths. In the Rb_2 experiment, off-resonant excitation by the two STIRAP laser fields was the limiting factor for the STIRAP transfer efficiency.

In the first paper presented in this thesis [Dan08] we were able to transfer the molecular population in Cs_2 from the original Feshbach level to a deeply bound level of the $X^1\Sigma_g^+$ electronic ground state with a binding energy of more than $hc \times 1000$ cm^{-1} or $h \times 30$ THz, bridging about one third of the total potential depth. This step constituted an important breakthrough because it demonstrated for the first time that molecules can be transferred from extremely weakly bound molecular levels, where the interaction between the atoms is mainly governed by the van der Waals interaction, to chemically bound levels deep in the potential without destroying the quantum-gas character of the sample. In these experiments, a large difference not only in binding energy but also in mean internuclear distance, reflected by extremely small Franck-Condon factors, was bridged.

Shortly thereafter, the rovibrational ground states of both the shallow triplet $a^3\Sigma^+$ potential and the singlet $X^1\Sigma^+$ electronic ground state were reached in KRb [Ni08] at JILA. Transfer to the $|v = 0, J = 0>$ level of the $X^1\Sigma^+$ electronic ground state resulted in a near quantum degenerate gas of heteronuclear molecules in an optical dipole trap. Here, v and J are the vibrational and rotational quantum numbers, respectively. In heteronuclear molecules, transfer to the rovibronic ground state can be accomplished in a single two-photon step due to a favorable run of the excited state potentials [Stw04] and the absence of the *gerade - ungerade* symmetry for exchange of the nuclei. In Rb_2, the rovibrational ground state of the triplet $a^3\Sigma_u^+$ potential with a binding energy of $\sim hc \times 230$ cm^{-1} was reached [Lan08b] with the molecules being trapped in an optical lattice.

Then, also in the framework of this thesis, it was possible to produce for the first time an ultracold high-density sample of molecules in a single hyperfine sublevel of the $|v = 0, J = 0 > X^1\Sigma_g^+$ rovibronic ground state where also the motional degrees of freedom are controlled by trapping each molecule in the motional ground state of an individual well of an optical lattice [Dan10b]. Both the Innsbruck experiment on Cs_2 and the JILA experiment on KRb are now capable of producing a sample of rovibronic ground state molecules in a defined hyperfine sublevel [Dan10b, Osp10a].

Ultracold molecules in an optical lattice

The creation of an ultracold high-density sample of rovibronic ground-state molecules in an optical lattice is of considerable interest for a variety of applications. For precision measurements involving ultracold molecules, the sample is ideally trapped in an optical lattice [DeM08, Zel08, Tak05] and quantum computation schemes with ultracold molecules rely on optical lattices [DeM02]. It furthermore constitutes an ideal starting point for future quantum gas studies, both for the creation of novel quantum phases [Gór02, Bar08, Lah09, Pup09] and quantum simulation [Pup09] as well as for molecular Bose-Einstein condensation [Jak02]. It has been predicted that an adiabatic transition exists from the many-body ground state in an optical lattice, i. e. the Mott-insulator state in the limit of a deep lattice [Gre02, Blo08], to a molecular BEC [Jak02]. Thus, by adiabatically releasing the rovibronic ground-state molecules from the optical lattice, it should be possible to form a molecular BEC. The experimental realization of a Mott-insulator state with ultracold atoms [Gre02] was a major breakthrough, establishing an important link between atomic physics and condensed matter physics. Ultracold molecules and especially dipolar molecules have the potential to substantially contribute to the understanding of complex systems, such as those encountered in solid state physics, by enabling experiments with full control over the parameter space. The optical lattice enables ultimate control over the motion of the molecules and perfectly shields the molecules from inelastic collisions during molecule production and transfer to the rovibronic ground state.

The production of ultracold Feshbach molecules in an optical lattice [Tha06] was a major step. Due to the high local density, Feshbach association can reach near unit efficiency for two atoms that are trapped at the same site of an optical lattice. Feshbach molecules from fermionic atoms [Stö06] as well as fermionic Feshbach molecules [Osp06] have been created in optical lattices. Weakly bound ultracold molecules in an optical lattice have also been formed by optical Raman transitions [Rom04, Ryu05].

The STIRAP work on the Rb_2 triplet state in Innsbruck was carried out in an optical lattice [Lan08b]. In these experiments, the optical lattice had a wavelength far from a magic wavelength and hence the lattice potential was significantly lower for triplet molecules in $|v = 0>$ than for the initial Feshbach molecules. Therefore, the STIRAP process led to a projection on several different motional states for the $|v = 0>$ molecules and hence to loss of motional state control [Lan09b].

Volz *et al.* produced a sample with exactly one Feshbach molecule at each site

of an optical lattice [Vol06], starting from an atomic Mott-insulator with a maximized number of lattice sites that are occupied by exactly two atoms. Due to the harmonic external confinement, the atom number distribution in the atomic Mott-insulator is inhomogeneous. Shells with a constant number of precisely n atoms per lattice site, where $n = 1, 2, 3 \ldots$, are separated by narrow superfluid regions [Blo08]. Theoretically, up to 53% of the atoms can be loaded into doubly occupied lattice sites making up the central $n = 2$ Mott shell by appropriately choosing the strength of an additional external harmonic confinement during lattice loading.

Our preparation procedure for rovibronic ground-state molecules in an optical lattice initially follows the experiment by Volz and coworkers. We produce an atomic Mott insulator where we aim to maximize the size of the two-atom Mott shell and associate pairs of atoms to weakly bound molecules. Starting from this lattice-trapped sample, we were able to produce a sample of deeply bound singlet $X^1\Sigma_g^+$ molecules in an optical lattice [Dan09a], populating the same intermediate ground-state level as in our previous work in free space [Dan08]. Taking these experiments one important step further, we transferred the molecular population all the way to the rovibronic ground state in the optical lattice [Dan10b]. One crucial aspect of this work is that we were able to maintain control over the motional state of the rovibronic ground state molecules by operating the optical lattice near a magic wavelength that gives equal trapping potentials for the initial Feshbach state and the $|v = 0>$-molecules. An alternative approach would be to spectroscopically resolve [Rom04] the lattice vibrational levels during the STIRAP transfer.

Our results on the production of a high-density ultracold sample of rovibronic ground-state molecules in an optical lattice can readily be generalized to heteronuclear molecules, such as KRb [Ni08, Osp06], LiCS [Dei08b], NaCs [Hai09] or RbCs [Pil09, Sag05], opening up the possibility to study dipolar quantum phases in optical lattices.

1.3 Coherent optical population transfer

Coherent optical transfer and in particular the STIRAP technique [Ber98] are extremely attractive tools for the manipulation of the internal quantum state of ultracold molecules. The STIRAP method allows for complete population transfer despite the fact that a spontaneously decaying intermediate level is used. Furthermore, it offers the possibility to fully control the final quantum state of the molecule and at the same time it is robust against variation of the parameters once certain requirements are fulfilled. STIRAP was developed in the context of molecular beam experiments in an effort to transfer molecules to high vibrational states [Gau88, Gau90], whereas the concept of population transfer with suitably delayed pulses and adiabatic population following had already been recognized in theoretical work [Ore84]. STIRAP relies on the existence of a dark state $|a^0>$ of the form $|a^0> = \cos\Theta|1> - \sin\Theta|3>$, where $|1>$ and $|3>$ are the initial and the final molecular states, respectively. The mixing

angle Θ is defined by $\tan\Theta = \Omega_1(t)/\Omega_2(t)$, where $\Omega_1(t)$ is the time-dependent Rabi frequency of laser L_1 linking $|1>$ to the excited intermediate level $|2>$ and $\Omega_2(t)$ is the Rabi frequency for laser L_2 linking $|2>$ and $|3>$. Note that there is no contribution from the leaky excited state level $|2>$ that would lead to spontaneous decay out of the three-level system. As is well known, in the STIRAP process, the population is adiabatically rotated from the initial level $|1>$ to the final level $|3>$ by a pulse sequence where Lasers L_1 and L_2 deliver time-dependent overlapping pulses with L_2 preceding L_1. During the STIRAP process, the population adiabatically follows the zero energy eigenstate [Ber98]. The effect of decay from the intermediate state is strongly suppressed by the counterintuitive pulse sequence [Vit97]. In order to ensure adiabaticity in the STIRAP process, the Rabi frequencies have to be sufficiently high and the STIRAP transfer time τ_p has to be sufficiently long, which is commonly expressed as an adiabaticity criterion $\Omega_{eff}\tau_p > 10$, where $\Omega_{eff} = \sqrt{\Omega_1^2 + \Omega_2^2}$ is the effective Rabi frequency [Ber98]. Depending on the system under study, this criterion can limit the population transfer efficiency. The achievable peak Rabi frequencies can be limited by low Franck-Condon overlap or finite available laser power. Long STIRAP transfer times τ_p, on the other hand, pose stringent conditions on the required narrow relative linewidth of the involved lasers.

It has been shown that even in a situation where several Λ-systems exist in parallel, such as with magnetic substates, efficient population transfer is possible as long as certain criteria are fulfilled [Mar96, Sho95, Mar95]. STIRAP and a series of variations of the technique have successfully been employed in a variety of contexts, including population transfer in solid state systems [Kle07]. An overview of an effort to combine STIRAP with coherent control concepts is given in Ref. [Krá07]. One extension of the classical STIRAP technique that is particularly important in the context of the experiments presented in this thesis is the extension to multilevel systems [Sho91, Mal97] that will be discussed in chapter 6.

1.4 Overview

This thesis contains five papers, each of which is presented in a separate chapter. Each paper is accompanied by a short introduction and by a statement about the author's contributions to the work. Only papers in peer-reviewed journals are discussed whereas conference proceedings [Dan09c] are omitted. In parallel to the effort to produce quantum gases of rovibronic ground state molecules, we investigate Cs as an atomic quantum gas with tunable interactions in optical lattices and in reduced dimensions. Work on Cs in optical lattices has been discussed in the thesis of Mattias Gustavsson [Gus08] and the experiments on quantum gases in reduced dimensions will be covered in the PhD thesis of Elmar Haller [Hal10]. Here, in chapter 8, an introduction to these experiments is given and five papers are presented.

The optical-lattice Cs BEC machine is described in detail in the PhD thesis of Mat-

tias Gustavsson [Gus08] and in the diploma theses of Peter Unterwaditzer [Unt05], Anton Flir [Fli06], Gabriel Rojas Kopeinig [Roj07], and Manfred Mark [Mar07c]. This machine is the second generation Cs BEC apparatus. The original Cs BEC machine built in Rudi Grimm's group is described in the PhD theses of Tino Weber [Web03], Jens Herbig [Her05], Tobias Kraemer [Kra06a], and Michael Mark [Mar03], and in the diploma theses of Michael Mark [Mar03] and Harald Schöbel [Sch07]. The author's diploma thesis [Dan07] on the original Cs BEC machine describes preparatory work for the current project on rovibronic ground-state molecules and gives a simplified introduction to molecular structure. The work on molecular state transfer in Rb_2 in Innsbruck is described in the PhD theses of Gregor Thalhammer [Tha07], Klaus Winkler [Win07a], and Florian Lang [Lan09a].

Chapter 2 reports on the first creation of a quantum gas of deeply bound ground-state molecules. The molecular population was coherently transferred from the initial weakly bound Feshbach level by STIRAP to the $|v = 73, J = 2>$ level of the $X^1\Sigma_g^+$ electronic ground state with a binding energy of more than hc $\times$ 1000 cm^{-1}, showing that deeply bound rovibrational ground state levels can efficiently be populated without destroying the quantum-gas character of the sample.

Chapter 3, *Precision molecular spectroscopy for ground state transfer of molecular quantum gases*, presents the high-resolution molecular spectroscopy on electronically excited levels necessary for STIRAP transfer to deeply bound ground-state levels.

Chapter 4, *Dark resonances for ground state transfer of molecular quantum gases*, discusses the molecular spectroscopy for transfer from the intermediate ground-state level $|v = 73, J = 2>$ to the rovibronic ground state. Data for the spectrocopy on the electronically excited states and for two-photon dark resonances involving $|v = 73>$ and $|v=0>$, is presented.

Chapter 5, *Deeply bound ultracold molecules in an optical lattice*, describes the production of an ultracold sample of molecules in rovibrational level $|v=73, J=2>$ in a three-dimensional optical lattice.

In Chapter 6, *An ultracold high-density sample of rovibronic ground-state molecules in an optical lattice*, we report on the first creation of a sample of ultracold rovibronic ground state molecules in an optical lattice. The molecules reside in a single hyperfine quantum level of the rovibronic ground state. Each ground-state molecule is trapped at an individual lattice site in a defined quantum state of the external motion, namely the lattice ground vibrational level, and we reach a high filling factor in the lattice. The lifetime of the sample is on the order of 8 seconds.

Chapter 7 gives an outlook on improvements of the STIRAP process and future experiments.

Chapter 8 discusses our research on atomic quantum gases with tunable interactions.

The appendix gives technical details of the STIRAP setup.

The following publications are included in this thesis:

1. J. G. Danzl, E. Haller, M. Gustavsson, M. J. Mark, R. Hart, N. Bouloufa, O. Dulieu, H. Ritsch, and H.-C. Nägerl. Quantum gas of deeply bound ground state molecules. *Science*, **321,** 1062 (2008).

2. J. G. Danzl, M. J. Mark, E. Haller, M. Gustavsson, N. Bouloufa, O. Dulieu, H. Ritsch, R. Hart, and H.-C. Nägerl. Precision molecular spectroscopy for ground state transfer of molecular quantum gases. *Faraday Discussions*, **142,** 283 (2009).

3. M. J. Mark, J. G. Danzl, E. Haller, M. Gustavsson, N. Bouloufa, O. Dulieu, H. Salami, T. Bergeman, H. Ritsch, R. Hart, and H.-C. Nägerl. Dark resonances for ground state transfer of molecular quantum gases. *Applied Physics B*, **95,** 219 (2009)

4. J. G. Danzl, M. J. Mark, E. Haller, M. Gustavsson, R. Hart, A. Liem, H. Zellmer, and H.-C. Nägerl. Deeply bound ultracold molecules in an optical lattice. *New J. Phys.*, **11,** 055036 (2009).

5. J. G. Danzl, M. J. Mark, E. Haller, M. Gustavsson, R. Hart, J. Aldegunde, J. M. Hutson, and H.-C. Nägerl. An ultracold high-density sample of rovibronic ground-state molecules in an optical lattice. *Nature Phys.*, advance online publication 21 Feb. 2010, DOI: 10.1038/NPHYS1533.

6. M. Gustavsson, E. Haller, M. J. Mark, J. G. Danzl, G. Rojas-Kopeinig, and H.-C. Nägerl. Control of interaction-induced dephasing of Bloch oscillations. *Phys. Rev. Lett.*, **100,** 080404 (2008).

7. M. Gustavsson, E. Haller, M. J. Mark, J. G. Danzl, R. Hart, A. J. Daley, and H.-C. Nägerl. Interference of interacting matter waves. Preprint available at *arXiv:0812.4836* (2008).

8. E. Haller, M. Gustavsson, M. J. Mark, J. G. Danzl, R. Hart, G. Pupillo, and H.-C. Nägerl. Realization of an excited, strongly correlated quantum gas phase. *Science*, **325,** 1224 (2009).

9. E. Haller, R. Hart, M. J. Mark, J. G. Danzl, L. Reichsöllner, and H.-C. Nägerl. Inducing transport in a dissipation-free lattice with super Bloch oscillations. Preprint available at *arXiv:1001.1206* (2010).

10. E. Haller, M. J. Mark, R. Hart, J. G. Danzl, L. Reichsöllner, V. Melezhik, P. Schmelcher, and H.-C. Nägerl. Confinement-induced resonances in low-dimensional quantum systems. Preprint available at *arXiv:1002.3795* (2010).

Chapter 2

Publication: Quantum gas of deeply bound ground state molecules

Originally published in *Science* Express on 10 July 2008
Science 22 August 2008:
Vol. 321, no. 5892, pp. 1062 - 1066
DOI: 10.1126/science.1159909

This paper** reports on the creation of a quantum gas of molecules in a deeply bound rovibrational level of the electronic ground state. Atoms in a BEC are associated to weakly bound molecules and then transferred with STIRAP [Ber98] in a two-photon transition to a specific rovibrational level of the singlet electronic ground state potential. The transfer bridges a binding energy difference of $>hc \times 1000\ cm^{-1}$ or $h \times 30$ THz, which constitutes about one third of the total binding energy of the rovibronic ground state, whereas previous experiments [Win07b, Osp08] had only reached binding energies less than 10^{-4} of the ground state potential depth. This step is crucial because it converts the initial loose bond mediated by van der Waals interaction into a tight chemical bond. A second two-photon transition, now between deeply bound levels both in the electronic ground state and in the electronically excited state – and hence with much better Franck-Condon factors – can then be added to transfer the population to $|v = 0>$, as discussed in chapter 6. In Cs_2, a homonuclear molecule, we decided on this 4-photon scheme because the additional g/u symmetry that results from exchange of the identical nuclei poses additional limitations on which electronically excited states can be used in the transfer. Furthermore, an unfavorable shape of the excited-state potentials leads to prohibitively low transition rates for a single two-photon transfer to the rovibronic ground state. It is not excluded, however, that in the future an excited-state potential that allows for a single two-photon step can be identified.

**The author of the present thesis developed the strategy and designed the experiments for transfer to the rovibronic ground-state in a 4-photon scheme together with H.-C. N. based on information about molecular transition strengths provided by N. B. and O. D.. He built the laser setup for STIRAP transfer including the frequency comb setup. The author performed all the experiments with support from E. H., M. J. M., M. G., and R. H. and he analyzed the data. E. H., M. G., and M. J. M. made important contributions by building and maintaining the BEC machine. The simulations for STIRAP transfer and dark resonance spectroscopy were done by H. R.. The paper was written by J. G. D. and H.-C. N. and all authors commented on the manuscript. Here, the final accepted version of the paper is given, before the journal's copy editing process.

The scheme was developed based on Franck-Condon factors from *ab initio* molecular structure calculations [Bou07] for the $(A^1\Sigma_u^+ - b^3\Pi_u)0_u^+$ coupled states. Unfortunately, there was no spectroscopic data available in the region of the potential relevant to the molecular state transfer. Strong spin-orbit interaction leads to strong coupling between the states in the heavy alkali dimers, leading to irregularities in the spectra and making them difficult to interpret [Ami99]. Our spectroscopic measurements on the excited state level structure are discussed in chapters 3 and 4. In contrast to other alkali dimers like KRb [Wan07, Pas07] or Rb_2 [Tsa97], even though there was extensive knowledge about the energy level structure near threshold [Mar07a] and in deeply bound regions of the potential [Wei85, Ami02], the dissociation energy of the Cs dimer had only been known [Ami02] to an uncertainty of $\pm$ hc $\times$ 0.45 cm^{-1} previous to this work. This uncertainty is large when compared to the resolution of the two-photon dark resonance spectroscopy that we applied to identify deeply bound target levels and the frequency-step size on the order of a few MHz required for this type of spectroscopy.

Efficient transfer to the target level was achieved despite the extremely low Franck-Condon factors in the 4-photon scheme. Our simulations show that the transfer efficiency is currently limited by a combination of laser linewidth and limited adiabaticity. Future technical improvements of the laser setup as described in chapter 7 will reduce the relative laser linewidth of the STIRAP lasers and allow for longer STIRAP times that should in turn improve adiabaticity and overall efficiency. In case it turns out in future studies that there is some residual coupling to unwanted molecular levels that lead to losses out of the three-level system, these levels could be shifted out of resonance by working at a higher magnetic field. Such weak residual couplings might either occur with excited state levels or in a Λ-type configuration with ground-state levels. At present, an analysis of the excited-state hyperfine structure is under way [Ber10, Dul10]. The couplings in such a parallel Λ-system would be far too weak for coherent population transfer, because the transition strengths even in our main Λ-system are low. Nevertheless, such weak couplings could lead to non-adiatatic excitation to a bright state followed by spontaneous decay and hence loss out of the three-level system.

We performed two important tests on the sample of deeply bound ground-state molecules. First, the coherence of the transfer was tested in a Ramsey-type experiment. Second, we tested heating of the sample by the transfer. This latter test is particularly significant because it determines whether the quantum-gas character of the sample is maintained during the transfer. The two-photon transition takes away about h $\times$ 32 THz of binding energy, or, in temperature units, $k_B \times 1500$ K, whereas the molecular sample has an energy on the order of a few $k_B \times$ nK. We find that the sample is not heated during the transfer.

In conclusion, these results show that the preparation of a quantum gas of molecules in specific rovibrational states is possible.

Quantum Gas of Deeply Bound Ground State Molecules

Johann G. Danzl[1*], Elmar Haller[1], Mattias Gustavsson[1], Manfred J. Mark[1], Russell Hart[1], Nadia Bouloufa[2], Olivier Dulieu[2], Helmut Ritsch[3], Hanns-Christoph Nägerl[1]

[1]Institut für Experimentalphysik und Zentrum für Quantenphysik, Universität Innsbruck, Technikerstraße 25, 6020 Innsbruck, Austria

[2]Laboratoire Aimé Cotton, CNRS, Université Paris-Sud Bât. 505, 91405 Orsay Cedex, France

[3]Institut für Theoretische Physik und Zentrum für Quantenphysik, Universität Innsbruck, Technikerstraße 25, 6020 Innsbruck, Austria

[*]To whom correspondence should be addressed; E-mail: johann.danzl@uibk.ac.at.

Molecular cooling techniques face the hurdle of dissipating translational as well as internal energy in the presence of a rich electronic, vibrational, and rotational energy spectrum. Here, we create a translationally ultracold, dense quantum gas of molecules bound by more than 1000 wavenumbers in the electronic ground state. Specifically, we stimulate with 80% efficiency a two-photon transfer of molecules associated on a Feshbach resonance from a Bose-Einstein condensate of cesium atoms. In the process, the initial loose, long-range electrostatic bond of the Feshbach molecule is coherently transformed into a tight chemical bond. We demonstrate coherence of the transfer in a Ramsey-type experiment and show that the molecular sample is not heated during the transfer. Our results show that the preparation of a quantum gas of molecules in specific rovibrational states is possible and that the creation of a Bose-Einstein condensate of molecules in their rovibronic ground state is within reach.

Ultracold samples of molecules are ideally suited for fundamental studies in physics and chemistry, ranging from few-body collisional physics *(1,2,3,4)*, ultracold chemistry *(5)*, and high resolution spectroscopy *(6,7)*, to quantum gas preparation, molecular Bose-Einstein condensation *(8)*, and quantum processing *(9)*. For many of the proposed experiments full control over the molecular wave function in specific

deeply bound rovibrational states is needed. High densities are required for molecular quantum gas studies. Only in the rovibronic ground state, i.e. the lowest vibrational and rotational energy level of the electronic ground state, is collisional stability assured. However, direct molecular cooling towards high phase space densities seems yet out of reach *(10)*, whereas techniques like Feshbach association *(11)* and photoassociation *(12)* either produce molecules exclusively in weakly bound rovibrational levels, or suffer from low production rates and low state selectivity.

In order to produce a quantum gas of molecules in their absolute ground state, Jaksch *et al. (13)* proposed a scheme for homonuclear alkali molecules in which the technique of stimulated two-photon transfer is repeatedly applied to molecules associated from a high-density sample of ultracold atoms. The initially very loosely bound molecules are transferred in successive steps to the rovibrational ground state of the singlet $X^1\Sigma_g^+$ molecular potential. The advantage of this scheme is that it is fully coherent, not relying on spontaneous processes, and that it involves only a very small number of intermediate levels. It promises that a ground state binding energy of typically 0.5 eV can be carried away without heating the molecular sample. It essentially preserves phase space density, allowing the molecular sample to inherit the high initial phase space density from the atomic sample. However, to realize this scheme, several challenges have to be met. First, there is a large difference in internuclear separation that has to be bridged: the overlap between the radial wave function of the least bound molecules with the radial wave functions of deeply bound molecular levels is extremely low, potentially leading to prohibitively low transition rates for the two-photon transitions. Second, the scheme requires the identification of suitable intermediate molecular levels while strictly avoiding parasitic excitations. Third, a large difference in binding energy has to be overcome. On a more technical side, the lasers driving the two-photon transitions at widely different wavelengths need to have extremely low relative short term phase jitter and high long term frequency stability to allow for coherence and reproducibility. In important experiments, Winkler *et al. (14)* and recently Ospelkaus *et al. (15)* demonstrated highly efficient two-photon transfer into lower lying molecular levels starting from weakly bound dimer molecules, which were associated from ultracold atoms on a Feshbach resonance *(11)*. However, the transferred molecules are still weakly bound. Their binding energy, on the order of the atomic hyperfine splitting, is less than 10^{-4} of the binding energy of the rovibrational ground state, and wave function overlap with this state is still negligible.

Here we demonstrate the crucial step towards full control of the molecular wave function and towards the formation of a Bose-Einstein condensate (BEC) of molecules in their rovibronic ground state by linking weakly bound molecular states with deeply bound rovibrational states. We coherently transfer an ultracold quantum gas of weakly bound cesium Feshbach molecules to the rovibrational level $|v = 73, J = 2>$ of the singlet $X^1\Sigma_g^+$ potential, bound by 1061 cm^{-1} (or $h\times$31.81 THz), corresponding to more than one fourth of the binding energy of the rovibrational ground state. To achieve this result, we overcome low wave function overlap by using a suitable intermediate excited molecular state while avoiding excitation into loss channels, and we reference

the transfer lasers to a frequency comb, allowing us to flexibly bridge binding energy differences of more than 1000 cm^{-1}.

Figure 2.1 shows the energy of the relevant molecular and atomic states. Our experiment starts with a cigar-shaped BEC of cesium atoms in the lowest hyperfine sublevel $F = 3, m_F = 3$ in an optical dipole trap. For BEC production, we essentially follow the procedure detailed in *(16)*. For Feshbach molecule production out of the BEC, we ramp up the offset magnetic field from the initial value of 2.1 mT to about 5.0 mT in 10 ms. We then ramp down, sweeping across a d-wave Feshbach resonance at 4.8 mT after about 1 ms as shown in Figure 2.1B *(17,18)*. Our procedure *(17)* gives an ultracold and dense sample of up to 11000 molecules every 10 s at densities above 1×10^{11} cm^{-3}. For the state transfer experiments discussed here, we do not separate the molecules from the original BEC. Upon lowering the magnetic field, the molecules are transferred from the initial state $|d\rangle$ to a still weakly bound s-wave molecular state $|s\rangle$ of the lowest hyperfine channel ($F_1 = 3, F_2 = 3$) via an avoided crossing *(18)*. The index $i = 1, 2$ denotes the i-th atom.

Upon further lowering the magnetic field to about 2.2 mT, the molecules enter into a closed channel s-wave molecular state $|a\rangle$ via a second, broad avoided crossing *(18)*. This state belongs to the uppermost hyperfine channel ($F_1 = 4, F_2 = 4$) and thus has an effective binding energy of more than $2 \times h\nu_{Cs}$. Here h is Planck's constant and $\nu_{Cs} \approx 9.19$ GHz is the Cs clock frequency. Similar to $|s\rangle$ this state is a mixture of the $X^1\Sigma_g^+$ ground state and the lowest triplet $a^3\Sigma_u^+$ state, coupled by hyperfine interaction, and it has zero rotational angular momentum. At a field of 1.9 mT, it has a binding energy of 5 MHz$\times h$ with respect to the $F = 3, m_F = 3$ two-atom asymptote *(18)*. As one might expect, we find that optical transition rates as measured below are improved when using this effectively more deeply bound state as the initial state for two-photon transfer instead of state $|s\rangle$. We shut off the trap and perform all subsequent experiments in free flight. This does not affect the particle density immediately, but reduces it during the later detection procedure, which takes about 6ms, in order to avoid collisions between atoms and weakly bound dimers and hence loss. We detect molecules in $|a\rangle$ via states $|s\rangle$ and $|d\rangle$ by first applying a magnetic field gradient for atom-molecule Stern-Gerlach separation, then reversing the magnetic field ramp, and finally dissociating them on the Feshbach resonance at 4.8 mT, and imaging the resulting atoms *(17)*.

Efficient two-photon transfer via the stimulated Raman adiabatic passage (STIRAP) technique *(19,14)* relies on a suitable choice for the excited state $|e\rangle$. In our case this state must have singlet character so that it can be used as a transfer state to deeply bound levels of the $X^1\Sigma_g^+$ potential. In general, it must be well separated from other states, which otherwise could be off-resonantly excited. It should thus be situated far to the red of the excited $S_{\frac{1}{2}}+P_{\frac{1}{2}}$ potential asymptote to avoid the high density of excited molecular states near that asymptote. We have performed optical loss spectroscopy starting from state $|a\rangle$ in the wavelength range from 1120 to 1130 nm, about 2300 cm^{-1} to the red of the cesium D_1 line. For this measurement we recorded the number of remaining molecules in $|a\rangle$ as a function of excitation wave-

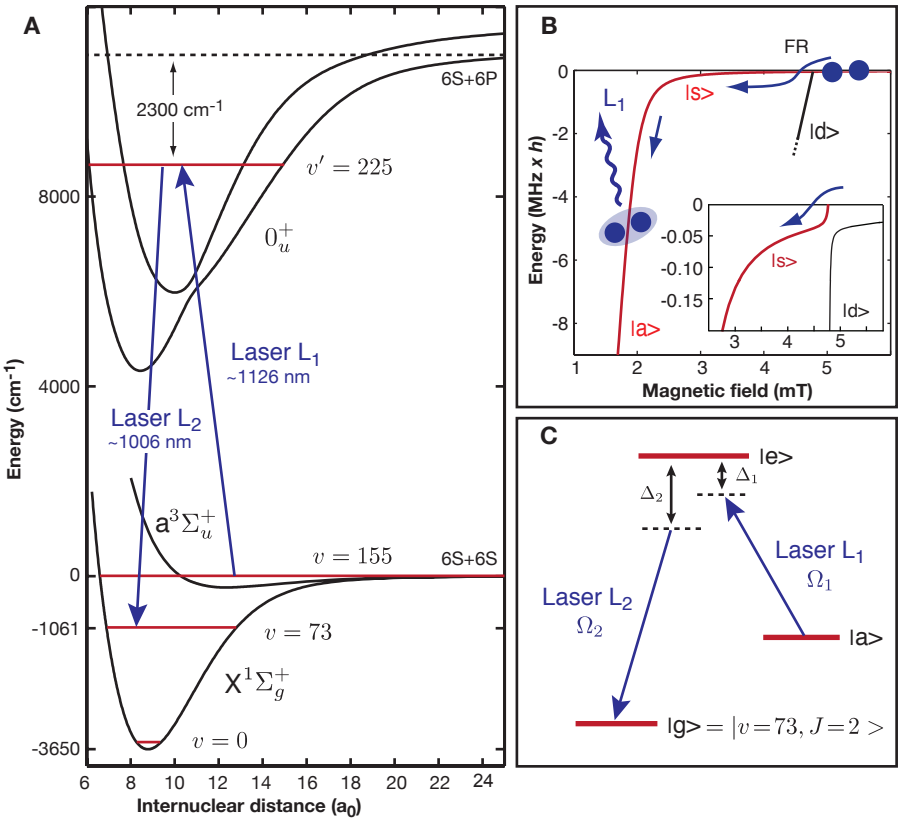

Figure 2.1: **A** Molecular level scheme for Cs_2. Molecules in a weakly bound Feshbach level are transferred to rovibrational level $|v=73, J=2>$ of the singlet $X^1\Sigma_g^+$ potential with a binding energy of 1061 cm^{-1} in a two-photon STIRAP process with wavelengths near 1126 nm and 1006 nm via the 225th level of the electronically excited $(A^1\Sigma_u^+ - b^3\Pi_u)\ 0_u^+$ potentials. The $X^1\Sigma_g^+$ potential has about 155 vibrational levels. **B** Zeeman diagram showing the energy of all relevant weakly bound molecular levels for initial Feshbach molecular state preparation *(18)*. The binding energy is given with respect to the $F = 3, m_F = 3$ two-atom asymptote. The molecules are produced on a d-wave Feshbach resonance at 4.8 mT (see inset) and then transferred to the weakly bound s-wave state $|s>$ on an avoided state crossing. Further lowering of the magnetic offset field to 1.9 mT transfers the molecules from $|s>$ to state $|a>$, the starting state for the STIRAP transfer. **C** STIRAP transfer scheme *(19)*. The molecules are transferred from the initial state $|a>$ to the final state $|g>=|v = 73, J = 2>$ by means of two overlapping laser pulses for which laser L_2 is pulsed on prior to L_1. The detunings and Rabi frequencies of L_i are Δ_i and Ω_i, $i = 1, 2$.

length and found two progressions of lines, which we assign to the potential curves of the mixed $(A^1\Sigma_u^+ - b^3\Pi_u)\, 0_u^+$ excited states and to the $(1)^3\Sigma_g^+$ excited state, respectively. For the present experiments, we choose for $|e>$ a level of the 0_u^+ progression which is 8879.63(1) cm^{-1} above the $F = 3, m_F = 3$ two-atom asymptote, corresponding to a transition wavelength of 1126.173(1) nm (Figure 2.1A). We measure all wavelengths on a home-built wavemeter. We identify this previously unknown level as the 225th one of the 0_u^+ system, with an uncertainty of two in the absolute numbering.

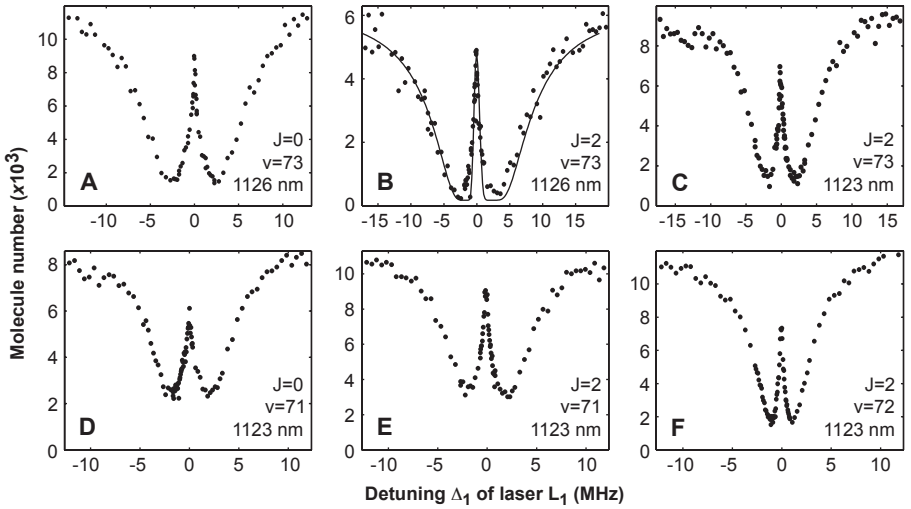

Figure 2.2: Dark resonances for vibrational levels $v = 71, 72$, and 73. Laser L_2 is held on resonance, while the detuning Δ_1 of L_1 is scanned. We record the number of molecules in $|a>$ while both lasers are pulsed on simultaneously. **A**, **B**, and **C** show dark resonances involving $v = 73$ for excitation with L_1 near 1126 nm into $J = 0$ and 2 and for excitation with L_1 near 1123 nm into $J = 2$, respectively. **D**, **E**, and **F** show the neighboring levels $v = 71$ and 72 for excitation near 1123 nm. The solid line in B is the result of a three-level model calculation matched to the data giving $\Omega_1 = 2\pi\times 2$ kHz $\sqrt{I_1/(\mathrm{mW/cm^2})}$ and $\Omega_2 = 2\pi\times 11$ kHz $\sqrt{I_2/(\mathrm{mW/cm^2})}$ for a pulse time of 5 μs at intensities of $I_1 = 4\times 10^5$ mW/cm^2 for L_1 and $I_2 = 2\times 10^5$ mW/cm^2 for L_2 assuming a laser linewidth of 2 kHz.

The ground state level $|g>$ with vibrational quantum number $v = 73$ is well known from conventional molecular spectroscopy *(20,21)*. However, its binding energy, as well as the binding energy of all deeply bound vibrational levels, has only been known with an uncertainty of about ± 0.45 cm^{-1} prior to the present experiments *(21)*. We search for $|g>$ by exciting the transitions from $|a>$ to $|e>$ with laser L_1 and from $|e>$ to $|g>$ with laser L_2 simultaneously. The two light fields create a molecule-molecule dark state. The molecules initially in $|a>$ are lost unless the second laser L_2 is on two-photon resonance, provided that the Rabi frequency Ω_2 on the second transition is equal to or greater than Ω_1, the Rabi frequency on the first transition. For coherence, stability, and reproducibility, we lock both lasers to independent narrow-band optical resonators,

which we reference to an optical frequency comb *(22)*. The comb is not calibrated, but it allows precise differential frequency measurements and provides long-term stability needed for systematic line searches *(23)*. We find the resonance condition with vibrational level $v = 73$ at 1005.976(1) and 1005.982(1) nm, corresponding to rotational quantum numbers $J = 0$ and 2. Identification of J is possible since the rotational energy splitting is well known. Figures 2.2A and B show typical molecular dark resonances when we set L_2 on resonance and step the detuning Δ_1 of L_1 near 1126.173 nm. Figure 2.2C shows a dark resonance involving $v = 73$, $J = 2$ using a different excited molecular state $|e'>$, which is excited with L_1 near 1123.104 nm.

Figures 2.2D-F show dark resonances involving the neighboring vibrational levels $v = 71$ and $v = 72$. These $X^1\Sigma_g^+$-levels were easily found based on previously acquired Cs_2 spectra *(21)*. We determine the binding energy of these levels with respect to the atomic $F_1 = 3, F_2 = 3$ asymptote at zero magnetic field to be 1060.9694(10), 1088.3101(10), 1115.9148(10) cm^{-1} for $v = 73, 72, 71$ with $J = 0$, respectively. The binding energy of the rovibrational ground state $v = 0$ is thus 3628.7053(14) cm^{-1}, which represents an improvement in precision of more than two orders of magnitude compared to the previous determination *(21)*. Fitting the data for the dark resonances with a three-level model taking into account off-resonant excitations and laser line widths, we determine the molecular transition strengths as given by the normalized Rabi frequencies for the transitions $|a>$ to $|e>$ and $|e>$ to $|v = 73, J = 2>$ to be $\Omega_1 = 2\pi \times 2$ kHz $\sqrt{I/(\mathrm{mW/cm^2})}$ and $\Omega_2 = 2\pi \times 11$ kHz $\sqrt{I/(\mathrm{mW/cm^2})}$, respectively. A comparison with a typical atomic transition strength of $\Omega_a = 2\pi \times 5$ MHz $\sqrt{I/(\mathrm{mW/cm^2})}$ giving $|\Omega_1/\Omega_a|^2 < 10^{-6}$ reflects the minuteness of the wave function overlap.

We are now in a position to carry out coherent transfer using the STIRAP technique. For $|g>$ we choose the vibrational level with $v = 73, J = 2$. This level will allow us to reach the rovibrational ground state $v = 0, J = 0$ with a second STIRAP step in view of the selection rule $\Delta J = 0, \pm 2$. STIRAP uses a counterintuitive overlapping pulse sequence in which L_2 is pulsed on prior to L_1. As is well known *(19)*, STIRAP relies on the existence of a dark state of the form $|D>= \alpha(t)|a> + \beta(t)|g>$. With sufficient adiabaticity, the function $|\alpha(t)|^2$ decreases smoothly from 1 to 0, while the function $|\beta(t)|^2$ increases smoothly from 0 to 1. The initial state $|a>$ is thus rotated via $|D>$ into the final state $|g>$. The criterion for adiabaticity is $\tau_p \Omega^2 \gg (2\pi)^2 \Gamma$, where τ_p is the pulse overlap time, $\Omega \approx \Omega_1 \approx \Omega_2$ is the peak Rabi frequency during the pulse, and $\Gamma \approx 2\pi \times 4$ MHz is the (spontaneous) decay rate from the upper state $|e>$ as determined from our loss measurements. This criterion is quite stringent, in particular in view of the low wave function overlap that enters into Ω. An upper (experimental) limit for τ_p is given by the relative laser coherence time for L_1 and L_2. We choose τ_p to be approximately 10 μs. For detection, we apply the reverse STIRAP sequence after a waiting time $\tau_w \approx 10$ μs to transfer the molecules back into $|a>$. During this time we leave laser L_1 on to assure that all possible residual population in state $|a>$ is removed.

We perform double STIRAP about 3 ms after the production of the Feshbach mole-

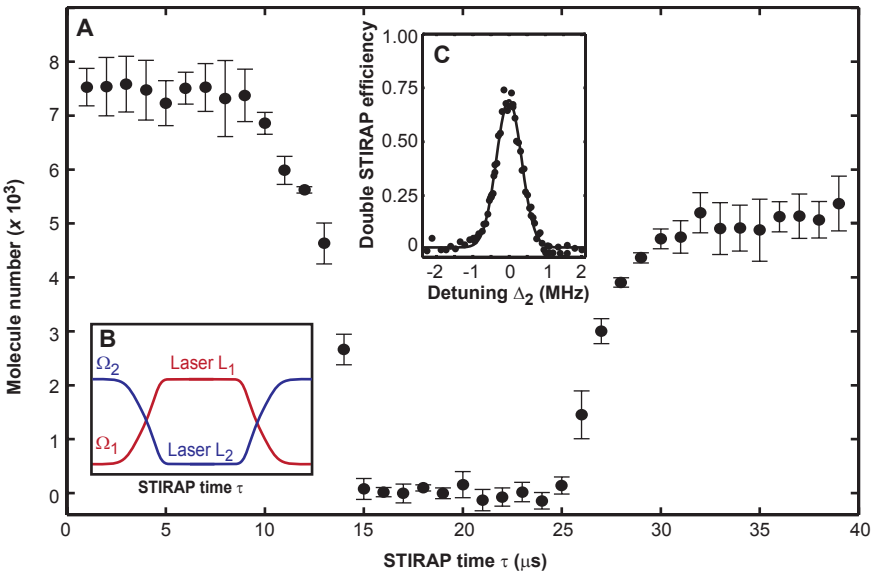

Figure 2.3: STIRAP transfer from the weakly bound state $|a>$ to the deeply bound state $|g>=|v=73, J=2>$ and back to $|a>$. **A** shows the number of molecules in state $|a>$ as a function of STIRAP time τ for $\Delta_1 \approx 0 \approx \Delta_2$. The measured pulse overlap begins at 5 μs and ends at about 15 μs. The second pulse overlap starts at 25 μs and ends at about 33 μs. **B** schematically shows the timing for the Rabi frequencies Ω_i, $i = 1, 2$, during the double STIRAP sequence. Laser L_1 is left on after the first STIRAP sequence to clear out any remaining population in $|a>$. **C** Double STIRAP efficiency as a function of the detuning Δ_2 of laser L_2 for $\Delta_1 \approx 0$. The solid line is a gaussian fit with a FWHM of 811 kHz. The peak Rabi frequencies are $\Omega_1 \approx 2\pi\times 3$ MHz and $\Omega_2 \approx 2\pi\times 6$ MHz. The error bars refer to the 1-sigma error in determining the particle number.

cules and 1 ms after shutting off the trap. Figure 2.3A shows the molecular population in $|a>$ as a function of the STIRAP time τ, and Figure 2.3B shows the timing sequence for the double transfer scheme. For recording the time evolution of the population we interrupt the transfer process after time τ and measure the remaining population in $|a>$. The molecules in $|a>$ initially disappear during the first STIRAP sequence. They are now in level $|v = 73, J = 2>$ of the singlet $X^1\Sigma_g^+$ potential. Then a large fraction of them returns in the course of the reverse STIRAP sequence. For this particular measurement both lasers are on resonance. The peak Rabi frequencies are $\Omega_1 \approx 2\pi\times 3$ MHz and $\Omega_2 \approx 2\pi\times 6$ MHz. We typically obtain an overall efficiency of more than 65% for the double transfer process, corresponding to single pass efficiencies of more than 80%, assuming equal efficiencies for both passes. Figure 2.3C shows the double pass efficiency as a function of detuning Δ_2 of laser L_2. Simulations for the three-level system show that the $\sim$800 kHz full width at half maximum of the efficiency curve is compatible with a combination of laser power broadening and Fourier broadening. Our simulations also show that higher transfer efficiencies can be expected for an optimized

STIRAP pulse sequence in which both peak Rabi frequencies are equal. Molecules not transferred by STIRAP are resonantly excited to $|e>$ and then lost from our three-level system by spontaneous emission into a multitude of ground state levels.

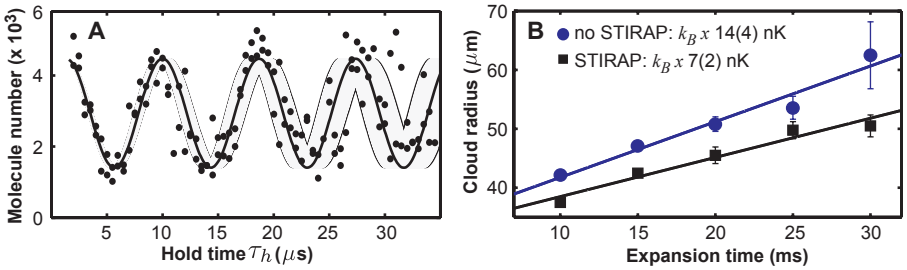

Figure 2.4: **A** Ramsey-type experiment. The population in the initial state $|a>$ oscillates as the hold time τ_h during which both transfer lasers are off is increased. The solid line is a sinussoidal fit to the data up to $\tau_h = 20$ μs. Its frequency f is 115(2) kHz, in good agreement with the expected value of 113 kHz. The thin lines are borders to a region that is given by varying f by ±6 kHz, illustrating the estimated jitter in the two-photon detuning $|\Delta_2 - \Delta_1|$. **B** Comparison of the rate of expansion in the horizontal direction for the molecular sample without and with STIRAP transfer. The top curve (circles) shows the Thomas-Fermi radius r of the molecular sample as a function of expansion time without STIRAP. The linear fit gives a rate of expansion of dr/dt = 1.0(1) mm/s, corresponding to an energy of $k_B \times 14(4)$ nK. The bottom curve (squares) shows the expansion after double STIRAP with dr/dt = 0.7(1) mm/s, corresponding to $k_B \times 7(2)$ nK.

We demonstrate coherence of the transfer process in a Ramsey-type experiment *(14)*, halting the transfer process by simultaneously shutting off both lasers 12 μs into the first STIRAP sequence when a balanced superposition of $|a>$ and $|g>$ has been created with $|\alpha(\tau)|^2 \approx \frac{1}{2} \approx |\beta(\tau)|^2$. After a hold time τ_h we resume the STIRAP transfer, with the roles of lasers L_1 and L_2 reversed. Thus, for $\tau_h = 0$ the population will simply be rotated back into the initial state. A three-level calculation shows that the population in the initial state $|a>$ is expected to oscillate at the rate of the two-photon detuning $|\Delta_2 - \Delta_1|/(2\pi)$. Figure 2.4A shows the initial state population for $\Delta_1 \approx 0$ and $\Delta_2 \approx 2\pi \times 113$ kHz as a function of τ_h. Indeed, the population oscillates with a frequency at $|\Delta_2 - \Delta_1|/(2\pi)$, however with marked increase in phase jitter on the time scale of 30 μs. We attribute this apparent loss of phase coherence to a slow relative frequency drift of lasers L_1 and L_2, leading to a slightly different two-photon detuning from one experimental run to the next. In Figure 2.4A, we have added a region indicating a frequency jitter of ±6 kHz. This value is compatible with the present long-term stability of our lasers. Note that the frequency drift does not affect an individual STIRAP process as the transfer efficiency is very robust against laser detuning as shown in Figure 2.3C.

We now show that the molecular sample is not heated during the transfer process and is indeed in the quantum gas regime. Specifically, we measure and compare the rate of expansion of the molecular sample in state $|a>$ without and with the double

transfer process. In our regime the energy scale for expansion is usually set by the mean field of the BEC, resulting in typical expansion energies for the atoms in the range from $k_B \times 2$ nK to $k_B \times 10$ nK, where k_B is Boltzmann's constant, depending on the strength of the atomic interaction *(24)*. We find that the initial magnetic field ramping excites collective motion of the BEC in the form of a breathing mode as a result of a change in the mean field potential due to a change in atomic interaction strength *(16)*. The breathing is transformed into expansion of the sample when the trap is shut off. We follow the expansion by monitoring the change of the Thomas-Fermi radius r of the sample. Figure 2.4B shows this radius along the horizontal direction as a function of expansion time without and with STIRAP. Without STIRAP, we obtain from a linear fit an expansion rate of $dr/dt = 1.0(1)$ mm/s, corresponding to an energy of $k_B \times 14(4)$ nK. With STIRAP, the rate is $dr/dt = 0.7(1)$ mm/s, corresponding to an energy of $k_B \times 7(2)$ nK. Both values are compatible with a separate measurement of the expansion of the atomic BEC for the same magnetic field ramp. Interestingly, the rate for the case with STIRAP is lower. We speculate that STIRAP with the tightly focused laser beams L_1 and L_2 preferentially transfers molecules in the center of the sample and is hence responsible for some selection in velocity space.

It should now be possible to add a second STIRAP step for transfer into the rovibrational ground state $v = 0, J = 0$. A suitable two-photon transition at readily available laser wavelengths is via the 68th excited state level of the 0_u^+ potential near 1329 nm (up) and 991 nm (down) with comparatively good wave function overlap at the level of $|\Omega/\Omega_a|^2 \approx 10^{-4}$. We expect that searching for dark resonances will be straightforward as now all two-photon transition energies are known to 10^{-3} cm^{-1}. Molecules in $v = 0, J = 0$ cannot further decay into a lower state upon a two-body collision, and they are thus expected to allow the formation of an intrinsically stable molecular BEC. The high speed of our STIRAP transfer will allow us to perform in-situ as well as time-of-flight imaging for direct characterization of the spatial and momentum distribution of the molecular ensemble.

With our technique any low-lying vibrational state can be coherently populated in a controlled fashion with full control over the rotational quantum number, allowing, e.g., state-specific collisional studies and high-precision molecular spectroscopy with possible implications for fundamental physics *(6,7)*. Our procedure can be adapted to other species, in particular to heteronuclear alkali dimers such as RbCs *(25)* and KRb *(15)* for the creation of dipolar quantum gases *(26)*. For heteronuclear alkali dimers a single two-photon transfer step might suffice as a result of favorable wave function overlap *(27)*. We expect that the combination of our technique with Feshbach molecule production out of a Mott-insulator state in a three-dimensional lattice *(28)* will increase the initial Feshbach molecule production efficiency, avoiding collective excitations as a result of magnetic field ramping and inhibiting collisional loss, and will provide full control over all internal and external quantum degrees of freedom of the ground state molecules.

References and Notes

1. C. Chin, T. Kraemer, M. Mark, J. Herbig, P. Waldburger, H.-C. Nägerl, R. Grimm, *Phys. Rev. Lett.* **94**, 123201 (2005).

2. T. Kraemer, M. Mark, P. Waldburger, J. G. Danzl, C. Chin, B. Engeser, A. D. Lange, K. Pilch, A. Jaakkola, H.-C. Nägerl, R. Grimm, *Nature* **440**, 315 (2006).

3. P. Staanum, S. D. Kraft, J. Lange, R. Wester, M. Weidemüller, *Phys. Rev. Lett.* **96**, 023201 (2006).

4. N. Zahzam, T. Vogt, M. Mudrich, D. Comparat, P. Pillet, *Phys. Rev. Lett.* **96**, 023202 (2006).

5. R. V. Krems, *Int. Rev. Phys. Chem.* **24**, 99 (2005).

6. T. Zelevinsky, S. Kotochigova, J. Ye, *Phys. Rev. Lett.* **100**, 043201 (2008).

7. D. DeMille, S. Sainis, J. Sage, T. Bergeman, S. Kotochigova, E. Tiesinga, *Phys. Rev. Lett.* **100**, 043202 (2008).

8. Ultracold Fermi Gases, Proceedings of the International School of Physics "Enrico Fermi", Course CLXIV, edited by M. Inguscio, W. Ketterle, and C. Salomon (IOS Press, Amsterdam, 2008).

9. D. DeMille, *Phys. Rev. Lett.* **88**, 067901 (2002).

10. J. Doyle, B. Friedrich, R. V. Krems, F. Masnou-Seeuws, *Eur. Phys. J. D* **31**, 149 (2004).

11. T. Köhler, K. Góral, P. S. Julienne, *Rev. Mod. Phys.* **78**, 1311 (2006).

12. K. M. Jones, E. Tiesinga, P. D. Lett, P. S. Julienne, *Rev. Mod. Phys.* **78**, 483 (2006).

13. D. Jaksch, V. Venturi, J. I. Cirac, C. J. Williams, P. Zoller, *Phys. Rev. Lett.* **89**, 040402 (2002).

14. K. Winkler, F. Lang, G. Thalhammer, P. v. d. Straten, R. Grimm, J. Hecker Denschlag, *Phys. Rev. Lett.* **98**, 043201 (2007).

15. S. Ospelkaus, A. Pe'er, K.-K. Ni, J. J. Zirbel, B. Neyenhuis, S. Kotochigova, P. S. Julienne, J. Ye, D. S. Jin, arXiv:0802.1093 (2008).

16. T. Weber, J. Herbig, M. Mark, H.-C. Nägerl, R. Grimm, *Science* **299**, 232 (2003).

17. J. Herbig, T. Kraemer, M. Mark, T. Weber, C. Chin, H.-C. Nägerl, R. Grimm, *Science* **301**, 1510 (2003).

18. M. Mark, F. Ferlaino, S. Knoop, J.G. Danzl, T. Kraemer, C. Chin, H.-C. Nägerl, R. Grimm, *Phys. Rev. A* **76**, 042514 (2007).

19. K. Bergmann, H. Theuer, B. W. Shore, *Rev. Mod. Phys.* **70**, 1003 (1998).

20. W. Weickenmeier, U. Diemer, M. Wahl, M. Raab, W. Demtröder, W. Müller, *J. Chem. Phys.* **82**, 5354 (1985).

21. C. Amiot and O. Dulieu, *J. Chem. Phys.* **117**, 5155 (2002).

22. Laser L_1 near 1126 nm and laser L_2 near 1006 nm are continuous-wave grating-stabilized tunable diode lasers with up to 26 mW and 5 mW of power at the sample position, respectively, both focused to a $1/e^2$-waist of about 25 μm for sufficiently high Rabi frequencies. We estimate the laser linewidth for both lasers to be on the order of 1 kHz. The laser beams propagate horizontally at an angle of 80° with the long axis of the BEC with vertical linear polarization. Copropagation assures that the imparted photon recoil during STIRAP is minimal, corresponding to an energy of $k_B \times 0.4$ nK, with Boltzmann's constant k_B. The beam intensity is controlled by acousto-optical modulators, allowing pulse lengths down to 1 μs.

23. The wavemeter calibration is currently not sufficient to allow absolute numbering of the frequency comb teeth.

24. T. Kraemer, J. Herbig, M. Mark, T. Weber, C. Chin, H.-C. Nägerl, R. Grimm, *Appl. Phys. B* **79**, 1013 (2004).

25. J. M. Sage, S. Sainis, T. Bergeman, D. DeMille, *Phys. Rev. Lett.* **94**, 203001 (2005).

26. K. Góral, L. Santos, M. Lewenstein, *Phys. Rev. Lett.* **88**, 170406 (2002).

27. W. C. Stwalley, *Eur. Phys. J. D* **31**, 221 (2004).

28. T. Volz, N. Syassen, D. M. Bauer, E. Hansis, S. Dürr, G. Rempe, *Nature Physics* **2**, 692 (2006).

29. We thank the team of J. Hecker Denschlag, the LevT team in our group, and T. Bergeman for very helpful discussions and M. Prevedelli for technical assistance. We are indebted to R. Grimm for generous support and gratefully acknowledge funding by the Austrian Ministry of Science and Research (BMWF) and the Austrian Science Fund (FWF) in form of a START prize grant and by the European Science Foundation (ESF) in the framework of the EuroQUAM collective research project QuDipMol.

Chapter 3

Publication: Precision molecular spectroscopy for ground state transfer of molecular quantum gases

Faraday Discussion 142 (2009)
Cold and ultracold molecules
pp. 283 - 295
DOI: 10.1039/b820542f

This paper** presents the spectroscopic measurements on the first optical transition of our 4-photon transfer scheme to the rovibronic ground state. Two important conditions have to be met for an intermediate excited state level to be suitable for STIRAP transfer. First, it must provide for adequate coupling both with the initial ground-state level and with the final target level. Preferentially, the two transitions should be of approximately equal strength. Second, unwanted couplings between molecular levels induced by the STIRAP lasers must be avoided. These levels could belong to the 3-level system, as was the case in the first STIRAP transfer with ultracold Rb_2 molecules [Win07b]. Alternatively, coupling could be with additional levels outside the 3-level STIRAP system in either the same or different electronic potentials. The transition strengths in the Cs_2 4-photon scheme are extremely weak, as evidenced by the low normalized Rabi frequencies given in the paper, but sufficient to drive the STIRAP process.

The following points were considered when choosing the intermediate ground and excited state levels for STIRAP to the rovibronic ground state: (1) All four transitions in the 4-photon scheme should be of sufficient and comparable strength. (2) A large detuning of all transitions from the excited state asymptote was chosen in order to decrease the chances of coupling to unwanted molecular levels. The first electronically excited intermediate level is $\sim h \times 2300\ cm^{-1}$ below the potential asymptote. When the second laser is switched on at the beginning of the STIRAP sequence when all the population resides in the initial Feshbach level, it could potentially lead to unwanted coupling between the Feshbach state and a parasitic level in the electronically excited state and hence to rapid loss. By choosing less detuning from the excited state asymptote, where the density of levels is much higher than further down in the potential, the chances of such an accidental loss process would have been higher. (3)

**The author of the present thesis contributed to this paper the same way as in the paper discussed in chapter 2. He assigned the molecular lines to either the 0_u^+ system or the (1) triplet state whereas the vibrational numbering was based on calculations by N. B. and O. D.. Here, the final accepted version of the paper is given.

All laser frequencies were chosen such that they would fall within the spectral range of our femtosecond Erbium-fiber frequency comb (see appendix) used as a reference for the STIRAP lasers. (4) All STIRAP lasers are grating-stabilized diode lasers. For practical reasons, the wavelengths had to be chosen such that laser diodes would be commercially available.

For ground-state transfer, we chose the $(A^1\Sigma_u^+ - b^3\Pi_u)0_u^+$ coupled system [Dul95] as electronically excited states. As a peculiarity in the heavy alkali dimers, such as Rb_2 [Ami99] and most notably Cs_2, the singlet $A^1\Sigma_u^+$ and the triplet $b^3\Pi_u$ states are strongly mixed by spin-orbit coupling. This modifies the Franck-Condon factors and hence optical transition strengths from ground state levels. However, for excitation from Feshbach levels, despite the strong triplet mixing in the excited state, we still rely on a singlet $X^1\Sigma_g^+$ contribution to the Feshbach state due to the presence of the g/u symmetry. This is different for heteronuclear molecules where the g/u symmetry is absent and where excitation to an excited state level of mixed singlet/triplet character can hence take place from the inner turning point of the triplet $a^3\Sigma^+$ component of the Feshbach molecules [Stw04, Ni08].

One interesting aspect of our spectroscopic measurements is that the transition strengths to levels in the electronically excited state depend on the choice of initial Feshbach state. Within the particular Feshbach state that we use as a starting state for STIRAP, the transition strengths also depend on the precise value of the magnetic field that determines whether this state acquires the character of the lowest atomic hyperfine scattering channel or of an excited hyperfine channel.

In addition to the $(A^1\Sigma_u^+ - b^3\Pi_u)0_u^+$ coupled system, the $(1)^3\Sigma_g^+$ state can be excited from Feshbach molecules, in this case from their $a^3\Sigma_u^+$ component. However, for transfer to the rovibronic ground state, this molecular potential would not be suitable because transitions to the $X^1\Sigma_g^+$ ground state are dipole forbidden.

Precision molecular spectroscopy for ground state transfer of molecular quantum gases

Johann G. Danzl,[a] Manfred J. Mark,[a] Elmar Haller,[a] Mattias Gustavsson,[a]
Nadia Bouloufa,[b] Olivier Dulieu,[b] Helmut Ritsch,[c] Russell Hart,[a]
and Hanns-Christoph Nägerl[a]

[a] Institut für Experimentalphysik und Zentrum für Quantenphysik,
Universität Innsbruck,
Technikerstraße 25, A–6020 Innsbruck, Austria.
E-mail: johann.danzl@uibk.ac.at

[b] Laboratoire Aimé Cotton, CNRS, Université Paris-Sud, Bât. 505,
91405 Orsay Cedex, France.

[c] Institut für Theoretische Physik und Zentrum für Quantenphysik,
Universität Innsbruck,
Technikerstraße 25, A–6020 Innsbruck, Austria.

One possibility for the creation of ultracold, high-phase-space-density quantum gases of molecules in the rovibronic ground state relies on first associating weakly-bound molecules from quantum-degenerate atomic gases on a Feshbach resonance and then transfering the molecules via several steps of coherent two-photon stimulated Raman adiabatic passage (STIRAP) into the rovibronic ground state. Here, in ultracold samples of Cs_2 Feshbach molecules produced out of ultracold samples of Cs atoms, we observe several optical transitions to deeply bound rovibrational levels of the excited 0_u^+ molecular potentials with high resolution. At least one of these transitions, although rather weak, allows efficient STIRAP transfer into the deeply bound vibrational level $|v = 73>$ of the singlet $X^1\Sigma_g^+$ ground state potential, as recently demonstrated[1]. From this level, the rovibrational ground state $|v = 0, J = 0>$ can be reached with one more transfer step. In total, our results show that coherent ground state transfer for Cs_2 is possible using a maximum of two successive two-photon STIRAP processes or one single four-photon STIRAP process.

3.1 Introduction

Ultracold and dense molecular samples in specific deeply bound rovibrational levels are of high interest for fundamental studies in physics and chemistry. They are expected to find applications in high resolution spectroscopy and fundamental tests[2,3], few-body collisional physics[4,5], ultracold chemistry[6], quantum processing[7], and in the field of dipolar quantum gases and dipolar Bose-Einstein condensation[8,9]. Ideally, full control over the molecular wave function is desired, i.e. full (quantum) control over the internal and external degrees of freedom of the molecules. High phase space densities are needed for molecular quantum gas studies. For many of the envisaged studies and applications, initial preparation of the molecular sample in the rovibronic ground state, i.e. the lowest energy level of the electronic ground state, is desired. Only in this state one can expect sufficient collisional stability.

But how is it possible to produce dense samples of ultracold molecules in the rovibrational ground state? Laser cooling of atoms, which has lead to the production of quantum degenerate atomic Bose and Fermi gases[10], can so far not be adapted to the case of molecular systems as suitable cycling transitions are not available. Versatile non-optical cooling and slowing techniques such as buffer gas cooling and Stark deceleration in combination with molecule trapping[11,12,13] have been developed, but high molecular densities and in particular high phase space densities are yet to be reached. An alternative route to producing ultracold molecular samples is given by first producing ultracold atomic samples and then associating molecules out of the atomic sample. While this technique is so far limited to the production of selected species of dimer molecules, it has the advantage that ultra-low temperatures and high particle densities are easily inherited from the atomic precursor sample. There are essentially two association techniques, photoassociation[14] and magnetically induced Feshbach association[15,16]. In photoassociation experiments[17,18,19,20], ultracold samples of deeply bound molecules have been created. Additional techniques such as vibrational cooling[19] should allow selective pumping into the rovibrational ground state and open up the prospect for high molecular phase space densities. In Feshbach association experiments[21,22], high-density samples of weakly bound molecules are produced. For dimer molecules composed of Fermions, collisional stability of the highly excited molecules is assured as a result of a Pauli blocking effect, and molecular Bose-Einstein condensation could be achieved in the limit of extremely weak binding[23].

Here, we are interested in combining the techniques of Feshbach association and coherent molecular state transfer to produce quantum gases of molecules in the rovibrational ground state $|v = 0, J = 0>$ of the lowest electronic state. As usual, v and J are the vibrational and rotational quantum numbers, respectively. The molecules, produced on a Feshbach resonance and hence initially very loosely bound, are to be transferred in a few successive steps of coherent two-photon laser transfer to the rovibrational ground state, acquiring more and more binding energy in each step. The general idea is sketched in Fig. 3.1A for the case of Cs_2. Each two-photon step involves an excited state level. Population transfer into this level needs to be avoided

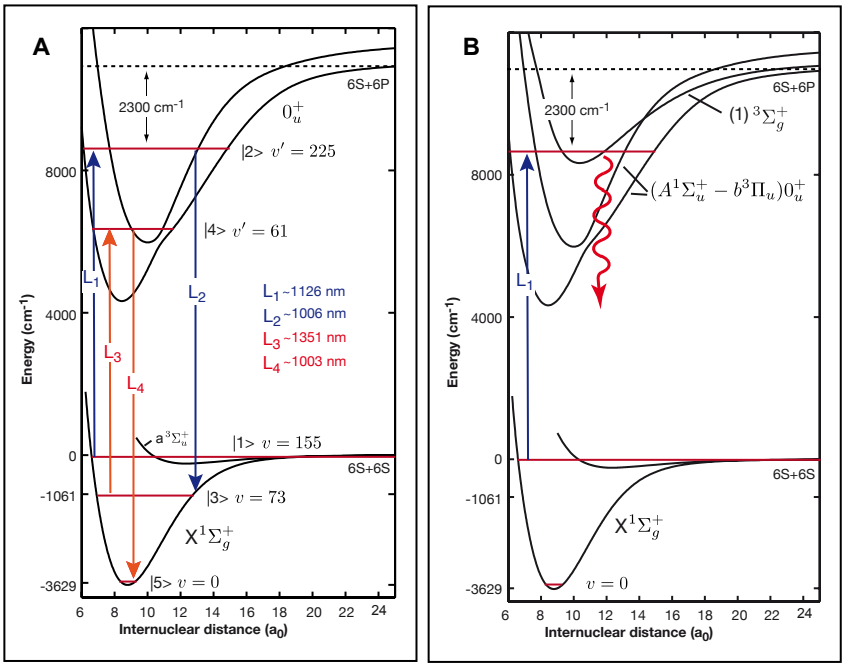

Figure 3.1: (**A**) Simplified molecular level scheme for Cs_2 showing the relevant ground state and excited state potentials involved in rovibrational ground state transfer. Molecules in a weakly bound Feshbach level $|1>= |v \approx 155>$ (not resolved near the $6S_{\frac{1}{2}} + 6S_{\frac{1}{2}}$ two-atom asymptote, but shown in Fig. 3.2) are to be transferred to the rovibrational ground state level $|5>= |v = 0, J = 0>$ of the singlet $X^1\Sigma_g^+$ potential with a binding energy of 3629 cm^{-1} by two sequential two-photon STIRAP processes involving lasers L_1 and L_2 near 1126 nm and 1006 nm and lasers L_3 and L_4 near 1351 nm and 1003 nm. The intermediate ground state level $|3>= |v = 73, J = 2>$ has a binding energy of 1061 cm^{-1}. (**B**) Probing candidate levels for $|2>$ belonging to the electronically excited coupled $(A^1\Sigma_u^+ - b^3\Pi_u)$ 0_u^+ potentials. Here, we search for $|2>$ in loss spectroscopy with laser L_1 in a region near 8890 cm^{-1} above the $6S_{\frac{1}{2}} + 6S_{\frac{1}{2}}$ asymptote, corresponding to an excitation wavelength range of 1118 to 1134 nm. The wiggly arrow indicates loss from the excited levels due to spontaneous emission. Also shown is the excited $(1)^3\Sigma_g^+$ potential, for which we find several levels.

to prevent loss due to spontaneous emission. One possibility is to use the technique of stimulated Raman adiabatic passage (STIRAP)[24], which is very robust and largely insensitive to laser intensity fluctuations. The scheme has several advantages. First, production of Feshbach molecules out of a quantum degenerate atomic sample can be very efficient[25]. Second, the optical transition rate on the first transition starting from the Feshbach molecules is greatly enhanced in comparison to the free atom case. Further, the scheme is fully coherent, not relying on spontaneous processes, allowing high state selectivity, and involving only a comparatively small number of intermediate levels. A ground state binding energy of typically 0.5 eV for an alkali dimer can be removed essentially without heating the molecular sample, as the differential photon

recoil using pairwise co-propagating laser beams driving the two-photon transitions is very small. If losses and off-resonant excitations can be avoided, the scheme essentially preserves phase space density and coherence of the initial particle wave function, allowing the molecular sample to inherit the high initial phase space density from the atomic precursor sample.

Certainly, several challenges have to be met: Going from weakly bound Feshbach to tightly bound ground state molecules corresponds to a large reduction in internuclear distance. Consequently, the radial wave function overlap between successive levels is small, and a compromise has to be found between the number of transitions and the minimum tolerable wave function overlap. To keep the complexity of the scheme low, one or at most two two-photon transitions are desirable. Accordingly, suitable intermediate levels have to be identified that allow a balanced division of wave function overlap, as given by the Franck-Condon factors, between the different transitions. For example, for a four-photon transition scheme with Cs_2 as shown in Fig. 3.1A the Franck-Condon factors are all on the order of 10^{-6}. We emphasize that the identification of the first excited level and hence of the first transition starting from the Feshbach molecules is of crucial importance. Detailed calculations determining the wave function overlap are generally missing, and estimates on the Franck-Condon factors using hypothetical last bound states of either the singlet or triplet potentials of an alkali dimer molecule do not necessarily reflect the transition dipole moments adequately. In addition, for electronic molecular states or energy regions where spectroscopic data is missing, the precise energy of the excited state levels above the atomic threshold is known only with a large uncertainty, which can approach the vibrational spacing of up to a few nanometers. Hence, considerable time has to be spent on searching for weak transitions starting from the initial Feshbach molecules.

In a pioneering experiment, Winkler *et al.*[26] demonstrated that the STIRAP technique can efficiently be implemented with quantum gases of weakly bound Feshbach molecules. In this work, the transferred molecules, in this case Rb_2, were still weakly bound with a binding energy of less than 10^{-4} of the binding energy of the rovibronic ground state, and the intermediate excited state level was close to the excited-atom asymptote. Here, we observe several optical transitions starting from a weakly bound Feshbach level to deeply bound rovibrational levels of the mixed excited $(A^1\Sigma_u^+ - b^3\Pi_u)\ 0_u^+$ molecular potentials of the Cs_2 molecule in a wavelength range from 1118 to 1134 nm, far to the red of the atomic D_1 and D_2 transitions. The Cs_2 molecular potentials are shown in Fig. 3.1A. We observe the levels as loss from an ultracold sample of Cs_2 Feshbach molecules as shown in Fig. 3.1B. We observe two progressions, one that we attribute to the $(A^1\Sigma_u^+ - b^3\Pi_u)\ 0_u^+$ potentials and one that we associate to the triplet $(1)^3\Sigma_g^+$ potential. From the loss measurements, we determine the transition strengths and find that the stronger transitions should be suitable for STIRAP to an intermediate, deeply bound rovibrational level of the singlet $X^1\Sigma_g^+$ potential with $v = 73$. Recently, we could implement STIRAP into $|v = 73, J = 2\rangle$[1]. For the case of the dimer molecule KRb, Ni *et al.*[27] could demonstrate quantum gas transfer all the way into the rovibrational ground state $|v = 0, J = 0\rangle$ of the singlet $X^1\Sigma^+$ molecular potential.

Here, the transfer could be achieved in only a single step as a result of the favorable run of the excited state potentials, which is generally the case for heteronuclear molecules composed of alkali atoms[28]. Also recently, transfer to the rovibrational ground state level of the lowest triplet $a^3\Sigma_u^+$ state of Rb_2 could be achieved[29].

3.2 Preparation of a sample of weakly bound Feshbach molecules

We produce ultracold samples of molecules on two different Feshbach resonances, one near 1.98 mT and one near 4.79 mT[30]. In both cases, essentially following the procedure detailed in Ref. [31], we first produce an ultracold sample of typically 2×10^5 Cs atoms in the lowest hyperfine sublevel $F=3,\ m_F=3$ in a crossed optical dipole trap. As usual, F is the atomic angular momentum quantum number, and m_F its projection on the magnetic field axis. The trapping light at 1064.5 nm is derived from a single-frequency, highly-stable Nd:YAG laser. The offset magnetic field value for evaporative cooling is 2.1 mT. We support optical trapping by magnetic levitation with a magnetic field gradient of 3.1 mT/cm. We then produce weakly bound Feshbach molecules out of the atomic sample[22]. We produce a sample every 8 s, i.e. our spectroscopic measurements are performed at a rate of one data point every 8 s. In order to be able to search for optical transitions over large frequency ranges it is advantageous to work with the shortest possible sample preparation times. For this reason we stop evaporative cooling slightly before the onset of Bose-Einstein condensation (BEC), which also makes sample preparation somewhat less critical. The temperature of the initial atomic sample is then typically about 100 nK. At higher temperatures and hence lower phase space densities the molecule production efficiency is reduced, so that there is a trade off between ease of operation and molecule number. We note that for our ground state transfer experiments reported in Ref. [1] we produce a pure atomic BEC at the expense of longer sample preparation times.

The spectrum of weakly-bound Feshbach levels near the two-free-atom asymptote is shown in Fig. 3.2[30]. For molecule production at the Feshbach resonance at 4.79 mT, we first ramp the magnetic field from the BEC production value to 4.9 mT, about 0.1 mT above the Feshbach resonance. We produce the molecular sample on a downward sweep at a typical sweep rate of 0.025 T/s. The resulting ultracold sample contains up to 11000 molecules, immersed in the bath of the remaining ultracold atoms. The resonance at 4.79 mT is a d-wave resonance[30], and hence the molecules are initially of d-wave character, i.e. $\ell = 2$, where ℓ is the quantum number associated with the mechanical rotation of the nuclei. However, there is a weakly bound s-wave Feshbach state ($|s>=|\ell=0>$) belonging to the open scattering channel right below threshold. This state couples quite strongly to the initial d-wave state, resulting in an avoided state crossing (as shown in the inset to Fig. 3.2), on which the molecules are transferred to the s-wave state $|s>$ upon lowering the magnetic field[30,1]. Upon further lowering the

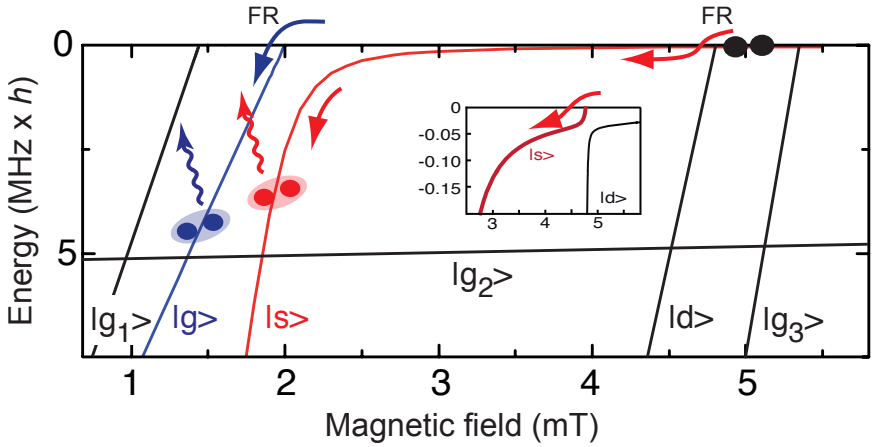

Figure 3.2: Initial Feshbach molecule production: Zeeman diagram showing the energy of weakly bound Feshbach levels[30] and the Feshbach resonances (FR) used in the present work. The binding energy is given with respect to the $F = 3, m_F = 3$ two-atom asymptote. The molecules are produced either on a d-wave Feshbach resonance at 4.79 mT (see inset) and then transferred to the weakly bound s-wave state $|s>$ on an avoided state crossing, or on a g-wave Feshbach resonance at 1.98 mT, resulting in molecules in level $|g>$. In the first case, further lowering of the magnetic offset field to below 2.0 mT changes the character of the $|s>$ level from open-channel to closed-channel dominated[30]. The levels $|s>$ and $|g>$ are both candidate levels for the initial level $|1>$ shown in Fig. 3.1. For completeness, further g-wave Feshbach levels, $|g_1>$, $|g_2>$, and $|g_3>$ are shown. Level $|g_2>$ connects $|g>$ to $|s>$ and can be used for Feshbach state transfer[30]. Level $|g_3>$ is a further interesting candidate level for $|1>$ with low nuclear spin contribution[30].

magnetic field to less than 2.0 mT, the molecules acquire more and more character of a closed channel s-wave state on a second, very broad avoided crossing. Here, we perform spectroscopy in this transition range from open channel to closed channel s-wave character. At a magnetic field value of 2.0 mT, the binding energy of the molecules is near 5 MHz$\times h$ with respect to the $F = 3, m_F = 3$ two-atom asymptote, where h is Planck's constant.

For molecule production at the Feshbach resonance at 1.98 mT, we simply ramp the magnetic field down from the initial BEC production value. Again, we produce an ultracold molecular sample with about 11000 molecules. The molecules in $|g>$ have g-wave character, i.e. $\ell = 4$. When we lower the magnetic field to 1.6 mT, the binding energy of the molecules is also near 5 MHz$\times h$ with respect to the $F = 3, m_F = 3$ two-atom asymptote.

For spectroscopy, we release the molecules from the trap after magnetic field ramping is completed and perform all subsequent experiments in free flight without any other light fields on except for the spectroscopy laser.

For molecule detection in both cases, we reverse the magnetic field ramps[22]. The g-wave molecules are dissociated on the g-wave Feshbach resonance at 1.98 mT, and

the *s*-wave molecules are dissociated on the *d*-wave Feshbach resonance at 4.79 mT. Prior to the reverse magnetic field ramp, we apply a magnetic field gradient of 3.1 mT/cm for about 5 ms to separate the molecular sample from the atomic sample in a Stern-Gerlach-type experiment. Finally, we detect atoms by standard absorption imaging. The minimum number of molecules that we can detect is on the order of 200 molecules.

3.3 Spectroscopy

We perform optical spectroscopy on Feshbach molecules in the wavelength region around 1125 nm. Based on selection rules, there are two sets of electronically excited states that we address in the spectroscopic measurements presented here, namely the $(A^1\Sigma_u^+ - b^3\Pi_u)\ 0_u^+$ coupled state system and the purely triplet $(1)^3\Sigma_g^+$ state. We first discuss transitions to the 0_u^+ coupled state system. Transitions to the latter state are discussed in Sec. 3.3.2.

3.3.1 Transitions to the $(A^1\Sigma_u^+ - b^3\Pi_u)\ 0_u^+$ coupled electronically excited states

For ground state transfer, we are primarily interested in transitions from Feshbach levels to rovibrational levels of the $(A^1\Sigma_u^+ - b^3\Pi_u)\ 0_u^+$ electronically excited states. In the heavy alkali dimers, most notably in Cs_2, the $A^1\Sigma_u^+$ state and the $b^3\Pi_u$ state are strongly coupled by resonant spin-orbit interaction[32,33], yielding the 0_u^+ coupled states in Hund's case (c) notation. The singlet component of the 0_u^+ states allows us to efficiently couple to deeply bound $X^1\Sigma_g^+$ state levels, specifically to the $|v=73, J=2>$ level of the ground state potential, as has recently been shown in a coherent transfer experiment[1]. We have chosen to do spectroscopy in the wavelength range of 1118 nm to 1134 nm above the $6S_{\frac{1}{2}}+6S_{\frac{1}{2}}$ dissociation threshold of the Cs_2 dimer. This corresponds to a detuning of roughly 2300 cm^{-1} from the cesium D_1 line and to an energy range of approximately 12572 cm^{-1} to 12450 cm^{-1} above the rovibronic ground state $X^1\Sigma_g^+\ |v=0, J=0>$. This region was chosen in order to give a balanced distribution of transition strengths in a 4-photon transfer scheme to the rovibronic ground state. In addition, the wavelengths of the four lasers used in the transfer experiments were chosen such that they lie within the wavelength range covered by the infrared fiber-based frequency comb that we use as a frequency reference in the state transfer experiments.

The transitions of interest here lie outside the energy regions for which Fourier transform spectroscopic data was obtained at Laboratoire Aimé Cotton from transitions to the $X^1\Sigma_g^+$ state[34]. The vibrational progression of the 0_u^+ states is highly perturbed by the resonant spin-orbit coupling and exhibits an irregular vibrational spacing. Molecular structure calculations are complicated by the spin-orbit coupling and calculated term values are highly sensitive to the coupling. Prior to the experiments discussed here the absolute energies of the vibrational levels of the $(A^1\Sigma_u^+ - b^3\Pi_u)\ 0_u^+$

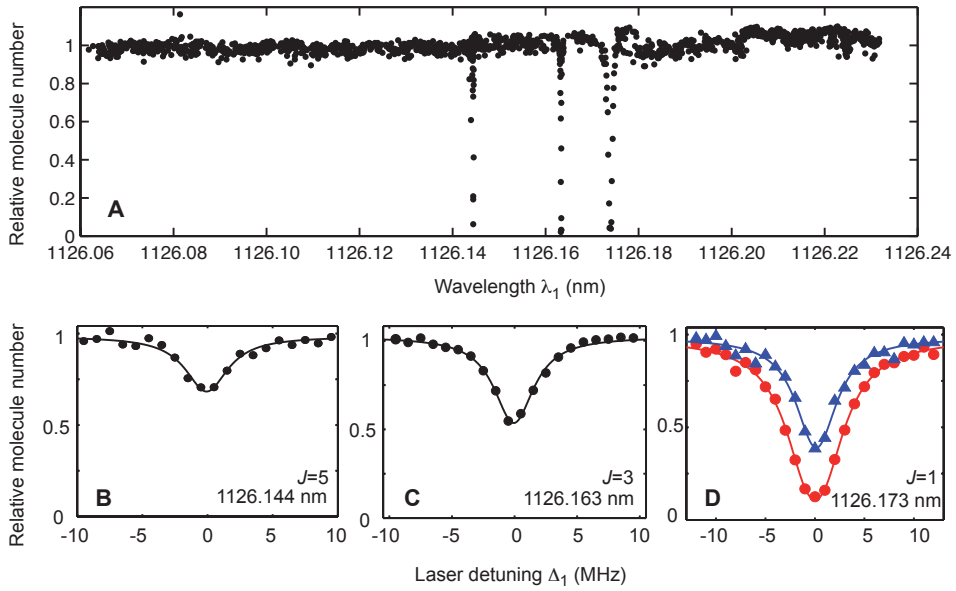

Figure 3.3: Loss resonances for excitation from the initial Feshbach level $|s>$ to the 0_u^+ system. (**A**) Typical scan showing the relative number of molecules in $|s>$ as a function of laser wavelength λ_1 near 1126 nm. Three resonances can be identified, corresponding to $|J=5>$, $|J=3>$, and $|J=1>$, from left to right. The sample is irradiated with laser light at an intensity of 1×10^6 mW/cm^2 for $\tau = 200\ \mu$s. The laser is locked to a narrow band optical resonator that is tuned via a piezoelectric element with a step size of approximately 40 MHz. Wavelength is measured on a home-built wavemeter. The molecule number is normalized to the atom number measured in the same individual realization of the experiment to cancel out fluctuations that stem from shot-to-shot atom number fluctuations and then normalized to unity. (**B**), (**C**), and (**D**) show measurements of the three individual lines with $|J=5>$, $|J=3>$, and $|J=1>$ at reduced intensity in order to avoid saturation. The solid lines represent fits as described in the text. The spectroscopy laser is stabilized to an optical resonator and the resonator is in turn referenced to an optical frequency comb, which allows precise and reproducible tuning of the frequency. The transition to $|J=1>$ in panel (**D**) is recorded at an intensity of 1.5×10^4 mW/cm^2 (circles) and 6×10^3 mW/cm^2 (triangles), (**B**) and (**C**) are recorded at 1×10^6 mW/cm^2 and 2×10^5 mW/cm^2, respectively. The pulse duration is $\tau = 10\ \mu$s.

excited state levels were poorly known in the region of interest from 1118 nm to 1134 nm. We therefore perform a broad range search by irradiating the weakly-bound Feshbach molecules at a fixed wavelength for a certain irradiation time τ of up to $\tau = 6$ ms and by recording the number of remaining molecules as a function of laser frequency. In one run of the experiment one particular laser frequency is queried. We thus take data points at the repetition rate of our experiment, which is given by the sample preparation time of 8 seconds. Based on the available laser intensity from L_1 and an estimate of the dipole transition moments for the strongest expected lines, we chose a frequency

step size of about 100 MHz to 150 MHz for initial line searching. We obtain the laser light at 1118 nm to 1134 nm from a grating-stabilized external cavity diode laser. For coarse frequency scanning, the laser is free running and tuned via a piezoelectric element on the grating of the laser. For more precise measurements, we lock the laser to a narrow-band optical resonator that can be tuned via a piezoelectric element. Fig. 3.3 A shows a typical loss spectrum starting from Feshbach state $|s>$ for excitation near 1126 nm, measured at a magnetic field of 1.98 mT. In this particular case we find three resonances, which we associate with the rotational splitting of the excited state level, $J = 5, 3, 1$, where J is the rotational quantum number. Based on molecular structure calculations we identify this level as the 225th one of the 0_u^+ progression with an uncertainty of about two in the absolute numbering. We zoom in on these three transitions in Fig. 3.3 B, C, and D and record loss resonances at reduced laser intensity in order to avoid saturation of the lines. For these measurements, the laser is locked to the narrow-band optical resonator and the resonator in turn is stabilized to the optical frequency comb to assure reproducibility and long term frequency stability. As one can expect, the loss is strongest on the transition to the $|J = 1>$ level, and it is weakest on the transition to $|J = 5>$. The width of all lines gives an excited state spontaneous decay rate of around $2\pi \times 2$ MHz, in agreement with the typical expected lifetimes of excited molecular levels. The transition to $|J = 1>$ shown in Fig. 3.3 D is of special interest to the current work. It has been used as intermediate excited state level for coherent transfer to $X^1\Sigma_g^+$ $|v = 73, J = 2>$ in our recent experiments[1].

By fitting to a series of such measurements, obtained with different laser intensities, a two level model that takes into account decay from the upper level, we determine the transition strength as given by the normalized Rabi frequency. As a result of optical excitation, for small saturation the number N of Feshbach molecules decays as a function of laser detuning Δ_1 according to $N(\Delta_1) = N_0 \exp(-\tau\Omega_1^2/(\Gamma(1 + 4\pi^2\Delta_1^2/\Gamma^2)))$, where N_0 is the molecule number without laser irradiation and τ is the irradiation time. From the fit we obtain the Rabi frequency on resonance Ω_1 and the excited state spontaneous decay rate Γ. We determine the normalized Rabi frequency to $\Omega_1 = 2\pi \times 2$ kHz $\sqrt{I/(\mathrm{mW/cm^2})}$ for $|J = 1>$, where I is the laser intensity. This value is sufficient to perform STIRAP given the available laser power[1]. The corresponding transition strengths for $|J = 3>$ and $|J = 5>$ are $\Omega_1 = 2\pi \times 0.3$ kHz $\sqrt{I/(\mathrm{mW/cm^2})}$ and $\Omega_1 = 2\pi \times 0.1$ kHz $\sqrt{I/(\mathrm{mW/cm^2})}$, respectively. The absolute values of these transition strengths bear an estimated uncertainty of 20 % because the laser beam parameters for the spectroscopy laser are not well determined.

We also record the time dependence of the molecular loss on some of the stronger lines. For this, we step the laser irradiation time τ from 0 to 150 μs, while laser L_1 is kept on resonance. The result is shown in Fig. 3.4 A for the transition at 1126.173 nm for two different values of the excitation laser intensity.

We note that the transition strength for a particular line starting from Feshbach level $|s>$ strongly depends on the value of the magnetic field, as evidenced in Fig. 3.4 B. Loss resonances for the transition at 1126.173 nm at 1.9 mT and 2.2 mT are shown.

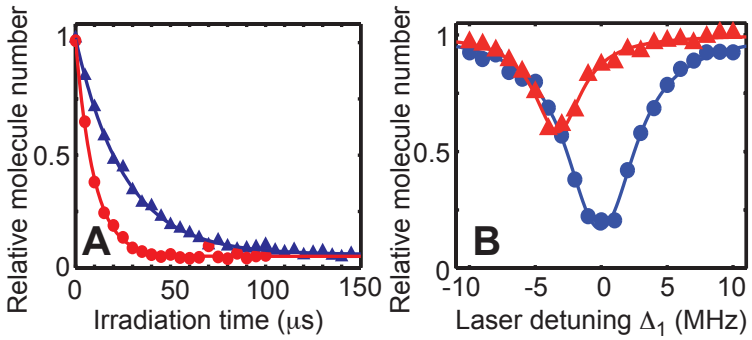

Figure 3.4: Loss of molecules for excitation near 1126.173 nm from Feshbach level $|s>$. (**A**) Time dependence of molecular loss on resonance at 1126.173 nm for two different laser intensities, 5.7×10^5 mW/cm^2 (circles) and 2.1×10^5 mW/cm^2 (triangles). The magnetic offset field is 1.9 mT. The fitted exponential decay gives the decay constants $\tau_d = 9.7\pm0.6\,\mu$s (circles) and $\tau_d = 25.5\pm1\,\mu$s (triangles). (**B**) Loss of molecules in $|s>$ as a function of laser detuning Δ_1 near 1126 nm with an irradiation time of $\tau = 10\,\mu$s for two values of the magnetic field, 1.9 mT (circles) and 2.2 mT (triangles). In both cases, the excited state spontaneous decay rate was determined to $\approx 2\pi\times2$ MHz. At higher magnetic fields, Feshbach level $|s>$ acquires more open-channel character, reducing radial wave function overlap with the excited rovibrational levels. The shift in transition frequency is essentially the result of the change in binding energy as seen in Fig. 3.2.

For ground state transfer[1], we choose a magnetic field of around 1.9 mT, which is somewhat below the magnetic field region where state $|s>$ is strongly curved, but above the avoided state crossing with state $|g_2>$, as seen in Fig. 3.2. The pronounced bending of $|s>$ is the result of a strong avoided crossing between two s-wave Feshbach levels[30]. For magnetic field values beyond 3.0 mT the level $|s>$ can be associated to the $F_1=3, F_2=3$ asymptote, where $F_i, i=1,2$, is the atomic angular momentum quantum number of the i-th atom, respectively. Below 2.0 mT the level $|s>$ can be associated to the $F_1=4, F_2=4$ asymptote. It is hence of closed channel character and much more deeply bound with respect to its potential asymptote, effectively by twice the atomic hyperfine splitting, improving the radial wave function overlap with the excited state levels. This increases the transition strength. Trivially, the resonance frequency is shifted as the binding energy is reduced for larger magnetic field values. Coupling to the excited state level is reduced from $\Omega_1 = 2\pi\times2$ kHz $\sqrt{I/(\mathrm{mW/cm^2})}$ to $\Omega_1 = 2\pi\times1$ kHz $\sqrt{I/(\mathrm{mW/cm^2})}$ when the magnetic field is changed from 1.9 mT to 2.2 mT.

As will be discussed in Sec.3.4 it is advantageous to be able to choose different Feshbach states as a starting state for ground state transfer experiments. Therefore, we probe transitions from Feshbach level $|g>$ to $(A^1\Sigma_u^+ - b^3\Pi_u)\ 0_u^+$ levels. Fig. 3.5 shows loss resonances to the same excited state levels as shown in Fig. 3.3, only that now the initial Feshbach level is $|g>$ instead of $|s>$. In this case, the transition to $|J=3>$ is the strongest, while the transition to $|J=1>$ is very weak, but can be detected.

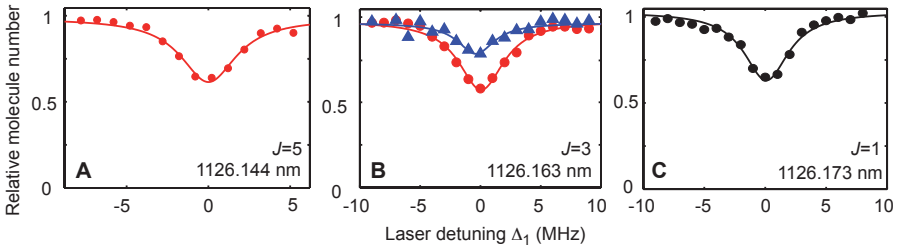

Figure 3.5: Loss resonances for excitation from the initial Feshbach level $|g>$. **(A)**, **(B)**, and **(C)** show the loss for excitation to $|J=5>$, $|J=3>$, and $|J=1>$, corresponding to the resonances shown in Fig. 3.3. The laser intensities are 1.5×10^4 mW/cm^2 for panel **(A)** and for the circles in panel **(B)**. The second resonance in **(B)** (triangles) is measured with 5.6×10^3 mW/cm^2. **(C)** The line at 1126.173 nm is measured at 1×10^6 mW/cm^2. All measurements are done with an irradiation time of $\tau = 10\ \mu$s. From a series of such measurements at different intensities we determine the line strengths for $|J=5>$, $|J=3>$, and $|J=1>$ to $\Omega_1 = 2\pi\times1$ kHz $\sqrt{I/(\mathrm{mW/cm^2})}$, $\Omega_1 = 2\pi\times1$ kHz $\sqrt{I/(\mathrm{mW/cm^2})}$, and $\Omega_1 = 2\pi\times0.1$ kHz $\sqrt{I/(\mathrm{mW/cm^2})}$, respectively.

A comparison of the transition strengths from $|g>$ to the excited state level $|J=3>$, giving $\Omega_1 = 2\pi\times1$ kHz $\sqrt{I/(\mathrm{mW/cm^2})}$ versus $|s>$ to $|J=1>$ giving $\Omega_1 = 2\pi\times2$ kHz $\sqrt{I/(\mathrm{mW/cm^2})}$ shows that level $|g>$ could also be potentially used as a starting level for coherent population transfer to deeply bound levels of the ground state but requires longer STIRAP times in order to assure sufficient adiabaticity[24]. The $|J=3>$ excited state level in turn couples to $|J=2>$ in the ground state, the level used in our previous work[1].

In addition to the transition near 1126 nm we find a series of other excited state levels that we assign to the $(A^1\Sigma_u^+ - b^3\Pi_u)\ 0_u^+$ coupled state system. These are listed in Table 3.1. The assignment to either the $(A^1\Sigma_u^+ - b^3\Pi_u)\ 0_u^+$ system or to the $(1)^3\Sigma_g^+$ electronically excited state discussed below is primarily based on the spacing between neighboring vibrational levels and in addition on the pattern of loss resonances associated with each particular vibrational level. Resonant spin-orbit coupling in the case of the 0_u^+ states leads to an irregular vibrational spacing. In contrast, the $(1)^3\Sigma_g^+$ state is not perturbed by spin-orbit interaction and therefore has a regular vibrational progression. The levels near 1126 nm and near 1123 nm have been used to detect dark resonances with deeply bound levels of the $X^1\Sigma_g^+$ state[1]. The ability to couple to these essentially purely singlet ground state levels unambiguously assigns the corresponding excited state levels to the 0_u^+ system. The data given in Table 3.1 does not represent a fully exhaustive study of the $(A^1\Sigma_u^+ - b^3\Pi_u)\ 0_u^+$ coupled states in the wavelength range of interest. In fact, for the most part we observe those levels of the 0_u^+ system that have a dominant $A^1\Sigma_u^+$ state contribution, as determined from molecular structure calculations.

Table 3.1: Observed excited state levels in the wavelength range from 1118 nm to 1134 nm. Transitions were measured from Feshbach state $|s>$ to the first electronically excited state, addressing both $(A^1\Sigma_u^+ - b^3\Pi_u)0_u^+$ levels and $(1)^3\Sigma_g^+$ levels. Levels are given according to the excitation wavelength (WL) from $|s>$, which essentially corresponds to the $F = 3, m_F = 3$ two-atom asymptote. The data is taken at a magnetic field of 1.98 mT. Wavemeter accuracy is about 0.001 nm. The energy of these levels above the rovibronic ground state $X^1\Sigma_g^+$ $|v = 0, J = 0>$ is given in the second column, where the binding energy of the rovibronic ground state is taken from Ref. [1]. The assignment to either the coupled $(A^1\Sigma_u^+ - b^3\Pi_u)0_u^+$ system or to the $(1)^3\Sigma_g^+$ is based on the vibrational spacing and similarities in the substructure of the levels. The levels marked with $*$ have been used for dark resonance spectroscopy coupling to deeply bound levels of the $X^1\Sigma_g^+$ state[1]. The ability to couple to such levels unambiguously reflects an important singlet component stemming from the $A^1\Sigma_u^+$ state and therefore clearly assigns these levels to the 0_u^+ system. The quantum numbers given for the 0_u^+ levels are coupled channels quantum numbers derived from molecular structure calculations and bear an uncertainty of two in the absolute numbering. The calculations show that these levels have about 70% $A^1\Sigma_u^+$ state contribution. Two further levels observed near 1120.17 nm and 1117.16 nm that belong to the 0_u^+ progression are not given in the table since no further measurements have been done on these levels. The level near 1129.5 nm exhibits a somewhat richer structure than the other levels assigned to 0_u^+ and than exemplified in Fig. 3.3. Levels assigned to the $(1)^3\Sigma_g^+$ state form a regular vibrational progression and show a more complex substructure than the levels attributed to the 0_u^+ system, as exemplified in Fig. 3.6. For these levels, the transition wavelength to one of the most prominent features is given, since an in-depth analysis of the rotational and hyperfine structure remains to be done. The vibrational numbering for the $(1)^3\Sigma_g^+$ levels is the same as in Ref[35].

WL [nm]	Energy above $X^1\Sigma_g^+$ $\|v=0>$ [cm^{-1}]	Assignment
1132.481	12458.875	0_u^+ $\|v' = 221, J = 1>$
1129.492	12482.245	0_u^+
1126.173$*$	12508.332	0_u^+ $\|v' = 225, J = 1>$
1123.104$*$	12532.598	0_u^+ $\|v' = 226, J = 1>$
1133.680	12449.536	$(1)^3\Sigma_g^+$ $\|v' = 32>$
1130.510	12474.274	$(1)^3\Sigma_g^+$ $\|v' = 33>$
1127.379	12498.838	$(1)^3\Sigma_g^+$ $\|v' = 34>$
1124.274	12523.334	$(1)^3\Sigma_g^+$ $\|v' = 35>$
1121.196	12547.756	$(1)^3\Sigma_g^+$ $\|v' = 36>$
1118.155	12572.013	$(1)^3\Sigma_g^+$ $\|v' = 37>$

3.3.2 Transitions to the $(1)^3\Sigma_g^+$ electronically excited state

The Feshbach levels that serve as starting levels for the spectroscopy are of mixed $X^1\Sigma_g^+$ and $a^3\Sigma_u^+$ character. In the wavelength range explored here, excitation to the $(1)^3\Sigma_g^+$ electronically excited triplet state is possible from the $a^3\Sigma_u^+$ component of the Feshbach molecules. In fact, for a heavy molecule as Cs_2, the $(1)^3\Sigma_g^+$ state is better described by the two separate electronic states 0_g^- and 1_g, denoted by Hund's case (c) notation. The $(1)^3\Sigma_g^+$ has been previously studied by Fourier transform spectroscopy[35]. This state is not of prime interest for the present work as transitions from this state down to the $X^1\Sigma_g^+$ ground state are expected to be strongly suppressed, but would be important for STIRAP transfer into the rovibrational ground state level of the shallow triplet $a^3\Sigma_u^+$ potential[29]. Certainly, it is important to be able to distinguish rovibrational levels belonging to the $(1)^3\Sigma_g^+$ state from the ones belonging to the 0_u^+ system, because otherwise time would be wasted in searching for ground state dark resonances that are very weak or even do not exist. Fig. 3.6 A shows a typical loss spectrum for one of the lines that we detected near 1127.37 nm. Due to hyperfine splitting, levels of triplet character exhibit a much richer substructure than the 0_u^+ levels used for ground state transfer. Several components can be identified as a result of rotational and excited state hyperfine splitting. Zoomed-in regions are shown in Fig. 3.6 B, C, D, and E. We have observed a regularly spaced series of optical transitions which we attribute to the $(1)^3\Sigma_g^+$ excited state as listed in Table 3.1. The level energies are well reproduced by the Dunham coefficients determined in Ref. [35]. The vibrational numbering used here is the same as in that work. However, it relies on the absolute energy position of the potential, T_e, which was not determined precisely in Ref. [35]. By fixing T_e to the value given in Ref. [35] we get good agreement with our data.

3.4 Conclusion

We have performed optical spectroscopy starting from weakly bound Cs_2 Feshbach molecules into deeply bound rovibrational levels of the mixed excited state 0_u^+ system and the excited triplet $(1)^3\Sigma_g^+$ state. At least one of the observed transitions, namely the one at 1126.173 nm starting from the Feshbach level $|s>$ to the excited level $|v' = 225, J = 1>$ of the 0_u^+ system, at an offset magnetic field value of 1.9 mT, is strong enough to allow efficient STIRAP transfer into deeply bound rovibrational levels of the singlet $X^1\Sigma_g^+$ ground state potential. The use of this transition for STIRAP has recently been demonstrated in Ref. [1]. In that work, the deeply bound rovibrational level $|v = 73, J = 2>$ of the $X^1\Sigma_g^+$ ground state potential was populated in the molecular quantum gas regime with 80% efficiency. The rovibrational ground state $|v = 0, J = 0>$ of the $X^1\Sigma_g^+$ ground state potential can thus be reached from the atomic threshold with a maximum of two two-photon STIRAP transfers. Dark resonances connecting $|v = 73, J = 2>$ to $|v = 0, J = 0>$ have recently been observed[36], and two-step STIRAP into $|v = 0, J = 0>$ has recently been implemented[37]. For future experiments, the use of

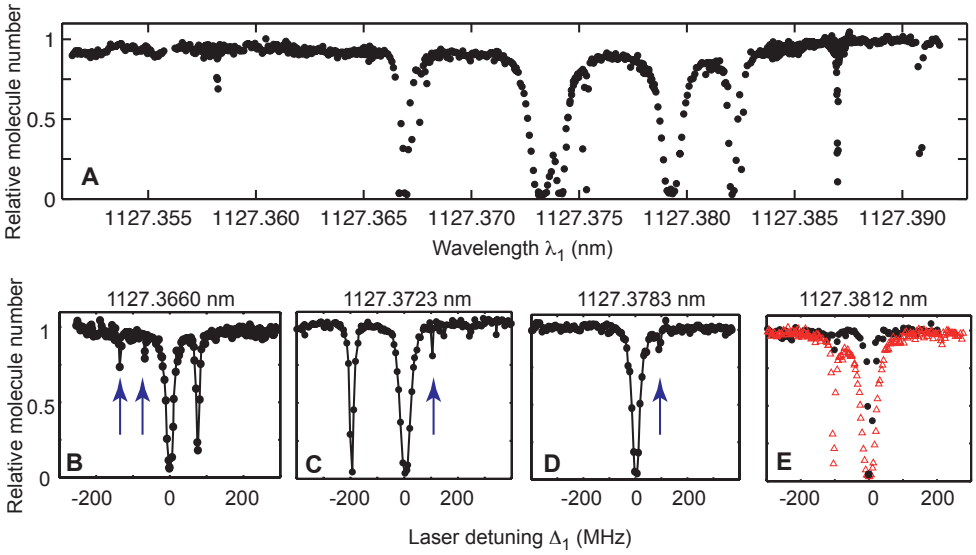

Figure 3.6: Loss of molecules for excitation near 1127.17 nm from Feshbach level $|s>$ to the triplet $(1)^3\Sigma_g^+$ state. (**A**) represents a broad scan with laser irradiation at an intensity of 5×10^5 mW/cm^2 for $\tau = 100\ \mu$s at a step size of 20 MHz. A rich structure due to rotation and excited state hyperfine splitting can be seen which is qualitatively different from the spectrum shown in Fig. 3.3. The lines are greatly broadened by the high intensity and long irradiation time. The spectroscopy laser is locked to a narrow band optical resonator that is stepped via a piezoelectric element. Scans of about 750 MHz were recorded as a function of piezo voltage on the resonator. Voltage was converted to wavelength for each scan by a linear interpolation. (**B**)-(**E**) represent scans over some of the observed features at a reduced intensity of 8×10^4 mW/cm^2 and an irradiation time of $\tau = 10\ \mu$s in order to reduce broadening of the lines. The step size is about 7 MHz. Resonator piezo voltage is converted to frequency with an estimated error of 10 %. The absolute wavelength accuracy is limited by wavemeter calibration to 0.001 nm, the relative accuracy is about a factor of 10 better. The vertical arrows indicate weak lines that have been verified in additional scans with higher power. In panel (**E**) the power was somewhat increased for an additional measurement (triangles) that emphasizes such a weak line.

Feshbach level $|g>$ as the initial state might be advantageous. Level $|g>$ can be more easily populated, as the Feshbach resonance connected to this level is at a low magnetic field value of 1.98 mT[30], where the atomic background scattering length has a moderate value of 155 a_0, where a_0 is Bohr's radius. The use of this resonance avoids excitation of collective motion of the atomic BEC as a result of a large mean field interaction near the Feshbach resonance at 4.79 mT[1], where the atomic background scattering length is about 935 a_0. The transition starting from level $|g>$ appears to be strong enough to allow STIRAP, this time via the excited state level $|v' = 225, J = 3>$ of the 0_u^+ system. An attractive strategy for the production of a BEC of ground state molecules relies on the addition of a three-dimensional optical lattice. Starting from the atomic

BEC, pairs of atoms at individual lattice sites can be produced in a superfluid-to-Mott-insulator transition[38] with high efficiencies of almost 50%[39]. These pairs can then be very efficiently associated on a Feshbach resonance[40] and subsequently transferred to the rovibronic ground state with STIRAP. The lattice has the advantage of shielding the molecules against inelastic collisions during the association process and subsequent state transfer. In particular, it should allow long STIRAP pulse durations, allowing us to resolve the weak hyperfine structure of ground state molecules[41]. As proposed by Jaksch *et al.*[42], dynamical melting of the Mott-insulator state should ideally result in the formation of a BEC of molecules in the rovibronic ground state in a Mott-insulator-to-superfluid-type transition.

Acknowledgements

We are indebted to R. Grimm for generous support and we thank T. Bergeman, H. Salami, J. Hutson, J. Aldegunde, and E. Tiemann for valuable discussions. We gratefully acknowledge funding by the Austrian Ministry of Science and Research (BMWF) and the Austrian Science Fund (FWF) in form of a START prize grant and by the European Science Foundation (ESF) in the framework of the EuroQUAM collective research project QuDipMol. R.H. acknowledges support by the European Union in form of a Marie-Curie International Incoming Fellowship (IIF).

References

1. J. G. Danzl, E. Haller, M. Gustavsson, M. J. Mark, R. Hart, N. Bouloufa, O. Dulieu, H. Ritsch, and H.-C. Nägerl, *Science*, 2008, **321**, 1062, published online 10 July 2008; 10.1126/science.1159909.

2. T. Zelevinsky, S. Kotochigova, and J. Ye, *Phys. Rev. Lett.*, 2008, **100**, 043201.

3. D. DeMille, S. Sainis, J. Sage, T. Bergeman, S. Kotochigova, and E. Tiesinga, *Phys. Rev. Lett.*, 2008, **100**, 043202.

4. P. Staanum, S. D. Kraft, J. Lange, R. Wester, and M. Weidemüller, *Phys. Rev. Lett.*, 2006, **96**, 023201.

5. N. Zahzam, T. Vogt, M. Mudrich, D. Comparat, and P. Pillet, *Phys. Rev. Lett.*, 2006, **96**, 023202.

6. R. V. Krems, *Int. Rev. Phys. Chem.*, 2005, **24**, 99.

7. D. DeMille, *Phys. Rev. Lett.*, 2002, **88**, 067901.

8. K. Góral, L. Santos, and M. Lewenstein, *Phys. Rev. Lett.*, 2002, **88**, 170406.

9. M. Baranov, L. Dobrek, K. Góral, L. Santos, and M. Lewenstein, *Phys. Scr.*, 2002, **T102**, 74.

10. K. Southwell (ed.), Ultracold matter, *Nature (Insight)*, 2002, **416**, 205.

11. J. Doyle, B. Friedrich, R.V. Krems, and F. Masnou-Seeuws, *Eur. Phys. J. D*, 2004, **31**, 149.

12. R. V. Krems, *Phys. Chem. Chem. Phys.*, 2008, **10**, 4079.

13. S. Y. T. van de Meerakker, H. L. Bethlem, and G. Meijer, *Nature Phys.*, 2008, **4**, 595.

14. For a review on photoassociation, see: K. M. Jones, E. Tiesinga, P. D. Lett, and P. S. Julienne, *Rev. Mod. Phys.*, 2006 **78**, 483.

15. T. Köhler, K. Góral, and P. S. Julienne, *Rev. Mod. Phys.*, 2006, **78**, 1311.

16. F. Ferlaino, S. Knoop, and R. Grimm, in: Cold Molecules: Theory, Experiment, Applications, edt. by R. V. Krems, B. Friedrich, and W. C. Stwalley (publication expected in March 2009), preprint at arXiv:0809.3920.

17. A. N. Nikolov, J. R. Ensher, E. E. Eyler, H. Wang, W. C. Stwalley, and P. L. Gould, *Phys. Rev. Lett.*, 2000, **84**, 246.

18. J. M. Sage, S. Sainis, T. Bergeman, and D. DeMille, *Phys. Rev. Lett.*, 2005, **94**, 203001.

19. M. Viteau, A. Chotia, M. Allegrini, N. Bouloufa, O. Dulieu, D. Comparat, and P. Pillet, *Science*, 2008, **321**, 232.

20. J. Deiglmayr, A. Grochola, M. Repp, K. Mörtlbauer, C. Glück, J. Lange, O. Dulieu, R. Wester, and M. Weidemüller, *Phys. Rev. Lett.*, 2008, **101**, 133004.

21. C. A. Regal, C. Ticknor, J. L. Bohn, and D. S. Jin, *Nature*, 2003, **424**, 47.

22. J. Herbig, T. Kraemer, M. Mark, T. Weber, C. Chin, H.-C. Nägerl, and R. Grimm, *Science*, 2003, **301**, 1510, published online 21 August 2003; 10.1126/science.1088876.

23. For an overview, see: Ultracold Fermi Gases, *Proceedings of the International School of Physics Enrico Fermi, Course CLXIV*, edited by M. Inguscio, W. Ketterle, and C. Salomon (IOS Press, Amsterdam, 2008).

24. K. Bergmann, H. Theuer and B. W. Shore, *Rev. Mod. Phys.*, 1998, **70**, 1003.

25. M. Mark, T. Kraemer, J. Herbig, C. Chin, H.-C. Nägerl, and R. Grimm, *Europhys. Lett.*, 2005, **69**, 706.

26. K. Winkler, F. Lang, G. Thalhammer, P. v. d. Straten, R. Grimm, and J. Hecker Denschlag, *Phys. Rev. Lett.*, 2007, **98**, 043201.

27. K.-K. Ni, S. Ospelkaus, M. H. G. de Miranda, A. Pe'er, B. Neyenhuis, J. J. Zirbel, S. Kotochigova, P. S. Julienne, D. S. Jin, and J. Ye, published online September 18, 2008, *Science* DOI: 10.1126/science.1163861.

28. W. C. Stwalley, *Eur. Phys. J. D*, 2004, **31**, 221.

29. F. Lang, K. Winkler, C. Strauss, R. Grimm, and J. Hecker Denschlag, Phys. Rev. Lett., 2008, **101**, 133005.

30. M. Mark, F. Ferlaino, S. Knoop, J. G. Danzl, T. Kraemer, C. Chin, H.-C. Nägerl, and R. Grimm, *Phys. Rev. A*, 2007, **76**, 042514.

31. T. Weber, J. Herbig, M. Mark, H.-C. Nägerl, and R. Grimm, *Science*, 2003, **299**, 232.

32. O. Dulieu and P. Julienne, *J. Chem. Phys.*, 1995, **103**, 60.

33. C. Amiot, O. Dulieu, and J. Vergès, *Phys. Rev. Lett.*, 1999, **83**, 2316.

34. H. Salami, T. Bergeman, O. Dulieu, D. Li, F. Xie, and L. Li, manuscript in preparation (2008).

35. C. Amiot and J. Vergès, *Chem. Phys. Lett.*, 1985, **116**, 273.

36. M. J. Mark, J. G. Danzl, E. Haller, M. Gustavsson, N. Bouloufa, O. Dulieu, H. Salami, T. Bergeman, H. Ritsch, R. Hart, and H.-C. Nägerl, manuscript submitted for publication, 2008, preprint at arXiv:0811.0695.

37. J. G. Danzl, M. J. Mark, E. Haller, M. Gustavsson, N. Bouloufa, O. Dulieu, H. Salami, T. Bergeman, H. Ritsch, R. Hart, H.-C. Nägerl, manuscript in preparation.

38. M. Greiner, O. Mandel, T. Esslinger, T. W. Hänsch, and I. Bloch, *Nature*, 2002, **415**, 39.

39. S. Dürr, 2008, private communication.

40. G. Thalhammer, K. Winkler, F. Lang, S. Schmid, R. Grimm, and J. Hecker Denschlag, *Phys. Rev. Lett.*, 2006, **96**, 050402.

41. J. Aldegunde and J. M. Hutson, 2008, preprint at arXiv:0810.4709.

42. D. Jaksch, V. Venturi, J. I. Cirac, C. J. Williams, and P. Zoller, *Phys. Rev. Lett.*, 2002, **89**, 040402.

Chapter 4

Publication: Dark resonances for ground state transfer of molecular quantum gases

Applied Physics B
Published online 19 February 2009
Vol. 95, no. 2, pp. 219-225
DOI: 10.1007/s00340-009-3407-1

In this paper** we discuss the high-resolution molecular spectroscopy that forms the basis for the transfer of the molecular population from the intermediate ground state level $|v=73, J=2>$ reached in Ref. [Dan08] to the rovibronic ground state $X^1\Sigma_g^+$ $|v=0, J=0>$. Similar to the first STIRAP step of the 4-photon transfer scheme, a rovibrational level of the $(A^1\Sigma_u^+ - b^3\Pi_u)0_u^+$ coupled system is chosen as an intermediate excited state level in the transfer. Interestingly, the particular level that was chosen for the transfer has a very strong contribution from the $b^3\Pi_u$ triplet state even though the two involved ground-state levels are of pure singlet character. Levels of predominant $b^3\Pi_u$ character provide more favorable Franck-Condon factors in this region of the potential than levels of predominantly $A^1\Sigma_u^+$ character. These latter levels would give excellent coupling for the fourth STIRAP transition but almost vanishing transition strength for the third transition of the 4-photon scheme.

In addition, the dark state spectroscopy on the fourth transition of the 4-photon scheme is presented in this paper. Identification of the rovibronic ground state was straight forward because the energy difference between the intermediate ground state level $|v=73, J=2>$ and the rovibronic ground state $|v=0, J=0>$ was precisely known from Fourier transform spectroscopy [Wei85, Ami02].

**The author of the present thesis planned the experiments and performed all spectroscopic measurements with support from M. J. M., E. H., M. G. and R. H.. M. J. M. and E. H. made important contributions by maintaining and improving the BEC machine. The author analyzed the data and together with N. B., O. D., H. S., and T. B. assigned the molecular transitions. The paper was written by J. G. D. and H.-C. N. with input from all authors. This is the final accepted version of the paper.

Dark resonances for ground state transfer of molecular quantum gases

Manfred J. Mark[1], Johann G. Danzl[1]*, Elmar Haller[1], Mattias Gustavsson[1], Nadia Bouloufa[2], Olivier Dulieu[2], Houssam Salami[3], Tom Bergeman[3], Helmut Ritsch[4], Russell Hart[1] & Hanns-Christoph Nägerl[1]

[1]Institut für Experimentalphysik und Zentrum für Quantenphysik, Universität Innsbruck, Technikerstraße 25, A–6020 Innsbruck, Austria

[2]Laboratoire Aimé Cotton, CNRS, Université Paris-Sud, Bât. 505, 91405 Orsay Cedex, France

[3]Department of Physics and Astronomy, SUNY Stony Brook, NY 11794-3800, USA

[4]Institut für Theoretische Physik und Zentrum für Quantenphysik, Universität Innsbruck, Technikerstraße 25, A–6020 Innsbruck, Austria

*e-mail: johann.danzl@uibk.ac.at

One possible way to produce ultracold, high-phase-space-density quantum gases of molecules in the rovibronic ground state is given by molecule association from quantum-degenerate atomic gases on a Feshbach resonance and subsequent coherent optical multi-photon transfer into the rovibronic ground state. In ultracold samples of Cs_2 molecules, we observe two-photon dark resonances that connect the intermediate rovibrational level $|v = 73, J = 2>$ with the rovibrational ground state $|v = 0, J = 0>$ of the singlet $X^1\Sigma_g^+$ ground state potential. For precise dark resonance spectroscopy we exploit the fact that it is possible to efficiently populate the level $|v = 73, J = 2>$ by two-photon transfer from the dissociation threshold with the stimulated Raman adiabatic passage (STIRAP) technique. We find that at least one of the two-photon resonances is sufficiently strong to allow future implementation of coherent STIRAP transfer of a molecular quantum gas to the rovibrational ground state $|v = 0, J = 0>$.

4.1 Introduction

Laser cooling of atoms and the production of quantum degenerate atomic Bose and Fermi gases have revolutionized the field of atomic physics [1]. For molecular systems, ultralow temperatures and high phase space densities are much more difficult to achieve. Laser cooling of molecules has not yet been demonstrated, and with alternative cooling and slowing techniques such as buffer gas cooling and Stark deceleration high phase space densities are yet out of reach [2,3,4]. In photoassociation experiments from magneto-optical traps, [5,6,7,8,9], cold samples of deeply bound molecules in the lowest vibrational levels have been created. Yet, the phase space densities are far away from the quantum degenerate regime. In the limit of extremely weak binding, molecular Bose-Einstein condensation has been achieved [10] by using the trick of first cooling an atomic Fermi gas to high phase space densities and subsequently associating pairs of atoms to molecules. For molecules composed of fermions, collisional stability of the highly excited molecules is assured as a result of a Pauli blocking effect. Here, we are interested in ultracold and dense molecular systems in specific deeply bound rovibrational levels. Such samples are of high interest for fundamental studies in physics and chemistry, ranging from ultracold chemistry [11] and few-body collisional physics [12,13] to high resolution spectroscopy [14,15], to applications in quantum processing [16], and to the formation of dipolar quantum gases and dipolar Bose-Einstein condensates [17,18]. For these experiments full control over the molecular wave function is desired. In addition, high densities are required for molecular quantum gas studies. Only in the rovibronic ground state, i.e. the lowest energy level of the electronic ground state, is collisional stability assured.

For the production of molecular quantum gases in the absolute ground state, we follow a scheme in which the technique of stimulated two-photon transfer is repeatedly applied to molecules associated on a Feshbach resonance from a high-density sample of ultracold atoms such as a Bose-Einstein condensate (BEC). The initially very loosely bound molecules are to be transferred in a few successive steps to the rovibrational ground state, acquiring more and more binding energy. The scheme has several advantages. It is fully coherent, not relying on spontaneous processes, allowing high state selectivity, and it involves only a comparatively small number of intermediate levels. The scheme is expected to allow the removal of a ground state binding energy of typically 0.5 eV for an alkali dimer without appreciably heating the molecular sample. It essentially preserves phase space density and coherence of the particle wave function, allowing the molecular sample to inherit the high initial phase space density from the atomic sample. Ideally, the scheme will ultimately result in the formation of a molecular BEC. A major challenge is given by the low radial wave function overlap between successive molecular levels, potentially leading to prohibitively low transition rates for the two-photon transitions that could only be compensated by the use of further (smaller) transfer steps.

In a crucial experiment, Winkler *et al.* [19] demonstrated that coherent two-photon transfer by means of the stimulated Raman adiabatic passage (STIRAP) technique [20]

can efficiently be implemented with quantum gases of weakly bound Feshbach molecules. In this work, the transferred molecules, in this case Rb_2, were still weakly bound with a binding energy of much less than 10^{-4} of the binding energy of the rovibrational ground state. In particular, wave function overlap of the final level with the rovibrational ground state is negligible. Nevertheless, an important result of this experiment was the demonstration that, even with excitation near the excited S+P asymptote, parasitic excitation of unwanted molecular transitions by the STIRAP laser beams can largely be avoided. Recently, Danzl *et al.* [21] showed efficient coherent STIRAP transfer into deeply bound rovibrational levels in the quantum gas regime. More specifically, transfer into the rovibrational level $|v = 73, J = 2>$ of the singlet $X^1\Sigma_g^+$ molecular potential of the Cs dimer was demonstrated. This level is bound by 1061 wavenumbers, more than one-fourth of the binding energy of the rovibrational ground state. Here, as usual, v and J denote the vibrational and rotational quantum numbers, respectively. This intermediate level was chosen as to give a balanced distribution for the wave function overlap in a four-photon transfer scheme to the ground state, i.e. to assure that all four dipole transition moments are of comparable magnitude. This level can thus serve as a transfer state towards the rovibrational ground state $|v = 0, J = 0>$, allowing coherent ground state transfer with two two-photon transitions. Also recently, Ni *et al.* [22] have demonstrated transfer all the way into the rovibrational ground state $|v = 0, J = 0>$ of the singlet $X^1\Sigma^+$ molecular potential in a quantum gas of KRb molecules. The transfer could be achieved in a single step as a result of the favorable run of the excited state potentials in the case of heteronuclear alkali dimers [23]. Also, the lowest rovibrational level of the Rb_2 triplet $a^3\Sigma_u^+$ potential has recently been populated in the quantum gas regime using the STIRAP technique [24].

Here, in an ultracold and dense sample of Cs molecules, we present two-photon dark resonances connecting the rovibrational level $|v = 73, J = 2>$ of the Cs dimer singlet $X^1\Sigma_g^+$ molecular potential with the rovibrational ground state $|v = 0, J = 0>$. Starting from $|v = 73, J = 2>$, we first perform molecular loss spectroscopy by laser excitation in the wavelength range from 1329 nm to 1365 nm. We searched for suitable rovibrational levels of the $A^1\Sigma_u^+(0_u^+)$ and $b^3\Pi_u(0_u^+)$ excited electronic states which are mixed due to spin-orbit coupling. Hereafter, these states will be referred to as the $(A - b)\, 0_u^+$ system. These levels are 9893 to 10091 wavenumbers above the rovibronic ground state, corresponding to a wavelength range from 1011 nm to 991 nm for the transition to the rovibronic ground state. We then perform dark state spectroscopy by simultaneous laser irradiation near 1350 nm and 1000 nm. We find several dark resonances, from which we derive normalized transition strengths and find that at least one of the two-photon transitions is favorable for ground state transfer.

4.2 Molecular energy levels and laser transitions

Fig.4.1 shows the energy of the relevant Cs_2 molecular states and the optical transitions for our transfer scheme. State |1> is the initial weakly bound Feshbach state that

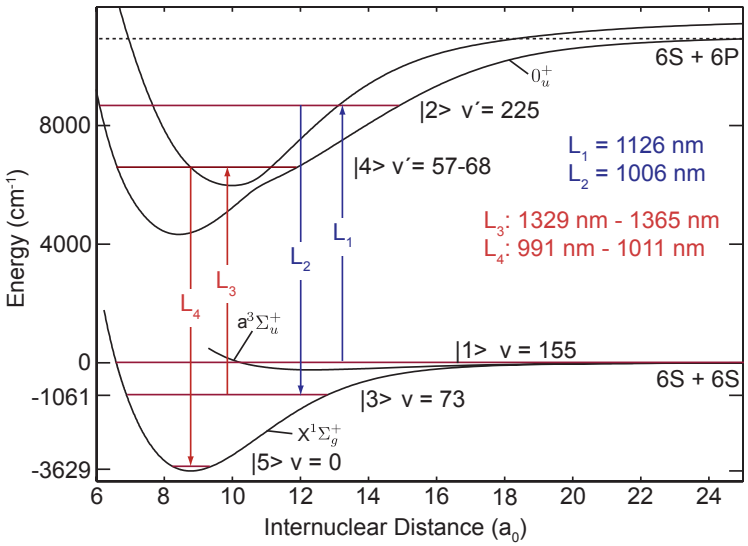

Figure 4.1: Molecular level scheme for Cs_2. Molecules in a weakly bound Feshbach level |1>= $|v \approx 155>$ (not resolved near the 6S+6S asymptote) are transferred to the rovibrational level |3>= $|v = 73, J = 2>$ of the singlet $X^1\Sigma_g^+$ ground state potential with a binding energy of 1061 cm^{-1} by a two-photon STIRAP process [21] involving lasers L_1 and L_2 near 1126 nm and 1006 nm. The following two-photon transition from |3> to |5>= $|v = 0, J = 0>$ and also to $|v = 0, J = 2>$ is then probed by lasers L_3 and L_4 near 1350 nm and 1000 nm, respectively. Level |2> is the 225th level of the electronically excited $(A - b)\ 0_u^+$ system. Here, we probe suitable candidate levels for |4>, connecting |3> to |5>. These candidate levels also belong to the $(A - b)\ 0_u^+$ system and include levels with coupled channels vibrational numbers $v' = 57$ to 68. The position of the vertical arrows is not meant to reflect the internuclear distance at which the transition takes place.

we populate out of an atomic BEC of Cs atoms via Feshbach association [25]. For the transfer from |1> to the ro-vibrational ground state |5>= $|v = 0, J = 0>$, three intermediate levels |2>, |3>, and |4> are needed. All five molecular levels are coupled by two two-photon transitions in a distorted M-shaped configuration as shown in Fig.4.2. Levels |2> and |4> belong to the $(A - b)\ 0_u^+$ system. We have identified level |2> as the 225th one of the $(A - b)\ 0_u^+$ system, with an uncertainty of 2 in the absolute numbering, and |3> is the level with $v = 73$ and $J = 2$ of the $X^1\Sigma_g^+$ ground state potential [21]. A two-photon laser transition with laser L_1 at 1126 nm and laser L_2 at 1006 nm couples |1> to |3> via |2>. There are now several possibilities for coupling |3> to |5>, differing in the choice of the excited level |4>. The aim of this work is to identify a suitable level |4> from the $(A - b)\ 0_u^+$ system with sufficient wave function overlap with both |3> and |5>. We search for level |4> in the energy range of 9893 to 10091 cm^{-1} above the rovibrational ground state |5>. Molecular structure calculations as outlined in Sec. 4.4 show that in this range there are candidate states for |4> that have dipole transition matrix elements with both |3> and |5> of comparable magnitude, allowing optimum

STIRAP performance. The wavelengths for the lasers L_3 and L_4 driving the associated two-photon transition are near 1350 nm and 1000 nm, respectively. We derive all laser light for driving the molecular transitions from highly stable, widely tunable diode laser systems with kHz linewidths. For short term stability, the lasers are all locked to narrow-band optical resonators. For long term stability, the optical resonators are referenced to an infrared, fiber-laser-based frequency comb, covering the wavelength range from about 980 nm to about 2000 nm.

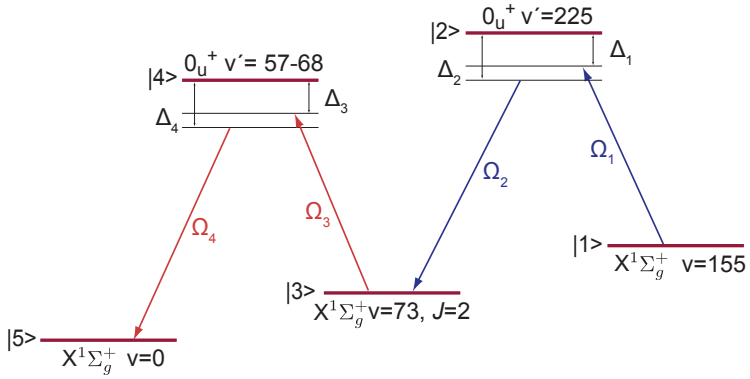

Figure 4.2: 5-level distorted M-scheme. The one-photon-detunings and Rabi frequencies of L_i are Δ_i and Ω_i, $i = 1,2,3,4$. For STIRAP to $|v = 73, J = 2>$ the detunings for L_1 and L_2 are $\Delta_1 \approx 0 \approx \Delta_2$.

4.3 Preparation of a molecular quantum gas in $|v = 73, J = 2>$

Our sample preparation procedure follows Ref. [21]. In summary, we first produce a cigar-shaped BEC of typically 1.5×10^5 cesium atoms in the lowest hyperfine sublevel $F = 3$, $m_F = 3$ in a crossed optical dipole trap. As usual, F is the atomic angular momentum quantum number, and m_F its projection. The trapping light at 1064.5 nm is derived from a single-frequency, highly-stable Nd:YAG laser. Using a d-wave Feshbach resonance at 4.8 mT [26] we then produce a quantum gas of weakly bound Feshbach molecules out of the BEC [25]. For this, we first ramp the magnetic field from the BEC production value of 2.0 mT to 4.9 mT, slightly above the Feshbach resonance. The molecules are produced on a downward sweep at a typical sweep rate of 0.025 mT/ms. The resulting ultracold sample contains up to 11000 molecules, immersed in the bath of the remaining BEC atoms. For the present experiments we shut off the trap and perform all subsequent measurements in free flight. This reduces the particle

density, in particular during the later detection stage of the experiment, and hence reduces atom-molecule collisional loss, thus increasing the molecular signal. Following two avoided state crossings while further sweeping the magnetic field to lower values, we transfer the molecules via a weakly bound, open channel *s*-wave molecular state into the still weakly bound, closed channel *s*-wave molecular state |1> by magnetic field ramping [21]. This is the starting state for the subsequent optical transfer. As with all other weakly bound Feshbach states, it belongs to both the $X^1\Sigma_g^+$ ground state potential and the lowest triplet $a^3\Sigma_u^+$ potential and is hence of mixed character. It has zero rotational angular momentum. At a field of 1.9 mT, it has a binding energy of 5 MHz×h, where h is Planck's constant, with respect to the $F = 3, m_F = 3$ two-atom asymptote [26]. We detect molecules in |1> by reverse magnetic field ramping, leading to dissociation on the Feshbach resonance at 4.8 mT, and subsequent imaging of the resulting atoms [25].

We transfer the molecules from |1> to the rovibrational level |3>= $|v = 73, J = 2>$ with the STIRAP technique [21]. For this, about 3 ms after molecule production, with the magnetic field ramping completed, laser L_2 at 1006 nm is pulsed on first and then laser L_1 at 1126 nm. Both lasers are on resonance within a few kHz. The pulse overlap time is about 10 μs. With peak Rabi frequencies of $\Omega_1 \approx 2\pi\times 3$ MHz and $\Omega_2 \approx 2\pi\times 6$ MHz we transfer about 80 % of the molecules to |3 >. We find that the molecular sample is not heated as a result of the STIRAP transfer. A residual kinetic energy on the order of $k_B \times 10$ nK comes from the expansion energy of the initial atomic sample. Our current procedure allows us to produce a sample of up to 8000 molecules in state |3> every 12 s. For the loss spectroscopy as detailed below, we irradiate the molecules in |3> with light near 1350 nm for a certain waiting time. We then measure the fraction of molecules that have remained in |3>. For this, we transfer the remaining molecules back to |1> using the reverse STIRAP process and determine the number of molecules in |1>. Without irradiation with light near 1350 nm we transfer more than 65% of the molecules from |1> to |3> and back to |1> [21].

4.4 Loss spectroscopy

In the heavy alkali dimers, most notably Cs_2, the $A^1\Sigma_u^+$ and $b^3\Pi_{0u}$ states are strongly mixed by spin-orbit coupling even in the lowest levels of the A state, leading to a mixed singlet-triplet character of the levels. Paradoxically, the levels of predominantly triplet $b^3\Pi_{0u}$ character are of special interest here for transfer to the rovibrational ground state $|v = 0, J = 0>$ of the singlet $X^1\Sigma_g^+$ electronic ground state. As determined by data fits described below, the predominantly $b^3\Pi_{0u}$ levels happen to have significant singlet character over the regions of internuclear distance that are most important for transitions of interest in this work and thus couple to levels of the $X^1\Sigma_g^+$ state in a two-photon transition. For STIRAP transfer, they provide a more balanced distribution of Franck-Condon factors than the levels of predominantly $A^1\Sigma_u^+$ character.

To model the strongly interacting $A^1\Sigma_u^+$ and $b^3\Pi_{0u}$ states, a coupled channels ap-

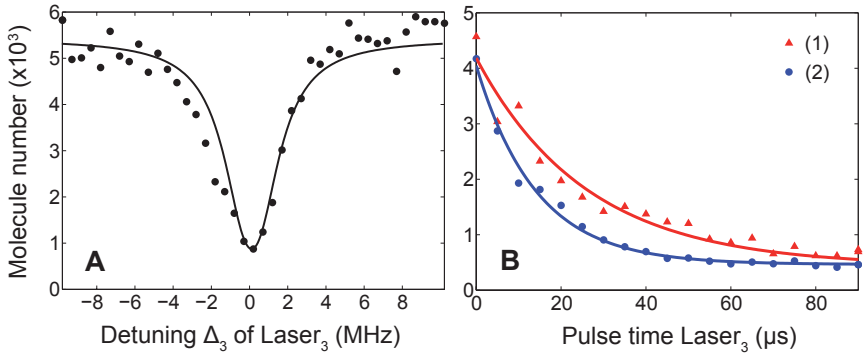

Figure 4.3: Loss resonances for excitation near 1351 nm from $|3>= |v = 73, J = 2>$ of the $X^1\Sigma_g^+$ ground state potential. **(A)** Loss of molecules in $|3>$ as a function of laser detuning Δ_3 near 1351 nm after a waiting time of 20 μs. The solid line represents a model calculation matched to the data yielding an excited state natural linewidth of $2\pi \times 2$ MHz. **(B)** Time dependence of molecular loss on resonance at 1351 nm for two different laser intensities. (1) 270 ± 80 mW/cm^2, (2) 570 ± 80 mW/cm^2. The fitted exponential decay gives the decay constants $\tau_d = 26 \pm 4$ μs for 270 mW/cm^2 and $\tau_d = 14 \pm 2$ μs for 570 mW/cm^2.

proach is needed. The calculations used to characterize the level structure of these interacting states in Cs_2 [27] employed methods developed from previous work on A and b states of K_2 [28,29], RbCs [30], Na_2 [31], and Rb_2 [32]. The DVR approach [33] was used to calculate eigenvalues for coupled channels. Similar computational approaches, differing in the detailed numerical methods, have been applied recently also to the A and b states of NaRb [34].

Prior to the present experiments, the energies of the Cs_2 $(A - b)$ 0_u^+ levels in the energy range of interest were approximately established by fits to two sets of data using the coupled channels approach. High resolution data was obtained by Fourier transform spectroscopy (FTS) at Laboratoire Aimé Cotton (LAC) using transitions to the $X^1\Sigma_g^+$ state. The second set of data, from Tsinghua and Temple Universities, contained, besides additional high resolution $(A - b) \rightarrow X$ transitions, lines from $2^3\Delta_{1g} \rightarrow b^3\Pi_{0u}$ emission [35] in an energy range that lies somewhat below the region of interest for the present work. This made it possible to establish the vibrational numbering for the $b^3\Pi_{0u}$ state and to construct a potential for this state. The coupled channels fit determined the spin-orbit coupling function between the A and the b state and hence the singlet-triplet mixing. The calculated energies for the highly mixed $(A - b)$ 0_u^+ levels above the minimum of the A state exhibited an overall rms deviation of about 0.07 cm^{-1} as compared with the high resolution observations. However, the predominantly $b^3\Pi_{0u}$ levels were only established to about ± 2 cm^{-1} in the region of interest for the ground state transfer. This region is above that for which data was obtained from $2^3\Delta_{1g} \rightarrow b^3\Pi_{0u}$ emission [35], but lower than the regime where $b^3\Pi_{0u}$ levels acquire sufficient singlet character to be observed in the FTS work.

v'	C	J	Excitation wavelength from $X^1\Sigma_g^+$ $\|v=73, J=2>$ [nm]	Energy above $X^1\Sigma_g^+$ $\|v=0, J=0>$ [cm^{-1}]	De-excitation wavelength to $X^1\Sigma_g^+$ $\|v=0, J=0>$ [nm]
57	A (7)	1	1365.148	9893.002	n. m.
57	A (7)	3	1365.131	9893.094	n. m.
*58	b (50)	0	1362.893	9905.126	n. m.
*59	A (8)	0	1357.748	9932.927	n. m.
60	b (51)	1	1357.091	9936.497	n. m.
60	b (51)	3	1357.071	9936.606	n. m.
61	b (52)	1	1351.367	9967.707	1003.240
61	b (52)	3	1351.347	9967.816	n. m.
*62	A (9)	0	1350.388	9973.068	n. m.
63	b (53)	1	1345.725	9998.729	1000.128
63	b (53)	3	1345.705	9998.839	n. m.
*64	A (10)	0	1343.082	10013.351	n. m.
65	b (54)	1	1340.162	10029.576	997.052
65	b (54)	3	1340.143	10029.682	n. m.
66	A (11)	1	1335.833	10053.759	994.653
66	A (11)	3	1335.816	10053.853	n. m.
*67	b (55)	0	1334.675	10060.249	n. m.
68	b (56)	1	1329.257	10090.794	991.003
68	b (56)	3	1329.238	10090.902	n. m.

Table 4.1: Levels of the $(A-b)\ 0_u^+$ system in the region 9893 cm^{-1} to 10091 cm^{-1} above $X^1\Sigma_g^+$ $|v=0, J=0>$. The first column gives the coupled channels vibrational numbers of the individual levels. Levels marked with * have not been searched for and the level energies given are those determined from the coupled channels calculations. The column labeled 'C' gives the predominant contribution to the overall vibrational wave function, which is either predominantly $A^1\Sigma_u^+$ or predominantly $b^3\Pi_{0u}$, indicated by A and b, respectively. The number in brackets gives the order within the two progressions of levels with either predominantly $A^1\Sigma_u^+$ or predominantly $b^3\Pi_{0u}$ character. Both the $|J=1>$ and the $|J=3>$ rotational levels were identified for all oberved excited state levels. The wavemeter accuracy gives a typical uncertainty in wavelength of ±0.002 nm, which translates into ±0.011 cm^{-1} uncertainty in the value for the energy above $|v=0, J=0>$. The energy relative to $X^1\Sigma_g^+$ $|v=0, J=0>$ of experimentally determined levels is based on the measured excitation wavelength from $X^1\Sigma_g^+$ $|v=73, J=2>$ and the $X^1\Sigma_g^+$ $|v=73>$ level energy from Ref. [37], which introduces an additional uncertainty of 0.001 cm^{-1}. Deexcitation wavelengths are obtained from dark resonance spectroscopy involving the respective intermediate excited state level and the rovibronic ground state $X^1\Sigma_g^+$ $|v=0, J=0>$. n. m.: not measured

Because of the uncertainty in the positions of mixed $(A - b)$ levels in this region, we decided to perform a systematic, broad-range search around expected transition energies in the wavelength range from 1329 nm to 1365 nm. For this, we perform double STIRAP from |1> to |3> and back with a waiting time of typically τ = 1 ms. During the waiting time, we irradiate the sample with laser L_3 at an estimated intensity of $5 \cdot 10^4$ mW/cm^2. Laser L_3 is a diode laser with grating feedback. On the timescale of our experiment, the resonator of the laser is sufficiently stable, allowing systematic tuning of the laser without locking the laser to its external resonator. We step the laser frequency in units of typically 20 MHz by tuning the piezo element on the grating. We monitor the laser wavelength with a home-built wavemeter at approximately 300 MHz accuracy. For the initial broad range line search we increased the repetition rate of the experiment by stopping evaporative cooling slightly before condensation sets in. Data points are taken essentially at the cycle rate of the experiment which is given by the sample production time. We step the laser with each experimental cycle and look for a dip in the molecule number. Once such a dip is found, typically consisting of a few data points, we perform a more precise scan by locking the laser to the external, highly-stable resonator and then the external resonator to the infrared frequency comb. This allows us to detune the laser with kHz precision. Fig.4.3 (A) shows a typical loss resonance near 1351 nm. We reduce the laser intensity such that on resonance at most 80% of the molecules are lost within 20 μs. From such measurements the transition strength as given by the normalized Rabi frequency and the natural linewidth of the excited state can be deduced. The typical width of the excited state molecular levels that we have identified is $2\pi \times 2$ MHz, in agreement with typical expected lifetimes. Fig.4.3 (B) shows a measurement of the time dependence of the molecular loss. Here, we step the waiting time τ from 0 to 50 μs, while the laser is kept on resonance. In total, we have found 7 excited levels belonging to the $(A - b)\ 0_u^+$ system. They are listed in Table 4.1 along with the dominant overall character (either $A^1\Sigma_u^+$ state or $b^3\Pi_{0u}$ state) of the vibrational wave function as determined from the coupled state calculations. Within the wavelength range from 1329 nm to 1365 nm, theory predicts the existence of 5 more levels of the $(A - b)\ 0_u^+$ system, whose energies are also displayed in Table 4.1. For most of them, the wave function overlap is not expected to be favorable for STIRAP transfer to X $^1\Sigma_g^+$ $|v = 0>$. However, an improved model of the energy level structure, based on all the data except one FTS point with a large residual, fits the observed transitions to a rms residual error of 0.02 cm^{-1}, indicating that additional resonances can be found with searches over very limited ranges of laser frequency.

4.5 Dark resonances with $|v = 0, J = 0>$ and $|v = 0, J = 2>$

In our recent work [21] we have greatly improved the value for the binding energy of the rovibrational ground state |5>= $|v = 0, J = 0>$ by determining the binding energy of $|v = 73>$ and using well-known data from conventional molecular spectroscopy [36,37]. Our measurement was limited by the calibration of our wavemeter, not al-

lowing us to determine the number of the teeth of the frequency comb, and by the precision of the spectroscopy data. Searching for |5> in dark state spectroscopy is now a straightforward task as only a range of about 0.002 cm^{-1} needs to be scanned. We do this by exciting the transitions from |3> to |4> with laser L_3 and from |4> to |5> with laser L_4 simultaneously. The intensity for L_4 is typically $5 \cdot 10^4$ mW/cm^2. As is well known, the two light fields create a molecule-molecule dark state. The molecules initially in |3> are lost unless laser L_4 is on two-photon resonance, provided that the Rabi frequency Ω_4 on the fourth transition is equal to or greater than Ω_3, the Rabi frequency on the third transition. We look for the resonance condition with the rovibrational ground state $|v=0, J=0>$ for some of the excited levels that we found above. Table 4.1 lists the observed transition wavelengths. We check that we can identify the level with rotational quantum number $J = 2$ as the rotational energy splitting is well known. Fig.4.4 shows typical molecular dark resonances when we set L_4 on resonance and step the detuning Δ_3 of L_3 near 1350 nm. From a three-level model matched to the data for the dark resonances, taking into account off-resonant excitations and laser line widths, we determine the molecular transition strengths as given by the normalized Rabi frequencies. One of the two-photon transitions appears to be a particularly good candidate for STIRAP ground state transfer. It involves the excited state level |4> with vibrational number $v' = 61$ of the $(A - b)\, 0_u^+$ system at $\sim$ 1351 nm. For the transition from |3> to |4> and from |4> to |5> the normalized Rabi frequencies are $\Omega_3 = 2\pi\times 6$ kHz $\sqrt{I/(\mathrm{mW/cm^2})}$ and $\Omega_4 = 2\pi\times 5$ kHz $\sqrt{I/(\mathrm{mW/cm^2})}$, respectively. These values carry an estimated error of 50% as the laser beam parameters for L_3 and L_4 are not well determined. A comparison with a typical atomic transition strength of $\Omega_a = 2\pi\times 5$ MHz $\sqrt{I/(\mathrm{mW/cm^2})}$ giving $|\Omega_3/\Omega_a|^2 \approx 10^{-6}$ and $|\Omega_4/\Omega_a|^2 \approx 10^{-6}$ reflects the minuteness of the wave function overlap. Nevertheless, their value is sufficient for STIRAP as seen in our recent work [21]. Also, they are of similar magnitude. This facilitates STIRAP, for which the peak Rabi frequencies should be approximately equal for optimum performance.

4.6 Conclusion

We observe several two-photon dark resonances that connect the intermediate rovibrational level $|v = 73, J = 2>$ of the $X^1\Sigma_g^+$ ground state potential with the rovibrational ground state $|v = 0, J = 0>$. At least one of the two-photon transitions is sufficiently strong for implementing STIRAP to $|v=0, J=0>$ in the quantum gas regime, paving the way for the realization of a BEC of ground state molecules. STIRAP can in principle be implemented in two ways, either in the form of two sequential two-photon STIRAP steps, or in the form of four-photon STIRAP [38,39]. An attractive strategy for the production of a BEC of ground state molecules relies on the addition of an optical lattice. Starting from an atomic BEC, pairs of atoms at individual lattice sites are produced in a superfluid-to-Mott-insulator transition [40]. These pairs can then be very efficiently associated on a Feshbach resonance and subsequently transfered to the

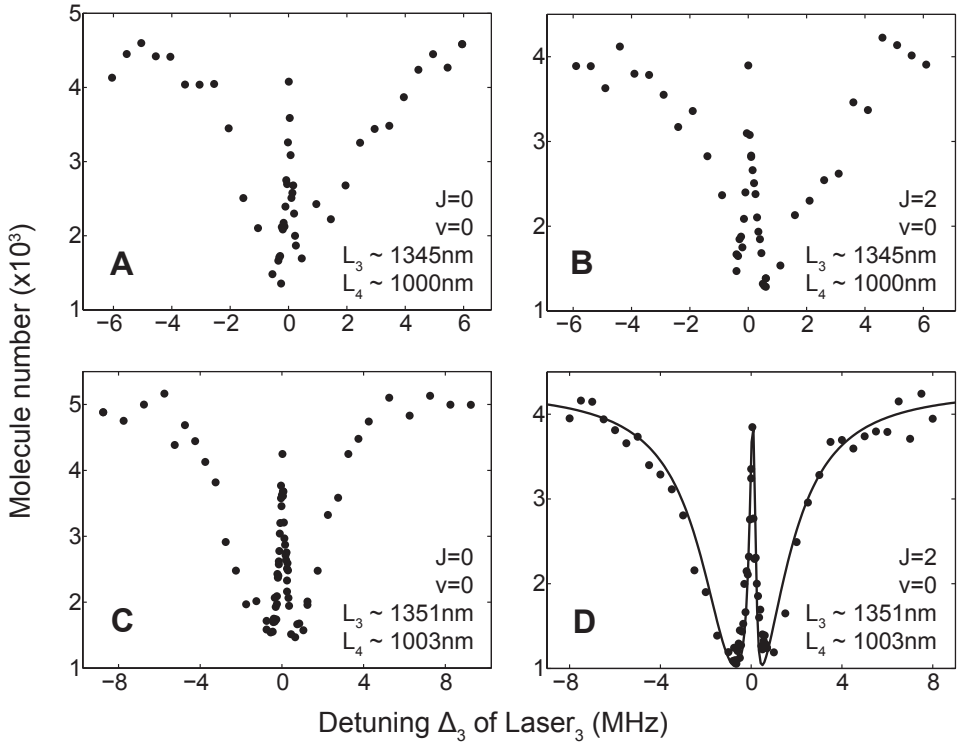

Figure 4.4: Dark resonances involving $X^1\Sigma_g^+$ state levels $|v = 73, J = 2>$ and $|v = 0>$ for two different intermediate levels. **(A** and **B)** Dark resonances with $X^1\Sigma_g^+$ $|v = 0, J = 0>$ and $|v = 0, J = 2>$ involving the 0_u^+ excited state level $|v' = 63, J = 1>$ at an excitation wavelength near 1345 nm. **(C** and **D)** Dark resonances with $X^1\Sigma_g^+$ $|v = 0, J = 0>$ and $|v = 0, J = 2>$ involving the excited state level $|v' = 61, J = 1>$ at an excitation wavelength near 1351 nm. The solid line in **(D)** is the result of a model calculation, solving the three-level master equation including laser bandwidth and loss, matched to the data giving $\Omega_3 = 2\pi\times 6$ kHz $\sqrt{I/(\mathrm{mW/cm^2})}$ and $\Omega_4 = 2\pi\times 4$ kHz $\sqrt{I/(\mathrm{mW/cm^2})}$ for $X^1\Sigma_g^+$ $|v = 0, J = 2>$. The corresponding calculation for $X^1\Sigma_g^+$ $|v = 0, J = 0>$ yields $2\pi\times 5$ kHz $\sqrt{I/(\mathrm{mW/cm^2})}$.

rovibronic ground state with STIRAP. The lattice has the advantage of shielding the molecules against inelastic collisions during the association process and subsequent state transfer. As proposed by Jaksch *et al.* [41], dynamical melting of the lattice should ideally result in the formation of a BEC of molecules in the rovibronic ground state in a Mott-insulator-to-superfluid-type transition.

Acknowledgements

We are indebted to R. Grimm for generous support and we thank E. Tiemann for valuable discussions and C. Amiot for providing the FTS data of LAC on Cs_2. We gratefully acknowledge funding by the Austrian Ministry of Science and Research (BMWF) and the Austrian Science Fund (FWF) in form of a START prize grant and by the European Science Foundation (ESF) in the framework of the EuroQUAM collective research project QuDipMol. R.H. acknowledges support by the European Union in form of a Marie-Curie International Incoming Fellowship (IIF). The work at Stony Brook was supported by the US NSF, under grant PHY0652459.

4.7 References

1. K. Southwell (ed.), Ultracold matter, Nature (Insight) **416** 205–246 (2002).
2. J. Doyle, B. Friedrich, R.V. Krems, and F. Masnou-Seeuws, Eur. Phys. J. D **31**, 149 (2004).
3. R.V. Krems, Phys. Chem. Chem. Phys. **10**, 4079 (2008).
4. S.Y.T. van de Meerakker, H.L. Bethlem, and G. Meijer, Nature Phys. **4**, 595 (2008).
5. For a review on photoassociation, see: K. M. Jones, E. Tiesinga, P.D. Lett, and P. S. Julienne, Rev. Mod. Phys. **78**, 483 (2006).
6. A.N. Nikolov, J.R. Ensher, E.E. Eyler, H. Wang, W.C. Stwalley, and P.L. Gould, Phys. Rev. Lett. **84**, 246 (2000).
7. J.M. Sage, S. Sainis, T. Bergeman, and D. DeMille, Phys. Rev. Lett. **94**, 203001 (2005).
8. M. Viteau, A. Chotia, M. Allegrini, N. Bouloufa, O. Dulieu, D. Comparat, and P. Pillet, Science **321**, 232 (2008).
9. J. Deiglmayr, A. Grochola, M. Repp, K. Mörtlbauer, C. Glück, J. Lange, O. Dulieu, R. Wester, and M. Weidemüller, Phys. Rev. Lett. **101**, 133004 (2008).
10. For an overview, see: Ultracold Fermi Gases, *Proceedings of the International School of Physics Enrico Fermi, Course CLXIV*, edited by M. Inguscio, W. Ketterle, and C. Salomon (IOS Press, Amsterdam, 2008).
11. R. V. Krems, Int. Rev. Phys. Chem. **24**, 99 (2005).
12. P. Staanum, S. D. Kraft, J. Lange, R. Wester, and M. Weidemüller, Phys. Rev. Lett. **96**, 023201 (2006).

13. N. Zahzam, T. Vogt, M. Mudrich, D. Comparat, and P. Pillet, Phys. Rev. Lett. **96**, 023202 (2006).

14. T. Zelevinsky, S. Kotochigova, and J. Ye, Phys. Rev. Lett. **100**, 043201 (2008).

15. D. DeMille, S. Sainis, J. Sage, T. Bergeman, S. Kotochigova, and E. Tiesinga, Phys. Rev. Lett. **100**, 043202 (2008).

16. D. DeMille, Phys. Rev. Lett. **88**, 067901 (2002).

17. K. Góral, L. Santos, and M. Lewenstein, Phys. Rev. Lett. **88**, 170406 (2002).

18. M. Baranov, L. Dobrek, K. Góral, L. Santos, and M. Lewenstein, Phys. Scr. **T102**, 74 (2002).

19. K. Winkler, F. Lang, G. Thalhammer, P. v. d. Straten, R. Grimm, and J. Hecker Denschlag, Phys. Rev. Lett. **98**, 043201 (2007).

20. K. Bergmann, H. Theuer, and B. W. Shore, Rev. Mod. Phys. **70**, 1003 (1998).

21. J. G. Danzl, E. Haller, M. Gustavsson, M. J. Mark, R. Hart, N. Bouloufa, O. Dulieu, H. Ritsch, and H.-C. Nägerl, Science **321**, 1062 (2008), published online 10 July 2008; 10.1126/science.1159909.

22. K.-K. Ni, S. Ospelkaus, M. H. G. de Miranda, A. Pe'er, B. Neyenhuis, J.J. Zirbel, S. Kotochigova, P.S. Julienne, D.S. Jin, and J. Ye, published online September 18, 2008, Science DOI: 10.1126/science.1163861.

23. W.C. Stwalley, Eur. Phys. J. D **31**, 221 (2004).

24. F. Lang, K. Winkler, C. Strauss, R. Grimm, and J. Hecker Denschlag, Phys. Rev. Lett. **101**, 133005 (2008).

25. J. Herbig, T. Kraemer, M. Mark, T. Weber, C. Chin, H.-C. Nägerl, and R. Grimm, Science **301**, 1510 (2003); published online 21 August 2003; 10.1126/science.1088876.

26. M. Mark, F. Ferlaino, S. Knoop, J.G. Danzl, T. Kraemer, C. Chin, H.-C. Nägerl, and R. Grimm, Phys. Rev. A **76**, 042514 (2007).

27. H. Salami, T. Bergeman, O. Dulieu, D. Li, F. Xie, and L. Li, manuscript in preparation (2008).

28. C. Lisdat, O. Dulieu, H. Knöckel and E. Tiemann, Eur. Phys. J. D **17**, 319 (2001).

29. M. R. Manaa, A. J. Ross, F. Martin, P. Crozet, A. M. Lyyra, L. Li, C. Amiot and T. Bergeman, J. Chem. Phys. **117**, 11208 (2002).

30. T. Bergeman, C. E. Fellows, R. F. Gutterres and C. Amiot, Phys. Rev. A, **67**, 050501 (2003).

31. P. Qi, J. Bai, E. Ahmed, A. M. Lyyra, S. Kotochigova, A. J. Ross, C. Effantin, P. Zalicki, J. Vigué, G. Chawla, R. W. Field, T.-J. Whang, W. C. Stwalley, H. Knöckel, E. Tiemann, J. Shang, L. Li, and T. Bergeman, J. Chem. Phys. **127**, 044301 (2007).

32. H. Salami, T. Bergeman, B. Beser, J. Bai, E. Ahmed, S. Kotochigova, A. M. Lyyra, J. Huennekens, C. Lisdat, O. Dulieu, P. Crozet and A. J. Ross, manuscript in preparation (2008).

33. D. Colbert and W. H. Miller, J. Chem. Phys. **96**, 1982 (1992).

34. O. Docenko, M. Tamanis, R. Ferber, E. A. Pazyuk, A. Zaitservkii, A. V. Stolyarov, A. Pashov, H. Knöckel and E. Tiemann, Phys. Rev. A **75**, 042503 (2007).

35. F. Xie, D. Li, L. Tyree, L. Li, V. Sovkov, V. S. Ivanov, S. Magnier, and A. M. Lyyra, J. Chem. Phys. **128**, 204313 (2008).

36. W. Weickenmeier, U. Diemer, M. Wahl, M. Raab, W. Demtröder, and W. Müller, J. Chem. Phys. **82**, 5354 (1985).

37. C. Amiot and O. Dulieu, J. Chem. Phys. **117**, 5155 (2002).

38. B. W. Shore, K. Bergmann, J. Oreg, and S. Rosenwaks, Phys. Rev. A **44**, 7442 (1991).

39. E. Kuznetsova, P. Pellegrini, R. Côté, M.D. Lukin, and S.F. Yelin, arXiv:0806.0821 (2008).

40. M. Greiner, O. Mandel, T. Esslinger, T.W. Hänsch, and I. Bloch, Nature **415**, 39 (2002).

41. D. Jaksch, V. Venturi, J. I. Cirac, C. J. Williams, and P. Zoller, Phys. Rev. Lett. **89**, 040402 (2002).

Chapter 5

Publication: Deeply bound ultracold molecules in an optical lattice

New Journal of Physics
Focus issue on cold and ultracold molecules
Published 14 May 2009
Vol. 11, 055036
DOI: 10.1088/1367-2630/11/5/055036

This paper** presents the production of a sample of ultracold deeply-bound molecules in level $|v = 73, J = 2>$ of the $X^1\Sigma_g^+$ potential in an optical lattice. It takes the experiments in Ref. [Dan08] a significant step further by trapping the molecules at the individual sites of an optical lattice. We load a BEC of Cs atoms into an optical lattice and drive the superfluid-to-Mott insulator quantum phase transition [Gre02]. In the paper presented here, we reach a fraction of about 30% of atoms at doubly occupied lattice sites, which is not optimal yet. Lattice loading was further optimized for the experiments discussed in chapter 6 in order to maximize the filling factor in the lattice. To reach the same starting level for STIRAP as in our previous work [Dan08] we implemented transfer between Feshbach levels via avoided level crossings [Mar07a].

We find that the STIRAP transfer efficiency in the lattice is similar to our previous work [Dan08] where the experiments were performed in free flight. For STIRAP in an optical lattice, besides fulfilling the criteria discussed in the previous chapters, it must be ensured that the lattice wavelength is chosen such that the lattice light does not lead to optical excitation of the molecules that would lead to loss. In addition, the lattice light must not create unwanted molecular coherences that might compete with the STIRAP transfer process. We operate the lattice at a wavelength of 1064.5 nm. When the energy of a lattice photon is added to the energy of the $|v=73, J=2>$ ground state level, the $(A^1\Sigma_u^+ - b^3\Pi_u)0_u^+$ coupled system is reached about half way between the potential minimum and the excited state potential asymptote. Therefore, the lattice light can lead to off-resonant excitation to nearby excited state levels. This is particularly true because the effective dynamical polarizability is such that the molecules are trapped at the intensity maxima of the lattice. This limits the lifetime to about 20 ms

**The author of the present thesis did all the measurements presented in this paper together with M. J. M., E. H., and R. H.. Lattice loading and production of Feshbach molecules was optimized by M. J. M.. J. G. D. analyzed the data and the paper was written by J. G. D. and H.-C. N. and all authors commented on the manuscript. The final accepted version of the paper is given here.

for molecules in $|v = 73, J = 2>$. This lifetime is in sharp contrast to the lifetime of 8 s achieved for rovibronic ground state molecules in an optical lattice as discussed in chapter 6. There, the detuning of the lattice light from the nearest allowed transitions is much larger, on the order of 7 THz.

We measure the dynamical polarizability for $|v = 73>$ molecules at the particular wavelength of our lattice and find a value that is about 30 % of the polarizability of Feshbach molecules. Due to nearby optical transitions and associated resonant structures in the molecular polarizability, the value of the molecular polarizability is a sensitive function of lattice wavelength in this regime. The potential depths and hence the shapes of the motional wave functions of the initial Feshbach molecules and the $|v = 73>$-molecules are not matched. In contrast, the lattice wavelength is chosen in such a way that it ensures motional state control for transfer from Feshbach levels to $|v=0>$ of the $X^1\Sigma_g^+$ electronic ground state potential, as discussed in chapter 6. There, the intermediate level $|v=73>$ is either only very briefly populated or hardly populated at all during transfer to $|v=0>$.

Deeply bound ultracold molecules in an optical lattice

Johann G. Danzl[a], Manfred J. Mark[a], Elmar Haller[a], Mattias Gustavsson[a], Russell Hart[a], Andreas Liem[b], Holger Zellmer[c], and Hanns-Christoph Nägerl[a]

[a] Institut für Experimentalphysik und Zentrum für Quantenphysik, Universität Innsbruck, Technikerstraße 25, A–6020 Innsbruck, Austria

[b] JT Optical Engine GmbH + Co. KG, Prüssingstraße 41, D–07745 Jena, Germany

[c] Hochschule für Technik, Wirtschaft und Kultur Leipzig, Gutenbergplatz 2-4, D–04103 Leipzig, Germany

We demonstrate efficient transfer of ultracold molecules into a deeply bound rovibrational level of the singlet ground state potential in the presence of an optical lattice. The overall molecule creation efficiency is 25%, and the transfer efficiency to the rovibrational level $|v=73, J=2>$ is above 80%. We find that the molecules in $|v=73, J=2>$ are trapped in the optical lattice, and that the lifetime in the lattice is limited by optical excitation by the lattice light. The molecule trapping time for a lattice depth of 15 atomic recoil energies is about 20 ms. We determine the trapping frequency by the lattice phase and amplitude modulation technique. It will now be possible to transfer the molecules to the rovibrational ground state $|v=0, J=0>$ in the presence of the optical lattice.

5.1 Introduction

The generation of molecular quantum gases and molecular Bose-Einstein condensates (BEC) has been a major goal for the field of atomic and molecular physics. It has been achieved for the case of two fermionic atoms that pair up to form a bosonic dimer molecule in the limit of vanishing binding energy [1,2] at ultralow temperatures. In this limit, collisional stability is assured, and this has allowed the investigation of the BEC-BCS crossover [3]. Here, we are interested in the opposite limit of deeply bound molecules. Collisional stability is expected only for the rovibronic ground state, and most likely it will be necessary that one prepares the lowest molecular hyperfine sublevel [4] to avoid hyperfine changing collisions. Our approach to producing a quantum gas of ground state molecules is based on laser cooling of atoms to the point of quantum degeneracy, followed by molecule association on a Feshbach resonance and subsequent coherent two-photon molecule transfer [5,6,7,8,9,10]. In principle, this approach

combines high molecular densities and ultralow temperatures with full state selectivity. For optimization of both the initial molecule creation process and the transfer process, the use of a three-dimensional optical lattice has been proposed, as illustrated in Fig. 5.1 C. In a superfluid-to-Mott-insulator phase transition doubly occupied lattice sites can be favored [11,12], and collisional relaxation during the transfer can, at least in principle, be fully avoided. It should be possible that one finally creates a molecular BEC by dynamical melting of the lattice after the two-photon transfer [13].

In the present work, we report on two-photon transfer into a deeply bound rovibrational level by means of the stimulated Raman adiabatic passage (STIRAP) technique [14,8] in the presence of a three-dimensional optical lattice. We extend our previous work of transfering Cs_2 molecules to rovibrational level $|v = 73, J = 2>$ of the $^1\Sigma_g^+$ electronic ground state in the quantum gas regime [5] by first using the superfluid-to-Mott-insulator phase transition to efficiently produce pairs of atoms at the wells of the lattice. The pairs are then associated to weakly bound molecules on a Feshbach resonance. Subsequently, the molecules are transferred by magnetic field ramping to the starting state for optical transfer. From there, they are efficiently transferred to the deeply bound rovibrational level $|v=73, J=2>$ by means of STIRAP. Note that in our previous work [5] all experiments were performed in free flight. Fig. 5. 1 A shows the relevant molecular states for the Cs dimer molecule and the transitions involved. We find that the molecules in $|v=73, J=2>$ are trapped in the lattice with a $1/e$-trapping time of about 20 ms, limited by scattering of lattice light. We measure the trapping frequency of the molecules in the lattice and find that the polarizability in $|v=73, J=2>$ is about 30% of that of the Feshbach molecules. It will now be possible that one adds a second STIRAP transfer step to reach the rovibronic ground state $|v = 0, J = 0>$, giving full quantum control over the external and internal degrees of freedom for the molecules.

5.2 Preparation of Feshbach molecules in the optical lattice

To produce an ultracold sample of Feshbach molecules trapped at the individual sites of an optical lattice we first produce an atomic BEC with typically 1×10^5 Cs atoms in the lowest hyperfine sublevel $F = 3,\ m_F = 3$ in a crossed optical dipole trap. As usual, F is the atomic angular momentum quantum number, and m_F its projection on the magnetic field axis. For BEC production, we essentially follow the procedure detailed in Ref.[15]. We set the atomic scattering length to a value of 210 a_0, where a_0 is Bohr's radius, by tuning the magnetic offset field to 2.1 mT. At this value, three-body losses are minimal [16]. We then drive the superfluid-to-Mott-insulator phase transition [17] by exponentially ramping up the power in a three-dimensional optical lattice within about 400 ms while simultaneously ramping up the harmonic confinement in the dipole trap. The lattice is generated by three mutually orthogonal, retro-reflected laser beams

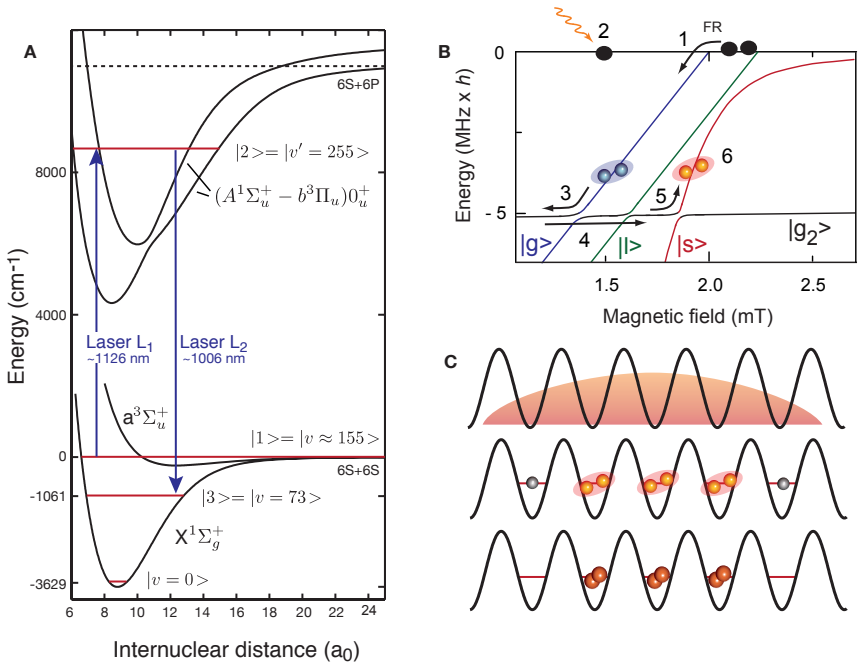

Figure 5.1: **A** Molecular level scheme for Cs_2. Molecules in a weakly bound Feshbach level |1> are transferred to rovibrational level |3>= $|v = 73, J = 2>$ of the singlet $X^1\Sigma_g^+$ potential in the presence of an optical lattice. Level |3> with a binding energy of 1061 cm^{-1} is reached in a two-photon STIRAP process with wavelengths near 1126 nm and 1006 nm via the 225th level of the electronically excited ($A^1\Sigma_u^+$–$b^3\Pi_u$) 0_u^+ potentials. The $X^1\Sigma_g^+$ potential has about 155 vibrational levels. **B** Zeeman diagram showing the energy of all relevant weakly bound levels for initial Feshbach molecular state preparation [23]. The binding energy is given with respect to the $F = 3, m_F = 3$ two-atom asymptote. The molecules are first produced on a g-wave Feshbach resonance at 1.98 mT in state |g> (1). Residual atoms are removed by a combined microwave and resonant light pulse (2). The molecules are then transferred to the weakly bound s-wave state |1>= |s> (6), the starting state for the STIRAP transfer, via three avoided state crossings involving state $|g_2>$ by slow (3,5) and fast magnetic field ramps (4). **C** Lattice based ground state transfer. Top: The BEC is adiabatically loaded into the three-dimensional optical lattice, creating a Mott-insulator state. Middle: Atoms at doubly occupied sites are converted to Feshbach molecules. Atoms at singly occupied sites are removed thereafter. Bottom: The molecules are subsequently transferred to the deeply bound rovibrational level |3>= $|v = 73, J = 2>$ while shielded from collisions by the lattice potential.

at a wavelength of $\lambda = 1064.5$ nm, each with a $1/e$-waist of about 350 μm. For the atoms, we achieve a well depth of up to 40 E_R, where $E_R = h^2/(2m\lambda^2) = k_B \times 64\,\mathrm{nK}$ is the atomic photon recoil energy with the mass m of the Cs atom. h is Planck's constant, and k_B is Boltzmann's constant. Throughout the paper we give lattice depths in units of the atomic recoil energy. The lattice light as well as the light for the dipole trap beams is derived from a single-frequency, narrow-band, highly-stable Nd:YAG

laser that is amplified to up to 20 W without spectral degradation in a home-built fiber amplifier [18]. The power in each lattice beam is controlled by an acousto-optical intensity modulator and an intensity stabilization servo. While ramping up the lattice potential, the power in the two dipole trap beams is increased to assure that the central density in the trap is sufficiently high to allow the preferential formation of atom pairs at the central wells of the lattice, but not too high in order to avoid triply occupied sites. We typically ramp the lattice to a depth of 15 to 25 E_R. Typically about 30% of the atoms reside at doubly occupied lattice sites. We estimate this number from the molecule production efficiency. This value is not optimal yet, as loading from a parabolic potential should give a maximum of 53% [12,19].

We now produce Feshbach molecules on a Feshbach resonance [20,21,22] near a magnetic field value of $B = 1.98$ mT [23] in the presence of the optical lattice [24,11]. Fig. 5. 1 B shows the relevant weakly bound Feshbach levels. The resonance at 1.98 mT is quite narrow, but it lies at a conveniently low value of the magnetic field, allowing us to simply lower the magnetic offset field from the BEC production value and ramp over the resonance with a rate of about 0.006 T/s. The molecules produced are then in level $|g>$. These molecules have g-wave character, i.e. $\ell = 4$, where ℓ is the quantum number associated with the mechanical rotation of the nuclei [25]. After association, atoms remaining at singly occupied lattice sites are removed by microwave transfer to $F = 4$ and a resonant light pulse. Starting from level $|g>$ we have recently identified transitions to deeply bound excited rovibrational levels of the Cs_2 mixed $(A^1\Sigma_u^+ - b^3\Pi_u)\ 0_u^+$ excited states [7]. These transitions should allow STIRAP transfer to the target rovibrational level $|v = 73, J = 2>$ of the electronic ground state, but for the present work we have decided to use Feshbach level $|s>$ as the starting state as in our previous work [5] so that the transfer performances with and without the presence of the lattice can be compared. To reach level $|s>$ from level $|g>$, we have implemented Feshbach state transfer as realized in Ref.[23] using a combination of slow and fast magnetic field ramps. In brief, we first transfer the molecules from $|g>$ to level $|g_2>$ by lowering the magnetic field B sufficiently slowly to a value of 1.22 mT, thereby following the upper branch of an avoided crossing near 1.33 mT as shown in Fig. 5. 1 B. We then increase B abruptly to a value of 1.67 mT, thereby jumping the two crossings with levels $|g>$ and $|l>$. The maximum magnetic field rate of change is $\sim$ 2000 T/s. We finally follow slowly on the upper branch of the avoided crossing with $|s>$ at 1.85 mT, stopping at $B = 1.9$ mT. Our procedure allows us to essentially transfer all molecules from $|g>$ to $|s>$. For molecule detection, we reverse the magnetic field ramps to level $|g>$, dissociate the molecules at the Feshbach resonance at $B = 1.98$ mT and detect the resulting atoms by standard absorption imaging [21].

For comparison with our data obtained below we first measure the lifetime of the weakly-bound Feshbach molecules in the optical lattice. Typical lifetime measurements for these molecules are shown in Fig. 5. 2 A-C. In such measurements, we record the number of remaining molecules as a function of hold time in the lattice. The lifetime of the molecules depends strongly on which Feshbach level is used and on the value of the magnetic field B. For example, for molecules in level $|g>$ at $B = 1.82$

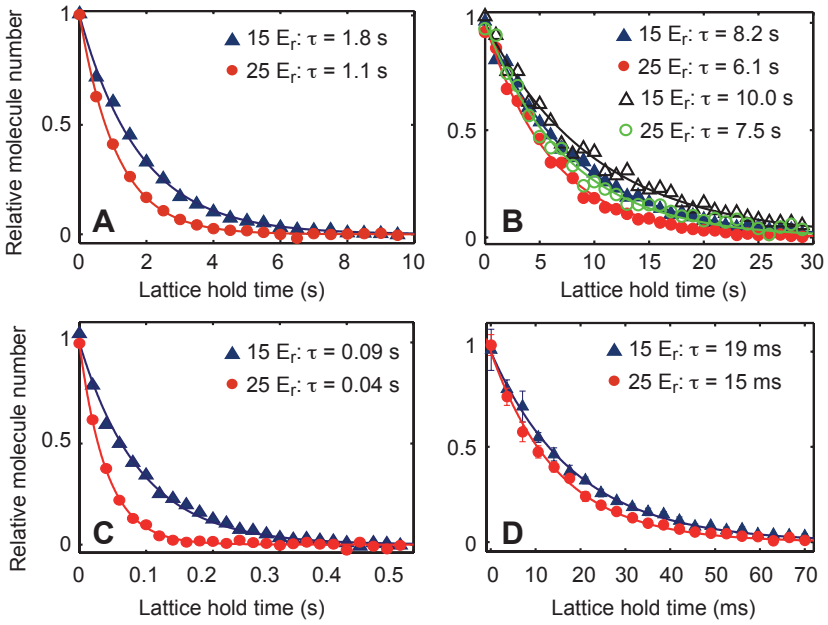

Figure 5.2: Lifetime measurements of ultracold molecules trapped in the optical lattice. **A**, **B**, and **C** show the decay of trapped Feshbach molecules, while **D** shows the decay for molecules in $|3\rangle = |v = 73, J = 2\rangle$ of the $X^1\Sigma_g^+$ ground state potential. In all cases, the triangles (circles) correspond to a lattice depth of 15 E_R (25 E_R). All lifetimes τ are determined from exponential fits to the data as shown by the the solid lines. **A** Lifetime of state $|g\rangle$. **B** Lifetime of state $|g_2\rangle$ (filled symbols) and of state $|s\rangle$ at $B = 2.9$ mT (open symbols). **C** Lifetime of state $|s\rangle$ at $B = 1.9$ mT, from where we drive the STIRAP transfer. **D** Lifetime of molecules in the rovibrational level $|3\rangle = |v = 73, J = 2\rangle$. The STIRAP lasers are switched off during the hold time in $|3\rangle$. In **D**, each data point is the average of 4 experimental runs, error bars correspond to the 1σ statistical uncertainty. The typical uncertainty for the lifetimes is one unit of the last digit given.

mT the lifetime is 1.8 s at a lattice depth of 15 E_R, while in level $|s\rangle$ the lifetime is 0.09 s at $B = 1.9$ mT and 10 s at $B = 2.9$ mT for the same lattice depth. We attribute this strong dependence of the lifetime of molecules in $|s\rangle$ to the fact that the molecular character changes strongly from being predominantly closed channel dominated to being open channel dominated as the magnetic field is increased [22], reducing wave function overlap with excited molecular levels. We always determine the lifetime for two values of the lattice depth, 15 E_R and 25 E_R. In all cases, the lifetime is reduced for higher lattice depth, indicating residual optical excitation by the lattice light. Nevertheless, the long lifetimes reflect the fact that the lattice perfectly shields the molecules from inelastic molecule-molecule collisions, which would otherwise limit the lifetime to a few ms at the given molecular densities [24].

5.3 Lattice-based STIRAP transfer

We implement two-photon STIRAP transfer to the deeply bound rovibrational level $|3>=|v=73, J=2>$ of the $^1\Sigma_g^+$ electronic ground state potential in a similar way as in our previous work [5], except that now the molecules are trapped at the individual wells of the optical lattice. In brief, laser L_1 near a wavelength of 1126 nm, driving the transition from $|1>=|s>$ to $|2>$, where $|2>$ is a deeply bound level of the mixed $(A^1\Sigma_u^+ - b^3\Pi_u)\ 0_u^+$ excited states, is pulsed on after laser L_2, which drives the transition from $|3>$ to $|2>$ at 1006 nm, see Fig. 5.1 A. The pulse (or pulse overlap) time τ_p is typically $\tau_p = 10\ \mu$s for the present experiments. A schematic time course for the transition Rabi frequencies is shown in Fig. 5.3 C. We estimate the peak Rabi frequencies to be $2\pi \times 3$ MHz for the transition at 1126 nm and $2\pi \times 6$ MHz for the transition at 1006 nm [5]. After a variable hold time τ_h, we reverse the pulse sequence to transfer the molecules back to $|s>$. For short τ_h below 40 μs we typically leave L_1 on between the two STIRAP pulse sequences. For longer τ_h we switch L_1 off to avoid any residual optical excitation of molecules in $|v=73, J=2>$ and possible effects of dipole forces generated by the tightly focused laser beam L_1.

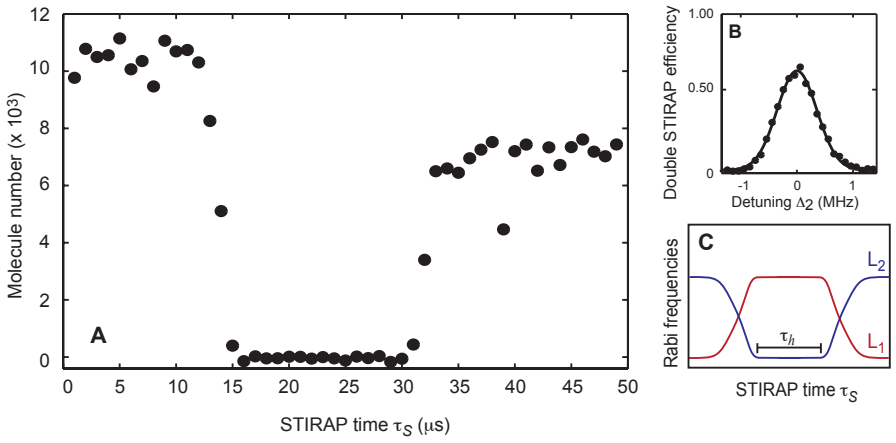

Figure 5.3: STIRAP transfer from the weakly bound state $|1>=|s>$ to the deeply bound rovibrational level $|3>=|v=73, J=2>$ and back to $|1>$ in the optical lattice. **A** shows the number of molecules in state $|1>$ as a function of STIRAP time τ_S for both lasers on resonance (laser detunings $\Delta_1 \approx 0 \approx \Delta_2$). The measured pulse overlap begins at about 5 μs and ends at about 15 μs. The second pulse overlap starts at 30 μs and ends at about 38 μs. The lattice depth is 15 E_R. Data points represent a single experimental realization, not an average over several runs. The data point at 39 μs represents a "bad shot", which occasionally occurs. **B** Double STIRAP efficiency as a function of the detuning Δ_2 of laser L_2 for $\Delta_1 \approx 0$. The solid line is a Gaussian fit with a full width at half maximum of 830 kHz. **C** schematically shows the timing for the Rabi frequencies, Ω_i, $i = 1, 2$, for lasers L_1 and L_2 during the double STIRAP sequence. For short hold times $\tau_h < 40\ \mu$s laser L_1 is left on after the first STIRAP sequence as shown here. For longer hold times $\tau_h > 40\ \mu$s we shut off L_1 to avoid possible optical excitation.

The result of double STIRAP transfer in the optical lattice is shown in Fig. 5.3 A. Here, $\tau_p = 10\ \mu$s and $\tau_h = 15\ \mu$s. As in our previous work [5], we interrupt the transfer after a given STIRAP time τ_S and record the number of molecules in the initial state $|s>$. The molecules first disappear, and then a sizable fraction of about 65% returns after the reverse STIRAP transfer. Thus, as in our previous work [5], the single pass efficiency is about 80% when both lasers are on resonance. Fig. 5.3 B shows the double STIRAP transfer efficiency as a function of the detuning Δ_2 of laser L_2 from the excited intermediate level while laser L_1 is held on resonance (detuning $\Delta_1 \approx 0$). A Gaussian fit yields a full width at half maximum of 830 kHz. With τ_p so short, we do not resolve molecular hyperfine structure in $|v=73, J=2>$.

We find that the molecules transferred to $|v=73, J=2>$ are trapped at the individual wells of the lattice. The $1/e$-lifetime is about 19 ms for a lattice depth of 15 E_R. This is much shorter than the lifetime of Feshbach molecules as shown above, but sufficiently long to allow future implementation of a second lattice-based STIRAP step to the rovibronic ground state $|v=0, J=0>$, for which the lifetime is expected to be much longer as discussed below. We determine the lifetime by repeating the double STIRAP transfer while increasing the hold time τ_h in steps of 3.5 ms. The result is shown in Fig. 5.2 D. The number of molecules can be well fit by an exponentially decaying function as a function of τ_h. For a higher lattice depth of 25 E_R, the lifetime is reduced to 15 ms. We thus attribute the reduced molecular lifetime to off-resonant scattering of lattice light, exciting the molecules to levels of the $(A^1\Sigma_u^+ - b^3\Pi_u)\ 0_u^+$ states, which then in turn leads to loss into other ground state rovibrational levels that we do not detect. Note that in the wavelength region of our trapping laser, the lifetime is expected to show strong variations as a function of trapping laser wavelength due to the presence of excited state levels. Hence, also the polarizability as discussed in the next section should strongly depend on the wavelength of the laser generating the lattice light.

5.4 Determination of molecule trapping parameters

We determine the molecular trapping frequency $\omega_{|v=73>}$ for molecules in $|v=73, J=2>$ by modulating the lattice phase and, alternatively, by modulating the lattice amplitude. In the first case, we primarily excite transitions from the lowest band in the lattice to the first excited band and then to higher bands. In the second case, we primarily excite into the second excited band and then to higher bands. For sufficiently strong modulation, molecules are lost from the lattice, as tunneling to neighboring sites and hence inelastic collisions with neighboring molecules become more probable. We thus expect to detect increased molecular loss if the modulation frequency is tuned into resonance with the inter-band transitions. The results are shown in Fig. 5.4. At a lattice depth of 15 E_R, we observe resonant loss at 5.2 kHz in the case of phase modulation and at 10.1 kHz in the case of amplitude modulation of the lattice. Phase modulation at 22 E_R and amplitude modulation at 20 E_R yield resonances at 6.5 kHz and 12.2 kHz, respectively. These values for different trap depths are consistent with

each other when compared with a calculation of the band structure. For comparison, to determine the trapping frequency ω_F of the Feshbach molecules in level $|g>$, we measure that phase modulation (amplitude modulation) of a 15 E_R deep lattice leads to loss at a modulation frequency of 9.4 kHz (18.4 kHz). Relating the dynamical polarizability $\alpha_{|v=73>}$ of the deeply bound molecules in $|v = 73 >$ to the dynamical polarizability α_F of the Feshbach molecules via $\alpha_{|v=73>}/\alpha_F = \omega^2_{|v=73>}/\omega^2_F$, we obtain that the molecular polarizability in $|v=73, J=2>$ is $\sim 30\%$ of the polarizability of the Feshbach molecules at the wavelength of our trapping light.

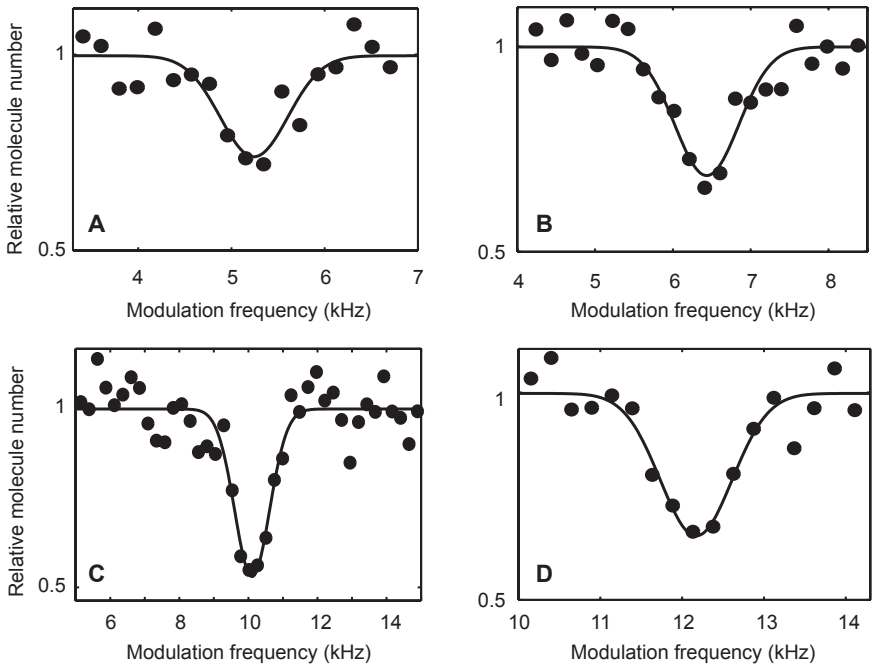

Figure 5.4: Trapping of deeply bound molecules in the wells of the optical lattice. While the molecules reside in level $|3>= |v = 73, J = 2>$, one of the lattice beams of the 3 dimensional optical lattice is either phase modulated (**A** and **B**) or amplitude modulated (**C** and **D**). As the frequency of the phase or amplitude modulation is scanned, a series of resonances due to transfer to higher bands arise, reflected in a decrease in molecule number. The respective resonances at the lowest modulation frequency are shown here. For phase modulation ("shaking" of the lattice), this corresponds to the first lattice band, for amplitude modulation to the second band. To determine the center frequency, the resonances are fit by a Gaussian. The lattice depth is 15 E_R, 22 E_R, 15 E_R, and 20 E_R in **A**, **B**, **C**, and **D**, respectively.

5.5 Conclusion

We have transferred an ultracold sample of Cs_2 molecules to the deeply bound rovibrational level $|v=73, J=2>$ of the singlet $X^1\Sigma_g^+$ potential in the presence of an optical

lattice. We essentially find the same transfer efficiency as in our previous work [5] where no lattice was used. The transferred molecules are trapped, and we have determined their polarizability in this particular level. The trapping time is sufficiently long to allow for subsequent lattice-based STIRAP transfer to the rovibronic ground state $|v = 0, J = 0>$ by means of a second two-photon transition [6]. A lower bound for the STIRAP pulse time and hence for the minimal required trapping time is set by the time needed to resolve the molecular hyperfine structure. This minimal time is the inverse of three times the ground state hyperfine coupling constant $c_4 \approx 14$ kHz [4], giving 24 μs. Hence a compromise can easily be found between Fourier-resolving the molecular hyperfine structure and keeping the STIRAP pulse time sufficiently short in view of finite laser coherence time and finite trapping time. Note that for optimum transfer efficiency also the hyperfine structure of the intermediate state needs to be resolved, which requires longer STIRAP times also for the first transfer step.

For Cs_2 molecules in the rovibronic ground state $|v = 0, J = 0>$ we expect much longer trapping times in the lattice as optical excitation at 1064.5 nm into excited molecular states can only occur in a far off-resonant process. At this wavelength transitions to the $(A^1\Sigma_u^+ - b^3\Pi_u)\ 0_u^+$ states are relevant. These are possible only to levels that have a sizable singlet contribution stemming from the $A^1\Sigma_u^+$ state. 0_u^+ levels below the minimum of the $A^1\Sigma_u^+$ state, corresponding to a wavelength of ~ 1041 nm as measured from the rovibronic ground state [26], have little singlet component and hence these transitions are strongly suppressed. We thus expect the formation of a stable molecular quantum gas in $|v = 0, J = 0>$ when the lattice depth is lowered and the molecules are released into a larger-volume optical dipole trap, possibly allowing the observation of Bose-Einstein condensation of ground state molecules.

Our technique can readily be applied to other molecular systems, e.g. heteronuclear dimers such as RbCs [27] and KRb [9]. These dimers carry a sizable electric dipole moment. In the presence of the lattice, one should thus be able to exploit the long range nature of the dipole-dipole interaction and be able to prepare interesting novel quantum phases with nearest-neighbor interaction [28,29].

Acknowledgements

We are indebted to R. Grimm for generous support and we thank S. Knoop, N. Boloufa, and O. Dulieu for valuable discussions. We gratefully acknowledge funding by the Austrian Ministry of Science and Research (BMWF) and the Austrian Science Fund (FWF) in form of a START prize grant. R.H. acknowledges support by the European Union in form of a Marie-Curie International Incoming Fellowship (IIF).

References

1. Jochim S, Bartenstein M, Altmeyer A, Hendl G, Riedl S, Chin C, Hecker Denschlag J and Grimm R 2003 *Science* **302** 2101

2. Greiner M, Regal C A and Jin D S 2003 *Nature* **426** 537

3. For an overview, see: Ultracold Fermi Gases, *Proceedings of the International School of Physics Enrico Fermi, Course CLXIV*, edited by Inguscio M, Ketterle W and Salomon C (IOS Press, Amsterdam, 2008)

4. Aldegunde J and Hutson J M 2008, preprint at arXiv:0810.4709

5. Danzl J G, Haller E, Gustavsson M, Mark M J, Hart R, Bouloufa N, Dulieu O, Ritsch H and Nägerl H-C 2008 *Science* **321** 1062, published online 10 July 2008; 10.1126/science.1159909

6. Mark M J, Danzl J G, Haller E, Gustavsson M, Bouloufa N, Dulieu O, Salami H, Bergeman T, Ritsch H, Hart R and Nägerl H-C 2008, published online February 19 2009, *Appl Phys B* DOI 10.1007/s00340-009-3407-1

7. Danzl J G, Mark M J, Haller E, Gustavsson M, Bouloufa N, Dulieu O, Ritsch H, Hart R and Nägerl H C 2008 manuscript submitted for publication, preprint at arXiv:0811.2374

8. Winkler K, Lang F, Thalhammer G, Straten P v d, Grimm R and Hecker Denschlag J 2007 *Phys. Rev. Lett.* **98** 043201

9. Ni K-K, Ospelkaus S, de Miranda M H G, Peer A, Neyenhuis B, Zirbel J J, Kotochigova S, Julienne P S, Jin D S and Ye J 2008 *Science* **322** 231

10. Lang F, Winkler K, Strauss C, Grimm R and Hecker Denschlag J 2008 *Phys. Rev. Lett.* **101** 133005

11. Volz T, Syassen N, Bauer D M, Hansis E, Dürr S, Rempe G 2006 *Nature Physics* **2** 692

12. Dürr S 2008 private communication.

13. Jaksch D, Venturi V, Cirac J I, Williams C J, and Zoller P 2002 *Phys. Rev. Lett.* **89** 040402

14. Bergmann K, Theuer H and Shore B W 1998 *Rev. Mod. Phys.* **70** 1003

15. Weber T, Herbig J, Mark M, Nägerl H-C and Grimm R 2003 *Science* **299** 232

16. Kraemer T, Mark M, Waldburger P, Danzl J G, Chin C, Engeser B, Lange A D, Pilch K, Jaakkola A, Nägerl H-C and Grimm R 2006 *Nature* **440** 315

17. Greiner M, Mandel O, Esslinger T, Hänsch T W and Bloch I 2002 *Nature* **415** 39

18. Liem A, Limpert J, Zellmer H, Tünnermann A 2003 *Opt. Lett.* **28** 1537

19. Hansis E 2006, diploma thesis, Technische Universität München, unpublished

20. Regal C A, Ticknor C, Bohn J L and Jin D S 2003 *Nature* **424** 47

21. Herbig J, Kraemer T, Mark M, Weber T, Chin C, Nägerl H-C and Grimm R 2003 *Science* **301** 1510, published online 21 August 2003; 10.1126/science.1088876

22. Köhler T, Góral K and Julienne P S 2006 *Rev. Mod. Phys.* **78** 1311

23. Mark M, Ferlaino F, Knoop S, Danzl J G, Kraemer T, Chin C, Nägerl H-C and Grimm R 2007 *Phys. Rev. A* **76** 042514

24. Thalhammer G, Winkler K, Lang F, Schmid S, Grimm R and Hecker Denschlag J 2006 *Phys. Rev. Lett.* **96** 050402

25. Chin C, Vuletic V, Kerman A J, Chu S, Tiesinga E, Leo P J and Williams C J 2004 *Phys. Rev. A* **70** 2032701

26. Vergès J and Amiot C 1987 *Journal of Molecular Spectroscopy* **126** 393

27. Pilch K, Lange A D, Prantner A, Kerner G, Ferlaino F, Nägerl H-C and Grimm R 2008 manuscript submitted for publication, preprint at arXiv:0812.3287

28. Góral K, Santos L and Lewenstein M 2002 *Phys. Rev. Lett.* **88** 170406

29. Wall M L and Carr L D 2008 manuscript submitted for publication, preprint at arXiv:0812.1548

Chapter 6

Publication: An ultracold high-density sample of rovibronic ground-state molecules in an optical lattice

Nature Physics
advance online publication 21 February 2010
DOI: 10.1038/NPHYS1533

This paper** reports on the first realization of an ultracold sample of rovibronic ground-state molecules in an optical lattice. Each molecule is trapped in the motional ground state of an individual lattice site with a high lattice filling factor. The molecules reside in a precisely defined hyperfine sublevel of the rovibronic ground state. Hence, all quantum degrees of freedom of the molecules are controlled at the level of single quantum states.

We load a BEC of Cs atoms into an optical lattice and drive the superfluid-to-Mott-insulator transition under conditions that maximize the size of the 2-atom Mott shell [Blo08]. Hence, in the central region of the lattice, each lattice site is filled with exactly n=2 atoms. Similar to the experiments in Ref. [Vol06] we come close to the theoretical limit of 53% of all atoms loaded into doubly occupied sites. Following Feshbach association and removal of unpaired atoms, about 85% of lattice sites are occupied by a Feshbach molecule in the desired starting state for coherent optical transfer. The Feshbach molecules reside in the motional ground state of the lattice potential. These are then transferred either in a single 4-photon STIRAP step or in two consecutive two-photon STIRAP steps to the rovibronic ground state. As discussed in chapter 2, in Cs_2, a homonuclear molecule, a 4-photon scheme is preferred over a single two-photon step in order to overcome prohibitively low Franck-Condon factors. It is ensured that the transfer goes selectively to one particular hyperfine sublevel of the rovibronic ground state [Ald09] by angular momentum conservation rules. For molecular quantum gas studies, control of the hyperfine degree of freedom is of essential importance. In order to maximize phase-space density, all particles need to reside in the same internal

**The author of the present thesis developed the strategy for transfer to the rovibronic ground-state together with H.-C. N.. He built the STIRAP laser system and frequency comb setup. He designed and performed all the experiments with support from M. J. M., E. H., and R. H. and he analyzed the data. The calculations of molecular hyperfine structure were provided by J. A. and J. M. H.. The calculation of the lattice band structure were performed by M. J. M. and M. G. and M. J. M. analyzed the polarizability data together with J. G. D.. The paper was written by J. G. D. and H.-C. N. with input from all authors. Here, the final accepted version is given before the copy-editing process of the journal.

quantum state. For collisional experiments in the quantum regime, control of the hyperfine state is indispensable. Also in the KRb experiments, the hyperfine state of the rovibronic ground-state molecules can be controlled [Osp10a].

In contrast to the work on Rb_2 triplet molecules [Lan08b, Lan09b], motional state control in the lattice is maintained during the STIRAP process in the experiments on Cs_2. The optical lattice is operated close to a magic wavelength [Ye08], which gives equal light shifts [Gri00] for the initial Feshbach level and the rovibronic ground state. At the magic wavelength, the dynamical polarizabilities of the initial and the final molecular levels [Bou10] are matched. Hence, the lattice depths for the Feshbach molecules and for the $|v = 0>$-molecules, and therefore the shapes of the motional wave functions in the lowest lattice vibrational level, are almost identical. STIRAP, which is almost instantaneous on the timescale of the external motion, then projects the motional wavefunction associated with the Feshbach molecules in the lowest lattice vibrational level almost perfectly onto the motional wavefunction associated with the lowest lattice vibrational level for $|v=0>$-molecules. An independent test based on time-of-flight absorption imaging that yields information about the momentum distribution of the molecules confirmed that the ground-state molecules do indeed reside in the motional ground state of the lattice. It will be interesting to see in future theoretical and experimental studies whether and how the molecular polarizability depends on the rotational and hyperfine quantum numbers and the respective projection quantum numbers.

For any practical application, the lifetime of the sample has to be sufficiently long. We observe a very long lifetime of 8 s for the lattice-trapped sample of rovibronic ground-state molecules.

The most obvious possibility to transfer population from the Feshbach state to the rovibronic ground state in a 4-photon scheme is to first transfer the population to the intermediate ground state level $|v=73>$ in two-photon STIRAP and then in a second two-photon step further on to the rovibronic ground state. Malinovski and Tannor proposed a so-called "straddle" scheme for STIRAP in multilevel systems [Mal97]. This involved a counterintuitive pulse sequence for the first and last lasers and longer pulses spanning those with the inner lasers. As was then shown, all intermediate levels can be continuously coupled by constant and strong laser fields to yield an effective intermediate level [Vit98]. Only the first and the last laser deliver time-dependent delayed pulses similar to the classical three-level case. When the Rabi frequencies on the inner transitions are much higher than the Rabi frequencies of the first and last transition, population can be avoided not only in the intermediate excited state levels but also in the intermediate ground-state level. Therefore, the properties of the intermediate ground-state level become largely unimportant. A recent paper gives a theoretical analysis of straddle STIRAP in the context of ultracold molecules [Kuz08].

An ultracold, high-density sample of rovibronic ground-state molecules in an optical lattice

Johann G. Danzl[1*], Manfred J. Mark[1], Elmar Haller[1], Mattias Gustavsson[1], Russell Hart[1], Jesus Aldegunde[2], Jeremy M. Hutson[2] & Hanns-Christoph Nägerl[1*]

[1]Institut für Experimentalphysik und Zentrum für Quantenphysik, Universität Innsbruck, Technikerstraße 25, A–6020 Innsbruck, Austria

[2]Department of Chemistry, University of Durham, South Road, Durham, DH1 3LE, England

[*]e-mail: johann.danzl@uibk.ac.at; christoph.naegerl@uibk.ac.at

Control over all internal and external degrees of freedom of molecules at the level of single quantum states will enable a series of fundamental studies in physics and chemistry[1,2]. In particular, samples of ground-state molecules at ultralow temperatures and high number densities will allow novel quantum-gas studies[3] and future applications in quantum information science[4]. However, high phase-space densities for molecular samples are not readily attainable as efficient cooling techniques such as laser cooling are lacking. Here we produce an ultracold and dense sample of molecules in a single hyperfine level of the rovibronic ground state with each molecule individually trapped in the motional ground state of an optical lattice well. Starting from a zero-temperature atomic Mott-insulator state[5] with optimized double-site occupancy[6], weakly-bound dimer molecules are efficiently associated on a Feshbach resonance[7] and subsequently transferred to the rovibronic ground state by a stimulated four-photon process with >50% efficiency. The molecules are trapped in the lattice and have a lifetime of 8 s. Our results present a crucial step towards Bose-Einstein condensation of ground-state molecules and, when suitably generalized to polar heteronuclear molecules, the realization of dipolar quantum-gas phases in optical lattices[8,9,10].

Recent years have seen spectacular advances in the field of atomic quantum gases. Ultracold atomic samples have been loaded into optical lattice potentials, allowing the realization of strongly-correlated many-body systems and enabling the direct observation of quantum phase transitions with full control over the entire parameter space[5]. Molecules with their increased complexity are expected to play a crucial role in future generation quantum gas studies. For example, the long-range dipole-dipole force

between polar molecules gives rise to nearest-neighbour and next-nearest-neighbour interaction terms in the extended Bose-Hubbard Hamiltonian and should thus lead to novel many-body states in optical lattices in the form of striped, checkerboard, and supersolid phases[8,9,10].

An important prerequisite for all proposed molecular quantum gas experiments is the capability to fully control all internal and external quantum degrees of freedom of the molecules. For radiative and collisional stability, the molecules need to be prepared in their rovibronic ground state, i.e. the lowest vibrational and rotational level of the lowest electronic state, and preferably in its energetically lowest hyperfine sublevel. As a starting point for the realization of novel quantum phases, the molecular ensemble should be in the ground state of the many-body system. Such state control is only possible at ultralow temperatures and sufficiently high particle densities. While versatile non-optical cooling and slowing techniques have recently been developed for molecular ensembles[11] and photo-association experiments with atoms in magneto-optical traps have reached the rovibrational ground state[1], the achievable molecular phase-space densities are still far away from the point of quantum degeneracy. Here, we exploit the fact that high phase-space densities can readily be achieved for atoms and that atoms can efficiently be associated on Feshbach resonances to form molecules[7] with minimal loss of phase-space density when an optical lattice is present. Subsequent state transfer to a specific hyperfine sublevel of the rovibronic ground state by means of a stimulated multi-photon process then preserves phase-space density and hence the quantum-gas character of the molecular ensemble. This approach is expected to allow the preparation of a molecular ground-state BEC[12]. Note that some loss of phase-space density can be tolerated if the collisional properties of the ground-state molecules, a priori unknown, turn out to be sufficiently favorable to allow for a final stage of evaporative cooling or, alternatively, sympathetic cooling with atoms.

A crucial ingredient for our experiments is the presence of an optical lattice. It provides full control over the motional wave function and prevents collisional loss. It allows us in particular to maximize the efficiency for initial molecule production and the efficiency for ground-state transfer. For sufficiently high efficiency, a molecular Mott-insulator state is approximated by this preparation procedure[12], providing an excellent starting point for the precision measurements[13,14] and many-body and quantum information experiments[8,9,10] envisioned with ground-state molecules. In the quantum gas regime without the use of an optical lattice, molecular state transfer to deeply-bound rovibrational levels of the singlet $^1\Sigma$ ground-state potential has recently been implemented for Cs_2[15] and KRb[16]. For KRb, the rovibronic ground state was reached, resulting in a near-quantum-degenerate gas of fermionic ground-state molecules[16]. Transfer of molecules in the presence of an optical lattice has been implemented for Rb_2 molecules[17], and the lowest rovibrational level of the shallow triplet $a^3\Sigma_u^+$ potential was reached[18].

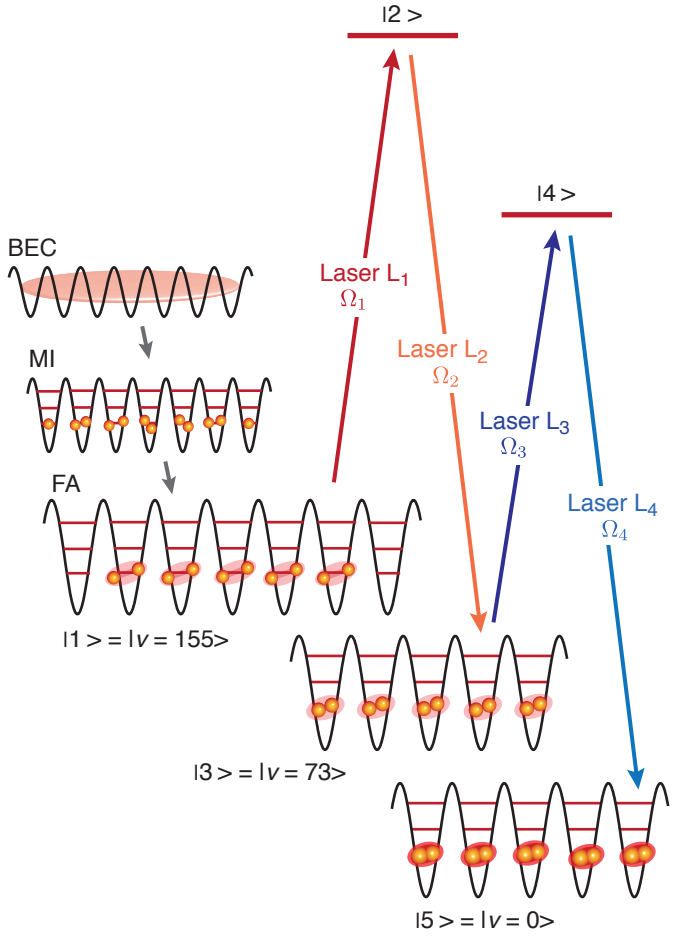

Figure 6.1: **Molecular quantum gas preparation procedure.** A BEC of Cs atoms is loaded into an optical lattice. By increasing the lattice depth, a Mott-insulator state (MI) with preferentially two atoms per site is created. Feshbach association (FA) subsequently converts atom pairs into weakly-bound molecules in state |1>. These are then transferred in the presence of the lattice to a specific hyperfine level $|I=6, M_I=6>$ of the rovibronic ground state $|5> = X^1\Sigma_g^+$ $|v=0, J=0>$ by a stimulated four-photon process (STIRAP) involving lasers L_i with Rabi frequencies Ω_i $i = 1, 2, 3, 4$, and three intermediate levels |2>, |3>, and |4>.

Our molecular quantum-gas preparation procedure is summarized in Fig. 6.1. We load a BEC of Cs atoms[19] into a three-dimensional optical lattice and drive the superfluid-to-Mott-insulator phase transition[5]. The atomic number distribution in the Mott-insulator state is inhomogeneous as a result of the external harmonic confinement. Shells with a constant number of precisely n atoms per lattice site, where $n = 1, 2, 3\ldots$, are separated by narrow superfluid regions[5]. We aim to maximize the size of the two-atom Mott shell in the central region of the lattice in order to obtain the highest number of lattice sites at which there are precisely two atoms (see the

Methods section). With up to 45(2)% of the atoms at doubly-occupied lattice sites we come close to the theoretical limit of 53% given the parabolic density profile of the BEC[6]. The atom pairs reside in the motional ground state at each well and are then associated[20] with 94(1)% probability to Cs_2 Feshbach molecules, which are subsequently transferred to the weakly-bound level $|1>$, the starting level for the optical transfer (see the Methods section)[21,15,22]. Atoms at singly-occupied sites are removed by a combination of microwave and optical excitation[20]. We now have a pure molecular sample with a high occupation of about 85(3)% in the central region of the lattice (see the Methods section). Each molecule is in the motional ground state of its respective well and perfectly shielded from collisional loss.

We employ stimulated Raman adiabatic passage (STIRAP)[23] involving four laser transitions to coherently transfer the molecules into the lowest rovibrational level $|5>=|v=0, J=0>$ of the ground state singlet $X^1\Sigma_g^+$ potential as shown in Fig. 6.2a, bridging a binding energy of $hc\times$ 3628.7 cm^{-1} $\approx h\times$ 109 THz[15]. Here, v and J are the vibrational and rotational quantum numbers, respectively, h is Planck's constant and c is the speed of light. For Cs_2, a homonuclear molecule, the four-photon process is preferred to a direct two-photon process because it allows us to overcome small Franck-Condon overlap. Lasers L_1 through L_4 couple $|1>$ and $|5>$ via three intermediate levels $|2>$,$|3>$, and $|4>$ (see the Methods section). For STIRAP in the presence of the lattice, the lattice light must not impede the transfer through optical excitation or by creating unwanted coherences. Also, the lattice wavelength has to be chosen such that the dynamical polarizabilities for $|1>$ and $|5>$ are closely matched in order to avoid excitation into higher motional states of the lattice as a result of motional wave-function mismatch[18]. We typically set the lattice depth to a value of 20 E_R for atoms, corresponding to 80 $\tilde{E}_R$ for Feshbach molecules with twice the polarizability and double the mass and 83 $\tilde{E}_R$ for molecules in $|v=0>$ at a lattice wavelength of 1064.5 nm, as determined below. Here, E_R ($\tilde{E}_R$) is the atomic (molecular) recoil energy.

Our experimental configuration ensures that only one particular molecular hyperfine sublevel is populated. The atomic BEC is prepared in the lowest hyperfine sublevel $|F_a=3, m_{Fa}=3>$, where F_a and m_{Fa} are the total atomic angular momentum and its projection on the magnetic field. Feshbach association and transfer between Feshbach levels via avoided crossings, as illustrated in Fig. 6.2b (see the Methods section), conserve[7] the total angular momentum projection $M_F = m_{Fa_1} + m_{Fa_2} = 6$. Fig. 6.2c shows the hyperfine structure of the target state, i.e. the rovibronic ground state $X^1\Sigma_g^+$ $|v=0, J=0>$. It splits into 28 hyperfine sublevels in the presence of a weak magnetic field, corresponding to the allowed values of the total nuclear spin $I = 0, 2, 4, 6$ and its $2I+1$ projections M_I for each value of I. The total energy splitting is $\sim h\times 270$ kHz at zero field[24] (see the Methods section). Importantly, there is only a single $M_I = M_F = 6$ sublevel of $|v=0, J=0>$, namely the $|I=6, M_I=6>$ level. This level we selectively populate by exploiting the dipole selection rule $\Delta M_F = 0$ for linear polarization along the axis of quantization. It is the lowest-energy hyperfine sublevel and hence the absolute energy ground state of the Cs dimer for magnetic fields above $\sim$ 13 mT.

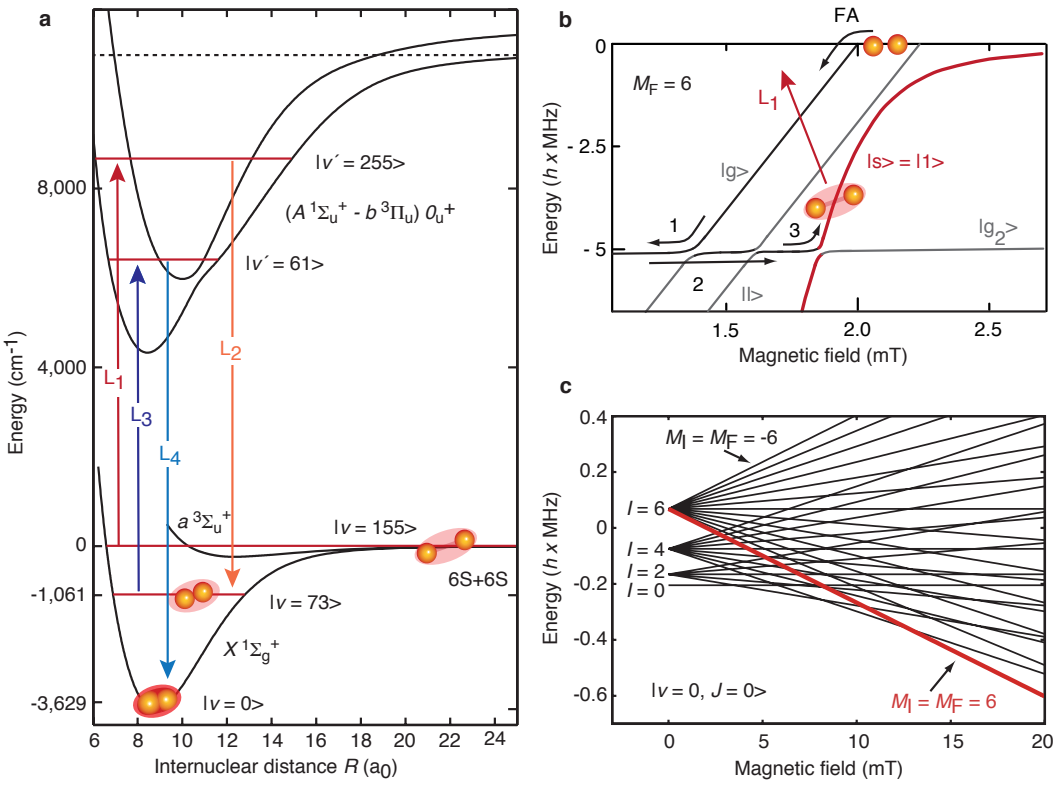

Figure 6.2: **Molecular potentials and level schemes for ground-state transfer. a**, The four-photon transfer from the weakly-bound Feshbach level $|1\rangle = |v \approx 155\rangle$ (not resolved near the 6S+6S asymptote) to the rovibrational ground state $|5\rangle = |v = 0, J = 0\rangle$ of the singlet $X^1\Sigma_g^+$ potential involves the deeply bound level $|3\rangle = |v = 73\rangle$ of the $X^1\Sigma_g^+$ potential[15] and the levels $|2\rangle = |v' = 225, J = 1\rangle$ and $|4\rangle = |v' = 61, J = 1\rangle$ of the electronically excited $(A^1\Sigma_u^+ - b^3\Pi_u)\ 0_u^+$ potentials[30,26]. The laser wavelengths for L_1, L_2, L_3, and L_4 are near 1126 nm, 1006 nm, 1351 nm, and 1003 nm, respectively. **b**, Zeeman diagram for weakly bound molecules near the 6S+6S asymptote. Molecules are associated at a g-wave Feshbach resonance[29] at 1.98 mT (FA) and then transferred to the desired starting level $|1\rangle = |s\rangle$ for optical transfer via three avoided level crossings by slow (arrows 1,3) and fast (arrow 2) magnetic field ramps[21]. The binding energy is given with respect to the $(F_{a_1} = 3, m_{Fa_1} = 3) \times (F_{a_2} = 3, m_{Fa_2} = 3)$ two-atom lowest hyperfine asymptote. All Feshbach levels are characterized by $M_F = 6$. **c**, Calculated Zeeman diagram for the hyperfine manifold of the rovibronic ground state $|5\rangle = |v = 0, J = 0\rangle$. The optical transfer goes selectively to level $|I = 6, M_I = 6\rangle$, indicated in red. This level becomes the lowest-energy absolute ground state for magnetic-field values above $\sim$ 13 mT. There are no avoided crossings between different hyperfine sublevels[24].

There are two possibilities for optical transfer from |1> to |5>. Sequential STIRAP (s-STIRAP) uses two consecutive two-photon STIRAP processes, first from |1> to |3> and then from |3> to |5>. The second scheme generalizes STIRAP[23,17] to the five-level system[25]: Four-photon STIRAP (4p-STIRAP) relies on the existence of a dark state of the form $|D> = (\Omega_2\Omega_4|1> - \Omega_1\Omega_4|3> + \Omega_1\Omega_3|5>)/A$ with time-dependent Rabi frequencies $\Omega_i = \Omega_i(t)$ for lasers L_i, $i = 1, 2, 3, 4$, and the appropriate normalization function $A = A(t)$. Similar to standard two-photon STIRAP, a counter-intuitive pulse sequence rotates the initial state |1> adiabatically into the final state, here |5>. For this, L_2 and L_3 couple the three intermediate levels while L_4 and L_1 deliver time-dependent overlapping pulses with L_4 preceding L_1. Fig. 6.3b and e show the timings for both schemes including the reverse sequence used for detecting the ground-state molecules after a certain hold time τ_h.

We investigate 4p-STIRAP to $|v = 0, J = 0>$ by interrupting the transfer sequence after a given 4p-STIRAP time τ and measuring the number of Feshbach molecules, as shown in Fig. 6.3a. The molecules are transferred to $|5>$ in a single step. No molecules in $|1>$ are detected during τ_h as the remaining Feshbach molecules are cleared by L_1 at the end of the transfer. When the pulse sequence is reversed, a large fraction of the molecules returns to $|1>$. Typically, 30% of the molecules are recovered after the full double 4p-STIRAP sequence. Almost all reside in the lowest band of the lattice as evidenced by band-mapping experiments[5]. The rectangular shape of the first Brillouin zone can be clearly seen in the momentum-space image shown in the lower inset of Fig. 6.3a. 92(3)% of the molecules can be found in the first Brillouin zone and hence had resided in the lowest lattice vibrational level. Assuming equal efficiencies for both transfers, the single-pass efficiency is 55%. The upper inset of Fig. 6.3a shows the double 4p-STIRAP efficiency versus detuning Δ_4 of L_4 from the ($|4> \rightarrow |5>$)-transition with all other lasers on resonance. With ground-state transfer efficiencies between 55% and 60%, about half of the lattice sites are occupied by a ground-state molecule. The solid lines in Fig. 6.3a represent a simulation of 4p-STIRAP that takes into account excited-state spontaneous decay and laser linewidth. Transfer times are typically 4 μs to 10 μs. The simulation yields that the transfer efficiency is currently limited by a combination of laser linewidth, which is about 10 kHz when averaged over 1 s, and imperfect adiabaticity due to finite available laser power to drive the extremely weak transitions of the 5-level scheme[15,26]. Molecules not transferred to $|5>$ as a result of insufficient phase coherence or limited adiabaticity are excited to either $|2>$ or $|4>$ by one of the lasers and are hence pumped into a multitude of rovibrational levels, which do not couple to the rovibrational ground state. For comparison, the double s-STIRAP efficiency from $|3>$ to $|v = 0, J = 0>$ and $|v = 0, J = 2>$ is shown in Fig. 6.3c and d, respectively. The solid lines represent a calculation matched to the data for standard 3-level STIRAP. With 55%-60%, the total ($|1> \rightarrow |5>$)-transfer efficiency for s-STIRAP is comparable to 4p-STIRAP.

A crucial prerequisite for efficient ground-state transfer without heating is good matching of the motional wave functions for the initial weakly-bound state and the final ground state. A mismatch leads to unwanted excitation of higher lattice vibra-

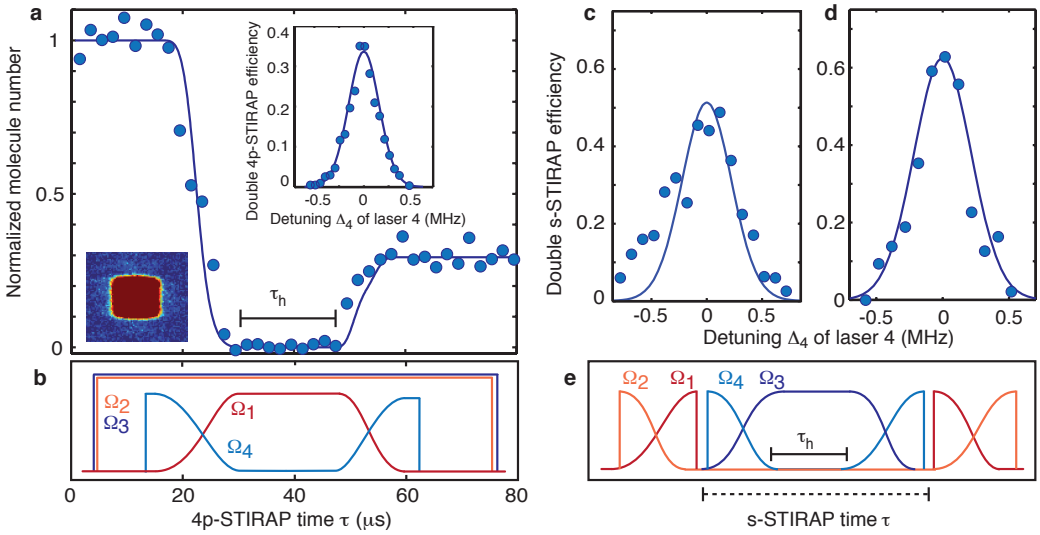

Figure 6.3: **STIRAP transfer to the rovibronic ground state** |5>= $|v=0, J=0>$ **and back. a**, 4p-STIRAP transfer and **b**, schematic timing for the Rabi frequencies Ω_i, $i = 1, 2, 3, 4$: Number of molecules in state |1> as a function of 4p-STIRAP time τ for all 4 lasers on resonance. The lattice depth is 80 $\tilde{E}_R$ and 83 $\tilde{E}_R$ for molecules in levels |1> and |5>, respectively. Data points represent a single experimental realization, not an average over several runs. The solid line is a 4p-STIRAP model calculation. τ_h is the hold time in |5>= $|v=0, J=0>$. Upper inset: double 4p-STIRAP efficiency as a function of the detuning Δ_4 of laser L_4 and corresponding model calculation. The peak corresponds to a single-pass efficiency of 57%. Lower inset: Band mapping of molecules after the double STIRAP sequence. The absorption images corresponding to data points beyond $\tau = 60\ \mu$s are averaged and smoothed with a Gaussian filter. The colour scale is chosen to emphasize any small population in higher bands. **c**, and **d**, s-STIRAP: Double STIRAP efficiency for the inner two-photon STIRAP from |3> to $|v=0, J=0>$ (**c**) and to $|v=0, J=2>$ (**d**) and back, corresponding to the dotted bar in the timing sequence in **e**, as a function of the detuning Δ_4 of laser L_4. The number of molecules is normalized to the initial number in |3>. All measurements are performed at an offset magnetic field of 1.9 mT.

tional levels or bands and hence to loss of state control. The lattice thus has to be operated at the magic wavelength condition[27], i.e. at a wavelength that gives equal light shifts for the initial and the final molecular states. Our experiment in fact shows, as discussed above, that hardly any population is transferred to higher lattice bands. We now measure the lattice band structure and determine the molecular polarizability of the ground-state molecules (see the Methods section). Molecules residing in the lowest band of the lattice are excited to the first (second) band by phase (amplitude) modulation of the light generating the lattice. Fig. 6.4 shows the measured band energies together with a calculation of the band structure as a function of lattice depth. On resonance, excitation to higher bands can readily be observed in momentum space as shown in inset **a**. For comparison, off-resonant modulation transfers hardly any

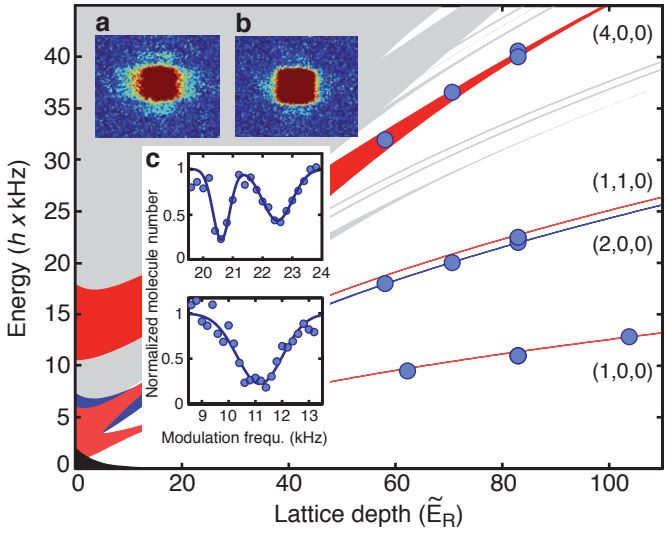

Figure 6.4: **Lattice band structure for $|v = 0>$ molecules.** Band energies as a function of lattice depth in units of the molecular recoil energy $\tilde{E}_R$ as measured by phase and amplitude modulation of the lattice. The lattice bands are labeled by (k, l, m), where k, l, and m give the number of vibrational quanta along the three spatial directions in the limit of a deep lattice. The horizontal position of the data points (filled circles, representing the position of excitation resonances as shown in inset **c**) is given by the molecular polarizability, which is determined by a fit of the data to the band structure. Inset **a** shows the molecular momentum distribution after transfer to higher lattice bands by resonant lattice amplitude modulation. The distribution represents an average of 5 experimental runs, smoothed with a Gaussian filter. For comparison, inset **b** shows that hardly any population is transferred to higher bands for off-resonant modulation. Inset **c** shows typical excitation spectra for amplitude (top) and phase (bottom) modulation at 83 $\tilde{E}_R$. For these, we determine the number of molecules in the first Brillouin zone as a function of the excitation frequency. The solid lines are Gaussian fits. The resonance at 22.5 kHz corresponds to excitation to the nearly-degenerate bands (2,0,0) and (1,1,0) (not resolved). The resonance at 20.6 kHz is a two-phonon excitation to (4,0,0).

population into higher bands (see inset **b**). We determine the band energies by taking modulation spectra as shown in inset **c**. We then use the band structure calculation to fit all measured resonance positions with the molecular dynamical polarizability $P_{|v=0>}$ as the single free parameter. These measurements are done for $|v = 0, J = 2>$. We obtain $P_{|v=0>} = 2.1(1) \times P_a$, where P_a is the atomic polarizability. For the initial, weakly-bound Feshbach molecules in level $|g>$ we obtain $P_{|g>} = 2.0(1) \times P_a$. Hence the magic wavelength condition is well fulfilled.

We measure the lifetime τ_e of the molecules in the lattice by varying the hold time τ_h for up to 20 s and recording the number of remaining molecules as shown in Fig. 6.5. To reduce inelastic light scattering, the lattice depth was adiabatically reduced to about 41.5 $\tilde{E}_R$ after the 4p-STIRAP transfer. An exponential fit gives a $1/e$-lifetime of $\tau_e = 8.1(6)$ s. We attribute this long lifetime to the large detuning $\Delta_L \approx 6.9$ THz

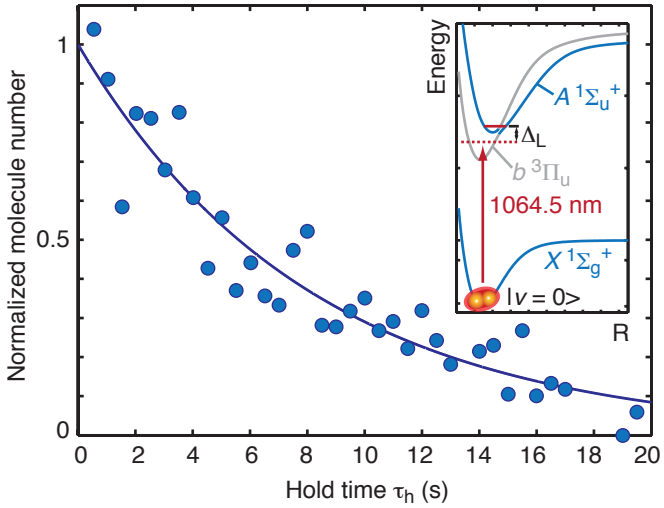

Figure 6.5: **Lifetime of trapped ground-state molecules in the optical lattice.** Normalized number of molecules in $|5\rangle = |v = 0, J = 0\rangle$ as a function of hold time τ_h. The solid line is an exponential fit, yielding a lifetime of 8.1(6)s. The inset schematically shows the excited-state potentials to which off-resonant optical excitation is possible (cf. Fig. 6.2a). Δ_L is the detuning of the lattice light at 1064.5 nm with respect to the lowest 0_u^+ level with $A^1\Sigma_u^+$ character. During the hold time, all STIRAP laser fields are turned off.

from the lowest 0_u^+ level with predominant $A^1\Sigma_u^+$ singlet contribution as shown in the inset to Fig. 6.5. Levels of the 0_u^+ system that lie below this are almost purely of $b^3\Pi_u$ character and thus make negligible contributions to the optical excitation rate.

We are now in a position to determine collisional properties of ultracold ground-state molecules in a fully state-selective way. At magnetic fields beyond 13 mT, where the level $|I = 6, M_I = 6\rangle$ becomes the absolute ground state, the sample should show collisional stability and thus allow the formation of a BEC of ground-state molecules when the lattice is adiabatically removed[12]. For Cs_2, formation of a trimer and an atom in a dimer-dimer collision is predicted to be energetically forbidden (R. Guérout and O. Dulieu, private communication, 2009). The long coherence times and the perfect decoupling from the environment in an optical lattice as demonstrated here will enable a new generation of precision measurements[13,14]. Furthermore, our results can readily be generalized to heteronuclear systems such as KRb[16] and RbCs[28], opening up the possibility to study dipolar quantum phases in optical lattices.

Methods

Lattice loading We first follow the procedure detailed in Ref.[22]. In brief, we produce an atomic BEC with typically 1×10^5 Cs atoms in the lowest hyperfine sublevel $|F_a = 3,\ m_{Fa} = 3\rangle$ in a crossed optical dipole trap. We then drive the superfluid-to-Mott-insulator phase transition[5] by exponentially ramping up the power in a three-

dimensional optical lattice within about 300 ms. The lattice is generated by three mutually-orthogonal, retro-reflected laser beams at a wavelength of $\lambda = 1064.5$ nm, each with a $1/e^2$-waist of about 350 μm. While ramping up the lattice potential, the power in the two dipole-trap beams is increased to ensure that the central density in the trap is sufficiently high to allow formation of atom pairs at the central wells of the lattice, but not too high to lead to triply occupied sites. Atoms at triply occupied sites would rapidly be cleared out by inelastic three-body collisions. We ramp the lattice to a depth of about 20 E_R before Feshbach association. Here, $E_R = h^2/(2m_a\lambda^2) = k_B{\times}64\,\mathrm{nK}$ is the atomic photon-recoil energy with the mass m_a of the Cs atom and Boltzmann's constant k_B. Up to 45(2)% of the atoms reside at doubly occupied lattice sites. We estimate this number from the number of molecules that we obtain and the molecule production efficiency.

For the molecules, the recoil energy is $\tilde{E}_R = h^2/(2 \times 2m_a\lambda^2)$. The polarizability of Feshbach molecules is twice the atomic polarizability. The same lattice that has a depth of 20 E_R for the atoms has thus a depth of 80 $\tilde{E}_R$ for the Feshbach molecules.

Feshbach association and Feshbach state transfer We efficiently produce weakly bound Cs_2 Feshbach molecules in the presence of the optical lattice by a magnetic field sweep[7] across a narrow g-wave Feshbach resonance with its pole at a magnetic field value of $B = 1.98$ mT[29,21]. The molecules are initially in level $|g>$, for which $\ell = 4$. Here, ℓ is the quantum number associated with the mechanical rotation of the nuclei[7]. We subsequently transfer the molecules via level $|g_2>$ with 95(3)% efficiency into level $|s> \equiv |1>$ with $\ell = 0$ by magnetic field ramping[21,22] as shown in Fig. 6.2b. For this level, the transitions to excited molecular levels are stronger than for the initial level $|g>$[30]. We obtain up to 2.5×10^4 Feshbach molecules in the lattice in the desired starting state. Assuming a perfect filling of the two-atom Mott-shell at the center of the trap, taking into account the efficiencies for molecule production and state transfer, and factoring in weak additional loss during sample purification, 85(3)% of the central lattice sites are occupied. We detect the molecules in $|1>$ by reversing the Feshbach state transfer sequence, dissociating the molecules at the Feshbach resonance and detecting the resulting atoms by standard absorption imaging[29].

Molecular states for ground state transfer The relevant molecular states for Cs_2 are shown in Fig. 6.2a. Levels $|2>$ and $|4>$ belong to the coupled $(A^1\Sigma_u^+ - b^3\Pi_u)0_u^+$ potentials[15]. We have recently identified suitable transitions linking $|1>$ to $|5>$, where levels $|2>$, $|3>$, and $|4>$ were chosen to give balanced transition strengths on the four optical transitions[30,26]. For $|3>$ we choose either $|v = 73, J = 2>$ or $|v = 73, J = 0>$ of the $X^1\Sigma_g^+$ ground state with a binding energy of $\sim hc \times 1061\ \mathrm{cm}^{-1}$.

Hyperfine structure of the rovibronic ground state The hyperfine levels are calculated using the molecular constants from Ref. [24] by constructing and diagonalizing a Hamiltonian matrix in an uncoupled basis set of functions representing the molecular

rotation and the spins of the two nuclei, using the matrix elements given in the Appendix of Ref. [24]. For $J = 0$ states the hyperfine structure is dominated by the scalar spin-spin coupling and the nuclear Zeeman effect, but for $J > 0$ additional terms are important.

STIRAP laser setup STIRAP lasers L_i with $i = 1, 2, 3, 4$ are continuous-wave grating-stabilized tunable diode lasers, which are stabilized to optical resonators for short-term stability and referenced to an optical frequency comb for long-term stability and reproducibility. We estimate the linewidth of the lasers to be about 10 kHz. In order to ensure minimum momentum recoil imparted on the molecules, the beams for lasers L_1 and L_2 are co-propagating. The beams for L_3 and L_4 are also co-propagating but run antiparallel to the beams of L_1 and L_2. All beams run horizontally and are linearly polarized with the polarization axis in the vertical direction, parallel to the direction of the magnetic field, which defines the axis of quantization. We operate at Rabi frequencies in the range of $2\pi\times$ (1 to 4) MHz.

Polarizability measurement For determining the ground state molecular polarizability, transfer to $|v = 0>$ is performed at a fixed lattice depth of 83 $\tilde{E}_R$ for $|v = 0>$ molecules. The lattice depth is then ramped to the desired value within 50 ms. For phase modulation of the lattice, the frequency of one lattice beam is usually modulated with a modulation depth of 2 MHz at the desired frequency for about 10 ms. For amplitude modulation, the intensity is typically modulated by 20% for about 10 ms.

References

1. Carr, L. D., DeMille, D., Krems, R. V. & Ye, J. Cold and ultracold molecules: science, technology and applications. *New. J. Phys.* **11,** 055049 (2009).

2. Krems, R. V. Cold controlled chemistry. *Phys. Chem. Chem. Phys.* **10,** 4079 – 4092 (2008).

3. Góral, K., Santos, L. & Lewenstein, M. Quantum phases of dipolar bosons in optical lattices. *Phys. Rev. Lett.* **88,** 170406 (2002).

4. DeMille, D. Quantum computation with trapped polar molecules. *Phys. Rev. Lett.* **88,** 067901 (2002).

5. Bloch, I., Dalibard, J. & Zwerger, W. Many-body physics with ultracold gases. *Rev. Mod. Phys.* **80,** 885–964 (2008).

6. Volz, T. *et al.* Preparation of a quantum state with one molecule at each site of an optical lattice. *Nature Phys.* **2,** 692–695 (2006).

7. Chin, C., Grimm, R., Julienne, P. & Tiesinga, E. Feshbach resonances in ultracold gases. *arXiv* 0812.1496v2 (2008).

8. Baranov, M. A. Theoretical progress in many-body physics with ultracold dipolar gases. *Physics Reports* **464,** 71–111 (2008).

9. Lahaye, T., Menotti, C., Santos, L., Lewenstein, M. & Pfau, T. The physics of dipolar bosonic quantum gases. *Rep. Prog. Phys.* **72,** 126401 (2009).

10. Pupillo, G., Micheli, A., Büchler, H. P. & Zoller, P. Condensed matter physics with cold polar molecules. Ch. *Cold Molecules: Theory, Experiment, Applications* (CRC Press, Boca Raton, 2009).

11. Friedrich, B. & Doyle, J. M. Why are cold molecules so hot? *ChemPhysChem* **10,** 604–623 (2009).

12. Jaksch, D., Venturi, V., Cirac, J. I., Williams, C. J. & Zoller, P. Creation of a molecular condensate by dynamically melting a Mott insulator. *Phys. Rev. Lett.* **89,** 040402 (2002).

13. DeMille, D. *et al.* Enhanced sensitivity to variation of m_e/m_p in molecular spectra. *Phys. Rev. Lett.* **100,** 043202 (2008).

14. Zelevinsky, T., Kotochigova, S. & Ye, J. Precision test of mass-ratio variations with lattice-confined ultracold molecules. *Phys. Rev. Lett.* **100,** 043201 (2008).

15. Danzl, J. G. *et al.* Quantum gas of deeply bound ground state molecules. *Science* **321,** 1062–1066 (2008).

16. Ni, K.-K. *et al.* A high phase-space-density gas of polar molecules. *Science* **322,** 231–235 (2008).

17. Winkler, K. *et al.* Coherent optical transfer of Feshbach molecules to a lower vibrational state. *Phys. Rev. Lett.* **98,** 043201 (2007).

18. Lang, F., Winkler, K., Strauss, C., Grimm, R. & Denschlag, J. H. Ultracold triplet molecules in the rovibrational ground state. *Phys. Rev. Lett.* **101,** 133005 (2008).

19. Kraemer, T. *et al.* Optimized production of a cesium Bose–Einstein condensate. *Appl. Phys. B* **79,** 1013–1019 (2004).

20. Thalhammer, G. *et al.* Long-lived Feshbach molecules in a three-dimensional optical lattice. *Phys. Rev. Lett.* **96,** 050402 (2006).

21. Mark, M. *et al.* Spectroscopy of ultracold trapped cesium Feshbach molecules. *Phys. Rev. A* **76,** 042514 (2007).

22. Danzl, J. G. *et al.* Deeply bound ultracold molecules in an optical lattice. *New J. Phys.* **11,** 055036 (2009).

23. Bergmann, K., Theuer, H. & Shore, B. W. Coherent population transfer among quantum states of atoms and molecules. *Rev. Mod. Phys.* **70,** 1003–1025 (1998).

24. Aldegunde, J. & Hutson, J. M. Hyperfine energy levels of alkali-metal dimers: Ground-state homonuclear molecules in magnetic fields. *Phys. Rev. A* **79,** 013401 (2009).

25. Malinovsky, V. S. & Tannor, D. J. Simple and robust extension of the stimulated Raman adiabatic passage technique to *N*-level systems. *Phys. Rev. A* **56,** 4929–4937 (1997).

26. Mark, M. J. *et al.* Dark resonances for ground-state transfer of molecular quantum gases. *Appl. Phys. B* **95,** 219–225 (2009).

27. Ye, J., Kimble, H. J. & Katori, H. Quantum state engineering and precision metrology using state-insensitive light traps. *Science* **320,** 1734–1738 (2008).

28. Pilch, K. *et al.* Observation of interspecies Feshbach resonances in an ultracold Rb-Cs mixture. *Phys. Rev. A* **79,** 042718 (2009).

29. Herbig, J. *et al.* Preparation of a pure molecular quantum gas. *Science* **301,** 1510–1513 (2003).

30. Danzl, J. G. *et al.* Precision molecular spectroscopy for ground state transfer of molecular quantum gases. *Faraday Discuss.* **142,** 283–295 (2009).

Acknowledgements We thank H. Ritsch, S. Dürr, N. Bouloufa, and O. Dulieu for valuable discussions. We are indebted to R. Grimm for generous support and to H. Häffner for the loan of a charge-coupled camera. We gratefully acknowledge funding by the Austrian Ministry of Science and Research (Bundesministerium für Wissenschaft und Forschung) and the Austrian Science Fund (Fonds zur Förderung der wissenschaftlichen Forschung) in form of a START prize grant and by the European Science Foundation within the framework of the EuroQUASAR collective research project QuDeGPM and within the framework of the EuroQUAM collective research project QuDipMol. R.H. is supported by a Marie Curie International Incoming Fellowship within the 7th European Community Framework Programme.

Author Contributions All authors contributed extensively to the work presented in this paper.

Competing Interests The authors declare that they have no competing financial interests.

Correspondence Correspondence and requests for materials should be addressed to H.-C. N. (email: christoph.naegerl@uibk.ac.at) or to J. G. D. (email: johann.danzl@uibk.ac.at).

Chapter 7

Outlook

7.1 Improved STIRAP efficiency and phase-locked laser system

Our simulations show that the STIRAP transfer efficiency to the rovibronic ground state is currently limited by a combination of laser linewidth [Has88] and limited available laser power to drive the extremely weak transitions in the 4-photon scheme, leading to non-perfect adiabaticity. Increasing the STIRAP efficiency will be important for maximizing the phase-space density for the creation of a BEC of ground-state molecules. Also, when releasing the ground-state molecules from the optical lattice for collisional experiments, it will avoid detrimental collisions with molecules that were nonadiabatically coupled to a bright state and then decayed to various ground-state levels during the STIRAP process. As discussed in the appendix, for the experiments presented in this thesis, the STIRAP lasers were individually locked to independent optical resonators with moderate finesse and the resonators were in turn referenced to an optical frequency comb for long term stability and reproducibility. The relative linewidth of the STIRAP lasers was on the order of 10 kHz. We have recently implemented a new locking scheme with all STIRAP lasers being phase-locked to a common reference laser via the optical frequency comb [Dan10a]. This will allow us to achieve relative linewidths on the order of Hz. There are several different schemes that would allow for narrow relative linewidths of the lasers. One option is to use ultra-high finesse optical resonators to achieve high absolute frequency stability [Ros08]. Diode lasers have been stabilized to optical resonators with sub-Hz linewidths (see e.g. Refs. [Aln08a, Aln08b]). Alternatively, the lasers can be phase-locked via an optical frequency comb. Care has to be taken then that noise contributions from the optical frequency comb are avoided. The comb needs to be stabilized to narrow linewidths or, alternatively, noise contributions from the comb need to be eliminated in the locking scheme. For example, a breathing movement of the comb modes in the frequency domain would lead to noise in the frequency difference of two cw-lasers phase locked to individual comb lines at different wavelengths. An overview over frequency combs and their applications for metrology is given in Ref. [Ye05]. For stabilization of the comb-repetition rate it is advantageous to phase lock one comb line to a highly stable laser in order to avoid a noise multiplication effect when the repetition rate is stabilized at its fundamental. We use an Erbium-fiber based frequency comb. Many of the fiber

combs available show excess noise when compared to Ti:sapphire combs, although fiber combs with narrow linewidths have been demonstrated [Swa06, McF06, Sch08]. One difficulty for tight phase-locking of the carrier-envelope offset phase to a reference is that the achievable feedback bandwidths are limited by a long excited state lifetime of erbium that creates a low pass behavior for feedback via the pump power of the femtosecond oscillator. Interestingly, the noise in the comb is correlated and can be described by an elastic tape model [Tel02]. This allows one to realize a transfer oscillator scheme and to compare frequency ratios of lasers operating at widely different wavelengths without extra noise contributions from the frequency comb [Ste02]. The applicability of this scheme to fiber combs has also been tested [Ben05]. We have implemented phase locking of the STIRAP lasers to a common reference lasers employing the transfer oscillator concept.

The improved phase coherence is expected to increase our STIRAP efficiency. In addition, it will allow us to use longer STIRAP times, improving adiabaticity and reducing Fourier broadening of the STIRAP pulses. The increased frequency resolution will also allow us to selectively address individual hyperfine levels by frequency discrimination in addition to the optical selection rules that we have taken advantage of in our experiments so far. In Cs_2, the total hyperfine splitting at zero magnetic field is only h $\times$ 300 kHz in the rovibronic ground state. In the presence of a weak magnetic field, the rovibronic ground state splits into 28 hyperfine sublevels. Given by the particular Feshbach level we use as a starting state, transfer to $|v = 0>$ has been done at low magnetic fields in contrast to the KRb and Rb_2 work, done at ~50 mT and ~100 mT, respectively [Ni08, Lan08b]. At low magnetic fields, the hyperfine splitting is very small, requiring exquisite frequency resolution to spectroscopically address individual levels. In addition, we will make an effort to elucidate the hyperfine structure of electronically excited levels. Weak coupling to unwanted excited state levels could potentially lead to loss out of our 5-level system. A theoretical study of excited state hyperfine structure is under way [Dul10, Ber10]. A hyperfine splitting for the mixed $(A - b)0_u^+$ states in Na_2 of several hundred MHz has been oberved [Atk82, Kat89], although the splittings might be considerably smaller in Cs_2 [Ber10].

7.2 Direct imaging of ground-state molecules

At present, the detection of rovibronic ground-state molecules is done by reversing the STIRAP pulse sequence, dissociating the Feshbach molecules on a Feshbach resonance and taking an absorption image of the resulting atoms. This detection scheme is adequate for many tasks. However, for a series of experiments it would be advantageous to directly image the ground-state molecules. These include e. g. time-of-flight imaging of the momentum distribution of the ground-state molecules or analysis of collisional experiments. At present, the achievable time-of-flight for ground-state molecules is limited by the small size of our STIRAP laser beams such that upon release from the trap, the molecules quickly fall out of the STIRAP beams and can hence not

be transferred back to the Feshbach state. Direct imaging of ground-state molecules after time-of-flight, yielding information about momentum space, will be instrumental for the detection of molecular Bose-Einstein condensation in the form of a bimodal momentum distribution.

For the study of hyperfine-state changing inelastic collisions in energetically excited hyperfine states, it will be helpful to have both a detection procedure that detects molecules only in the particular hyperfine sublevel that is populated by STIRAP and, alternatively, to have another detection procedure that images the whole population in the rovibronic ground state irrespective of the hyperfine substate. Detection by means of the reverse STIRAP process is completely hyperfine-state selective, whereas direct imaging of ground-state molecules can be designed to detect a series of hyperfine states.

Two of the most appealing options for direct imaging of ground-state molecules are absorption imaging and phase-contrast imaging, both of them being well established techniques in the field of ultracold quantum gases [Ket99]. Absorption imaging of atoms relies on a cycling transition such that many photons are scattered out of a laser beam. In contrast, due to the complex level structure, cycling transitions are, except for a few notable cases, absent in the case of molecules, such that each molecule scatters only one or slightly more than one photons before being lost. However, a very strong molecular transition will yield sufficient signal-to-noise ratio to directly image the ground-state molecules. In Cs_2, and also in other alkali dimers, the lowest vibrational levels of the $B^1\Pi_u$ state offer excellent Franck-Condon overlap with the rovibronic ground state [Bou08] and therefore constitute a natural choice. Absorption imaging for KRb ground-state molecules has recently been successfully implemented [Ye09].

Alternatively, phase-contrast imaging poses a very attractive option to detect ground-state molecules *in situ* in a non-destructive way. An ultracold high-density sample of molecules in an optical lattice will provide enough refractive index change for phase contrast imaging. The ground-state molecules feature number densities that are very similar to the densities in a typical atomic BEC where phase contrast imaging has been successfully applied [Ket99].

7.3 Quantum-state resolved collisional experiments

With the advent of ultracold molecules, where all degrees of freedom are controlled at the quantum level, a new regime of collisional studies will be entered, the fully quantum regime [Car09]. In Cs_2, we will now focus on elucidating the elastic and inelastic scattering properties of rovibronic ground-state molecules. STIRAP transfer goes selectively to one defined hyperfine sublevel, namley the $|I = 6, M_I = 6>$ level, where I and M_I are the molecular nuclear spin and its projection on the magnetic field axis, respectively. At low magnetic field values, this is an energetically excited hyperfine sublevel. At magnetic field values above ~13 mT, the $|I = 6, M_I = 6>$

becomes the lowest energy absolute ground state of the Cs dimer. This level is the molecular analogue of an atomic stretched state and might therefore be stable against inelastic two-body collisions even in the low magnetic field region. More probably, it will relax to some lower lying hyperfine level, most likely with collision rates that are close to the universal reaction rates predicted by quantum defect theory [Idz09]. In the magnetic field region above ~13 mT, where the $|I = 6, M_I = 6>$ level is the lowest energy state, the rovibronic ground-state molecules are expected to exhibit collisional stability. It would be exciting to find collisional resonances similar to magnetically tunable Feshbach resonances. Even though the nuclear magnetic moment that sets the scale for the Zeeman shifts of the rovibronic ground-state molecules is very small, such resonances might still be observable due to the high density of tetramer states below the dimer-dimer threshold.

Experimentally, we will prepare a sample of rovibronic ground-state molecules in the optical lattice where the molecules are initially perfectly shielded from inelastic collisions. We will then ramp the magnetic field to the desired value and release the molecules into an optical dipole trap where collisions can take place.

In order to analyze collisions between molecules in different hyperfine levels, one would need to transfer the population into different hyperfine sublevels. In contrast to heteronuclear molecules [Osp10a], transfer to other hyperfine sublevels with microwave two-photon Raman transitions via rotationally excited levels is not an option in homonuclear molecules. However, it is straight forward to employ coherent optical two-photon transitions, e. g. via a rotationally excited level of a low-lying vibrational level of the $B^1\Pi_u$ state. Given the excellent Franck-Condon overlap and the small energy to be bridged, population transfer with e. g. STIRAP should result in complete population transfer.

7.4 Bose-Einstein condensation of ground-state molecules

If the collisional properties of the rovibronic ground-state molecules turn out to be sufficiently favorable, it should be possible to reach Bose-Einstein condensation of ground-state molecules. One very attractive route to a BEC of ground-state molecules is to prepare a high-density ultracold sample of molecules in an optical lattice and then to adiabatically remove the optical lattice [Jak02]. The lattice increases the Feshbach association efficiency and, as mentioned above, shields the molecules from inelastic collisions. For sufficiently high efficiency, this procedure should directly result in the formation of a Bose-Einstein condensate. Some loss of phase-space density can be tolerated during the molecule production and transfer procedure. This could potentially be compensated for by direct evaporation of the molecules if the elastic collision rates are high enough. Alternatively, sympathetic cooling with atoms might be possible. When both the atoms and the molecules are prepared in the lowest hyperfine

sublevel, inelastic atom-molecule collisions should be suppressed and only three-body loss processes would play a role.

The most important obstacle to the formation of a molecular BEC would be an open channel for a chemical reaction of the type $Cs_2 + Cs_2 \rightarrow Cs_3 + Cs$, i. e. for the formation of a trimer and an atom in a dimer-dimer collision. In Cs_2, this channel is known to be energetically closed, as has been determined from molecular structure calculations [Gué09, Hut09]. The binding energy of two Cs_2 molecules in the rovibronic ground state in is 2×3628.7 cm^{-1} whereas the potential depth for the Cs_3 electronic ground state is ~5437 cm^{-1} [Gué09].

7.5 Precision measurements

Deeply bound vibrational levels of Cs_2 have been identified as an attractive system for precision measurements on the time evolution of fundamental constants [DeM08], specifically for the time evolution of the electron-to-proton mass ratio m_e/m_p. In particular, lattice trapped systems of ultracold molecules hold promise for precision metrology [Ye08, Zel08]. Our STIRAP laser setup is now phase locked to an optical frequency comb, constituting a clockwork for precision measurements [Hal06, Hän06]. However, a detailed analysis of the expected systematic effects still needs to be done. In addition, the complete level structure including hyperfine structure of all involved vibrational levels and a potential effect on the precision measurement has to be elucidated both theoretically and experimentally.

7.6 Extension to heteronuclear molecules

Our results can readily be generalized to the production of samples of heteronuclear ground-state molecules in optical lattices, such as RbCs [Pil09, Sag05], LiCs [Dei08b], or KRb [Ni08]. In order to load one atom of each species into an optical lattice [Osp06] from a doubly-degenerate atomic system, the interspecies scattering length has to be tuned to a value that is smaller than the two intraspecies scattering lengths.

In Innsbruck, we are pursuing the production of rovibronic ground-state molecules of RbCs in the quantum-gas regime. Similar to our work on Cs_2, we have chosen the $(A^1\Sigma^+ - b^3\Pi)$ coupled system [Ber03, Doc09, Lon09, Stw04] as electronically excited intermediate states for STIRAP to the rovibronic ground state, in contrast to the photoassociation work at Yale [Sag05]. Due to a more favorable run of the excited state potentials as compared to homonuclear molecules, STIRAP to $|v = 0>$ can be done in a single two-photon step [Ni08, Stw04]. A sample of polar molecules in an optical lattice will provide an extremely attractive platform for novel quantum gas studies [Gór02, Bar08, Pup09, Lah09].

In contrast to the experiments at JILA with fermionic KRb, the RbCs effort in Innsbruck will produce a sample of bosonic polar molecules. Unlike the KRb case

[Osp10b], where the chemical reaction KRb + KRb $\rightarrow$ K_2 + Rb_2 takes place at a near universal rate [Idz09], reactions of the type RbCs + RbCs $\rightarrow$ Rb_2 + Cs_2 are energetically forbidden. The binding energy of a RbCs molecule in the rovibronic ground state is ~3811 cm^{-1} [Fel99] (for the ^{85}Rb isotope) and the binding energies for the Cs dimer [Dan08, Wei85, Ami02] and the Rb dimer [Tsa97, Set00, Ami90] are ~3629 cm^{-1} and ~3965 cm^{-1}, respectively. Hence, chemical reactions of this type between RbCs molecules are endothermic by about 30 cm^{-1}. Similar to the Cs_2 case, the channel for the formation of a trimer and an atom in a dimer-dimer collision is predicted to be energetically closed in RbCs [Sol10]. The potential depth of the *B* doublet state is around 5636 cm^{-1} for the $RbCs_2$ molecule and around 5883 cm^{-1} for Rb_2Cs. Interestingly, in the case of $RbCs_2$, the *A* doublet state is predicted to be slightly deeper than the *B* state. The *A* doublet state binding energies are 5493 cm^{-1} for Rb_2Cs and 5773 cm^{-1} for $RbCs_2$. In fact, it turns out that inelastic collisions that lead to the formation of an atom and a trimer are energetically forbidden for all alkali metal dimers in the rovibrational ground state of the singlet ground potential [Żuc10].

RbCs is an attractive system for dipolar studies because it offers a high electric dipole moment of around 1.3 Debye [IM86, Aym05, Kot05] combined with a very high mass, yielding a high figure of merit in terms of static polarizability of the molecules [Dei08a].

Chapter 8

A tunable quantum gas in an optical lattice

There are two main thrusts of our experiment that are pursued in parallel: ultracold ground-state molecules and Cs as a quantum gas with tunable interactions in an optical lattice. The efforts to produce ultracold rovibronic ground-state molecules are discussed in detail in the previous chapters. This chapter gives an overview of our experiments on tunable quantum gases.

Interactions play an important role in the field of ultracold quantum gases. Even though particle interactions are not a prerequisite for Bose-Einstein condensation as a statistical mechanics phenomenon, the experimental realization of Bose-Einstein condensation by evaporative cooling and the stability of a BEC crucially depend on the scattering properties. In many instances, the macroscopic matter wave of a BEC can be described by a mean-field treatment in the form of the Gross-Pitaevskii equation [Pit03, Pet02]. In this nonlinear Schrödinger equation, the interaction strength enters in a term that is quadratic in the order parameter. Many of the exciting physics questions that can be addressed with ultracold atoms and BECs, such as particle correlations, are not captured by the Gross-Pitaevskii equation. When a system is confined to low dimensions, quantum correlations and quantum fluctuations are enhanced [Gia04]. Interactions play an important role for gases that are confined to low dimensions and for atoms in optical lattices [Blo08]. Ultracold atoms in deep optical lattices can be described with the Bose-Hubbard Hamiltonian [Jak98]. For the realization of the superfluid-to-Mott insulator quantum phase transition, the relative magnitude of the tunnel coupling J and the interaction energy U on a lattice site has to be tuned. Up to until very recently, most experiments with ultracold atoms in optical lattices have been carried out with a fixed magnitude of the contact interaction given by the scattering length of the atomic species employed. For example, in the pioneering experiments by Greiner and coworkers, the lattice depth was varied in order to observe this phase transition [Gre02]. Quantum phase transitions are driven by quantum fluctuations and hence also take place at zero temperature. As described below, in cesium we have the possibility to control the interaction strength as an important experimental parameter in addition to tuning the strength of the external confinement. With this, we achieve control over the entire parameter space, allowing us to drive the superfluid-to-Mott insulator transition solely by varying the interaction strength. In addition, this system is particularly suited for entering the strongly-correlated regime with atoms confined to low dimensions. In reduced dimensions, new strongly-correlated quantum phases arise, including the Tonks-Girardeau gas, the super-Tonks-Girardeau gas, and, in the

presence of an additional perturbation to the Hamiltonian, a series of insulating phases [Gia04]. In particular, the presence of an arbitrarily weak optical lattice potential commensurate with the atomic granularity allows us to drive a transition from a Tonks-Girardeau gas to a Mott-insulating phase, which is described within the framework of the sine-Gordon model [Büc03].

Interactions cause phase shifts in atom interferometers that can pose limits to the achievable accuracy. Control over the interaction strength also allows us to tune the contact interaction to zero in a matter wave interferometer and to investigate the role of interactions on the interferometer.

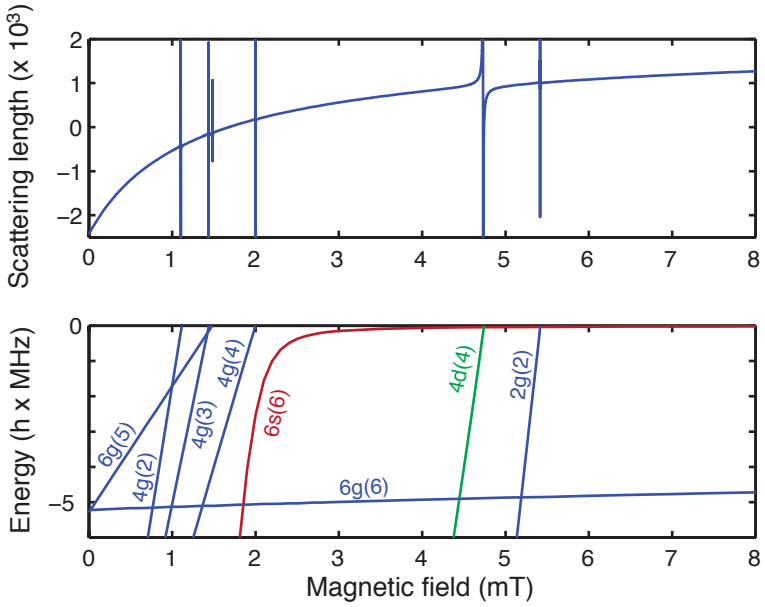

Figure 8.1: **Cesium scattering length and molecular structure near threshold. Top:** Scattering length as a function of magnetic field for two atoms in the lowest hyperfine channel $|F = 3, m_F = 3>$, showing the smoothly tunable scattering length with a zero crossing around 1.7 mT and a series of superimposed narrow Feshbach resonances where the scattering length diverges. **Bottom:** Corresponding molecular structure near threshold. The zero energy corresponds to two free atoms in the lowest hyperfine state $|F = 3, m_F = 3>$. Only levels with a total projection quantum number $M = 6$ are shown.The states are labelled according to $f, \ell, (m_f)$, where f is the quantum number associated with $\vec{f} = \vec{F}_1 + \vec{F}_2$ and m_f its projection [Chi04]. The quantum number associated with the mechanical rotation of the nuclei is ℓ, where $\ell = 0, 2, 4$ for s, d, and g-states, respectively. Only states up to $\ell = 4$ are shown, whereas a series of states with $\ell = 8$ exist in this magnetic field region but do not couple to the dissociation threshold. Where a bound state intersects the dissociation threshold, a Feshbach resonance arises if coupling between the bound state and the scattering state exists. Bound molecular levels are drawn as intersecting lines. In reality, the crossings between bound states are avoided. For the $6s(6)$ state, the very broad avoided crossing between two bare states is taken into account, resulting in a strong curvature of the state as a function of magnetic field. The data was kindly provided by Paul Julienne and Eite Tiesinga.

At ultralow temperatures, scattering is limited to s-wave scattering, characterized by zero angular momentum, $\ell = 0$. The scattering properties can be described by a single parameter, the s-wave scattering length a, irrespective of the short-range details of the interaction potential [Wei99]. In view of the extremely low collisional energies, the atomic hyperfine structure provides precisely defined collisional channels. The scattering length is intricately related to the molecular level structure right below the scattering threshold. For example, in the universal regime of vanishing binding energies, the binding energy of the least bound s-wave molecular state is given by $E_b = \hbar^2/(2\mu(a-\bar{a})^2)$ [Gri93], where $\hbar = h/(2\pi)$, μ is the reduced mass of the atom pair and $\bar{a}$ is the mean scattering length which is given by the range of the van der Waals potential. Fig. 8.1 shows the scattering length and the molecular structure near threshold for the lowest hyperfine scattering channel in Cs. There is an extremely weakly bound s-wave molecular state with a binding energy of a few tens of kHz below the lowest hyperfine asymptote [Chi04]. This state leads to a large background scattering length for Cs atoms in their lowest hyperfine state. There is a very broad avoided crossing with a second s-wave state that belongs to an excited hyperfine channel. The resulting dressed state, denoted $6s(6)$ in the figure, bends over in a Zeeman diagram such that at magnetic fields below ~2 mT, this state acquires more and more binding energy and hence the scattering length is reduced. The pole of the avoided crossing between the bound states is at -1.2 mT, leading to a zero-crossing of the scattering length at a magnetic field of ~1.7 mT. This peculiar level structure leads to a smoothly tunable scattering length at low magnetic fields from ~ -2500 a_0 at zero magnetic field to ~ 1240 a_0 at 7.6 mT. In addition, du to relativistic interactions that are particularly pronounced in the very heavy cesium atom [Chi04], even higher partial-wave molecular states couple to the threshold and lead to narrow Feshbach resonances. In Cs, there is a series of d- and g-wave resonances [Chi04, Mar07a] characterized by $\ell = 2$ and $\ell = 4$, respectively, at low magnetic fields, as can already be deduced from general properties of the van der Waals potential [Gao00].

In our experiments, we take advantage both of the broad tunability of the scattering length, allowing us in particular to set the scattering length to zero, and of the narrow Feshbach resonances that allow us to reach large absolute values of the scattering length beyond 4000 a_0 given the magnetic field control in our experiment. In the work on rovibronic ground-state molecules, we exploit the narrow Feshbach resonances for the formation of Feshbach molecules and the $6s(6)$ state is the starting state for STIRAP. Control over all experimental parameters including interactions is a key ingredient to our experiments.

In a first set of experiments presented in section 8.1, *Control of interaction-induced dephasing of Bloch oscillations*, we study the effects of interactions in a matter wave interferometer. Bloch oscillations arise as a single-particle effect when a particle subject to a constant force is Bragg-reflected from a periodic potential. In our case, the periodic potential is realized by an optical lattice along the vertical direction and the atoms are subject to the gravitational force. We can tune the net force by adjusting a magnetic field gradient that levitates the atoms. In an interacting sample, collisional

phase shifts lead to rapid dephasing of Bloch oscillations and limit the number of observable Bloch cycles to a few. Setting the interaction strength to zero, we were able to observe over 20 000 Bloch cycles, showing that interaction-induced phase shifts can be avoided and that non-interacting BECs can in principle form the basis for high-brightness, high-resolution atom interferometers. Interestingly, with the precision attained is these experiments for the control of the scattering length around zero, the weak dipole-dipole interaction between Cs atoms starts to play a role.

In section 8.2, *Interference of interacting matter waves*, we demonstrate control over the interaction-induced phase shifts in a matter-wave interferometer. We observe a coherent evolution in the matter-wave interferometer in the presence of interactions. By applying an appropriate external potential that compensates the interaction-induced phase shifts, we can prevent dephasing of Bloch oscillations for an interacting BEC. In addition, due to the coherent nature of the interaction-induced phase shifts, the momentum distribution of a dephased sample can be refocused by applying an appropriate external potential. We achieve exquisite momentum resolution in time-of-flight imaging by switching the interactions to zero upon release from the optical lattice and by expanding the sample for >150 ms in the presence of magnetic levitation. A detailed account of the experiments discussed in sections 8.1 and 8.2 is given in the PhD thesis of Mattias Gustavsson [Gus08].

Steep external potentials can be employed to confine atoms to low-dimensional geometries. We create an array of elongated tubes by means of two retroreflected laser beams. The energy scale associated with the transversal confinement is much larger than the energy scale associated with the kinetic and interaction energies of the atomic sample and hence the transversal degrees of freedom are frozen out. For a 1D system with strong repulsive interactions, a dramatic change of the atomic scattering properties is predicted as the *s*-wave scattering length approaches the transversal confinement length [Ols98]. In 3D-geometry, coupling between a molecular bound state and the incoming two-atom channel leads to a Feshbach resonance. In contrast, in 1D-geometry, coupling between the incident two-atom channel and a molecular bound state associated with a transversally excited level of the external confining potential leads to a so-called confinement-induced resonance (CIR).

In section 8.3, we employ the CIR to realize an excited, strongly correlated quantum gas phase, the super-Tonks-Girardeau gas (sTG) [Hal09]. The ground state of a system of strongly repulsively interacting bosons in 1D-geometry is the Tonks-Girardeau gas [Lie63, Gir60] where the particles show strong correlations and acquire many of the properties of fermions. The ground state for a system of attractively interacting bosons in 1D-geometry would be a cluster state that would quickly decay via molecular channels. However, starting from a Tonks-Girardeau gas, an excited quantum phase in the form of the sTG [Ast05] becomes accessible when switching from strong repulsive interactions to strong attractive interactions by crossing a CIR. One amazing propertey of the sTG phase is its metastability, which allows us to experimentally observe it.

In section 8.4, we further study the confinement-induced resonance and generalize

it to the case of asymmetric transversal confinement. We observe that the CIR splits for increasing asymmetry and we investigate its properties in the limiting case of 2D-confinement.

Section 8.5 revisits the topic of Bloch oscillations by investigating the properties of the oscillator under forced driving. In a periodic potential under the influence of a constant force and in the absence of dissipation, Bloch oscillations, but no net transport, arise. We find that a giant movement in position space arises when the force acting on the sample is periodically modulated with a periodicity that is close to the Bloch period. By appropriately choosing the phase of the driving oscillation in the case of resonant driving or switching the sign of the detuning at certain points for off-resonant driving, we can recover transport in this dissipationless system. The experiments presented in sections 8.3, 8.4, and 8.5 will be discussed in more detail in the thesis of Elmar Haller [Hal10].

8.1 Control of interaction-induced dephasing of Bloch oscillations

Phys. Rev. Lett., 29 February 2008:
Vol. 100 pp. 080404
DOI: 10.1103/PhysRevLett.100.080404

M. Gustavsson, E. Haller, M. J. Mark, J. G. Danzl**,
G. Rojas-Kopeinig, H.-C. Nägerl

Institut für Experimentalphysik und Forschungszentrum für Quantenphysik,
Universität Innsbruck,
6020 Innsbruck, Austria

We report on the control of interaction-induced dephasing of Bloch oscillations for an atomic Bose-Einstein condensate in an optical lattice. We quantify the dephasing in terms of the width of the quasi-momentum distribution and measure its dependence on time for different interaction strengths which we control by means of a Feshbach resonance. For minimal interaction, the dephasing time is increased from a few to more than twenty thousand Bloch oscillation periods, allowing us to realize a BEC-based atom interferometer in the non-interacting limit.

Ultracold atomic systems have initiated a revolution in the field of precision measurements. Laser cooled thermal samples are used for ultra-high resolution laser spectroscopy [1], they are at the heart of modern atomic fountain clocks [2,3], and they allow the realization of matter-wave interferometers for high-precision inertial sensing [4] and high-precision determination of fundamental constants [5]. Atomic Bose-Einstein condensates (BEC), the matter-wave analoga to the laser, combine high brightness with narrow spatial and momentum spread. In general, the resolution is limited only by the quantum mechanical uncertainty principle, and BECs could thus serve as ideal sources for precision measurements and in particular for matter wave interferometers [6]. Atom-atom interactions, however, have to be taken into account, as they lead to collisional dephasing and give rise to density dependent mean-field shifts in the interferometric signal. It is thus advisable to either operate a BEC-based atom interferometer in the dilute density limit, possibly sacrificing a high signal-to-noise ratio, or to find ways of reducing or even nulling the strength of the interaction altogether. Precisely the latter is feasible in the vicinity of magnetically induced Feshbach

**The author of the present thesis contributed to this work through experimental support, discussions on physics and technology, and in paper writing. Here, the final accepted version of the paper is given.

resonances where the atomic s-wave scattering length and hence the strength of the atom-atom contact interaction go through a zero crossing [7]. It is thus possible to experimentally investigate the reduction and even disappearance of interaction-induced effects on the interferometric signal as the scattering length is tuned towards zero by means of an externally controlled magnetic field.

A paradigm atom interferometric effect is the well-known phenomenon of Bloch oscillations [8]. Bloch oscillations for the mean quasi-momentum are the result of single atom interference as the atomic wavepacket, subject to a constant force, is Bragg reflected in the presence of a periodic optical lattice potential. They have been observed for ultracold thermal samples [8,9,5,10], for atoms in interacting BECs [11,12], and for ensembles of non-interacting quantum-degenerate fermions [12]. For the case of the interacting BEC, strong dephasing is found as evidenced by a rapid broadening and apparent smearing out of the momentum distribution in the first Brillouin zone, limiting the observation of Bloch oscillations to a few cycles for typical atomic densities in a BEC. In addition, the measured initial width of the momentum distribution is comparable to the extent of the Brillouin zone, as interaction energy is converted into kinetic energy upon release of the BEC from the lattice potential, thus greatly reducing the contrast of the oscillations [12].

In this Letter, we report on the control of interaction induced dephasing of Bloch oscillations for a BEC in a vertically oriented optical lattice under the influence of gravity. Control is obtained by means of a zero crossing for the atomic *s*-wave scattering length a. We observe the transition from an interacting BEC to a non-interacting BEC by measuring the rate of dephasing, given by the change of the width of the momentum distribution, as a function of a. We identify a clear minimum for the dephasing which we associate with the zero crossing for a. At the minimum more than 2×10^4 oscillations can be observed with high contrast, and the zero crossing can be determined with high precision. For our measurements at non-zero scattering length, we greatly reduce broadening of the momentum distribution by rapidly switching the interaction strength to zero upon release from the lattice potential. Our measurements indicate that BECs can indeed be used as a source for precision atom interferometry, as effects of the interaction can be greatly reduced. For a non-interacting BEC, we intentionally induce dephasing by means of a weak optical force gradient and observe collapse and revivals of Bloch oscillations.

The starting point for our experiments is an essentially pure BEC with typically 1×10^5 Cs atoms in the $|F=3,m_F=3\rangle$ hyperfine ground state sublevel confined in a crossed-beam dipole trap generated by one vertically (L_1, with $1/e^2$-beam diameter 256 μm) and one more tightly focused horizontally (L_2, with diameter 84 μm) propagating laser beam at a wavelength near 1064 nm. We support the optical trapping by magnetic levitation against gravity [13]. For BEC preparation, we basically follow the procedure described in Ref. [13,14]. The strength of the interaction can be tuned by means of a broad Feshbach resonance with a pole at -11.7 G. The resonance causes a zero crossing for the scattering length a near an offset magnetic field value of 17 G with a slope of 61 a_0/G [15]. Here, a_0 denotes Bohr's radius. The lattice potential is

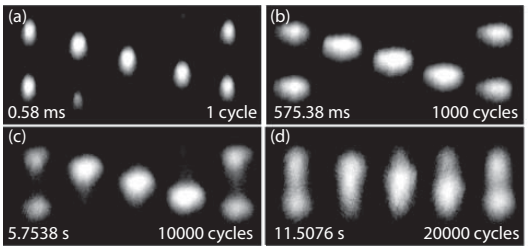

Figure 8.2: Long-lived Bloch oscillations for a non-interacting BEC with Cs atoms in the vertical lattice under the influence of gravity. Each picture shows one Bloch cycle in successive time-of-flight absorption images corresponding to the momentum distribution at the time of release from the lattice. Displayed are the first (a), the 1000^{th} (b), the 10000^{th} (c), and the 20000^{th} (d) Bloch cycle for minimal interaction near the zero crossing for the scattering length.

generated by a vertically oriented standing laser wave generated by retro-reflection, co-linear with L_1, but with much larger diameter of 580 μm. This allows independent control of lattice depth and radial (i.e. horizontal) confinement. The light comes from a home-built single-mode fiber amplifier [16] seeded with highly-stable light at $\lambda = 1064.4946(1)$ nm. We turn on the optical lattice potential exponentially to a depth of 7.9 E_R within 1000 ms, where $E_R = h^2/(2m\lambda^2) = k_B \times 64\,\text{nK}$ is the photon recoil energy and m is the mass of the Cs atom. The slow ramp assures that the BEC is adiabatically loaded into the lowest Bloch band of the lattice and it avoids horizontal excitations. We load between 40 to 65 lattice sites, depending on the initial vertical extent of the BEC. We then reduce the power in L_2 to zero within 300 μs. Subsequently, the magnetic field gradient needed for levitation is ramped down and a bias magnetic field is tuned to the desired value within 100 μs. For the present experiments, we adjust a in the range from -2 to $300\,a_0$ with magnetic bias fields from 17 to 23 G. The step in a leads to some unavoidable horizontal excitation as a result of the change of the Thomas-Fermi profile. We control the average bias field to about 1 mG. The confinement of the BEC in the lattice as given by L_1 gives horizontal trapping frequencies in the range of 5 to 10 Hz. We then let the atoms evolve in the lattice under the influence of the gravitational force for variable hold time T. Finally, we switch off the horizontal confinement and ramp the lattice depth adiabatically to zero within 300 μs to measure the momentum distribution by the standard time-of-flight technique, taking an absorption picture on a CCD camera. For some of the data we turn on the magnetic levitation field to allow for longer expansion times up to 100 ms. To minimize broadening of the distribution as a result of interaction we switch the scattering length to zero during the release and the initial time-of-flight.

We observe persistent Bloch oscillations when minimizing the effect of interactions at a magnetic field value of 17.12 G (see below). Fig. 8.2 (a)-(d) show the evolution of the momentum distribution during the first, the 1000^{th}, the 10000^{th}, and the 20000^{th} Bloch cycle. Initially, the momentum distribution exhibits narrow peaks. Their full width Δp [17] is as narrow as about 0.15 $\hbar k$, where $k = 2\pi/\lambda$. Very little broadening

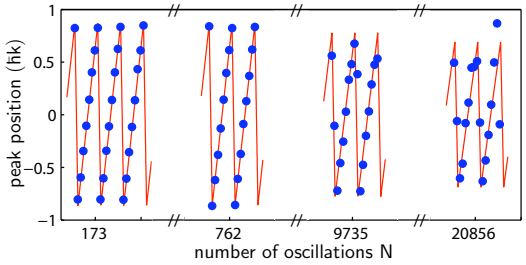

Figure 8.3: (color online). Position of the strongest peak in the momentum distribution as a function of the number N of Bloch oscillations (dots). More than 20000 cycles can be followed with high contrast. A fit to the data (solid curve) yields a Bloch period of 0.5753807(5) ms.

along the vertical direction is seen after the first 1000 cycles. Initial excitation of horizontal motion as a result of ramping the power in L_2 and switching the scattering length leads to some horizontal spreading. After 20000 cycles the distribution has started to spread out noticeably along the vertical direction.

Fig. 8.3 highlights the high number of Bloch oscillations, which we can observe for the case of minimal interaction strength. It shows how the strongest peak of the momentum distribution cycles through the first Brillouin zone with the typical saw-tooth behavior [8]. More than 20000 cycles can easily be followed. From a fit to the data we determine the Bloch period to 0.5753807(5) ms. Assuming that no additional forces act on the sample, the local gravitational constant is $g = 9.803821(9)\,\mathrm{m/s^2}$. The error is statistical only. While we took care to minimize magnetic field gradients, we expect them to be the dominant contribution to the systematic error.

In order to quantify the dephasing of Bloch oscillations we determine for each Bloch period the width Δp of the momentum distribution at the instant in time when the peak of the distribution is centered at zero momentum, i.e. for the central picture of each series shown in Fig. 8.2. Fig. 8.4 (a) displays Δp up to the 300$^{\mathrm{th}}$ Bloch cycle for different interaction strengths ranging from 0 to $300\,a_0$. For minimal interaction strength ($a \approx 0\,a_0$), we see no broadening of the distribution. Broadening can clearly be seen for $a = 25\,a_0$, and the rate of broadening then increases with increasing interaction strength. For $a \geq 50\,a_0$ the width Δp saturates within the chosen observation time to a value of about 1.3 $\hbar k$ as the momentum distribution completely fills the first Brillouin zone [18]. To a good approximation, we find that Δp initially increases linearly with time. In Fig. 8.4 (b) we plot Δp as a function of interaction strength for various fixed numbers of Bloch cycles. Δp appears to scale with the square root of the interaction strength. Both observations agree well with a simple model for the dephasing of Bloch oscillations, which predicts $\Delta p \propto \sqrt{a} \times T$ [19] for sufficiently short times T. In order to verify this model, we have performed numerical calculations solving the one-dimensional Gross-Pitaevskii equation in the presence of an optical lattice under the influence of gravity for the typical parameters of our experiment according to the method detailed in Ref. [20]. Via Fourier transform of the spatial wave function we

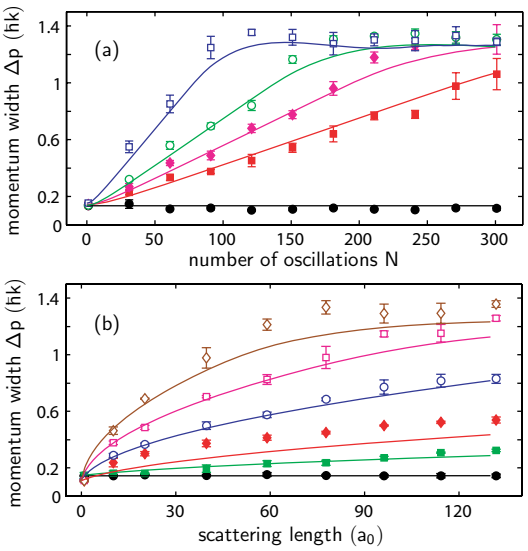

Figure 8.4: (color online). Width Δp of the momentum distribution for different interaction strengths. (a) Evolution of Δp as a function of the number N of Bloch cycles for different values of the scattering length ($a = 0, 25, 50, 100$, and $300\,a_0$ from bottom (full circles) to top (open squares). The solid curves are derived from a numerical model calculation, see text. (b) Width Δp for a fixed number of cycles $N = 1$ (full circles), 25 (full squares), 50 (full diamonds), 100 (open circles), 150 (open squares), and 200 (open diamonds) as a function of scattering length. The solid line represents the model calculation. All error bars correspond to ± one standard deviation resulting from 7 measurements. The data and the simulations correspond to the following parameters: lattice depth: 7.9 E_R, scattering length during lattice loading: 210 a_0, trapping frequencies in L_1 and L_2: 10 and 8 Hz, atom number in the BEC: 5×10^4.

determine the momentum distribution and its width. As shown in Fig. 8.4 (solid lines) we find very good agreement with our measurements with no adjustable parameters when we add a constant offset of 0.1 $\hbar k$ to all the numerical curves. This offset takes into account residual interactions during release from the lattice as a result of the finite magnetic switching speed, which leads to some artificial broadening of the distribution. We attribute the systematic discrepancy for the $N = 50$ data in Fig. 8.4 (b) to the horizontal motion which leads to modulations in the density that adds a modulation onto Δp also seen in Fig. 8.4 (a).

To find the value for the magnetic field that gives minimal broadening we measure Δp after 6951 cycles in the vicinity of the crossing. Fig. 8.5 plots Δp as a function of magnetic field. It shows a clear minimum, which we expect to correspond to the zero crossing for the scattering length. From a Gaussian fit we determine the center position of the minimum to be at 17.119(2) G. The one-sigma error takes into account our statistical error in magnetic field calibration. To our knowledge, this is the most precise determination of a minimum for the elastic cross section in ultracold atom scattering. We believe that our measurements are limited by the ambient magnetic

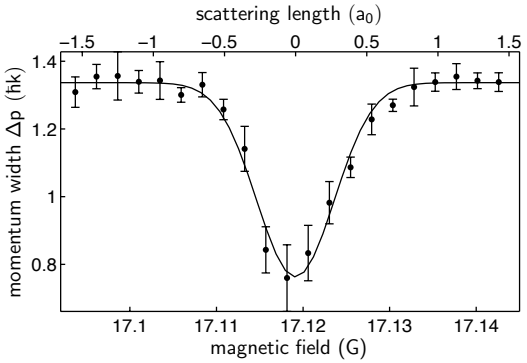

Figure 8.5: Broadening of the momentum distribution as a result of 6951 Bloch oscillations near the zero crossing for the scattering length. The width Δp is plotted as a function of magnetic field (dots). The solid line is a Gaussian fit with a rms-width of 4.5 mG. The fit is centered at 17.119(2) G. The zero for the scattering length scale on top was chosen to agree with this value.

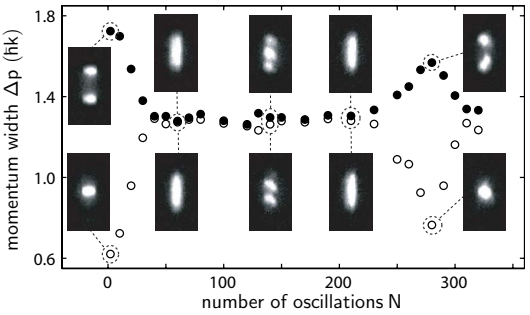

Figure 8.6: Collapse and revival of Bloch oscillations for the case of a non-interacting BEC with a vertical force gradient. The width Δp is plotted as a function of the number N of Bloch cycles for two cycle phases separated by π. For selected cycles ($N = 1, 70, 140, 210$, and 280) two absorption images corresponding to the two cycle phases are shown.

field noise, leading to a finite width for the distribution of the scattering length. In fact, a reduction of the atomic density gives longer decay times for the Bloch oscillations. Note that in the scattering length regime considered here the effect of the (magnetic) dipole-dipole interaction [21] should start to play a role.

Our capability to observe Bloch oscillations on extended time scales without interaction-induced dephasing allows us to study the effect of deliberately imposed dephasing. For this we apply a linear force gradient ∇F corresponding to harmonic trapping at $\nu = 40(1)$ Hz along the vertical direction by turning on laser beam L_2 during the hold time. Fig. 8.6 shows the widths Δp for two cycle phases separated by π as a function of the number N of Bloch cycles. The two phases correspond to the single- resp. symmetric double-peaked distribution. Both widths rapidly increase resp. decrease to the same value of 1.3 $\hbar k$ within about $N = 30$ oscillations. Here the

ensemble is dephased. It then remains dephased for about 200 cycles. Partial rephasing at intermediate times not reflected in the widths can be seen from the absorption images. Revival of the oscillations [22] happens around $N = 280$ when the values for both widths separate again [23]. This number agrees well with the expected value of $N_{\mathrm{rev}} = 292(15)$ given by $N_{\mathrm{rev}} = F_{\mathrm{grav}}/(\nabla F d) = mg/(m\omega^2 d)$, where F_{grav} is the gravitational force, $\omega = 2\pi\nu$, and $d = \lambda/2$ is the lattice spacing. Subsequently, the widths collapse again to the common value. In further measurements we see up to four collapses and revivals.

In summary, we have demonstrated the control of interaction-induced dephasing near a zero-crossing for the scattering length. On the crossing, we have realized a non-interacting BEC, which allows us to observe more than 20000 Bloch cycles, indicating a matter wave coherence time of more than 10 s. The broadening of the momentum distribution agrees well with results from theoretical models. We believe that the number of observable Bloch cycles is limited by residual interactions as a result of magnetic field noise. Our results open up exciting new avenues for precision measurements with quantum degenerate gases. For example, it is now possible to perform sensitive measurements of forces on short length scales, such as the Casimir-Polder force near a dielectric surface [24]. Future experimental work can now address the nature of the dephasing [25] by studying structure in the momentum distribution.

A similar experiment on long-lasting Bloch oscillations and control of the interaction strength has recently been performed with a BEC of ^{39}K atoms at LENS, Italy [26]. We thank A. Daley for theoretical support and for help with setting up the numerical calculations and A. Buchleitner and his group for useful discussions. We are grateful to A. Liem and H. Zellmer for valuable assistance in setting up the 1064-nm fiber amplifier system. We acknowledge contributions by P. Unterwaditzer and T. Flir during the early stages of the experiment. We are indebted to R. Grimm for generous support and gratefully acknowledge funding by the Austrian Ministry of Science and Research (BMWF) and the Austrian Science Fund (FWF) in form of a START prize grant.

1. S. A. Diddams *et al.*, Science **306**, 1318 (2004).

2. S. Bize *et al.*, J. Phys. B **38**, S449 (2005).

3. M. M. Boyd *et al.*, Phys. Rev. Lett. **98**, 083002 (2007).

4. A. Peters, K.Y. Chung, and S. Chu, Nature **400**, 849 (1999).

5. P. Cladé *et al.*, Phys. Rev. Lett. **96**, 033001 (2006).

6. S. Gupta *et al.*, Phys. Rev. Lett. **89**, 140401 (2002).

7. For a review, see T. Köhler, K. Góral, and P.S. Julienne, Rev. Mod. Phys. **78**, 1311 (2006).

8. M. Ben Dahan *et al.*, Phys. Rev. Lett. **76**, 4508 (1996).

9. R. Battesti *et al.*, Phys. Rev. Lett. **92**, 253001 (2004).

10. G. Ferrari *et al.*, Phys. Rev. Lett. **97**, 060402 (2006).

11. O. Morsch *et al.*, Phys. Rev. Lett. **87**, 140402 (2001).

12. G. Roati *et al.*, Phys. Rev. Lett. **92**, 230402 (2004).

13. T. Weber *et al.*, Science **299**, 232 (2003).

14. T. Kraemer *et al.*, Appl. Phys. B **79**, 1013 (2004).

15. P. Julienne (private communication).

16. A. Liem *et al.*, Opt. Lett. **28** 1537 (2003).

17. We define the full width Δp to be the root-mean-square (rms) diameter of the distribution.

18. The momentum distribution of a fully dephased interacting ensemble carries high-contrast substructure which will be discussed in a forthcoming publication.

19. D. Witthaut *et al.*, Phys. Rev. E 71, 036625 (2005). Note that for the quasi-one-dimensional case the interaction constant in Eq. (33) is proportional to $\sqrt{a}$, see [20].

20. A. Smerzi and A. Trombettoni, Phys. Rev. A **68**, 023613 (2003).

21. S. Giovanazzi, A. Görlitz, and T. Pfau, Phys. Rev. Lett. **89**, 130401 (2002).

22. A. V. Ponomarev and A. R. Kolovsky, Laser Physics **16**, 367 (2006).

23. Note that the revived Bloch cycles are subject to a phase shift, which depends on the vertical location of the harmonic trap minimum with respect to the lattice minima.

24. I. Carusotto *et al.*, Phys. Rev. Lett. **95**, 093202 (2005).

25. A. Buchleitner and A. R. Kolovsky, Phys. Rev. Lett. **91**, 253002 (2003).

26. M. Fattori *et al.*, Phys. Rev. Lett. **100**, 080405 (2008).

8.2 Interference of interacting matter waves

New Journal of Physics, in press

Mattias Gustavsson[1†], Elmar Haller[1], Manfred J. Mark[1],
Johann G. Danzl[1**], Russell Hart[1], Andrew J. Daley[2,3] and Hanns-Christoph Nägerl[1]

[1] Institut für Experimentalphysik und Zentrum für Quantenphysik,
Universität Innsbruck,
Technikerstraße 25, A–6020 Innsbruck, Austria

[2] Institut für Theoretische Physik und Zentrum für Quantenphysik,
Universität Innsbruck,
Technikerstraße 25, A–6020 Innsbruck, Austria

[3] Institut für Quantenoptik und Quanteninformation der Österreichischen Akademie
der Wissenschaften,
Technikerstraße 21a, A–6020 Innsbruck, Austria

e-mail: christoph.naegerl@uibk.ac.at

The phenomenon of matter wave interference lies at the heart of quantum physics. It has been observed in various contexts in the limit of non-interacting particles as a single particle effect. Here we observe and control matter wave interference whose evolution is driven by interparticle interactions. In a multi-path matter wave interferometer, the macroscopic many-body wave function of an interacting atomic Bose-Einstein condensate develops a regular interference pattern, allowing us to detect and directly visualize the effect of interaction-induced phase shifts. We demonstrate control over the phase evolution by inhibiting interaction-induced dephasing and by refocusing a dephased macroscopic matter wave in a spin-echo type experiment. Our results show that interactions in a many-body system lead to a surprisingly coherent evolution, possibly enabling narrow-band and high-brightness matter wave interferometers based on atom lasers.

Matter wave interference has been observed as a single particle effect for electrons [1], neutrons [2], atoms and molecules [3]. Macroscopic matter wave interference was

[†]Present address: Department of Physics, Yale University, P.O. Box 208120, New Haven, Connecticut 06511, USA

[**]The author of the present thesis contributed to this work through experimental support, discussions on physics and technology, and in paper writing. Here, the submitted version of the paper is given.

first directly observed in the case of two independent atomic Bose-Einstein condensates (BEC) that were brought to overlap [4]. This experiment validated the notion of the BEC as a macroscopic matter wave and coined the expression of the atom laser in analogy to the laser for the case of photons. Matter wave interferometers [5,6,7], in particular for applications to precision measurements, are typically operated in the dilute single particle limit [8,9,10] to avoid particle-particle interactions. Atom interferometers based on Bose-Einstein condensates (BEC) are expected to benefit from the extremely low momentum spread, the exceptional brightness, and the low spatial extent of the BEC [11], but they readily enter the nonlinear matter wave regime as a result of the interaction-induced mean field potential. A possible solution is to operate BEC-based interferometers in the non-interacting limit [12,13] by exploiting the cancellation of the scattering phase shift near a scattering resonance. This condition, however, is difficult or impossible to fulfill for most atomic species. In the present work we demonstrate a BEC-based multipath atom interferometer where the dynamics is dominated by interaction-induced phase shifts, and we show that full control and also cancellation of these phase shifts is possible. We realize the multipath interferometer by loading an interacting BEC into an optical lattice potential along one dimension, coherently splitting the BEC into several parts that are then each subject to different linear and nonlinear phase shifts. The linear phase shifts due to the gravitational force lead to the the well-known phenomenon of Bloch oscillations [14,15], whereas the interaction-induced nonlinear phase shifts cause the macroscopic wave function to first spread in momentum space as a function of time and then, surprisingly, to exhibit high-contrast interference. We demonstrate a high degree of coherence by reversing the nonlinear phase evolution, thereby refocusing the BEC momentum wave function. By application of an external potential we cancel the dominant mean-field contribution to the phase evolution and become sensitive to beyond-mean-field effects. A crucial ingredient of our experiments is the capability to tune a, the atomic scattering length which determines the strength of the interaction, by means of a Feshbach resonance [16]. In particular, a can be switched to zero to stop the interaction driven part of the evolution in the interferometer or to perform high resolution wave function imaging in momentum space.

Phase evolution in the matter wave interferometer

Our interferometer consists of a BEC adiabatically loaded into a 1D optical lattice potential with a superimposed harmonic trap, as illustrated in figure 8.7a. In the tight-binding regime, it is convenient to write the macroscopic wave function of the condensate, Ψ, in a basis [17] of wave functions $\Psi_j(z, r_\perp)$ centered at the position $z_j = jd$ of the individual lattice sites j, $\Psi(z, r_\perp, t) = \sum_j c_j(t)\Psi_j(z, r_\perp)$. Here, z is the coordinate along the (vertical) lattice direction, $r_\perp$ is the transverse coordinate, d is the distance between adjacent lattice sites and $c_j(t)$ are time-dependent complex amplitudes.

After the BEC is loaded into the lattice, we tilt the lattice potential by applying a strong force F along the lattice direction. In the limit $Fd \gg J$, where J is the

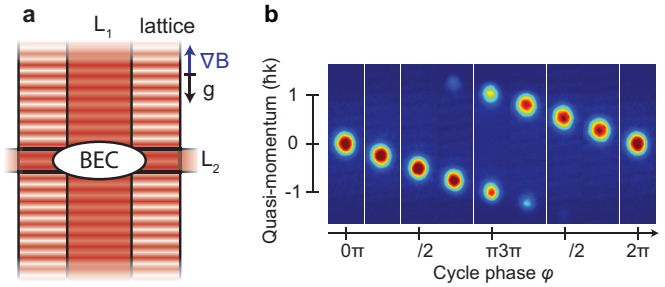

Figure 8.7: **BEC-based atom interferometer. a,** Experimental configuration: The tunable BEC is formed at the intersection of the vertical guide laser beam L_1 and a horizontal trapping beam L_2. The lattice is oriented along the vertical direction. Gravity, g, is initially compensated by a force due to a magnetic field gradient, ∇B. **b,** Imaging the first Brillouin zone (BZ): One cycle of Bloch oscillations for a non-interacting BEC as seen in time-of-flight absorption imaging, showing narrow peaks cycling through quasi-momentum space for cycle phases $\phi = 0$, $\pi/4$, $\pi/2$, ..., to 2π.

tunnelling matrix element, tunnelling between lattice sites is inhibited. The on-site occupation numbers $|c_j|^2$ are then fixed, and we can write $c_j(t) = c_j(0)e^{i\phi_j(t)}$, where the phase $\phi_j(t)$ evolves in time according to the local potential at each specific lattice site [21],

$$\begin{aligned} \hbar\frac{\partial\phi_j}{\partial t} &= Fdj + V_j^{\mathrm{trap}} + \mu_j^{\mathrm{loc}} \\ &= Fdj + \beta_{\mathrm{tr}} j^2 - \alpha_{\mathrm{int}} j^2. \end{aligned} \tag{8.1}$$

Here, the total potential at each lattice site j consists of three terms. The applied force leads to a term linear in j and causes Bloch oscillations [14,15] with angular frequency $Fd/\hbar$. The second term comes from an optional harmonic confinement, where $\beta_{\mathrm{tr}} = m\omega_{\mathrm{tr}}^2 d^2/2$ characterizes the strength of the confining potential and ω_{tr} is the trap frequency. Atom-atom interactions give rise to a third term, the local chemical potential μ_j^{loc}, which depends on the scattering length a and the site occupation number as [17] $\mu_j^{\mathrm{loc}} \propto \sqrt{a|c_j|^2}$. When the BEC is loaded in the Thomas-Fermi regime, as is done here, its initial value can be calculated in a simple way. The density distribution will be such that the local chemical potential mirrors the trapping potential that is present during loading into the lattice, $\mu_{\mathrm{loc}}^j = \mu - V_j^{\mathrm{trap}}$, with μ being the (global) chemical potential of the BEC. We then initially have $\mu_j^{\mathrm{loc}} = \alpha_{\mathrm{int}} j^2$, where $\alpha_{\mathrm{int}} = m\omega_{\mathrm{lo}}^2 d^2/2$ and ω_{lo} is the trap frequency during loading. Note that although the initial value of α_{int} is independent of the scattering length used at loading, a later change in scattering length will also change the value of α_{int}.

The phase terms proportional to j^2 lead to a nonlinear relative phase evolution between lattice sites, i.e., dephasing. This results in a time-varying interference pattern of the macroscopic matter wave, as we will demonstrate below. The key in our experiments is that we have full control over these nonlinear terms, not only over β_{tr} via

the external trapping potential, but also over the interaction term characterized by α_{int}, both via the initial density distribution, and, more importantly, via the scattering length a. By tuning the scattering length [16] from its initial value a to a', we can ramp α_{int} to a new value α'_{int}, which can in particular be set to zero for $a = 0$. Nonlinear phase terms for matter waves are well known in single particle quantum mechanics. They play an important role for matter wave Talbot interferences [5,18] and can be visualized in terms of so-called matter wave quantum carpets [19]. In these contexts, the phase terms arise from propagation. In our case, the nonlinear phase terms for $\alpha_{\mathrm{int}} \neq 0$ arise from interactions and thus lead to a density dependent many-body effect in the multipath atom interferometer.

In the preceding discussion, we have assumed that the minimum of the trapping potential is centered directly over one of the lattice minima. If this is not the case, the trapping potential term in equation (8.1) has to be modified to $\beta_{\mathrm{tr}}(j-\delta)^2 = \beta_{\mathrm{tr}} j^2 - 2\beta_{\mathrm{tr}}\delta j + const.$, where $\delta \in [0, 1]$ describes the offset of the trap center in the z-direction with respect to the lattice minima, and an analogous modification has to be done to the interaction term. This adds a small term linear in j and therefore leads to a slight modification of the Bloch oscillation frequency. In our experiments, δ is the only parameter that we do not fully control. It is constant on the timescale of a single experimental run, but it drifts over the course of minutes as the beam pointing of the horizontally propagating laser beam generating the trapping potential is not actively stabilized.

Interaction-induced matter wave interference

The starting point for our experiments is a BEC trapped in a crossed optical dipole trap and adiabatically loaded into an optical lattice, as illustrated in figure 8.7a. The sample preparation is described in appendix A. The gravitational force acting on the BEC is initially compensated using magnetic levitation [16]. We effectively start the multipath atom interferometer and hence the evolution of the interacting macroscopic wave function by turning off magnetic levitation and ramping down the vertical confinement created by laser beam L_2 within 0.3 ms, inducing Bloch oscillations in the lowest band of the lattice. With $Fd/\hbar \approx 2\pi\times 1740$ Hz and $J/\hbar \approx 2\pi\times 40$ Hz the on-site occupation numbers $|c_j|^2$ are fixed to their initial values. After an evolution time τ, we close the interferometer by ramping down the lattice in 1 ms and directly image the (vertical) quasi-momentum distribution in the first Brillouin zone (BZ). The ramp is adiabatic with respect to the bandgap and maps quasi-momentum onto real momentum [20], which is measured by taking an absorption image after a period of free expansion. Figure 8.7b shows absorption images of the first Bloch oscillation [14]. The Bloch period is about 0.58 ms and the peaks have a root mean square (rms) width of $0.2\hbar k$, where $k = \pi/d$ is the lattice wave vector, thus being well separated.

We study the evolution of the wave function at high resolution in momentum space by taking snapshots after extended time-of-flight. As illustrated in figure 8.8a, the BEC wave function spreads out in the BZ in about $N = 18$ Bloch cycles. Then, surprisingly,

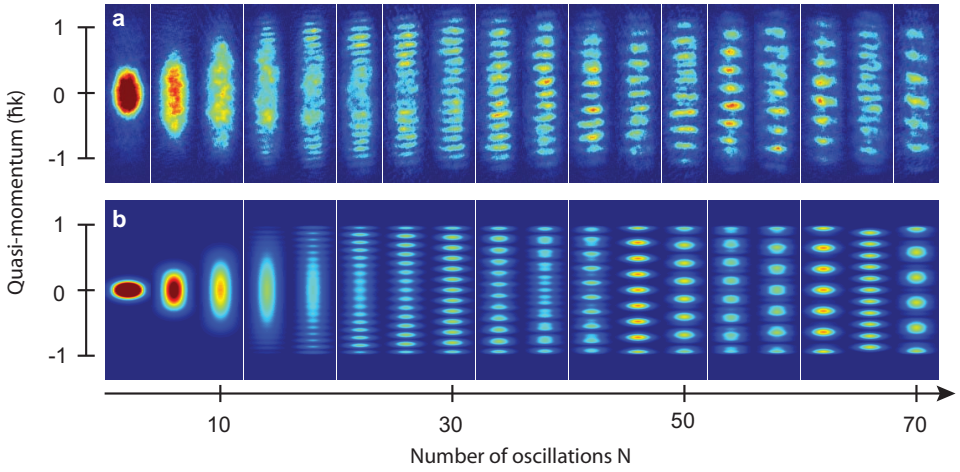

Figure 8.8: **Interaction induced macroscopic matter wave interference. a,** Experimental results showing the quasi-momentum distribution as a function of evolution time τ given in units of the Bloch period. The absorption images are taken in steps of 4 Bloch cycles for a BEC with an initial peak density of $n = 4 \times 10^{13}$ atoms/cm^3 loaded into about 35 lattice sites with $a = 190$ a$_0$. Each image corresponds to a single realization of the experiment. **b,** Evolution of the wave function in quasi-momentum space when the phase at the individual lattice sites evolves according to equation (8.2) with $\beta_{\rm tr} = 0$ (no external trap) for $n = 4 \times 10^{13}$ atoms/cm^3 loaded into 35 lattice sites with $a = 190$ a$_0$. $\alpha_{\rm int}$ is slightly rescaled to account for the reduction in density due to transversal dynamics, see text. In **a**, some additional broadening, largely due to the presence of the horizontal trapping potential during expansion, can be seen.

an interference pattern gradually develops at the edge of the BZ and later also becomes visible at the center of the BZ, while the number of interference maxima and minima changes as time progresses. Images are taken after an integer number of Bloch cycles for cycle phase $\phi = 0$, corresponding to the first image in figure 8.7b. The data is acquired with an interacting BEC with the scattering length set to 190 a$_0$, where a$_0$ is the Bohr radius, at an initial peak density of $n = 4 \times 10^{13}$ atoms/cm^3, occupying about 35 lattice sites after loading. We can follow the evolution of the interference pattern for more than $N = 100$ Bloch cycles, corresponding to times beyond 60 ms. This is about a factor 10 longer than the timescale for the initial broadening. We find that the number of maxima and minima in the interference pattern as measured after a fixed evolution time τ depends on the number of occupied lattice sites and on the trap frequency of the external harmonic confinement employed when loading the lattice. We also find that the measured quasi-momentum distribution for a given τ is reproducible from one experimental realization to the next, except that the pattern appears slightly shifted within the BZ after several experimental realizations. We attribute this to a drift of δ, the offset of the lattice minima from the dipole trap center, which leads to a small change of the Bloch frequency as noted before. We do not actively stabilize the vertical position of L$_2$ with respect to the lattice, and hence temperature variations in

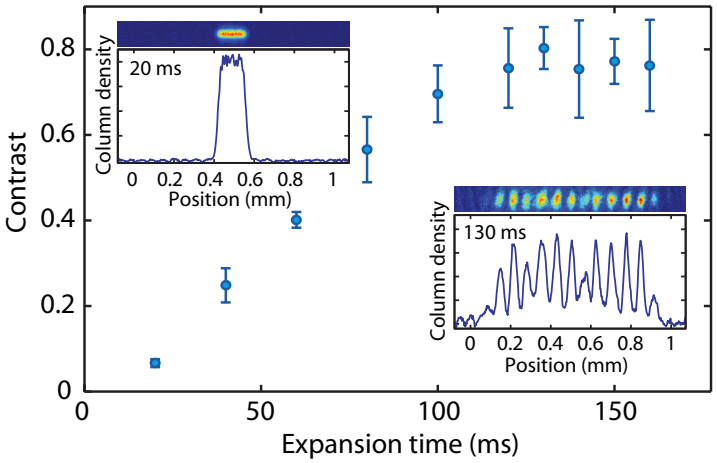

Figure 8.9: **Contrast of interference fringes.** Contrast of matter wave interference emerging during time-of-flight expansion for a BEC after $N = 40$ Bloch cycles, where the wave function completely fills the BZ. We define the contrast as $(I_{max} - I_{min})/(I_{max} + I_{min})$, where I_{max} (I_{min}) is the average value of the maxima (minima) of the central peak structure. Each data point is the average contrast of 10 experimental runs and the error bars indicate the 1σ statistical error. The insets show measured quasi-momentum distributions integrated along the transverse direction at two expansion times as indicated.

the laboratory slowly change δ.

We combine two techniques to achieve a high resolution in momentum space and to visualize the interference pattern. First, we minimize broadening of the distribution as a result of interactions by setting a to zero during the release from the lattice and the subsequent free expansion [12]. In addition, we use long expansion times, employing magnetic levitation to prevent the BEC being accelerated by gravity and falling out of the field of view. Figure 8.9 shows how the contrast emerges during the expansion for a BEC after $N = 40$ Bloch cycles. It takes more than 100 ms of expansion for the interference pattern to acquire full contrast. In general, we find that the contrast is improved when the horizontally confining beam L_1 is not switched off abruptly but is ramped down slowly within the first 55 ms of time-of-flight, reducing the horizontal expansion rate. However, this happens at the cost of some additional momentum broadening along the vertical direction. Our imaging techniques allow us to resolve structure in momentum space on a scale below $0.1\hbar k$ in a single shot absorption image.

To understand the interference structure and its evolution in time, we compute the total BEC wave function in quasi-momentum space for the case where the phase at each lattice site evolves according to equation (8.1) (details can be found in appendix B). Figure 8.8b shows the interference pattern for our experimental parameters according to this simple model. The experimental results are qualitatively very well reproduced by the model when we reduce α_{int} by 10 % compared to the value deduced

from our experimental parameters. This scale factor accounts primarily for the fact that our simple model does not take into account any horizontal dynamics. In particular, switching off L_2 when starting the evolution leads to an excitation of a radial breathing mode in the horizontal plane, reducing the density at each site and modulating it in time. To a first approximation, rescaling of α_{int} accounts for this. Nevertheless, the agreement between the experiment and the analytical model indicates that the dominant driving mechanism for the wave function spreading and interference is the nonlinear phase evolution. In particular, phase coherence is not lost, in contrast to previous experiments [22]. We test this coherence and demonstrate control over the phase evolution in two experiments.

Cancellation of dephasing using an external potential

Equation (8.1) suggests that the effect of interactions can be cancelled by the application of an external potential [23]. Indeed, choosing this potential to be equal to the initial loading potential, i.e. choosing $\alpha_{int} \approx \beta_{tr}$, allows us to observe persistent Bloch oscillations for an interacting BEC. This demonstrates that the detrimental effects of the mean field phase shift in a BEC matter wave interferometer can be compensated for. The BEC quasi-momentum distribution after $N = 40$ Bloch cycles is shown in figures 8.10a and 8.10b as a function of the strength of the external compensating potential, given by the power in laser L_2. When the external potential does not compensate for interactions, the condensate wave function is dephased and spreads over the whole BZ within less than $N = 20$ Bloch cycles. In contrast, when the external potential balances the effect of interactions, the BEC wave function does not spread out and Bloch oscillations are clearly visible. The time during which Bloch oscillations can be observed is now greatly extended compared to the case when the compensating potential is absent. The transition from a dephased to a non-dephased wave function as a function of confinement strength is quantified in figure 8.10c, where the rms-width Δp of the singly-peaked quasi-momentum distribution after $N = 40$ Bloch cycles is plotted as a function of the laser power in L_2. Figures 8.10d and 8.10e show the time evolution of the quasi-momentum distribution without and with the compensating potential while all other parameters are kept the same. Figure 8.10d essentially shows the broadening of the distribution as described before. Interestingly, the condensate wave function in the presence of a compensating potential shown in figure 8.10e dephases in a completely different way. Initially, the central peak shows no broadening. However, it is slowly depopulated, while a much broader background distribution is increasingly populated. After about 100 oscillations, the shape of the central peak starts to develop side lobes or splits in two, with the exact shape varying from one experimental run to the next. The timescale for the loss of interference is a factor 10 larger than the timescale on which the dephasing and hence the initial broadening takes place in the uncompensated case.

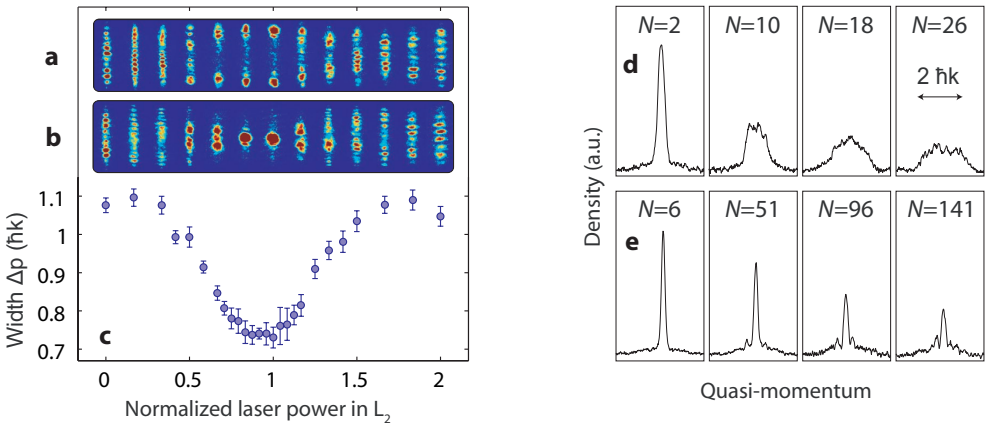

Figure 8.10: **Cancellation of interaction induced dephasing and observation of persistent Bloch oscillations. a-c,** Absorption images showing the quasi-momentum distribution for cycle phase $\phi = \pi$ (**a**) and $\phi = 0$ (**b**) after $N = 40$ Bloch cycles and (**c**) momentum width Δp for $\phi = 0$ as a function of confinement strength, normalized to the confinement strength at loading. **d** Momentum distribution for $\phi = 0$ as a function of the number N of Bloch cycles when no compensating potential is present, showing fast broadening. **e** The evolution of the momentum distribution for the case of optimum cancellation of interactions.

Rephasing of a dephased condensate

Second, we perform a matter wave spin-echo-type experiment. We initially proceed as shown in figure 8.8, letting the wave function evolve for a time corresponding to about $N = 40$ Bloch cycles until it is fully dephased and shows, upon measurement, a regular interference structure. We then essentially remove the effect of interactions by ramping to $a = 10\ a_0$ within 10 ms. By not switching the interaction entirely off and by ramping comparatively slowly we avoid excessive excitation of the radial breathing mode as a result of the change in the mean field potential at each site. At the same time, we gradually turn on the harmonic potential as given by the horizontal dipole trapping laser beam L_2 within 4 ms to approximately the same depth as during the initial BEC loading phase. From equation (8.1) we expect that the wave function now experiences a phase shift with a quadratic spatial dependence with opposite sign, allowing us to reverse the evolution and to recover the initial condition. Figure 8.11 shows the resulting quasi-momentum distributions. As time progresses, the wave function indeed refocuses while it continues to perform Bloch oscillations. As we do not control the value of δ for a particular run, we record about 10 distributions for each evolution time and select those that are symmetrical, corresponding to Bloch cycle phase $\phi = 0$ or $\phi = \pi$. For the chosen strength of the potential, refocusing happens after about 24 Bloch cycles after the ramp of a. This confirms that the initial broadening and dephasing mechanism must have been coherent. We note that we cannot avoid some excitation of the radial breathing mode as seen in the absorption images given in figure 8.11.

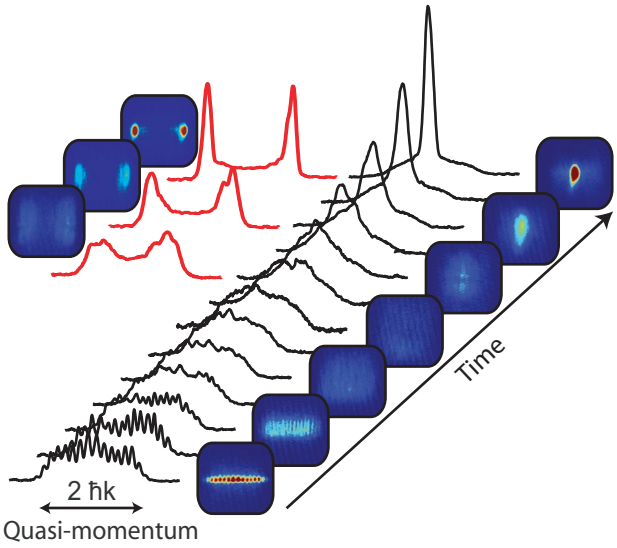

Figure 8.11: **Matter wave spin-echo-type experiment.** Rephasing of the BEC from a fully dephased wave function back into a narrow distribution after switching interactions to near zero and turning on an external potential. Time progresses from front to back. The black solid lines correspond to selected quasi-momentum distributions that refocus into the characteristic singly-peaked distribution (cycle phase $\phi = 0$), see text. They are separated in time by 1.15 ms or two Bloch cycles, and they are offset for clarity. The red solid lines correspond to selected distributions that refocus into the characteristic double-peaked distribution (cycle phase $\phi = \pi$). The images are absorption images corresponding to the adjacent quasi-momentum distributions. Some radial excitation is also present.

Discussion

Our results raise several important questions: To what extent can matter wave interferometry be performed in the presence of interactions? What sets the timescale for the eventual loss of interference contrast? Certainly, our simple analytic model does not predict any loss of contrast. In particular, it should be possible to completely eliminate the effect of interactions with the compensating external potential. However, there are several effects not included in the model that could cause the residual dephasing we observe. Motion in the radial direction, which causes the density and therefore the interaction energy to change over time, could lead to mixing of the different degrees of freedom and hence to additional dephasing. This might apply to our matter wave spin-echo experiment shown in figure 8.11, but in the experiment in figure 8.10 where we compensate interactions by means of the external potential there is hardly any radial excitation and this effect should not play a role. The appearance of dynamical instabilities [24,25,26] can be ruled out, as the force applied along the lattice is about 2.5 times stronger than the force needed for the instability to disappear [24]. Going beyond the mean-field treatment, a variety of factors can lead to dephasing. For example, at each lattice site there exists a superposition of number states, accumulating different

phases corresponding to their respective interaction energies [27,28]. This leads to an effective dephasing, as the phase on a particular lattice site becomes ill-defined. Basic estimates [27,28] indicate a dephasing time of about 20 ms for our system, on the same order as we observe.

These experiments constitute a clear demonstration of coherent dynamics in an interacting macroscopic quantum system. This coherence affords a large degree of control over the system, as demonstrated by the possibility to rephase the wave function using an external potential in order to reverse dephasing due to interactions. The control demonstrated here has potential application in matter-wave interferometry, and such a degree of control over the mean-field evolution also opens the possibility to probe beyond-mean-field effects in atom interferometers.

Acknowledgements

We thank E. Arimondo, O. Morsch, W. Schleich, A. Smerzi, D. Witthaut and A. Buchleitner and his group for helpful discussions. We are indebted to R. Grimm for generous support and gratefully acknowledge funding by the Austrian Ministry of Science and Research (Bundesministerium für Wissenschaft und Forschung) and the Austrian Science Fund (Fonds zur Förderung der wissenschaftlichen Forschung) in form of a START prize grant and through SFB 15. R.H. is supported by a Marie Curie International Incoming Fellowship within the 7th European Community Framework Programme.

Appendix

A. Sample preparation

Our experimental approach initially follows the procedure described in [12]. In brief, within 10 s we produce an essentially pure BEC with tunable interactions [16] in the Thomas-Fermi limit with up to 1.5×10^5 Cs atoms. The BEC is trapped in a crossed-beam dipole trap generated by a vertically (L_1) and a more tightly focused horizontally (L_2) propagating laser beam. The BEC is cigar-shaped with the long axis oriented along the direction of L_2. The trap frequencies are $(\omega_x, \omega_y, \omega_z) = 2\pi \times (39, 5, 39)$ Hz, where x denotes the horizontal direction perpendicular to L_2, y is the axial direction along L_2, and z is the vertical direction. We magnetically control the scattering length a in the range between $0\,a_0$ and $300\,a_0$ with a resolution of about $0.1\,a_0$. For BEC production, we work at $a = 210\,a_0$, where three-body losses are minimized [29]. Initially, we support the optical trapping by magnetic levitation against gravity [16]. As shown in figure 8.7a we superimpose an optical lattice with $d = \lambda/2$ along the vertical direction, where $\lambda = 1064.5$ nm is the wavelength of the lattice light. To load the BEC into the lattice, we stiffen the horizontal confinement within 1 s, leading to trap frequencies of $2\pi \times (41, 13, 39)$ Hz, and at the same time turn on the lattice potential exponentially to a depth of $8E_R$. Here, $E_R = h^2/(2m\lambda^2) = k_B \times 64$ nK is the photon recoil energy and

m the mass of the Cs atom. The BEC is thus gently loaded into the lattice, occupying about 25 to 35 lattice sites, with up to 7000 atoms at the central site.

B. Derivation of the BEC wave function in momentum space

Here, we outline the method used to calculate the images in figure 8.8b. Due to the comparatively small interaction energies in our system, the atoms are restricted to move in the lowest Bloch band and we can write the local wavefunction at lattice site j as $\Psi_j(r_\perp, z) = w_0^{(j)}(z)\Phi_\perp(\rho_j, r_\perp)$, where $w_0^{(j)}(z)$ is the lowest-band Wannier function localized at the j-th site and $\Phi_\perp(n_j, r_\perp)$ is a radial wave function depending on the occupation number $n_j = |c_j|^2$ at each site [17]. We can then write the total time-dependent wave function in momentum space as

$$\begin{aligned}\Psi(p_z, p_\perp, t) &= \textstyle\sum_j c_j(t) w_0^{(j)}(p_z)\Phi_\perp(n_j, p_\perp) \\ &= w_0^{(0)}(p_z) \textstyle\sum_j c_j(t) e^{-ip_z jd}\Phi_\perp(n_j, p_\perp). \end{aligned} \tag{8.2}$$

Transforming to quasi-momentum space and assuming that the phase at each lattice site evolves according to equation (8.1), we can write [21]

$$\Psi(q_z, p_\perp, t) = \sum_j c_j(0) e^{-i(q+\frac{Ft}{\hbar})jd}\, e^{-i(\beta_{\rm tr} j^2 - \alpha_{\rm int} j^2)t/\hbar}\Phi_\perp(n_j, p_\perp), \tag{8.3}$$

where q_z denotes the quasimomentum. The images in figure 8.8b show the BEC density distribution $|\Psi(q_z, p_\perp, t)|^2$ integrated along one radial direction, using a Thomas-Fermi wave function as radial wave function $\Phi_\perp(n_j, p_\perp)$.

We have compared the result in figure 8.8b with a numerical integration of the discrete nonlinear Schrödinger equation [17], which includes tunnelling between lattice sites, and find essentially identical results, confirming that tunnelling is inhibited.

References

1. Davisson C J and Germer L H 1927 *Nature* **119** 558
2. von Halban H and Preiswerk P 1936 *C.R. Acad. Sci.* **203,** 73
3. Estermann I and Stern O 1930 *Z. Phys.* **61** 95
4. Andrews M R, Townsend C G, Miesner H-J, Durfee D S, Kurn D M and W Ketterle 1997 *Science* **275** 637
5. Berman P R (ed) 1997 *Atom Interferometry* (New York: Academic Press)
6. Cronin A D, Schmiedmayer J and Pritchard, D E 2007 Atom interferometers *Preprint* arxiv:0712.3703
7. Hart R A, Xu X, Legere R and Gibble, K 2007 *Nature* **446** 892

8. Wicht A, Hensley J M, Sarajlic E and Chu S 2002 *Phys. Scr.* **T102** 82

9. Cladé P, de Mirandes E, Cadoret M, Guellati-Khélifa S, Schwob C, Nez F, Julien L and Biraben F 2006 *Phys. Rev. Lett.* **96** 033001

10. Fixler J B, Foster G T, McGuirk J M and Kasevich M A 2007 *Science* **315** 74

11. Gupta S, Dieckmann K, Hadzibabic Z and Pritchard D E 2002 *Phys. Rev. Lett.* **89** 140401

12. Gustavsson M, Haller E, Mark M J, Danzl J G, Rojas-Kopeinig G and Nägerl H-C 2008 *Phys. Rev. Lett.* **100** 080404

13. Fattori M, D'Errico C, Roati G, Zaccanti M, Jona-Lasinio M, Modugno M, Inguscio M and Modugno G 2008 *Phys. Rev. Lett.* **100** 080405

14. Ben Dahan M, Peik E, Reichel J, Castin Y and Salomon C 1996 *Phys. Rev. Lett.* **76** 4508

15. Anderson B P and Kasevich M A 1998 *Science* **282** 1686

16. Weber T, Herbig J, Mark M, Nägerl H-C and Grimm R 2003 *Science* **299** 232

17. Smerzi A and Trombettoni A 2003 *Phys. Rev. A* **68** 023613

18. Deng L, Hagley E W, Denschlag J, Simsarian J E, Edwards M, Clark C W, Helmerson K, Rolston S L and Phillips W D 1999 *Phys. Rev. Lett.* **83** 5407

19. Kaplan A E, Marzoli I, Lamb W E and Schleich W P 2000 *Phys. Rev. A* **61** 032101

20. Kastberg A, Phillips W D, Rolston S L, Spreeuw R J C and Jessen P S 1995 *Phys. Rev. Lett.* **74** 1542

21. Witthaut D, Werder M, Mossmann S and Korsch H J 2005 **71** 036625

22. Morsch O, Müller J H, Ciampini D, Cristiani M, Blakie P B, Williams C J, Julienne P S and Arimondo E 2003 *Phys. Rev. A* **67** 031603

23. Zhang R, Sapiro R E, Mhaskar R R and Raithel G 2008 *Phys. Rev. A* **78** 053607

24. Zheng Y, Koštrun M and Javanainen J 2004 *Phys. Rev. Lett.* **93** 230401

25. Cristiani M, Morsch O, Malossi N, Jona-Lasinio M, Anderlini M, Courtade E and Arimondo E 2004 *Opt. Express* **12** 4

26. Fallani L, De Sarlo L, Lye J E, Modugno M, Saers R, Fort C and Inguscio M 2004 *Phys. Rev. Lett.* **93** 140406

27. Li W, Tuchman A K, Chien H and Kasevich M A 2007 *Phys. Rev. Lett.* **98** 040402

28. Imamoğlu A, Lewenstein M and You, L 1997 *Phys. Rev. Lett.* **78** 2511

29. Kraemer T *et al.* 2006 *Nature* **440** 315

8.3 Realization of an excited, strongly-correlated quantum gas phase

Science 4 September 2009:
Vol. 325, no. 5945, pp. 1224 - 1227
DOI: 10.1126/science.1175850

Elmar Haller,[1] Mattias Gustavsson,[1] Manfred J. Mark,[1]
Johann G. Danzl,[1**] Russell Hart,[1] Guido Pupillo,[2,3]
Hanns-Christoph Nägerl[1*]

[1]Institut für Experimentalphysik und Zentrum für Quantenphysik, Universität Innsbruck,
Technikerstraße 25, A–6020 Innsbruck, Austria

[2]Institut für Theoretische Physik, Universität Innsbruck
Technikerstraße 25, A–6020 Innsbruck, Austria

[3]Institut für Quantenoptik und Quanteninformation
der Österreichischen Akademie der Wissenschaften
Technikerstraße 21a, A–6020 Innsbruck, Austria

[*]To whom correspondence should be addressed;
E-mail: Christoph.Naegerl@uibk.ac.at

Ultracold atomic physics offers myriad possibilities to study strongly correlated many-body systems in lower dimensions. Typically, only ground state phases are accessible. Using a tunable quantum gas of bosonic cesium atoms, we realize and control in one dimensional geometry a highly excited quantum phase that is stabilized in the presence of attractive interactions by maintaining and strengthening quantum correlations across a confinement-induced resonance. We diagnose the crossover from repulsive to attractive interactions in terms of the stiffness and the energy of the system. Our results open up the experimental study of metastable excited many-body phases with strong correlations and their dynamical properties.

In many-body quantum physics the interplay between strong interactions and confinement to a low-dimensional geometry amplifies the effects of quantum fluctuations and correlations. A remarkable example in one dimension is the Tonks-Girardeau (TG) gas, where bosons with strong repulsive interactions minimize their interaction

[**]The author of the present thesis contributed to this work through experimental support, discussions on physics and technology, and in paper writing. Here, the final accepted version of the paper is given.

energy by avoiding spatial overlap and acquire fermionic properties *(1,2)*. Evidence for this ground state phase was found using Bose-Einstein condensates (BEC) loaded into optical lattices *(3,4)*. While many-body quantum systems are usually found in their ground state phases, long-lived excited state phases are responsible for some of the most striking physical effects, examples ranging from vortex lattices in superfluids to subtle topological excitations in spin liquids *(5)*. However, the experimental realization of excited phases is difficult, as these usually quickly decay by intrinsic effects or by coupling to the environment. In this context, cold atoms *(6,7,3,4,8,9,10,11,12)* may provide unique opportunities for the realization of long-lived, strongly interacting, excited many-body phases due to the excellent decoupling from the environment and the tunability of interactions via, for example, Feshbach resonances.

For an ultracold one-dimensional (1D) system of bosons, we prepare a highly-excited many-body phase known as the super-Tonks-Girardeau (sTG) gas *(13)*. In this highly-correlated quantum phase, interactions are attractive, and rapid decay into a cluster-type ground state is in principle possible. However, a surprising property of this many-body phase is its metastability. Attractive interactions strengthen correlations between particle positions and ensure, similar to an effective long-range repulsive interaction, that particles rarely come together. To realize this exotic phase, we observe and exploit a 1D confinement-induced resonance (CIR) *(14,15)*. This resonance allows us to first enter deeply into the repulsive TG regime to establish strong particle correlations and then to switch interactions from strongly repulsive to strongly attractive. The frequency ratio of the two lowest-energy collective modes *(16)* provides accurate diagnostics for the crossover from the TG to the sTG regime. In particle loss and expansion measurements we study the time evolution of the system through the crossover.

We tune the strength of the interaction as characterized by the three-dimensional (3D) scattering length a_{3D} by means of a magnetically-induced Feshbach resonance *(17)*. For a 1D system, a CIR arises and strongly modifies the 1D scattering properties when a_{3D} approaches the harmonic oscillator length $a_\perp = \sqrt{\hbar/(m\omega_\perp)}$ of the transversal confinement with trap frequency $\omega_\perp$ *(15,14)*. Here, m is the mass of the particles and $\hbar$ is Planck's constant divided by 2π. More precisely, the coupling constant g_{1D} of the 1D δ-function contact potential $U_{1D}(z) = g_{1D}\delta(z)$ behaves as *(14)*

$$g_{1D} = -\frac{2\hbar^2}{m a_{1D}} = \frac{2\hbar^2 a_{3D}}{m a_\perp^2}\frac{1}{1 - C\, a_{3D}/a_\perp}, \tag{8.4}$$

where a_{1D} is the 1D scattering length defined by this equation and $C = 1.0326$ is a constant. Thus, the CIR allows tuning of g_{1D}. For values of a_{3D} less but close to $a_\perp/C$ ($a_{3D} \lesssim a_\perp/C$) the coupling parameter g_{1D} is large and positive, and for $a_{3D} \gtrsim a_\perp/C$ it is large and negative, leading to an effectively attractive interaction. For homogenous systems with $g_{1D} > 0$, it is customary to characterize the strength of interactions by the Lieb-Liniger parameter $\gamma = g_{1D}m/(\hbar^2 n_{1D})$, where n_{1D} is the linear 1D density of the system *(2,6)*. The TG gas corresponds to the limit $\gamma \gg 1$ or $g_{1D} \to \infty$. As interactions are increased, the system becomes strongly correlated and is fully dominated by its kinetic energy. In previous experiments, without the capability to tune a_{3D}, a maximum

of $\gamma \approx 5.5$ was achieved *(4)*, while an effective strength $\gamma_{\text{eff}} \approx 200$ was reached with an additional shallow lattice potential along the longitudinal direction *(3)*. In the former experiment, a saturation for the size and energy of the 1D system was observed, and in the latter experiment the momentum distribution was studied.

But what happens in the case of strong attractive interactions $g_{1D} \to -\infty$, i.e. $a_{1D} \gtrsim 0$? The ground state for a system of N attractively interacting bosons in 1D is a cluster state *(18,19)*, which one would expect, in a cold atom system, to decay quickly via molecular channels. However, by crossing the CIR from the TG side, i.e. switching interactions from $g_{1D} = +\infty$ to $g_{1D} = -\infty$, an excited gas-like phase, the sTG gas, should be accessible *(13)*. Is this excited phase stable, i.e. does it exist at all? The expectation is that the large kinetic energy inherited from the TG gas, in a Fermi-pressure like manner, prevents the gas from collapsing *(20)*. This stability can most simply be inferred from a Bethe-ansatz solution to the Lieb-Liniger model with attractive interactions *(21,20)*. This ansatz yields for the energy per particle $E/N \approx \hbar^2\pi^2 n_{1D}^2/[6m(1-n_{1D}a_{1D})^2]$, corresponding to the energy of a gas of hard rods *(1)*, for which a_{1D} represents the excluded volume. This results in a positive inverse compressibility and also in an increased stiffness of the systems as long as $n_{1D}a_{1D}$ is sufficiently small. Interestingly, in this phase the density correlations are even stronger than in the TG gas, as they show a power-law decay that is slower than for a TG gas *(13)*, indicating an effective long-range interaction.

We realize the crossover all the way from a non-interacting gas via the 1D mean-field Thomas-Fermi (TF) regime to a TG gas and then to a sTG gas. We exploit the fact that our 1D systems possess weak harmonic confinement along the axial direction characterized by the confinement length $a_\parallel$. Whereas the frequency ω_D of the lowest dipole mode depends only on the confinement, the frequency ω_C of the lowest axial compressional mode is sensitive to the various regimes of interaction *(16)*. For the non-interacting system one expects $R \equiv \omega_C^2/\omega_D^2 = 4$. This value then changes to $R = 3$ for weakly repulsive interactions in a 1D TF regime *(7)*. For increasing positive interaction strength, R is expected to change smoothly to 4 when entering the TG regime as the system becomes fermionized and hence effectively non-interacting. A rise beyond the value of 4, after crossing the CIR, would then constitute clear evidence for the sTG regime *(13)*. As a_{1D} is further increased, the system will finally become unstable and R is expected to turn over and drop towards zero. For a harmonically confined system, the point of instability is reached when the overall length of the system of hard rods, Na_{1D}, becomes of the order of the size $\sqrt{N}a_\parallel$ for the wave function of N non-interacting fermions, i.e. $A \equiv Na_{1D}/(\sqrt{N}a_\parallel) \approx 1$. We use A^2 as an alternative parameter to γ to characterize the strength of the interaction as it accounts for the harmonic confinement.

We start from a 3D Bose-Einstein condensate (BEC) with up to 2×10^5 Cs atoms with no detectable thermal fraction in a crossed-beam dipole trap with magnetic levitation *(22)*. Depending on the interaction regime to be studied, we then set the number of atoms in the BEC to values in the range of $(1-4) \times 10^4$ by means of forced radio-frequency evaporation. To confine the atoms in 1D, i.e. to freeze out transversal

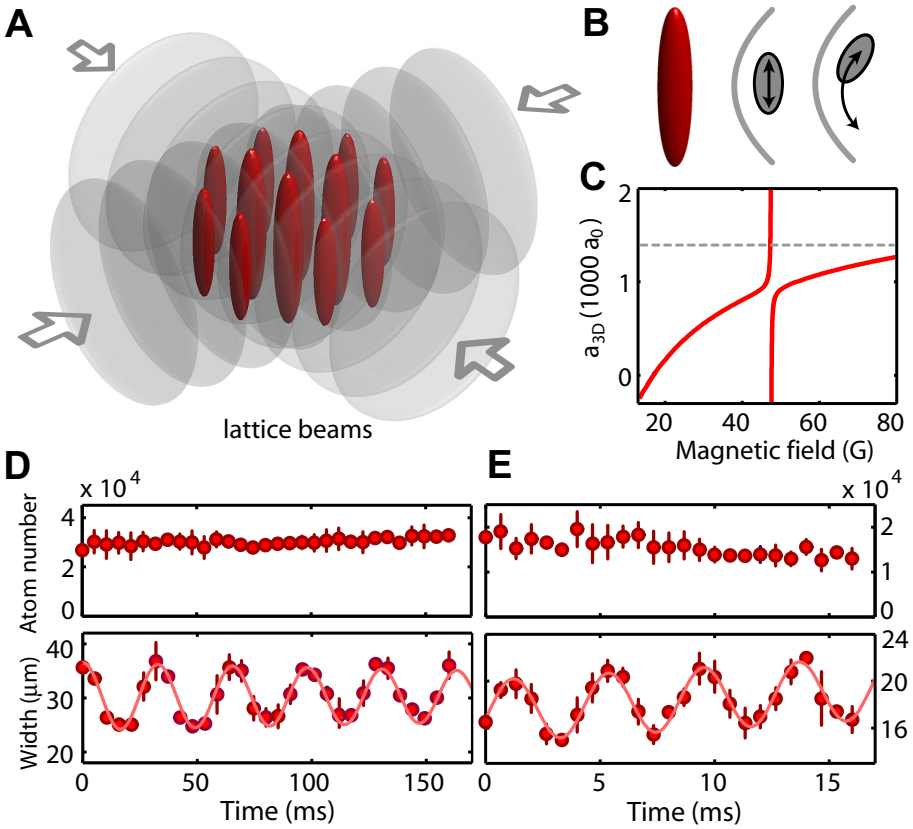

Figure 8.12: **A**, Experimental setup. The lattice potential is created by two retro-reflected laser beams confining the atoms to an array of one-dimensional tubes with equipotential surfaces shown in red. **B**, Along each tube (left) we excite the lowest compressional mode (center) and compare its frequency to the dipole mode (right). **C**, The strength of the interatomic interaction is adjusted by tuning the s-wave scattering length a_{3D}. The background scattering length rises gently from 0 to 1240 a_0 when the magnetic field B is tuned from 17 to 76 G. Further tuning is possible near a Feshbach resonance at 47.78(1) G to absolute values beyond 4000 a_0. The dashed line indicates $a_\perp/C$ for a transversal trap frequency of $\omega_\perp = 2\pi \times 13.1$ kHz. **D** and **E** present typical data sets for the compressional mode in the TG and sTG regime at $a_{3D} = 875(1)$ a_0 and $a_{3D} = 2300(200)$ a_0, respectively. The upper panels show the atom number, the lower panels show the $1/e$-cloud-width after time-of-flight. The solid lines in the lower panels are sinusoidal fits (see online material), yielding the oscillation frequencies $\omega_C = 2\pi \times 30.6(3)$ Hz and $\omega_C = 2\pi \times 241(1)$ Hz, respectively.

motion, we use a two-dimensional optical lattice *(12)*, which forms an array of vertically oriented elongated tubes with an aspect ratio that we set to values between 100 and 1000 (Fig. 8.12A). We occupy between 3000 – 6000 independent tubes with 8-25 atoms in the center tube. The interaction strength g_{1D} is controlled by magnetic tuning of a_{3D} by means of a combination of a broad and a narrow Feshbach resonance (Fig. 8.12C) with poles at $B = -11.1(6)$ G and $B = 47.78(1)$ G and widths of about 29.2

G and 164 mG, respectively *(23)*. The broad resonance provides a slow variation of a_{3D}, allowing us to gently tune a_{3D} from 0 a_0 near 17.119 G to about 1240 a_0 near 76 G, while the narrow resonance allows us to tune a_{3D} to absolute values beyond 4000 a_0 given our magnetic field control. We convert the applied magnetic field B into a_{3D} using the fit formula of Ref. *(23)*. A magnetic field gradient, used to levitate the atomic sample *(24)*, introduces a small spread in the value of a_{3D} across the sample.

To determine the oscillation frequencies ω_C and ω_D of the fundamental modes (Fig. 8.12 B), we excite each mode separately at a given value of the magnetic field B *(24)* and let the atoms evolve for a varying amount of hold time. The distribution is then imaged in momentum space by taking an absorption picture after release and expansion. To avoid possible broadening effects due to interaction during the initial expansion, a_{3D} is set to zero near $B = 17.119$ G at the moment of release. To extract the frequency, we determine for each hold time the axial $1/e$-width of the distribution and then fit a damped sinusoid with linear offset to this data. Typical measurements of ω_C are shown in Fig. 8.12 D and E. Whereas the atom number remains constant for $g_{1D} > 0$, we observe some atom loss and a slight broadening of the distribution for attractive 1D interactions. In all parameter regimes, the 1D system is sufficiently stable to allow a reliable measurement of ω_C.

First, we show that we can tune the system from the non-interacting regime deeply into the repulsive TG regime (Fig. 8.13). In agreement with expectations, the value for $R = \omega_C^2/\omega_D^2$ first drops from 4 to 3 and then increases back to 4 as γ is tuned by means of the gently-varying background scattering length. We find that the TG regime is fully reached for $\gamma > 50$. A further increase to values up to $\gamma \approx 500$ does not lead to changes for R. Note that, as a_{3D} approaches $a_\perp$, the divergence of g_{1D} according to Eq. 8.4 has to be taken into account when determining γ *(24)*. Heating of the system can be excluded as we can return to a 3D BEC without significant thermal background when ramping down the lattice potential.

The attractive regime is entered by crossing the CIR on the low-field wing of the 47.78 G Feshbach resonance. a_{1D} is now small and positive. The central results of this work are summarized in Fig. 8.14A and compared to the theoretical work of Ref. *(13)*. We plot $R = \omega_C^2/\omega_D^2$ as a function of the interaction parameter A^2. For reference, Fig. 8.14B plots a_{3D}, a_{1D}, and g_{1D} in the vicinity of the Feshbach resonance as a function of the magnetic field B. As the CIR is crossed and A^2 is increased, R rises beyond the value of 4. This provides clear evidence for the sTG regime as $R = 4$ is the maximal value for bosons with repulsive contact interaction. This increase is expected from the model of a gas of hard rods, and our data initially follows the prediction from this model. However, as A^2 is increased, R reaches a maximum and then starts to drop. The maximum of about 4.5 is reached for $A^2 \approx 3 \times 10^{-2}$. The existence of the maximum is in qualitative agreement with the results obtained from Monte-Carlo simulations *(13)*. The theoretical prediction, however, underestimates the measured R. This is probably due to the local density approximation, which may not be applicable to our system with low particle numbers. For comparison, the results from Fig. 8.13 for $\gamma \geq 1$ are shown. Note that $\gamma \approx 500$ corresponds to small values of $A^2 \approx 10^{-4}$. For this data,

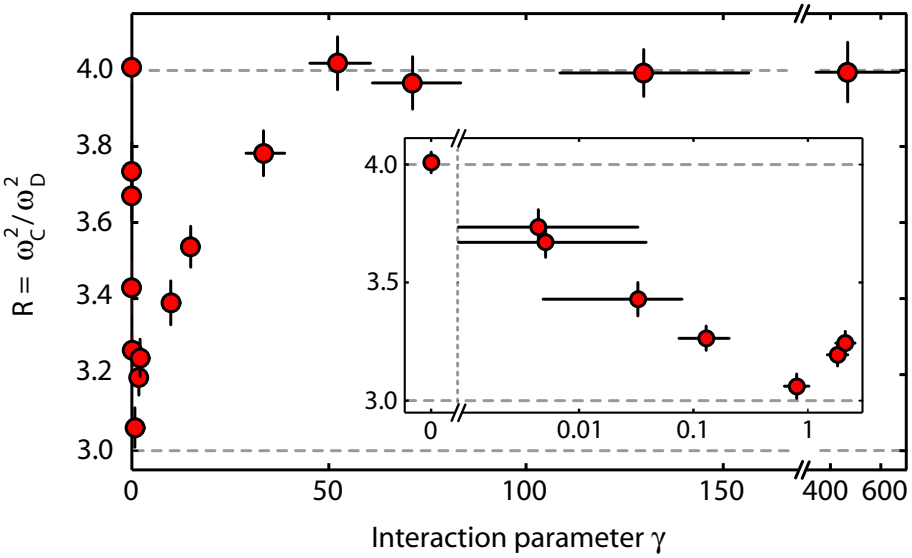

Figure 8.13: Transition from the non-interacting regime via the mean-field TF regime into the TG regime. The squared frequency ratio $R = \omega_C^2/\omega_D^2$ of the lowest compressional mode with frequency ω_C and the dipole mode with frequency ω_D serves as an indicator for the different regimes of interaction. For increasing interactions from $\gamma = 0$ to $\gamma \approx 500$ the system passes from the ideal gas regime ($R = 4$) to the 1D TF regime ($R \approx 3$) and then deeply into the TG regime ($R = 4$). The inset shows the transition from the non-interacting regime to the mean-field regime in more detail. The vertical error bars refer to standard error and the horizontal error bars reflect the uncertainty in determining a_{1D} and n_{1D} (see online material). The horizontal error bar on the data point at $\gamma = 0$ (not shown in the inset) is ± 0.03 a_0.

at higher particle numbers, there is excellent agreement with the theoretical prediction (solid line) in the entire crossover from the mean-field regime to the TG regime *(16)*.

We study the stability of the system in the crossover from the TG to the sTG regime and find further evidence for the existence of the CIR by recording particle loss and measuring the axial width of the atomic cloud after release from the tubes. The axial width is a measure for the kinetic energy of the system as interactions are instantly switched off upon release. Similar conditions are used as for the measurements on the sTG regime presented in Fig. 8.14. The TG regime is entered adiabatically to avoid the excitation of collective modes. The system is prepared at $a_{3D} = 887(1)$ a_0 at a magnetic field of $B = 42.77(2)$ G with about 11 atoms in the central tube. The magnetic field is then ramped to a specific value within 0.2 ms and the sample is held at this value for a variable hold time τ from 10 to 200 ms. $a_\perp$ is set to 1523(6) a_0. The results (Fig. 8.15) for different hold times τ in the tubes show that, for $\tau = 10$ ms, corresponding to the timescale of the measurements in the sTG regime shown in Fig. 8.14, the transition from the TG to the sTG regime appears very smooth. There is essentially no particle loss when the system is deep in the TG regime and close to the CIR. The loss gradually increases in the attractive regime as one moves to larger values of B and towards the

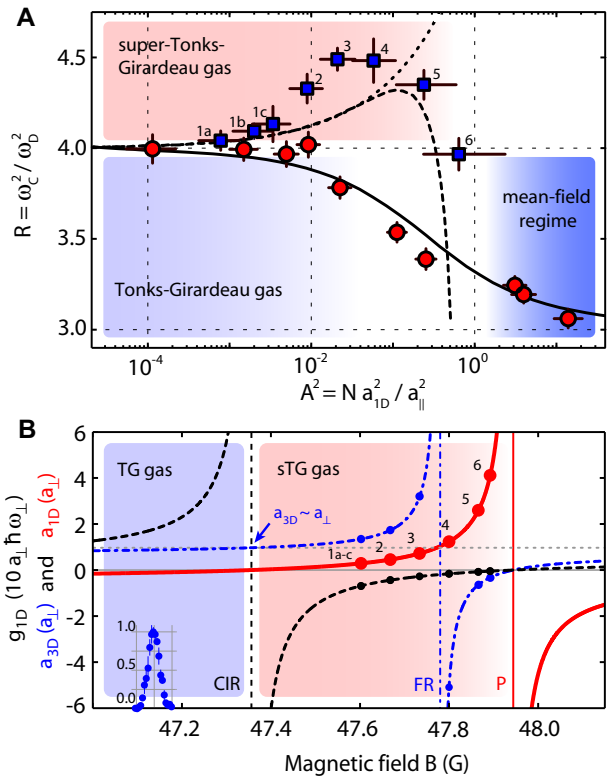

Figure 8.14: **A**, The ratio $R = \omega_C^2/\omega_D^2$ is plotted as a function of the interaction parameter $A^2 = Na_{1D}^2/a_\parallel^2$. The squares show the measurements in the attractive regime ($g_{1D} < 0$), providing evidence for the super-Tonks-Girardeau gas. The circles show the transition from the TF to the TG regime ($g_{1D} > 0$, same data as in Fig. 8.13 for $\gamma > 1$). The solid (dashed) line presents the theoretical data for $g_{1D} > 0$ ($g_{1D} < 0$) by Astrakharchik et al.*(13)*. The dotted line corresponds to the model of hard rods. For reference, the measurements for $g_{1D} < 0$ are numbered. Data points 1c to 6 are taken at $\omega_D = 2\pi \times 115.6(3)$ Hz. For data points 1a and 1b the trap frequency is $\omega_D = 2\pi \times 22.4(1)$ Hz and $\omega_D = 2\pi \times 52.3(1)$ Hz, respectively. For all measurements in the sTG regime $a_\perp = 1346(5)$ a_0. **B**, The parameters a_{3D} (dashed-dotted), a_{1D} (solid), and g_{1D} (dashed) are plotted in the vicinity of the Feshbach resonance (FR) at 47.78(1) G. The horizontal dotted line indicates the value of $a_\perp/C$. The pole of the CIR is at 47.36(2) G. a_{1D} has a pole (P) at 47.96(2) G. The bell-shaped curve at the bottom left indicates the atomic distribution as a function of the magnetic field determined from high-resolution microwave spectroscopy.

pole for a_{1D}. Correspondingly, the width of the sample exhibits a smooth behavior across the CIR, showing a slight increase for larger B. This behavior is consistent with the expectation of an increased energy in the sTG regime *(13)*.

For longer hold times, the data for the atom number and the sample width develop distinct features at the calculated position of the CIR. Evidently, the system is in a transient state. For $\tau = 50$ ms, the number of remaining atoms shows a dip that correlates with a peak in the kinetic energy of the sample. Both features become more

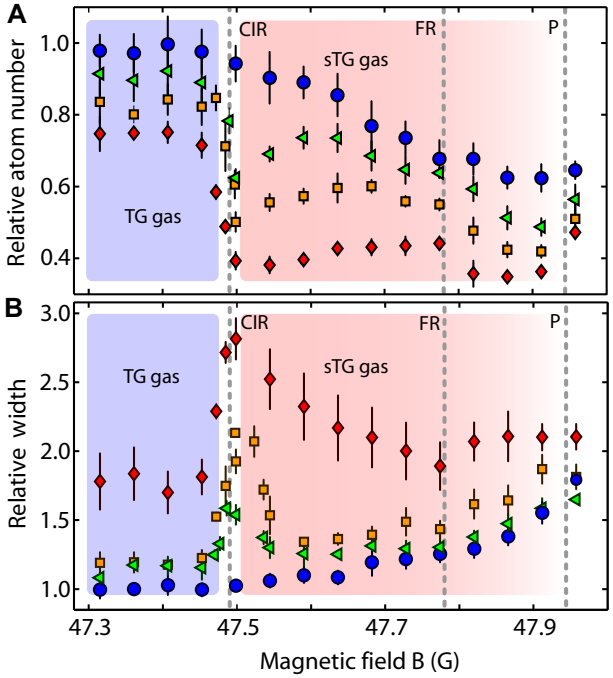

Figure 8.15: Stability and kinetic energy in the TG and sTG regimes. **A**, relative number of atoms remaining and **B**, relative $1/e$-width along the axial direction after 10 ms expansion, after a hold time τ = 10, 50, 100, and 200 ms (circles, triangles, squares, and diamonds, respectively) at a given magnetic field B. The position of the CIR, the pole of the Feshbach resonance (FR), and the pole for a_{1D} (P) are as indicated. For these measurements $a_\perp$ = 1523(6) a_0 and $\omega_D = 2\pi \times 115.6(3)$ Hz. The atom number is normalized to the initial value of $1.7(1) \times 10^4$ and the width is normalized to the initial value in the TG regime.

prominent and asymmetric for longer hold times (τ = 100 and 200 ms). Note that, in comparison, no pronounced effects are visible at the pole of the Feshbach resonance for a_{3D}. Our results must be connected to the fact that the energy spectrum of the system changes dramatically across the CIR, from the TG to the sTG regime *(19)*. The system acquires a deeply lying ground state together with a family of lower lying many-body excited states, potentially opening up new decay channels. Also, the CIR strongly modifies the two-body scattering problem, making formation of confinement-induced molecules in transversally excited trap states *(14)* possible.

The non-trivial time evolution observed in this system raises intriguing questions on possible coupling and decay mechanisms for strongly interacting excited many-body systems, in particular in the context of integrability of 1D systems *(25)*. Our results offer an example of the counter-intuitive effects that occur in many-body systems, and open up the possibility to study the dynamical properties of strongly-correlated systems with effective long-range interactions *(26,27)* under conditions where all parameters are tunable and, in fact, can be changed dynamically. Similar to magnetic Feshbach resonances in atomic scattering, we expect the confinement-induced reso-

nance demonstrated here to serve as a general tool to tailor interactions in 1D and possibly also in 2D systems *(28)*, allowing for the further investigation of strongly correlated phases in the context of cold atomic gases.

References and Notes

1. M. Girardeau, *J. Math. Phys.* **1**, 516 (1960).
2. E. H. Lieb, W. Liniger, *Phys. Rev.* **130**, 1605 (1963).
3. B. Paredes *et al.*, *Nature* **429**, 277 (2004).
4. T. Kinoshita, T. Wenger, D. S. Weiss, *Science* **305**, 1125 (2004).
5. F. Alet, A. M. Walczak, M. P. A. Fisher, *Physica A* **369**, 122 (2006).
6. D. S. Petrov, G. V. Shlyapnikov, J. T. M. Walraven, *Phys. Rev. Lett.* **85**, 3745 (2000).
7. H. Moritz, T. Stöferle, M. Köhl, T. Esslinger, *Phys. Rev. Lett.* **91**, 250402 (2003).
8. B. L. Tolra *et al.*, *Phys. Rev. Lett.* **92**, 190401 (2004).
9. D. S. Petrov, D. M. Gangardt, G. V. Shlyapnikov, *J. Phys. IV France* **116**, 3 (2004).
10. S. Hofferberth, I. Lesanovsky, B. Fischer, T. Schumm, J. Schmiedmayer, *Nature* **449**, 324 (2007).
11. N. Syassen *et al.*, *Science* **320**, 1329 (2008).
12. I. Bloch, J. Dalibard, W. Zwerger, *Rev. Mod. Phys.* **80**, 885 (2008).
13. G. E. Astrakharchik, J. Boronat, J. Casulleras, S. Giorgini, *Phys. Rev. Lett.* **95**, 190407 (2005).
14. T. Bergeman, M. G. Moore, M. Olshanii, *Phys. Rev. Lett.* **91**, 163201 (2003).
15. M. Olshanii, *Phys. Rev. Lett.* **81**, 938 (1998).
16. C. Menotti, S. Stringari, *Phys. Rev. A* **66**, 043610 (2002).
17. S. Inouye *et al.*, *Nature* **392**, 151 (1998).
18. J. B. McGuire, *J. Math Phys.* **6**, 432 (1965).
19. E. Tempfli, S. Zöllner, P. Schmelcher, *New J. Phys.* **10**, 103021 (2008).

20. M. T. Batchelor, M. Bortz, X. W. Guan, N. Oelkers, *J. Stat. Mech.* L10001 (2005).

21. G. E. Astrakharchik, D. Blume, S. Giorgini, B. E. Granger, *Phys. Rev. Lett.* **92**, 030402 (2004).

22. T. Weber, J. Herbig, M. Mark, H.-C. Nägerl, R. Grimm, *Science* **299**, 232 (2003).

23. A. D. Lange *et al.*, *Phys. Rev. A* **79**, 013622 (2009).

24. Material and methods are available as supporting material on *Science* Online.

25. T. Kinoshita, T. Wenger, D. S. Weiss, *Nature* **440**, 900 (2006).

26. M. Bockrath *et al.*, *Nature* **397**, 598 (1999).

27. H. Steinberg *et al.*, *Nature Phys.* **4**, 116 (2008).

28. D. S. Petrov, M. Holzmann, G. V. Shlyapnikov, *Phys. Rev. Lett.* **84**, 2551 (2000).

29. We thank S. Giorgini and C. Menotti for helpful discussions and for providing the theory curves shown in Fig. 8.14A. We are indebted to R. Grimm for generous support and to H. Häffner and his group for the loan of a CCD camera. We gratefully acknowledge funding by the Austrian Ministry of Science and Research (Bundesministerium für Wissenschaft und Forschung) and the Austrian Science Fund (Fonds zur Förderung der wissenschaftlichen Forschung) in form of a START prize grant and by the European Union through the STREP FP7-ICT-2007-C project NAME-QUAM (Nanodesigning of Atomic and MolEcular QUAntum Matter) and within the framework of the EuroQUASAR collective research project QuDeGPM. R.H. is supported by a Marie Curie International Incoming Fellowship within the 7th European Community Framework Programme.

Supporting Online Material
www.sciencemag.org
Materials and Methods

8.4 Confinement-induced resonances in low- dimensional quantum systems

submitted for publication

Elmar Haller[1], Manfred J. Mark[1], Russell Hart[1], Johann G. Danzl[1**],
Lukas Reichsöllner[1], Vladimir Melezhik[2], Peter Schmelcher[3],
and Hanns-Christoph Nägerl[1]

[1]Institut für Experimentalphysik and Zentrum für Quantenphysik,
Universität Innsbruck,
Technikerstraße 25, 6020 Innsbruck, Austria

[2]Bogoliubov Laboratory of Theoretical Physics, Joint Institute for Nuclear Research,
Dubna, 141980 Dubna, Russia

[3]Zentrum für Optische Quantentechnologien, Universität Hamburg,
Luruper Chaussee 149, 22761 Hamburg, Germany

We report on the observation of confinement-induced resonances in strongly interacting quantum-gas systems with tunable interactions for one- and two-dimensional geometry. Atom-atom scattering is substantially modified when the s-wave scattering length approaches the length scale associated with the tight transversal confinement, leading to characteristic loss and heating signatures. Upon introducing an anisotropy for the transversal confinement we observe a splitting of the confinement-induced resonance. With increasing anisotropy additional resonances appear. In the limit of a two-dimensional system we find that one resonance persists.

Low-dimensional systems have recently become experimentally accessible in the context of ultracold quantum gases. For a two-dimensional (2D) geometry, the Berezinskii-Kosterlitz-Thouless (BKT) transition has been observed [1], while in one dimension the strongly-correlated Tonks-Girardeau (TG) [2,3] and super-Tonks-Girardeau (sTG) gases [4] have been realized. For molecular gases, it was shown that strong dissipation leads to inhibition of loss and induces particle correlations [5]. In general, tight confinement that leads to a system of reduced dimensionality modifies the density of states and amplifies the role of quantum fluctuations. Particles can become correlated, e.g. in the limit of the strongly-interacting TG gas, where bosons acquire fermionic properties [6]. In the experiments steep optical potentials freeze out

**The author of the present thesis contributed to this work through experimental support, discussions on physics and technology, and in paper writing.

particle motion along one or two directions, and restrict the dynamics to a plane or to a line, respectively. Such quasi-2D or quasi-1D systems can be realized with ultracold gases when the kinetic and the interaction energy of the particles are insufficient to transfer the particles to transversally excited energy levels [7,8].

While the confinement removes motional degrees of freedom, it also provides an additional structure of discrete energy levels that can be used to modify the scattering process along the unconfined direction and by this to effectively control the interaction properties of the low-dimensional system [7,9]. As is well known, in three-dimensional (3D) geometry magnetically-induced Feshbach resonances (FBRs) [11,10] allow tuning of the inter-particle interaction strength. For atoms, a FBR occurs when the scattering state of two atoms is allowed to couple to a bound molecular state. Typically, scattering state and bound state are brought into degeneracy by means of the magnetically tunable Zeeman interactions. For particles in 1D and 2D geometry a novel type of scattering resonance occurs [7,8,9]. Coupling between the incident channel of two incoming particles and a transversally excited molecular bound state generates a so-called confinement-induced resonance (CIR) [7,9,12,13,14,15,16,17]. A CIR occurs when the 3D scattering length a_{3D} approaches the length scale that characterizes the transversal confinement, i.e. the harmonic oscillator length $a_\perp = \sqrt{\hbar/(m\omega_\perp)}$ for a particle with mass m and transversal trapping frequency $\omega_\perp$. Whereas in the weak confinement limit ($a_{3D} \ll a_\perp$) the 1D coupling parameter $g_{1D} = 2\hbar\omega_\perp a_{3D}$ increases linearly with $\omega_\perp$, the CIR leads to strong coupling and causes $g_{1D} = \frac{2\hbar^2 a_{3D}}{m a_\perp^2} \frac{1}{1-Ca_{3D}/a_\perp}$ to diverge at $a_\perp = Ca_{3D}$, where $C = 1.0326$ is a constant [7], [9]. Crossing the CIR allows tuning of interactions from strongly repulsive (g_{1D} large and positive) to strongly attractive (g_{1D} large and negative). The CIR thus represents a crucial ingredient for the control of interactions in a low-dimensional system. Recently, a CIR has been observed for a strongly-interacting 1D quantum gas of Cs atoms and was used to drive the crossover from a TG gas with strongly repulsive interactions to an sTG gas with strongly attractive interactions [4]. Here, for an ultracold quantum gas of Cs atoms with tunable interactions, we study the properties of CIRs by measuring particle loss and heating rate and, in particular, confirm the resonance condition $a_\perp = Ca_{3D}$ for symmetric 1D confinement. For the case of transversally anisotropic confinement we find that the CIR splits and, to our surprise, persists for positive a_{3D} even when the anisotropy reaches the limit of a 2D system.

Figure 8.16(a) reviews the basic mechanism that causes a CIR for zero collisional energy in 1D [9]. It is assumed that in 3D the scattering potential supports a single universal bound state for strong repulsive interactions (dotted line) [18]. The point where the incoming channel of two colliding atoms and the universal dimer state are degenerate marks the position of a 3D FBR (triangle). In 1D, strong transversal confinement shifts the zero-energy of the incoming channel (middle dashed line) and introduces a transversally excited state (upper dashed line). As a result of the strong confinement, which modifies the long-range part of the molecular potential, the universal dimer state with binding energy E_B (lower solid line) exists also for attractive

interactions [19] whereas the original 3D FBR has disappeared. Instead, there is a CIR (star) when the incoming scattering channel becomes degenerate with the transversally excited molecular bound state (upper solid line). It is assumed that the binding energy of this state is also E_B, shifted by $2\hbar\omega_\perp$[7]. In more detail, as depicted in Fig. 8.16(b), we assume that the energy levels of non-interacting atoms, as a result of cylindrically symmetric transversal confinement, can be approximated by those of a 2D harmonic oscillator with $E_{n_1,n_2} = \hbar\omega_\perp(n_1 + n_2 + 1)$ and quantum numbers n_1 and n_2 belonging to the two Cartesian directions. Scattering atoms in the transversal ground state $(0, 0)$ can couple to the excited states (n_1, n_2) if the parity of the total wave function is preserved [12]. The energetically lowest allowed excited states are threefold degenerate with an energy $E = 3\hbar\omega_\perp$ and with quantum numbers $(1, 1)$, $(2, 0)$ and $(0, 2)$. For the transversally symmetric confinement, they contribute towards a single CIR [9]. Unequal transversal trapping frequencies ω_1 and $\omega_2 = \omega_1 + \Delta\omega$ lift this degeneracy and shift the energy levels according to $E_{n_1,n_2} = \hbar\omega_1(n_1 + n_2 + 1) + \hbar\Delta\omega(n_2 + 1/2)$. One thus expects a splitting of the CIR.

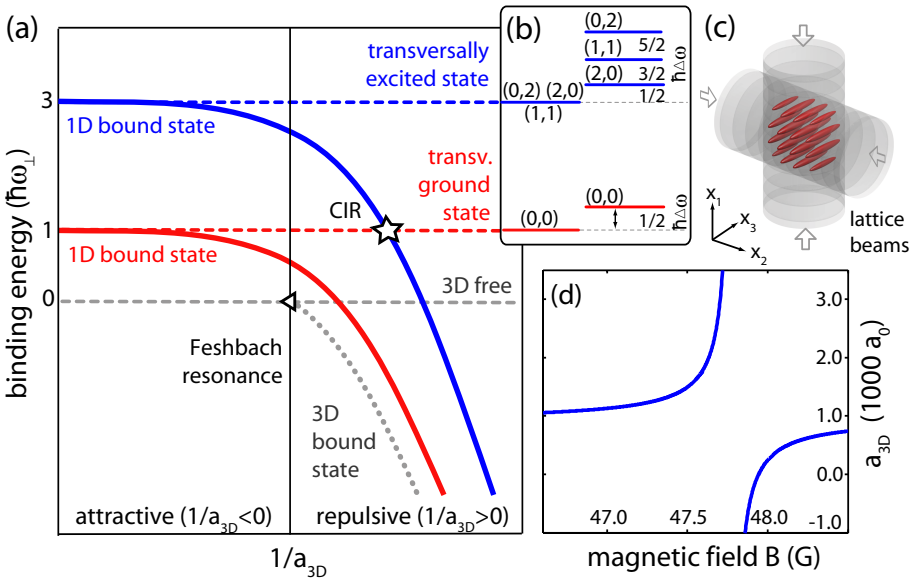

Figure 8.16: (color online) (a) Illustration of the mechanism responsible for a CIR, see Ref.[9] and text for details. The energy levels near a scattering resonance are plotted as a function of $1/a_{3D}$. The CIR occurs for $Ca_{3D} = a_\perp$ when scattering atoms are allowed to couple to transversally excited bound states. (b) indicates the shift and splitting for anisotropic confinement characterized by $\Delta\omega$. (c) Experimental configuration. Two laser beams create an optical lattice that confines the atoms to an array of approximately 3000 independent, horizontally-oriented elongated 1D tubes. (d) Tuning of a_{3D} is achieved by means of a FBR with a pole at $B = 47.78(1)$ G [21].

We start from a tunable Bose-Einstein condensate (BEC) of 1.0 to 1.4 $\times$ 10^5 Cs atoms in the energetically lowest hyperfine sublevel [20] confined in a crossed-beam optical dipole trap and levitated against gravity by a magnetic field gradient of

$|\nabla B| \approx 31.1$ G/cm. Tunability of a_{3D} is given by a FBR as shown in Fig. 8.16(d) with its pole at $B_0 = 47.78(1)$ G and a width of 164 mG. [20,21,4]. The resonance resides on top of a slowly varying background that allows tuning of a_{3D} from 0 to values of about 1000 a_0, where a_0 is Bohr's radius. Using the FBR, we can further tune to values up to $a_{3D} \approx 6000\ a_0$ given our magnetic field control with an uncertainty of $\Delta B \approx 10$ mG. We convert B into a_{3D} using the fit employed in Ref.[21]. The BEC is produced at $a_{3D} \approx 290\ a_0$. We load the atoms within 300 ms into an optical lattice, which is formed by two retro-reflected laser beams at a wavelength of $\lambda = 1064.49(1)$ nm and with a beam waist of approximately 350 μm, one propagating vertically and one propagating horizontally as illustrated in Fig. 8.16(c). These lattice beams confine the atoms to an array of approximately 3000 horizontally oriented, elongated 1D tubes with a maximum occupation of 60 atoms at a linear peak density of approximately $n_{1D} \approx 2/\mu$m. Weak longitudinal confinement results from the Gaussian-shaped intensity distribution of the beams. We raise the lattice to a depth of typically $V = 30\ E_R$, where $E_R = h^2/(2m\lambda^2)$ is the photon recoil energy. At this depth, the resulting transversal and longitudinal trap frequencies are $\omega_\perp = 2\pi \times 14.5$ kHz and $\omega_\parallel = 2\pi \times 16$ Hz and we then have $a_\perp \approx 1370\ a_0$. After loading we slowly ramp down $|\nabla B|$ in 50 ms and adiabatically increase a_{3D} to 915 a_0 in 100 ms to create a TG gas with well-defined starting conditions near the CIR [4]. To detect the CIR as a function of B, manifested by a loss resonance, we quickly set B in less than 200 μs to the desired value, wait for a hold time of typically $\tau = 200$ ms, and then measure the number N of remaining atoms by absorption imaging. For this, we re-levitate the atoms, ramp down the lattice beams adiabatically with respect to the lattice band structure, and allow for 50 ms of levitated expansion and 2 ms time-of-flight. Note that τ is chosen to be much longer than the lifetime of the sTG phase [4].

We observe the CIR in the form of an atomic loss signature as shown in Fig. 8.17. We attribute the loss near the resonance to inelastic three-body [22] or higher-order collisions [23], which lead to molecule formation and convert binding energy into kinetic energy, causing trap loss and heating, similar to the processes observed near a FBR [10]. In our case, inelastic two-body processes can be ruled out for energetic reasons and single-particle loss occurs on the timescale of tens of seconds. In Fig. 8.17(a) the CIR can be identified as a distinct "edge" for the atom number N. Initially, in the TG regime of strong repulsive interactions, here for $B < 47.35$ G, losses are greatly suppressed, but increase rapidly on the attractive side of the CIR. N drops to a minimum when B is increased and then recovers somewhat. A clear shift of the loss signature to lower values for B and hence lower values for a_{3D} can be discerned when the confinement is stiffened. When we identify the position of the edge with the position of the CIR, we find good agreement with the analytical result $Ca_{3D} = a_\perp$ as shown in Fig. 8.17(b). For comparison, we also plot the position of the minimum, which is shifted accordingly.

In Fig. 8.17(c) we juxtapose the loss and the heating rate that we measure in the vicinity of the CIR. For this, we measure the increase of the release energy within the first 100 ms. After holding the atoms for time τ at a given value of B, we decrease

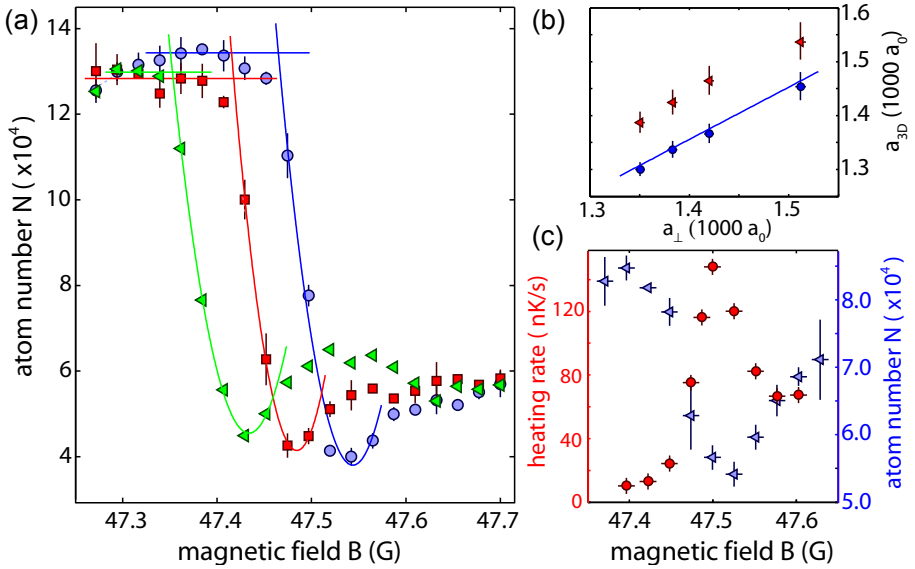

Figure 8.17: (color online) Particle loss and heating rates in the vicinity of a CIR. (a) The number N of remaining atoms after $\tau = 200$ ms shows a distinct drop ("edge") when B is scanned across the CIR. A clear shift of the position of the edge to lower values for B can be observed when the transversal confinement is stiffened, $\omega_\perp = 2\pi \times (0.84, 0.95, 1.05) \times 14.2(2)$ kHz (circles, squares, triangles). (b) Position of the edge (circles) as determined from the intersection point of a second-order polynomial fit to the minimum for N and the initial horizontal baseline as shown in (a), converted into values for a_{3D}. For comparison, the position of the minimum (triangles) is also shown. The solid line is given by $Ca_{3D} = a_\perp$ with the predicted value $C = 1.0326$. (c) Heating rates near the CIR (circles). For comparison, N is also shown (triangles). For this measurement, $\omega_\perp = 2\pi \times 12.0(2)$ kHz. All error bars reflect 1σ statistical uncertainty.

a_{3D} back to 250 a_0 in 20 ms, switch off the lattice potential and determine the release energy in the direction of the tubes from the momentum distribution in free space expansion. We observe an increase for the heating rate when the CIR is crossed. From a low value of 10 nK/s in the TG regime it rises to a maximum of approximately 150 nK/s and then drops to settle at some intermediate value. The position of the maximum agrees well with the maximum for atom loss. We check that the system's increase in energy is sufficiently small so that its 1D character is not lost. The release energy, even at maximal heating, remains below $k_B \times 30$ nK, which is far below the energy spacing of the harmonic oscillator levels, $\hbar\omega_\perp \approx k_B \times 600$ nK.

We now examine 1D systems with transversally anisotropic confinement. Starting from a lattice depth of $V = 25\ E_R$ along both transversal directions, yielding $\omega_\perp = \omega_1 = \omega_2 = 2\pi \times 13.2(2)$ kHz, we increase the horizontal confinement to frequencies up to $\omega_2 = 2\pi \times 16.5(2)$ kHz, corresponding to a lattice depth of 39 E_R, while keeping the depth of the vertical confinement constant. Fig. 8.18(a) shows a distinct splitting of the original CIR into two loss resonances, CIR_1 and CIR_2. The splitting increases

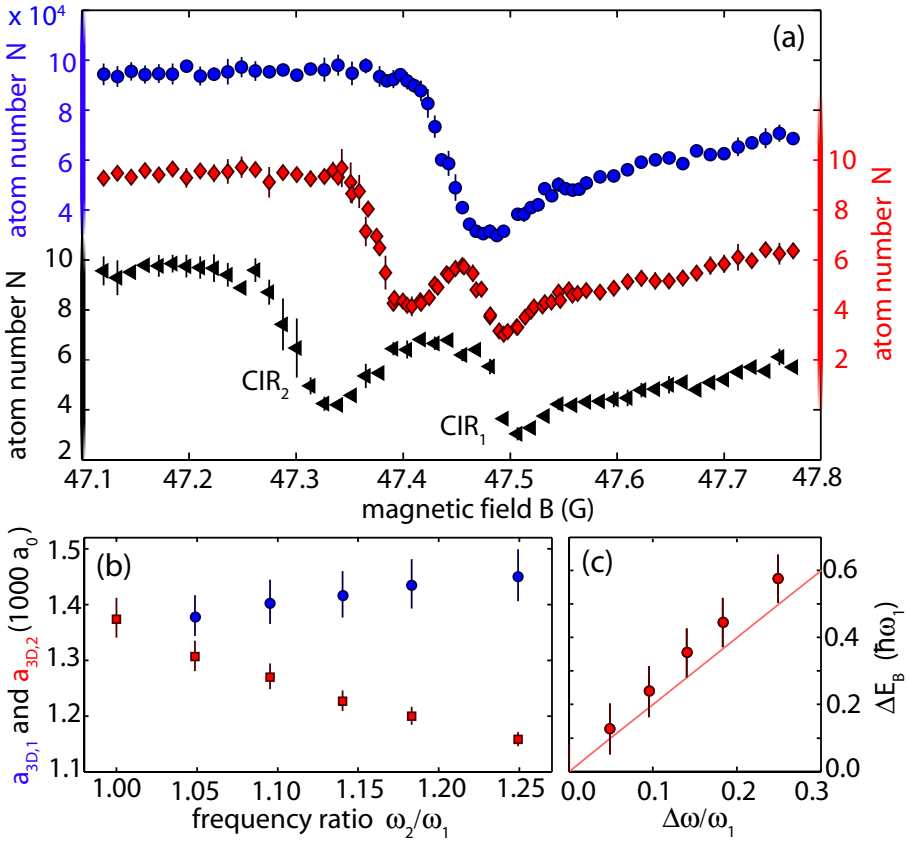

Figure 8.18: (color online) Splitting of a CIR for a 1D system with transversally anisotropic confinement. (a) As the horizontal confinement is stiffened, $\omega_2/\omega_1 = 1.00, 1.10, 1.18$ (circles, diamonds, triangles) for $\omega_1 = 2\pi \times 13.2(2)$ kHz, the CIR splits into CIR_1 and CIR_2. (b) Position of CIR_1 ($a_{3\mathrm{D},1}$, circles) and CIR_2 ($a_{3\mathrm{D},2}$, squares) as a function of the frequency ratio ω_2/ω_1. (c) Binding energy difference ΔE_B as determined from the implicit equation (see text) in comparison to the expectation from the simple harmonic oscillator model (solid line).

as the anisotropy is raised. In Fig. 8.18(b) we plot the 3D scattering length values $a_{3\mathrm{D},1}$ and $a_{3\mathrm{D},2}$ that we associate with the positions of CIR_1 and CIR_2 as a function of the frequency ratio ω_2/ω_1. For this, as it becomes difficult to assign an edge to both of them, we simply determine the associated atom number minima and subtract a constant offset of 88(7) a_0 as determined from the measurement shown in Fig. 8.17(b). One of the resonances, CIR_2, exhibits a pronounced shift to smaller values for $a_{3\mathrm{D}}$ as the horizontal confinement is stiffened. The second resonance, CIR_1, shows a slight shift towards higher values for $a_{3\mathrm{D}}$. We now use the lifting of the degeneracy for the energy levels as indicated in Fig. 8.16(b) to model the observed splitting of the CIR. We assume that the implicit equation $\zeta(1/2, -E_\mathrm{B}/(2\hbar\omega_\perp) + 1/2) = -a_\perp/a_{3D}$ for the binding energy E_B [9] remains approximately valid for sufficiently small $\Delta\omega$, taking $\omega_\perp = \omega_1$. Here, ζ is the Hurwitz zeta function. We translate the scattering

length values $a_{3D,1}$ and $a_{3D,2}$ into binding energies and calculate the energy difference $\Delta E_B = E_B(a_{3D,1}) - E_B(a_{3D,2})$, shown in Fig. 8.18(c). While this model does not explain the upward deviation seen for CIR_1, the difference ΔE_B is in reasonable agreement with the expected energy shift caused by the shifts of the excited harmonic oscillator states $(E_{0,2} - E_{2,0}) = 2\hbar\Delta\omega$ (solid line in Fig. 8.18(c)). We thus attribute CIR_2 to the stiffened confinement along the horizontal direction and hence to state $(0, 2)$, while CIR_1 corresponds to the unchanged confinement along the vertical direction and hence to state $(2, 0)$. Note that we do not detect a third resonance that could be associated with state $(1, 1)$.

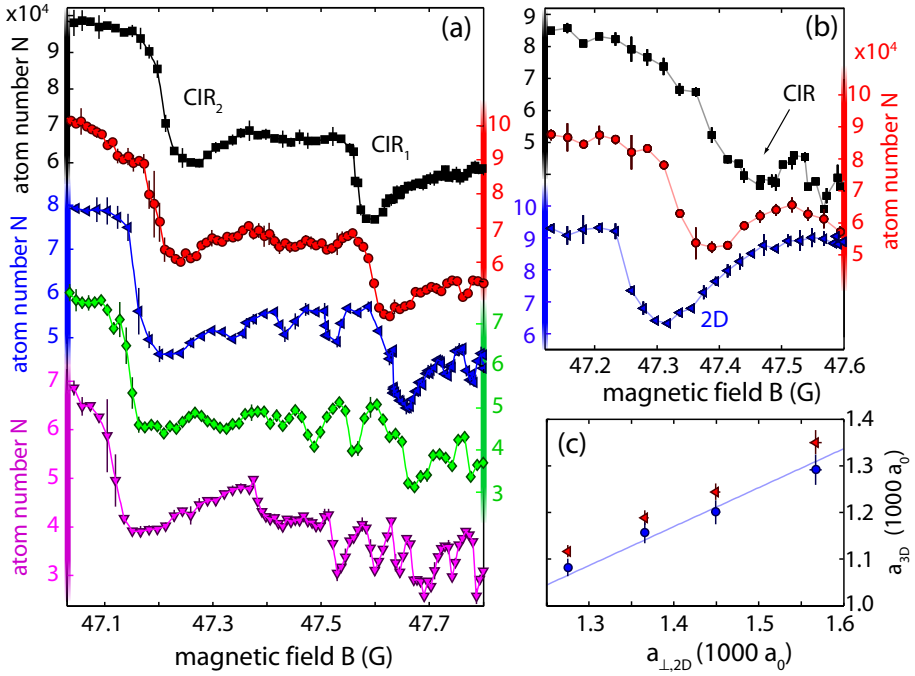

Figure 8.19: (color online) (a) Appearance of additional structure in the vicinity of CIRs for strongly anisotropic transversal confinement. The trap frequencies are $\omega_2 = 2\pi \times 16.6(2)$ kHz and $\omega_1/\omega_2 = 0.67, 0.60, 0.53, 0.49, 0.45$ from top to bottom. (b) Transition from 1D to 2D confinement. As the horizontal lattice is ramped down, CIR_2 shifts and persists, while CIR_1 disappears ($\omega_1 = 2\pi \times 13.0(2)$ kHz and $\omega_2/\omega_1 = 0.58, 0.42, 0.00$ for squares, circles, and triangles). (c) Scaling of the CIR's position in 2D, in analogy to the 1D case shown in Fig. 8.17(b). The position of the CIR as determined from the edge (circles) and, alternatively, from the minimum in atom number (triangles) shifts to lower values for a_{3D} as the confinement is stiffened and $a_{\perp,2D}$ is reduced. The solid line is a linear fit according to $C_{2D}a_{3D} = a_{\perp,2D}$ with $C_{2D} = 1.19(3)$.

We observe the appearance of additional structure in the measured loss curves when we increase the transversal anisotropy by weakening the confinement along one axis, here along the vertical direction. Fig. 8.19(a) shows the atom number after $\tau = 300$ ms for trapping frequency ratios ω_1/ω_2 from 0.67 to 0.45. Multiple loss

resonances appear close to the position of CIR_1. The number of resonances increases and the positions shift continuously as the confinement is weakened. We speculate that those resonances are a result of a coupling to additional excited states, resulting in a multi-channel scattering situation. Also the weakening of the confinement could induce sufficient anharmonicity to allow for violation of the parity rule [24].

Surprisingly, we find that one of the CIRs persists in the limit of a 2D system. Previous theoretical studies on 2D systems have predicted the appearance of a CIR for negative $a_{3\mathrm{D}}$, but not for positive $a_{3\mathrm{D}}$ [25,14]. In the experiment, we reduce the horizontal confinement while keeping the vertical confinement constant to probe the transition from the array of tubes to a stack of pancake-shaped, horizontally-oriented 2D systems. Trapping in the horizontal direction is still assured, now by the Gaussian profile of the vertically propagating laser beam, for which $\omega_2 = 2\pi \times 11$ Hz. Fig. 8.19(b) shows that the CIR associated with the tight confinement shifts to lower values for B and hence for $a_{3\mathrm{D}}$ as the horizontal confinement is weakened. In the limit of 2D confinement, one of the CIRs, and in fact all the additional structure observed above, have disappeared, but one resonance persists. To check that the observed resonance is indeed the result of the 2D confinement, we vary the confinement along the tight vertical direction. Fig. 8.19(c) plots the positions of edge and minimum of the loss signature as a function of $a_{\perp,2\mathrm{D}}$, the confinement length associated with this direction. When we again associate the edge with the pole of the resonance, we obtain $C_{2\mathrm{D}} a_{3\mathrm{D}} = a_{\perp,2\mathrm{D}}$ with $C_{2\mathrm{D}} = 1.19(3)$, where $C_{2\mathrm{D}}$ is a scaling factor similar to C for the 1D case.

In summary, we have investigated the properties of CIRs, which appear in low-dimensional quantum systems as a result of tight confinement and which replace "conventional" 3D Feshbach resonances to tune the effective atomic interaction strength. We observed a splitting of the CIR for anisotropic transversal confinement, the appearance of multiple resonances for strongly anisotropic confinement, and the survival of one resonance for positive $a_{3\mathrm{D}}$ in the limit of 2D confinement. We expect that CIRs will not only be used in 1D geometry to tune the effective interaction strength as recently demonstrated [4], but also in 2D geometry and mixed dimensions [26] for the study of strongly-interacting quantum systems.

We thank W. Zwerger for discussions and R. Grimm for generous support. We gratefully acknowledge funding by the Austrian Ministry of Science and Research and the Austrian Science Fund and by the European Union within the framework of the EuroQUASAR collective research project QuDeGPM. R.H. is supported by a Marie Curie International Incoming Fellowship within FP7. P.S. gratefully acknowledges financial support by the Deutsche Forschungsgemeinschaft. Financial support by the Heisenberg-Landau Program is appreciated by P.S. and V.S.M.

References

1. Z. Hadzibabic *et al.*, Nature **441**, 1118 (2006).

2. T. Kinoshita, T. Wenger, D. S. Weiss, Science **305**, 1125 (2004).

3. B. Paredes *et al.*, Nature **429**, 277 (2004).

4. E. Haller *et al.*, Science **325**, 1224 (2009).

5. N. Syassen *et al.*, Science **320**, 1329 (2008).

6. M. Girardeau, J. Math. Phys. **1**, 516 (1960).

7. M. Olshanii, Phys. Rev. Lett. **81**, 938 (1998).

8. D. S. Petrov, M. Holzmann, G. V. Shlyapnikov, Phys. Rev. Lett. **84**, 2551 (2000).

9. T. Bergeman, M. G. Moore, M. Olshanii, Phys. Rev. Lett. **91**, 163201 (2003).

10. C. Chin, R. Grimm, P. Julienne, E. Tiesinga, cond-mat:0812.1496v2.

11. S. Inouye *et al.*, Nature **392**, 151 (1998).

12. J.I. Kim, J. Schmiedmayer, P. Schmelcher, Phys. Rev. A **72**, 042711 (2005).

13. V.S. Melezhik, J.I. Kim, P. Schmelcher, Phys. Rev. A **76**, 053611 (2007).

14. P. Naidon, E. Tiesinga, W.F. Mitchell, P.S. Julienne, New J. Phys. **9**, 19 (2007).

15. S. Saeidian, V.S. Melezhik, P. Schmelcher, Phys. Rev. A **77**, 042721 (2008).

16. E. Tiesinga, C. J. Williams, F. H. Mies, P.S. Julienne, Phys. Rev. A **61**, 063416 (2000).

17. V.A. Yurovsky, Phys. Rev. A **71**, 012709 (2005).

18. I. Bloch, J. Dalibard, W. Zwerger, Rev. Mod. Phys. **80**, 885 (2008).

19. H. Moritz, T. Stöferle, M. Köhl, T. Esslinger, Phys. Rev. Lett. **91**, 250402 (2003).

20. T. Kraemer *et al.*, Appl. Phys. B **79**, 1013 (2004).

21. A.D. Lange *et al.*, Phys. Rev. A **79**, 013622 (2009).

22. T. Weber, J. Herbig, M. Mark, H.-C. Nägerl, R. Grimm, Phys. Rev. Lett. **91**, 123201 (2003).

23. F. Ferlaino *et al.*, Phys. Rev. Lett. **102**, 140401 (2009).

24. V. Peano, M. Thorwart, C. Mora, R. Egger, New J. Phys. **7**, 192 (2005).

25. D. S. Petrov, G. V. Shlyapnikov, Phys. Rev. A **64**, 012706 (2001).

26. G. Lamporesi *et al.*, arXiv:1002.0114.

8.5 Inducing transport in a dissipation-free lattice with super Bloch oscillations

submitted for publication

Elmar Haller[1], Russell Hart[1], Manfred J. Mark[1], Johann G. Danzl[1**], Lukas Reichsöllner[1], and Hanns-Christoph Nägerl[1]

[1]Institut für Experimentalphysik and Zentrum für Quantenphysik,
Universität Innsbruck,
Technikerstraße 25, 6020 Innsbruck, Austria

Particles in a perfect lattice potential perform Bloch oscillations when subject to a constant force, leading to localization and preventing conductivity. For a weakly-interacting Bose-Einstein condensate (BEC) of Cs atoms, we observe giant center-of-mass oscillations in position space with a displacement across hundreds of lattice sites when we add a periodic modulation to the force near the Bloch frequency. We study the dependence of these "super" Bloch oscillations on lattice depth, modulation amplitude, and modulation frequency and show that they provide a means to induce linear transport in a dissipation-free lattice. Surprisingly, we find that, for an interacting quantum system, super Bloch oscillations strongly suppress the appearance of dynamical instabilities and, for our parameters, increase the phase-coherence time by more than a factor of hundred.

Understanding the conduction of electrons through solids is of fundamental concern within the physical sciences. The simplified situation of an electron under a constant force F within a perfect, non-dissipative, periodic lattice was originally studied by Bloch and Zener [1] over 70 years ago. Their and subsequent studies revealed that the particle would undergo so-called Bloch oscillations (BOs), a periodic oscillation in position and momentum space, thereby quenching transport and hence resulting in zero conductivity. BOs can be viewed as periodic motion through the first Brillouin zone, resulting in a Bloch period $T_B = 2\hbar k/F$, where $k = \pi/d$ is the lattice wave vector for a lattice spacing d. They result from the interference of the particle's matter wave in the presence of the periodic lattice structure, requiring a coherent evolution of the wave during the time T_B. Generally, it is believed that conductance is restored via dissipative effects such as scattering from lattice defects or lattice phonons [2]. In

**The author of the present thesis contributed to this work through experimental support, discussions on physics and technology, and in paper writing.

bulk crystals, relaxation processes destroy the coherence of the system even before a single Bloch cycle is completed. These systems thus exhibit conductivity but prevent the observation of BOs. To observe BOs, the BO frequency $\nu_B = 1/T_B$ must be large compared to the rate of decoherence. In semiconductor superlattices, where the Bloch frequency is enhanced, a few cycles have been observed [3].

A recent approach to observe and study BOs is to use systems of ultracold atoms in optical lattice potentials with a force that is provided by gravity or by acceleration of the lattice potential. In these engineered potentials, generated by interfering laser waves, dissipation is essentially absent, and decoherence can be well-controlled [4]. Essentially all relevant system parameters are tunable, e.g. lattice depth and spacing, particle interaction strength, and external force, i.e. lattice tilt. For sufficiently low temperatures, a well-defined narrow momentum distribution can initially be prepared. BOs have been observed for thermal samples [5,6,7], for atoms in weakly-interacting Bose-Einstein condensates (BECs) [8,9,4], and for ensembles of non-interacting quantum-degenerate fermions [10]. Non-interacting BECs [11,12] are ideally suited to study BOs as interaction-induced dephasing effects are absent, allowing for the observation of more than 20000 Bloch cycles [11].

As for any oscillator, classical or quantum, it is natural that one investigates the properties of the oscillator under forced harmonic driving. The dynamics of a harmonically driven Bloch oscillator has recently been the subject of several theoretical [13,14,15,16] and experimental studies [17,19,18,20]. For example, modulation-enhanced tunneling between lattice sites [19,18] and spatial breathing of incoherent atomic samples [20] have been observed. Here, for a weakly-interacting atomic BEC in a tilted lattice potential, we demonstrate that harmonic driving can lead to directed center-of-mass motion and hence to transport. In this dissipationless system we thereby recover transport and obtain ballistic conductivity. More strikingly, for slightly off-resonant driving, we observe giant matter-wave oscillations that extend over hundreds of lattice sites. These "super Bloch oscillations" result from a beat between the usual BOs and the drive. They are rescaled BOs in position space and can also be used, by appropriate switching of the detuning or the phase, to engineer transport. Interestingly, forced driving leads to strongly reduced interaction-induced dephasing and greatly extends the time over which ordinary BOs can be observed.

The experimental starting point is a tunable BEC of 1.2×10^5 Cs atoms in a crossed beam dipole trap [21] adiabatically loaded within 400 ms into a vertically oriented 1D optical lattice [11] as illustrated in Fig. 8.20(a). The lattice spacing is $d = \lambda/2$, where $\lambda = 1064.49(1)$ nm is the wavelength of the light. Unless stated otherwise, we work with a shallow lattice with depth $V = 3.0(3)\ E_R$, where $E_R = h^2/(2m\lambda^2)$ is the photon recoil energy for particles with mass m. The atoms are initially levitated against gravity by means of a magnetic field gradient and spread across approximately 50 lattice sites with an average density near 5×10^{13} cm^{-3} in the central region of the sample. We control the strength of the interaction as measured by the s-wave scattering length a near a Feshbach resonance [21]. Throughout this work, unless stated otherwise, we work at $a = 11(1)\ a_0$, where a_0 is Bohr's radius. We initiate BOs by removing the

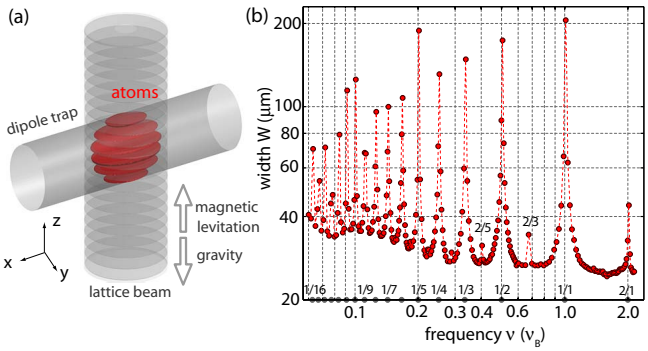

Figure 8.20: (color online) Experimental setup (a) and excitation spectrum (b) for atoms in a tilted periodic potential. The width W is plotted as a function of the drive frequency ν. The resonances correspond to a drastic spreading of the atomic wave packet as a result of modulation-assisted tunneling [19] when $\nu \approx i/j \times \nu_B$, where i, j are integers. The parameters are $F_0 = 0.096(1)mg$, $\Delta F = 0.090(4)mg$, $V = 3.0(3)\ E_R$, and $\tau = 2$ s. The dashed line is a guide to the eye.

dipole trap confinement in the vertical direction and by reducing the levitation in 1 ms to cause a force that is a small fraction of the gravitational force mg, for which ν_B is near 100 Hz. An additional harmonic modulation of the levitation gradient then results in an oscillating driving force $F(t) = F_0 + \Delta F \sin(2\pi\nu t + \phi)$, where F_0 is the constant force offset, ΔF is the amplitude of the modulation, ν is the modulation frequency, and ϕ is a phase difference between the BOs and the drive. After a given hold time τ we switch off all optical beams and magnetic fields and take in-situ absorption images after a short delay time of 800μs.

We first determine the excitation spectrum. Fig. 8.20(b) shows the $1/\sqrt{e}$-width W of the matter wave after $\tau = 2$ s as a function of ν. A series of narrow resonances at rational multiples of ν_B can clearly be identified. In agreement with recent experiments [19,18], we attribute these resonances to modulation-enhanced tunneling between lattice sites, leading to dramatic spreading of the atomic wave packet. Tunneling between nearest neighbor lattice sites is enhanced when ν_B is an integer multiple j of ν via a j-phonon process [22], while tunneling between lattice sites i lattice units apart is enhanced when ν is an integer multiple i of ν_B. Even combinations thereof, e.g. $i/j = 2/3$ or $2/5$, are detectable.

We now investigate the dynamics of the wave packet in more detail. For this, we use the resonance with $i = j = 1$ and choose $\nu = \nu_B + \Delta\nu$, where $\Delta\nu$ is the detuning. In Fig. 8.21(a)-(d) we present absorption images and spatial profiles for the weakly-interacting BEC. The time evolution for the width, shape, and center position of the BEC is dramatic. On resonance ($\Delta\nu = 0$), (c) and (d), the atomic ensemble spreads as it develops pronounced edges. Also, as we will see below, the center-of-mass motion depends crucially on the phase ϕ. Off resonance, (a) and (b), for small detuning $\Delta\nu = -1$ Hz, the wave packet exhibits giant oscillatory motion across hundreds of lattice

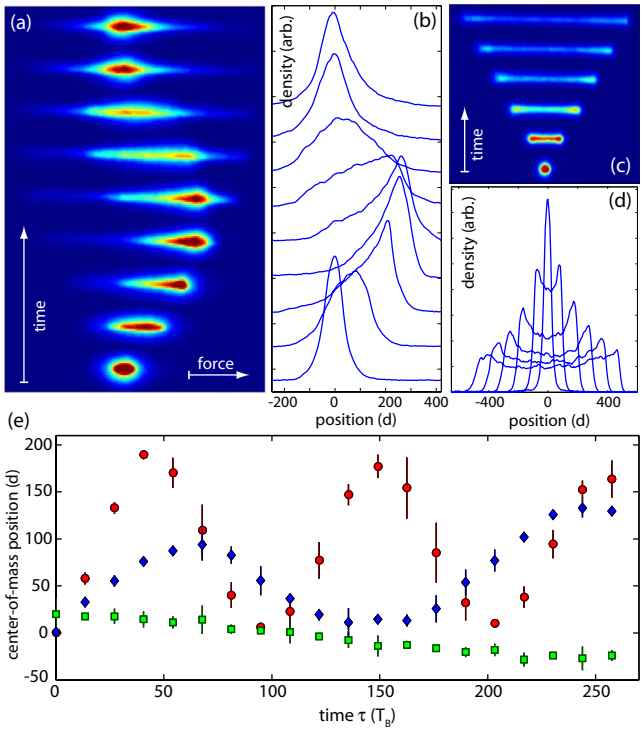

Figure 8.21: (color online) Observation of super Bloch oscillations and modulation-driven wave packet spreading. (a) and (b) In-situ absorption images and density profiles for off-resonant modulation ($\Delta\nu = -1$ Hz), showing giant oscillatory motion across more that 200 sites. (time steps of 120 ms, average of 4 images).(c) and (d) In-situ absorption images and density profiles for resonant modulation ($\Delta\nu = 0$ Hz), showing a wave packet that spreads symmetrically (time steps of 100 ms, average of 4 images). The phase ϕ was adjusted to allow for a symmetric spreading, corresponding to a calculated value of $\phi = \pi/2$. For (a)-(d), the parameters are $F_0 = 0.062(1)mg$, $\Delta F = 0.092(4)mg$, $V = 3.0(3)E_R$, $a = 11(1)$ a_0. (e) Center-of-mass motion for $a = 11(1)a_0$ (circles), $a = 90(1)a_0$ (diamonds), $a = 336(4)a_0$ (squares).

sites that we denote as "super Bloch oscillations" (sBO). Note that, for the parameters used here, the amplitude for ordinary BOs corresponds to about $4d = 2.1$ μm. Also the width and higher moments of the distribution show oscillatory behavior. In Fig. 8.21(e) we plot the center-of-mass position as a function of time for $\Delta\nu = -1$ Hz. At $a = 11(1)$ a_0 we typically observe sBOs over the course of several seconds. The dynamics of sBOs strongly depends upon the site-to-site phase evolution of the matter-wave. In fact, stronger interactions, e.g. $a = 90(1)$ a_0, distort the density profile of the driven BEC and alter the BEC's oscillation frequency and amplitude. For sufficiently strong interactions, no sBOs are observed. We also attribute the wave-packet spreading as seen after one cycle in Fig. 8.21(b) mostly to interactions. For the measurements above, we intentionally use a large modulation amplitude ΔF to enhance the amplitude of sBOs. However, all effects equally exist for $\Delta F \ll F_0$, as we will also demonstrate

below in Fig. 8.23(b).

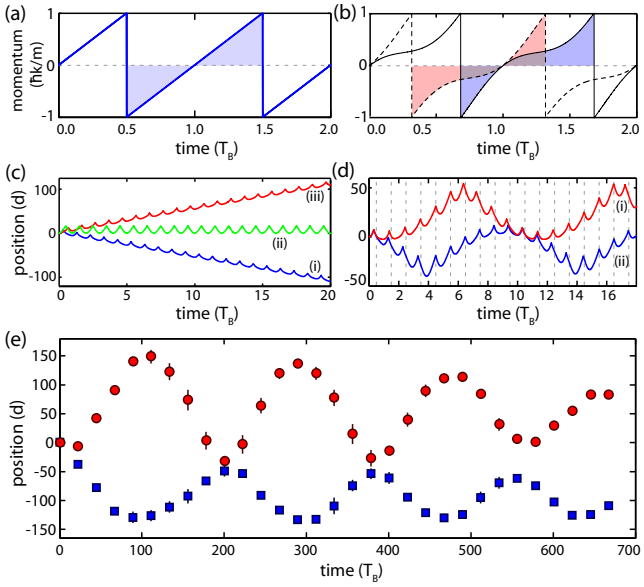

Figure 8.22: (color online) Results from a semi-classical model for sBOs. (a) For a constant force, here $F_0 = 0.06mg$, the velocity (in units of $\hbar k/m$) exhibits a symmetric, saw-tooth-like time evolution, typical for BOs. (b) Resonant modulation, here with $\Delta F = 0.8F_0$, alters the symmetric periodic velocity excursions of normal BOs ($\phi = 0$, solid line, $\phi = \pi$, dashed line), leading to a net-movement, (c), with $\phi = 0$ (i), $\phi = \pi/2$ (ii), and $\phi = \pi$ (iii). An additional detuning $\Delta\nu = \pm 0.1\nu_B$ results in a periodically changing phase difference and hence in giant oscillations in position space, (i) and (ii) in (d). On top of the motion, normal BOs can clearly be seen. The phase of sBOs depends on the sign of $\Delta\nu$, as shown by experimental data in (e), where $F_0 = 0.096(1)mg$, $\Delta F = 0.090(4)mg$, $\Delta\nu = 1$ Hz (circles), -1 Hz (squares).

It is useful to develop a simple semi-classical model to obtain a qualitative understanding of the origin of sBOs. The only elements of this model are that the wave packet is accelerated by the applied force and that, once the wave packet reaches the edge of the first Brillouin zone, it is Bragg reflected. This model does not include an effective mass and cannot be used to predict quantitative results. Fig. 8.22(a)-(d) shows the result of a numerical integration of the time-dependent acceleration $a(t) = F_0/m + \Delta F/m \sin(2\pi(\nu_B + \Delta\nu)t + \phi)$ with periodic Bragg reflection. For a constant acceleration $\Delta F = 0$, the wave packet's velocity shows the well-known saw-tooth-like time evolution that corresponds to BOs. The curve in (a) is symmetric, hence, there is no net movement, as indicated by the shaded regions of equal area. If, however, there is additional harmonic modulation at $\nu = \nu_B$, the velocity excursions will not be symmetric about zero, (b), and result in a net movement for each period, leading to linear motion, (c). Only for $\phi = \pi/2$ or $\phi = 3\pi/2$ symmetry is restored and no net movement will occur. Note that, in general, the velocity of the linear motion depends non-trivially on ϕ. Off-resonant modulation with $\Delta\nu \ll \nu_B$ induces a slowly-varying

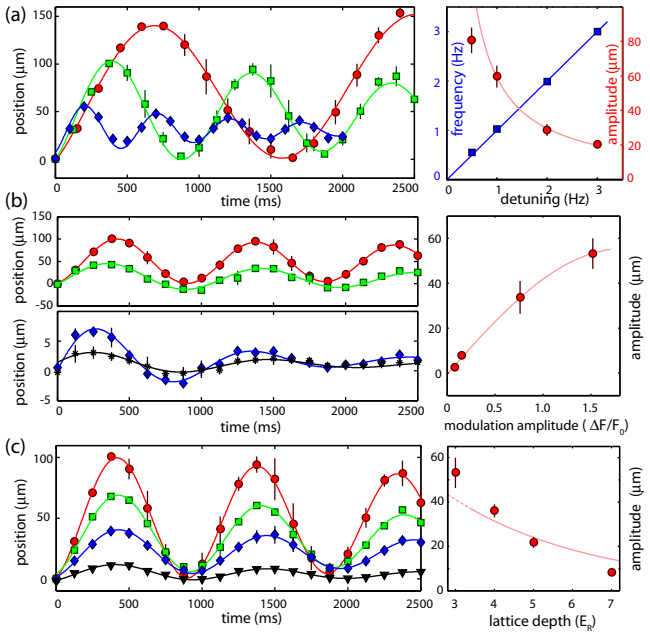

Figure 8.23: (color online) Quantitative analysis of sBOs. (a) The effect of the detuning $\Delta\nu$ on the oscillation frequency and the amplitude of sBOs, with $\Delta\nu = 0.5$ Hz (circles), 1 Hz (squares), 2 Hz (diamonds). Right: The solid lines are fits with linear and $\Delta\nu^{-1}$-dependence, respectively. (b) Dependence of the amplitude of sBOs on $\Delta F/F_0$. The data sets correspond to $\Delta F/F_0 = 1.52$ (circles), 0.76 (squares), 0.15 (diamonds), 0.08 (stars). Right: The solid line is a fit proportional to $B_1(\Delta F/F_0)$. (c) Amplitude of sBOs as a function of lattice depth, V= 3 E_R (circles), 4 E_R (squares), 5 E_R (diamonds), 7 E_R (stars). Right: The solid line is a fit proportional to J, for which we omit the first data point for the shallow lattice. If not stated otherwise, the parameters for all measurements shown here are $F_0 = 0.062(1)mg$, $\Delta F = 0.092(4)mg$, $\Delta\nu = -1$ Hz.

phase mismatch between the drive and the original Bloch period. This results in a slow oscillation of the net movement for each Bloch cycle, which finally sums up to a giant oscillation in position space, (d). Evidently, this oscillation is the result of a beat between the drive and the original BO. The initial direction of the motion depends on ϕ and $\Delta\nu$. In particular, a change in the sign of $\Delta\nu$ at a given ϕ can lead to opposite motion in position space, as verified experimentally in Fig. 8.22(e) for $\Delta\nu = \pm 1$ Hz.

A quantitative understanding of sBOs [16] can be obtained from an approach based on Wannier-Stark states [15]. In essence, the harmonic drive is expected to lead to a rescaling of the tunneling rate $J \rightarrow J_{\text{eff}} = JB_1(\Delta F/F_0)$ and the force $F_0 \rightarrow F_{\text{eff}} = h\Delta\nu/d$ for a stationary lattice with tilt. Here, B_1 is the first Bessel function of the first kind. The amplitude of sBOs is thus given by a new Wannier-Stark localization length $L_{\text{eff}} \approx J_{\text{eff}}/(dF_{\text{eff}})$ [16]. In this sense, sBOs are rescaled BOs. We quantitatively study the dependence of amplitude and period of sBOs on $\Delta\nu$, $\Delta F/F_0$, and V. The results are shown in Fig. 8.23. As expected, the period T is given by $1/\Delta\nu$. Also, the oscillation amplitude scales as $1/\Delta\nu$, and its Bessel-function dependence on

$\Delta F/F_0$ is well reproduced. Given our spatial resolution, we can observe sBOs down to $\Delta F/F_0 = 0.08$ (Fig. 8.23(b)). Note that sBOs can only be observed with sufficient wave function coherence and for well-defined initial conditions, i.e. for sufficient wave packet localization in the first Brillouin zone of the lattice. Nevertheless, incoherent atomic samples exhibit a breathing of the spatial distribution [20] as the oscillation period is insensitive to the initial conditions. In the work of Ref.[20], the breathing can be understood in terms of an incoherent sum over localized Wannier-Stark states that individually show a breathing motion with period T [15].

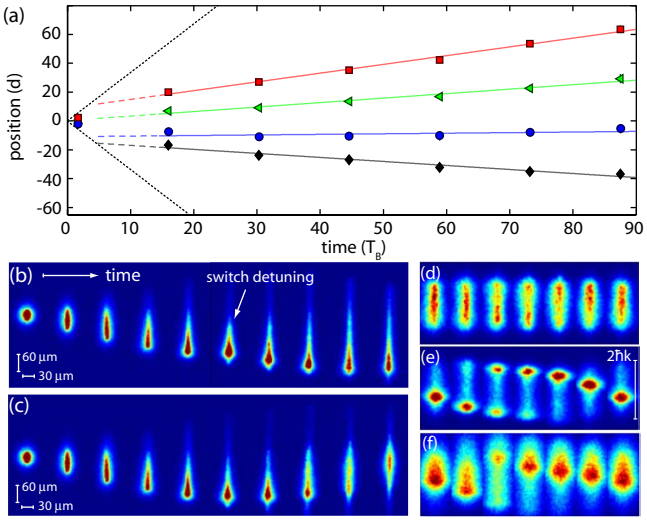

Figure 8.24: (color online) Inducing transport and suppressing interaction-induced dephasing. (a) Linear motion for resonant modulation. $\Delta\phi = 0°$ diamonds, 65° circles, 120° triangles, 190° squares. $\Delta\phi = 0°$ and $\Delta\phi = 190°$ were chosen to maximize the speed in opposite directions. The solid lines are linear fits to the data points excluding the first data point. For comparison we plot the linear motion that corresponds to a tunneling rate of J_{eff}, dotted lines. (b) Directed motion for off-resonant modulation. $\Delta\nu$ was switched from -1 Hz to 1 Hz after 400 ms. For comparison, (c) shows the oscillatory motion without switching (time steps of 80 ms). The parameters are $F_0 = 0.096(1)mg$, $\Delta F = 0.090(4)mg$. (d)-(f) BOs in quasi-momentum space after 10 BO cycles with no drive (d), after 17 BO cycles with drive (e), after 750 BO cycles with drive (f). The parameters are $F_0 = 0.096(1)mg$, $\Delta F = 0.045(3)mg$, $\Delta\nu = -1$ Hz. The time steps are 1 ms.

The results above provide two mechanisms to circumvent the localization inherent in BOs and to induce coherent transport in an otherwise insulating context. As shown in Fig. 8.24(a), resonant modulation ($\Delta\nu = 0$) causes directed motion of the wave packet's center-of-mass. For longer times, we find that the motion is approximately linear. The mean velocity depends on the relative phase ϕ of the Bloch oscillator and the drive. In the experiment, we varied ϕ via $\phi = \phi_0 + \Delta\phi$, where ϕ_0 is a constant phase offset, which depends on the details how BOs are initiated. For off-resonant modulation, transport can be induced by switching the sign of $\Delta\nu$ before a half-cycle of

a sBO is completed. The wave packet then continues to move in the original direction. This motion is shown in Fig. 8.24(b), where we switch the sign after 400 ms. For comparison, Fig. 8.24(c) shows a sBO with $T = 1$ s without switching.

Surprisingly, we find that harmonic modulation strongly reduces the effect of dephasing and wave-packet spreading in quasi-momentum space as a result of interactions. Fig. 8.24(d)-(f) shows single Bloch cycles in quasi-momentum space. Without modulation, the wave packet spreads across the first Brillouin zone within about 10 Bloch cycles. This phenomenon is well known in the context of interacting BECs and is attributed to the appearance of dynamical instabilities [23]. In contrast, with modulation, the quasi-momentum distribution remains narrow and BOs can still be well resolved after 750 Bloch cycles. Evidently, the effects of dynamical instabilities are strongly suppressed.

In summary, we have studied the coherent evolution of matter waves in tilted periodic potentials under forced driving and have observed giant sBOs, which result from a beat of BOs with the drive when a small detuning $\Delta\nu$ from the Bloch frequency is introduced. Localization as a result of BOs is broken, allowing us to engineer matter wave transport over macroscopic distances in lattice potentials with high relevance to atom interferometry [24]. We are now in a position to investigate the effect of interactions on driven transport, for which subdiffusive and chaotic dynamics have been proposed [25].

During the final preparation of the manuscript we became aware of related work on non-dissipative transport in a quantum ratchet [26]. We thank A. R. Kolovsky, A. Zenesini, and A. Wacker for discussions and R. Grimm for generous support. We acknowledge funding by the Austrian Ministry of Science and Research and the Austrian Science Fund and by the European Union within the framework of the EuroQUASAR collective research project QuDeGPM. R.H. is supported by a Marie Curie Fellowship within FP7.

References

1. F. Bloch, Z. Phys. **52**, 555 (1928); C. Zener, Proc. R. Soc. Lond. A **145**, 523 (1934).

2. Y. Kanemitsu, T. Ogawa, *Optical Properties of Low-Dimensional Materials* (World Scientific, Singapore 1995); N.W. Ashcroft, N.D. Mermin, *Solid State Physics* (Saunders College, Philadelphia, 1976)

3. K. Leo *et al.*, Solid State Comm. **84**, 943 (1992); J. Feldmann *et al.*, Phys. Rev. B **46**, 7252 (1992).

4. M. Gustavsson *et al.*, arXiv:0812.4836 (2008).

5. M. Ben Dahan *et al.*, Phys. Rev. Lett. **76**, 4508 (1996).

6. R. Battesti *et al.*, Phys. Rev. Lett. **92**, 253001 (2004).
7. G. Ferrari *et al.*, Phys. Rev. Lett. **97**, 060402 (2006).
8. B.P. Anderson and M.A. Kasevich, Science **27**, 1686 (1998).
9. O. Morsch *et al.*, Phys. Rev. Lett. **87**, 140402 (2001).
10. G. Roati *et al.*, Phys. Rev. Lett. **92**, 230402 (2004).
11. M. Gustavsson *et al.*, Phys. Rev. Lett. **100**, 080404 (2008).
12. M. Fattori *et al.*, Phys. Rev. Lett. **100**, 080405 (2008).
13. H.J. Korsch and S. Mossmann, Phys. Lett. A **317**, 54 (2003).
14. T. Hartmann *et al.*, New J. Phys. **6** (2004).
15. Q. Thommen, J. C. Garreau, and V. Zehnlé, Phys. Rev. A **65**, 053406 (2002); J. Opt. B **6**, 301 (2004).
16. A. Kolovsky and H.J. Korsch, arXiv0912.2587 (2009).
17. S.R. Wilkinson *et al.*, Phys. Rev. Lett. **76**, 4512 (1996).
18. V.V. Ivanov *et al.*, Phys. Rev. Lett. **100**, 043602 (2008).
19. C. Sias *et al.*, Phys. Rev. Lett. **100**, 040404 (2008).
20. A. Alberti *et al.*, Nature Phys. **5**, 547 (2009).
21. T. Kraemer *et al.*, Appl. Phys. B **79**, 1013 (2004).
22. A. Eckardt *et al.*, Phys. Rev. Lett. **95**, 200401 (2005).
23. B. Wu, Q. Niu, New J. Phys. **5**, 104 (2003).
24. A.D. Cronin, J. Schmiedmayer, and D.E. Pritchard, Rev. Mod. Phys. **81**, 1051 (2009).
25. A.R. Kolovsky, E.A. Gómez, and H.J.Korsch, arXiv0904.4549 (2009).
26. T. Salger *et al.*, Science **326**, 1241 (2009).

Appendix A

Optical Setup for STIRAP transfer

The lasers driving the STIRAP transitions must be phase coherent relative to each other on the timescale of the STIRAP transfer. In our experiments so far, we have employed short STIRAP pulses with a duration of a few microseconds, posing rather modest requirements on the stabilization of the STIRAP lasers. The relative linewidth of the STIRAP lasers is on the order of 10 kHz when averaged over 1 s. As discussed in section 7.1, the STIRAP efficiency would profit from decreased laser linewidth. In the following, we will describe the laser setup for the experiments in chapters 2 - 6. The improved setup with phase-locked STIRAP lasers will be described in a separate paper [Dan10a].

For STIRAP, we use four grating-stabilized external cavity diode lasers (DL100 from Toptica Photonics, Graefelfing, Germany) at wavelengths of roughly 1126 nm, 1006 nm, 1351 nm, and 1003 nm, resprectively. Each diode laser is locked to an optical resonator with the Pound-Drever-Hall (PDH) technique [Dre83]. In each of the 4 optical resonators, one of the two mirrors is mounted on a piezoelectric actuator (piezo), allowing to tune the resonance frequency. Without any further stabilization, the drifts of the resonators would be too large for STIRAP. We continuously measure the frequency of each laser by beating it against one spectral component of an optical frequency comb and we slowly feed back on the piezo of the optical resonator to keep the frequency of the STIRAP laser fixed.

The lock to the optical resonators was instrumental for the high precision molecular spectroscopy on the excited state intermediate levels and in the systematic search for the deeply bound ground state level $|v = 73>$. The excited state intermediate levels were largely unknown and the binding energy of the $|v = 73>$-level had been known to only about $\pm$ h $\times$ 15 GHz. We chose to stabilitze the lasers to optical resonators rather than phase-locking them to the optical frequency comb for the spectroscopy. The optical resonators had the advantage that a much larger frequency range could be systematically scanned without relocking the laser than with a phase lock to the comb, given the repetition rate of 100 MHz of our comb.

A.1 Optical frequency comb setup

We use a commercial Erbium fiber-based frequency comb at a center wavelength of ~1550 nm (model FFS from Toptica Photonics) with 100 MHz repetition rate with a single supercontinuum output. The supercontinuum spans a wavelength range from

roughly 980 nm to around 2000 nm. The repetition rate of the comb is stabilized to an ultra-low phase noise crystal oscillator (Wenzel Associates, Austin, Texas) at its fundamental frequency. The crystal is stabilized on a slow timescale to another ultralow noise crystal running at 10 MHz that is in turn stabilized to the global positioning system (GPS) time standard, yielding absolute frequencies. To stabilize the carrier-envelope offset (CEO) phase, we built a 1f-2f interferometer [Rei99, Ude02, Ye05]. The long wavelength part of the output spectrum is separated from the short wavelength spectral region by a shortpass dichroic mirror (reflectivity > 99.9 % at 45° for s-polarization: 1820 nm - 2360 nm, for p-polarization: 1890 nm -2240 nm, Layertec, Mellingen, Germany) with a cutoff wavelength at around 1600 nm. The long wavelength light is frequency doubled in a 10 mm long BBO crystal (Castech/ GWU Lasertechnik, Erftstadt, Germany) and superimposed with the short wavelength part on a polarizing beamsplitter cube. A $\lambda/2$-plate and a second polarizing cube project the polarizations on a common axis. An optical delay line in the long-wavelength branch assures equal path lengths for both arms. Comb lines that do not contribute to the beat signal are deflected with a grating. The beat signal is recorded with an InGaAs photodiode (G8376-05 from Hamamatsu) and amplified in a homebuilt photodiode amplifier. For locking the CEO phase, we use a commercial digital phase detector (model DXD200 from Menlo Systems, Martinsried, Germany) and a homebuilt PID circuit to feed back on the pump power for the fiber ring oscillator. In the short wavelength branch of the interferometer, three shortpass dichroic mirrors (Layertec 100791, 103933, and 105890) with edge wavelengths at 1135 nm, 1100 nm, and 990 nm separate out certain regions of the optical spectrum to generate beat notes with the four STIRAP lasers. For the beat notes between the diode lasers and the frequency comb, unwanted spectral components of the comb are deflected with a ruled diffractive grating from either Zeiss or Thorlabs.

With this optical setup that relied on optical resonators for short-term stability of the STIRAP lasers and on the comb for long-terms stabilization of the resonators, the noise properties of the comb were only of secondary importance. All reference frequencies except for the 100 MHz reference signal for the comb repetition rate are generated by direct digital synthesizers with a homebuilt design developed by Florian Schreck and Todd Meyrath (based on DDS model AD9852 from Analog Devices). The DDS are clocked with a 300 MHz signal from a radiofrequency generator that is synchronized to the 10 MHz GPS-stabilized signal.

A.2 Stabilization of the STIRAP lasers to optical resonators

Each STIRAP laser is stabilized to an individual optical resonator. Four resonators are mounted on a single Zerodur spacer (60 mm × 60 mm square cross section, 195 mm length, 4 bores for one cavity each, from Hellma Optik, Jena, Germany), three of which

are equipped with a piezo. The resonators are contained within a vacuum vessel which is temperature stabilized. The housing was once evacuated, however, no ion pump is attached to the housing. One additional resonator with piezo is contained in a separate housing in air at ambient pressure. The resonators have one flat and one curved mirror with a radius of 500 mm (reflectivity $\sim$ 99.8%, transmission $<$ 0.3% from 850 nm to 1510 nm, Layertec) and have a finesse of $\sim$1000. The mirrors have a wedge of 30'. For PDH locking, the laser beams to the optical resonators are phase modulated at 24 MHz to 50 MHz with an external electro-optic modulator (3 mm $\times$ 3 mm $\times$ 30 mm, lithium niobate, Döhrer Elektrooptik, Karlsbad, Germany). Feedback to the laser is via a fast branch acting on the laser diode current via a field-effect transistor (FET) in the laser head and via a slow branch to the piezo acting on the feedback grating in the laser head. The PID circuit for locking is homebuilt. The fast branch is realized with a single high-speed operational amplifier. The feedback bandwidths are between 1 and 3 MHz.

For the dark resonance spectroscopy on the second leg of the first STIRAP transition [Dan08], the frequency of the second laser had to be scanned over $\pm$15 GHz with a 5 MHz step after each cycle of the BEC machine while the first laser was kept on one-photon resonance. To achieve reproducible and at the same time widely tunable frequency locking, one laser was stabilized to the optical resonator without piezo and the spectroscopy laser was phase-locked to it in a tunable manner with a fast feedback loop.

For long-term stabilization of the optical resonators against slow drifts, the beat note beween each diode laser and the nearest comb line is detected with an InGaAs photodiode (G8376-05 from Hamamatsu Photonics or GAP-500 from GPD Optoelectronics, Salem, NH, USA), amplified (RF amplifier model RAM8), low pass filtered at 50 MHz and further amplified (low noise RF amplifiers from Miteq, e. g. model AU-1519, or ZFL500LN from Minicircuits). As frequency discriminators we either used a simple home-built fequency detector [Sch99] or a homebuilt digital phase and frequency detector based on a design that M. Prevedelli kindly provided to us [Cac05]. Feedback to the piezos of the optical resonators was provided by a homebuilt PI regulator with a low feedback bandwith of a fraction of a Hz. This low feedback bandwith was chosen in order to assure that short term stability of the laser frequency would be given by the passive stability of the optical resonator and that referencing to the comb would only compensate for slow drifts.

References

[Ald08] J. Aldegunde, B. A. Rivington, P. S. Żuchowski, and J. M. Hutson, *Hyperfine energy levels of alkali-metal dimers: Ground-state polar molecules in electric and magnetic fields*, Phys. Rev. A **78**, 033434 (2008).

[Ald09] J. Aldegunde and J. M. Hutson, *Hyperfine energy levels of alkali-metal dimers: Ground-state homonuclear molecules in magnetic fields*, Phys. Rev. A **79**, 013401 (2009).

[Aln08a] J. Alnis, A. Matveev, N. Kolachevsky, T. Udem, and T. W. Hänsch, *Subhertz linewidth diode lasers by stabilization to vibrationally and thermally compensated ultralow-expansion glass Fabry-Pérot cavities*, Phys. Rev. A **77**, 053809 (2008).

[Aln08b] J. Alnis, A. Matveev, N. Kolachevsky, T. Wilken, R. Holzwarth, and T. W. Hänsch, *Stable diode lasers for hydrogen precision spectroscopy*, Eur. Phys. J. ST **163**, 89 (2008).

[Ami90] C. Amiot, *Laser-induced fluorescence of Rb_2: The $(1)^1\Sigma_g^+(X)$, $(2)^1\Sigma_g^+$, $(1)^1\Pi_u$ (B), $(1)^1\Pi_g$, and $(2)^1\Pi_u$ (C) electronic states*, J. Chem. Phys. **93**, 8591 (1990).

[Ami99] C. Amiot, O. Dulieu, and J. Vergès, *Resolution of the apparent disorder of the Rb_2 $A^1\Sigma_u^+(0_u^+)$ and $b^3\Pi_u(0_u^+)$ spectra: A case of fully coupled electronic states*, Phys. Rev. Lett. **83**, 2316 (1999).

[Ami02] C. Amiot and O. Dulieu, *The Cs_2 ground electronic state by Fourier transform spectroscopy: Dispersion coefficients*, J. Chem. Phys. **117**, 5155 (2002).

[And95] M. H. Anderson, J. R. Ensher, M. R. Matthews, C. E. Wieman, and E. A. Cornell, *Observation of Bose-Einstein condensation in dilute atomic vapor*, Science **269**, 198 (1995).

[And06] A. André, D. DeMille, J. M. Doyle, M. D. Lukin, S. E. Maxwell, P. Rabl, R. J. Schoelkopf, and P. Zoller, *A coherent all-electrical interface between polar molecules and mesoscopic superconducting resonators*, Nature Phys. **2**, 636 (2006).

[Ast05] G. E. Astrakharchik, J. Boronat, J. Casulleras, and S. Giorgini, *Beyond the Tonks-Girardeau gas: Strongly correlated regime in quasi-one-dimensional Bose gases*, Phys. Rev. Lett. **95**, 190407 (2005).

[Ast08] G. E. Astrakharchik, G. Morigi, G. De Chiara, and J. Boronat, *Ground state of low-dimensional dipolar gases: Linear and zigzag chains*, Phys. Rev. A **78**, 063622 (2008).

[Atk82] J. B. Atkinson, J. Becker, and W. Demtröder, *Hyperfine structure of the 625 nm band in the a* $^3\Pi_u < -X^1\Sigma_g$ *transitions of* Na_2, Chem. Phys. Lett. **87**, 128 (1982).

[Aym05] M. Aymar and O. Dulieu, *Calculation of accurate permanent dipole moments of the lowest* $^{1,3}\Sigma^+$ *states of heteronuclear alkali dimers using extended basis sets*, J. Chem. Phys. **122**, 204302 (2005).

[Bah96] J. T. Bahns, W. C. Stwalley, and P. L. Gould, *Laser cooling of molecules: A sequential scheme for rotation, translation, and vibration*, J. Chem. Phys. **104**, 9689 (1996).

[Bar08] M. A. Baranov, *Theoretical progress in many-body physics with ultracold dipolar gases*, Physics Reports **464**, 71 (2008).

[Ben05] E. Benkler, H. Telle, A. Zach, and F. Tauser, *Circumvention of noise contributions in fiber laser based frequency combs*, Opt. Express **13**, 5662 (2005).

[Ber98] K. Bergmann, H. Theuer, and B. W. Shore, *Coherent population transfer among quantum states of atoms and molecules*, Rev. Mod. Phys. **70**, 1003 (1998).

[Ber03] T. Bergeman, C. E. Fellows, R. F. Gutterres, and C. Amiot, *Analysis of strongly coupled electronic states in diatomic molecules: Low-lying excited states of RbCs*, Phys. Rev. A **67**, 050501 (2003).

[Ber08] A. J. Berglund, J. L. Hanssen, and J. J. McClelland, *Narrow-line magneto-optical cooling and trapping of strongly magnetic atoms*, Phys. Rev. Lett. **100**, 113002 (2008).

[Ber10] T. Bergeman, private communication (2010).

[Bet99] H. L. Bethlem, G. Berden, and G. Meijer, *Decelerating neutral dipolar molecules*, Phys. Rev. Lett. **83**, 1558 (1999).

[Bet00] H. L. Bethlem, G. Berden, F. M. H. Crompvoets, R. T. Jongma, A. J. A. van Roij, and G. Meijer, *Electrostatic trapping of ammonia molecules*, Nature **406**, 491 (2000).

[Blo08] I. Bloch, J. Dalibard, and W. Zwerger, *Many-body physics with ultracold gases*, Rev. Mod. Phys. **80**, 885 (2008).

[Bou04] T. Bourdel, L. Khaykovich, J. Cubizolles, J. Zhang, F. Chevy, M. Teichmann, L. Tarruell, S. J. J. M. F. Kokkelmans, and C. Salomon, *Experimental study of the BEC-BCS crossover region in lithium 6*, Phys. Rev. Lett. **93**, 050401 (2004).

[Bou07] N. Bouloufa and O. Dulieu, private communication (2007).

[Bou08] N. Bouloufa and O. Dulieu, private communication (2008).

[Bou10] N. Bouloufa, O. Dulieu, and coworkers, *Calculation of the dynamical polarizability of* Cs_2 *molecules*, manuscript in preparation (2010).

[Büc03] H. P. Büchler, G. Blatter, and W. Zwerger, *Commensurate-incommensurate transition of cold atoms in an optical lattice*, Phys. Rev. Lett. **90**, 130401 (2003).

[Büc07a] H. P. Büchler, E. Demler, M. Lukin, A. Micheli, N. Prokof'ev, G. Pupillo, and P. Zoller, *Strongly correlated 2D quantum phases with cold polar molecules: Controlling the shape of the interaction potential*, Phys. Rev. Lett. **98**, 060404 (2007).

[Büc07b] H. P. Büchler, A. Micheli, and P. Zoller, *Three-body interactions with cold polar molecules*, Nature Phys. **3**, 726 (2007).

[Cac05] L. Cacciapuoti, M. de Angelis, M. Fattori, G. Lamporesi, T. Petelski, M. Prevedelli, J. Stuhler, and G. M. Tino, *Analog + digital phase and frequency detector for phase locking of diode lasers*, Rev. Sci. Instrum. **76**, 053111 (2005).

[Cam07] W. C. Campbell, E. Tsikata, H.-I. Lu, L. D. van Buuren, and J. M. Doyle, *Magnetic trapping and Zeeman relaxation of NH ($X^3\Sigma$)*, Phys. Rev. Lett. **98**, 213001 (2007).

[Car09] L. D. Carr, D. DeMille, R. V. Krems, and J. Ye, *Cold and ultracold molecules: Science, technology and applications*, New. J. Phys. **11**, 055049 (2009).

[Cha09] D. W. Chandler and K. E. Strecker, *The quest for cold and ultracold molecules*, ChemPhysChem **10**, 751 (2009).

[Chi00] C. Chin, V. Vuletić, A. J. Kerman, and S. Chu, *High resolution Feshbach spectroscopy of cesium*, Phys. Rev. Lett. **85**, 2717 (2000).

[Chi04] C. Chin, V. Vuletić, A. J. Kerman, S. Chu, E. Tiesinga, P. J. Leo, and C. J. Williams, *Precision Feshbach spectroscopy of ultracold Cs_2*, Phys. Rev. A **70**, 032701 (2004).

[Chi05] C. Chin, T. Kraemer, M. Mark, J. Herbig, P. Waldburger, H.-C. Nägerl, and R. Grimm, *Observation of Feshbach-like resonances in collisions between ultracold molecules*, Phys. Rev. Lett. **94**, 123201 (2005).

[Chi06] C. Chin and V. V. Flambaum, *Enhanced sensitivity to fundamental constants in ultracold atomic and molecular systems near Feshbach resonances*, Phys. Rev. Lett. **96**, 230801 (2006).

[Chi09] C. Chin, V. V. Flambaum, and M. G. Kozlov, *Ultracold molecules: new probes on the variation of fundamental constants*, New J. Phys. **11**, 055048 (2009).

[Chi10] C. Chin, R. Grimm, P. S. Julienne, and E. Tiesinga, *Feshbach resonances in ultracold gases*, Rev. Mod. Phys. (in press) (2010), preprint available at arXiv:0812.1496.

[Cou98] P. Courteille, R. S. Freeland, D. J. Heinzen, F. A. van Abeelen, and B. J. Verhaar, *Observation of a Feshbach resonance in cold atom scattering*, Phys. Rev. Lett. **81**, 69 (1998).

[Cro01] F. M. Crompvoets, H. L. Bethlem, R. T. Jongma, and G. Meijer, *A prototype storage ring for neutral molecules*, Nature **411**, 174 (2001).

[Dan07] J. G. Danzl, *Towards optical spectroscopy of ultracold cesium molecules*, Diploma thesis, University of Innsbruck (2007).

[Dan08] J. G. Danzl, E. Haller, M. Gustavsson, M. J. Mark, R. Hart, N. Bouloufa, O. Dulieu, H. Ritsch, and H.-C. Nägerl, *Quantum gas of deeply bound ground state molecules*, Science **321**, 1062 (2008), published online 10 July 2008.

[Dan09a] J. G. Danzl, M. J. Mark, E. Haller, M. Gustavsson, R. Hart, A. Liem, H. Zellmer, and H.-C. Nägerl, *Deeply bound ultracold molecules in an optical lattice*, New J. Phys. **11**, 055036 (2009).

[Dan09b] J. G. Danzl, M. J. Mark, E. Haller, M. Gustavsson, N. Bouloufa, O. Dulieu, H. Ritsch, R. Hart, and H.-C. Nägerl, *Precision molecular spectroscopy for ground state transfer of molecular quantum gases*, Faraday Discuss. **142**, 283 (2009).

[Dan09c] J. G. Danzl, M. J. Mark, E. Haller, M. Gustavsson, R. Hart, and H.-C. Nägerl, *Production of a quantum gas of rovibronic ground-state molecules in an optical lattice*, ICOLS Proceedings (2009).

[Dan10a] J. G. Danzl and coworkers, manuscript in preparation (2010).

[Dan10b] J. G. Danzl, M. J. Mark, E. Haller, M. Gustavsson, R. Hart, J. Aldegunde, J. M. Hutson, and H.-C. Nägerl, *An ultracold high-density sample of rovibronic ground-state molecules in an optical lattice*, Nature Phys. (2010), advance online publication 21 Feb 2010, DOI: 10.1038/NPHYS1533.

[Dav95] K. B. Davis, M. O. Mewes, M. R. Andrews, N. J. van Druten, D. S. Durfee, D. M. Kurn, and W. Ketterle, *Bose-Einstein condensation in a gas of sodium atoms*, Phys. Rev. Lett. **75**, 3969 (1995).

[Dei08a] J. Deiglmayr, M. Aymar, R. Wester, M. Weidemüller, and O. Dulieu, *Calculations of static dipole polarizabilities of alkali dimers: Prospects for alignment of ultracold molecules*, J. Chem. Phys. **129**, 064309 (2008).

[Dei08b] J. Deiglmayr, A. Grochola, M. Repp, K. Mörtlbauer, C. Glück, J. Lange, O. Dulieu, R. Wester, and M. Weidemüller, *Formation of ultracold polar molecules in the rovibrational ground state*, Phys. Rev. Lett. **101**, 133004 (2008).

[Dei09] J. Deiglmayr, P. Pellegrini, A. Grochola, M. Repp, R. Côté, O. Dulieu, R. Wester, and M. Weidemüller, *Influence of a Feshbach resonance on the photoassociation of LiCs*, New J. Phys. **11**, 055034 (2009).

[DeM02] D. DeMille, *Quantum computation with trapped polar molecules*, Phys. Rev. Lett. **88**, 067901 (2002).

[DeM08] D. DeMille, S. Sainis, J. Sage, T. Bergeman, S. Kotochigova, and E. Tiesinga, *Enhanced sensitivity to variation of m_e/m_p in molecular spectra*, Phys. Rev. Lett. **100**, 043202 (2008).

[Di 04] M. Di Rosa, *Laser-cooling molecules*, Eur. Phys. J. D **31**, 395 (2004).

[Did04] S. A. Diddams, J. C. Bergquist, S. R. Jefferts, and C. W. Oates, *Standards of time and frequency at the outset of the 21st century*, Science **306**, 1318 (2004).

[Doc09] O. Docenko, M. Tamanis, R. Ferber, T. Bergeman, S. Kotochigova, A. V. Stolyarov, A. de Faria Nogueira, and C. E. Fellows, *New spectroscopic data on the $A^1\Sigma^+$ and $b^3\Pi$ states of RbCs and revised analysis of strong perturbative interactions*, submitted for publication in PRA (2009).

[Don02] E. A. Donley, N. R. Clausen, S. T. Thompson, and C. E. Wieman, *Atom-molecule coherence in a Bose-Einstein condensate*, Nature **417**, 529 (2002).

[Doy04] J. Doyle, B. Friedrich, R. Krems, and F. Masnou-Seeuws, *Editorial: Quo vadis, cold molecules?*, Eur. Phys. J. D **31**, 149 (2004).

[Dre83] R. W. P. Drever, J. L. Hall, F. V. Kowalski, J. Hough, G. M. Ford, A. J. Munley, and H. Ward, *Laser phase and frequency stabilization using an optical resonator*, Appl. Phys. B **31**, 97 (1983).

[Dul95] O. Dulieu and P. S. Julienne, *Coupled channel bound states calculations for alkali dimers using the Fourier grid method*, J. Chem. Phys. **103**, 60 (1995).

[Dul06] O. Dulieu, M. Raoult, and E. Tiemann, *Cold molecules: a chemistry kitchen for physicists?*, J. Phys. B **39** (2006).

[Dul09a] O. Dulieu and C. Gabbanini, *The formation and interactions of cold and ultracold molecules: new challenges for interdisciplinary physics*, Rep. Prog. Phys. **72**, 086401 (2009).

[Dul09b] O. Dulieu and R. Guérout, private communication (2009).

[Dul10] O. Dulieu, N. Bouloufa, and A. Crubellier, private communication (2010).

[Efi70] V. Efimov, *Energy levels arising from resonant two-body forces in a three-body system*, Phys. Lett. B **33**, 563 (1970).

[Efi71] V. Efimov, *Weakly-bound states of three resonantly-interacting particles*, Sov. J. Nucl. Phys. **12**, 589 (1971).

[Eli03] M. S. Elioff, J. J. Valentini, and D. W. Chandler, *Subkelvin cooling NO molecules via "billiard-like" collisions with argon*, Science **302**, 1940 (2003).

[Eur04] *Special Issue: Ultracold polar molecules: Formation and collisions*, Eur. Phys. J. D **31** (2004).

[Far09] *Cold and ultracold molecules*, Faraday Discuss. **142** (2009).

[Fel99] C. E. Fellows, R. F. Gutterres, A. P. C. Campos, J. Vergès, and C. Amiot, *The RbCs $X^1\Sigma^+$ ground electronic state: new spectroscopic study*, J. Mol. Spect. **197**, 19 (1999).

[Fer09a] F. Ferlaino, S. Knoop, M. Berninger, W. Harm, J. P. D'Incao, H.-C. Nägerl, and R. Grimm, *Evidence for universal four-body states tied to an Efimov trimer*, Phys. Rev. Lett. **102**, 140401 (2009).

[Fer09b] F. Ferlaino, S. Knoop, and R. Grimm, *Ultracold Feshbach molecules*, in: R. V. Krems, B. Friedrich, and W. C. Stwalley (Eds.), *Cold molecules: Theory, experiment, applications*, Taylor & Francis, 2009, preprint available at arXiv:0809.3920v1.

[Fio98] A. Fioretti, D. Comparat, A. Crubellier, O. Dulieu, F. Masnou-Seeuws, and P. Pillet, *Formation of cold Cs_2 molecules through photoassociation*, Phys. Rev. Lett. **80**, 4402 (1998).

[Fla07] V. V. Flambaum and M. G. Kozlov, *Enhanced sensitivity to the time variation of the fine-structure constant and m_p/m_e in diatomic molecules*, Phys. Rev. Lett. **99**, 150801 (2007).

[Fli06] A. Flir, *Implementierung und Untersuchung von Raman-Seitenbandkühlung zur Erzeugung eines ultrakalten Cäsiumgases*, Diploma thesis, University of Innsbruck (2006).

[Fri09] B. Friedrich and J. M. Doyle, *Why are cold molecules so hot?*, ChemPhysChem **10**, 604 (2009).

[Gao00] B. Gao, *Zero-energy bound or quasibound states and their implications for diatomic systems with an asymptotic van der Waals interaction*, Phys. Rev. A **62**, 050702 (2000).

[Gau88] U. Gaubatz, P. Rudecki, M. Becker, S. Schiemann, M. Külz, and K. Bergmann, *Population switching between vibrational levels in molecular beams*, Chem. Phys. Lett. **149**, 463 (1988).

[Gau90] U. Gaubatz, P. Rudecki, S. Schiemann, and K. Bergmann, *Population transfer between molecular vibrational levels by stimulated Raman scattering with partially overlapping laser fields. A new concept and experimental results*, J. Chem. Phys. **92**, 5363 (1990).

[Gho09] S. Ghosal, R. J. Doyle, C. P. Koch, and J. M. Hutson, *Stimulating the production of deeply bound RbCs molecules with laser pulses: the role of spin–orbit coupling in forming ultracold molecules*, New J. Phys. **11**, 055011 (2009).

[Gia04] T. Giamarchi, *Quantum physics in one dimension*, Oxford University Press, 2004.

[Gir60] M. Girardeau, *Relationship between systems of impenetrable bosons and fermions in one dimension*, J. Math. Phys. **1**, 516 (1960).

[Gór02] K. Góral, L. Santos, and M. Lewenstein, *Quantum phases of dipolar bosons in optical lattices*, Phys. Rev. Lett. **88**, 170406 (2002).

[Gor08] A. V. Gorshkov, P. Rabl, G. Pupillo, A. Micheli, P. Zoller, M. D. Lukin, and H. P. Büchler, *Suppression of inelastic collisions between polar molecules with a repulsive shield*, Phys. Rev. Lett. **101**, 073201 (2008).

[Gre02] M. Greiner, O. Mandel, T. Esslinger, T. W. Hänsch, and I. Bloch, *Quantum phase transition from a superfluid to a Mott insulator in a gas of ultracold atoms*, Nature **415**, 39 (2002).

[Gre03] M. Greiner, C. A. Regal, and D. S. Jin, *Emergence of a molecular Bose-Einstein condensate from a Fermi gas*, Nature **426**, 537 (2003).

[Gri93] G. F. Gribakin and V. V. Flambaum, *Calculation of the scattering length in atomic collisions using the semiclassical approximation*, Phys. Rev. A **48**, 546 (1993).

[Gri00] R. Grimm, M. Weidemüller, and Y. B. Ovchinnikov, *Optical dipole traps for neutral atoms*, Adv. At. Mol. Opt. Phys. **42**, 95 (2000).

[Gri05] A. Griesmaier, J. Werner, S. Hensler, J. Stuhler, and T. Pfau, *Bose-Einstein condensation of chromium*, Phys. Rev. Lett. **94**, 160401 (2005).

[Gro09] N. Gross, Z. Shotan, S. Kokkelmans, and L. Khaykovich, *Observation of universality in ultracold ^{7}Li three-body recombination*, Phys. Rev. Lett. **103**, 163202 (2009).

[Gué09] R. Guérout, P. Soldán, M. Aymar, J. Deiglmayr, and O. Dulieu, *Core repulsion effects in alkali trimers*, Int. J. Quant. Chem. **109**, 3387 (2009).

[Gus08] M. Gustavsson, *A quantum gas with tunable interactions in an optical lattice*, Ph.D. thesis, University of Innsbruck (2008).

[Hai09] C. Haimberger, J. Kleinert, P. Zabawa, A. Wakim, and N. P. Bigelow, *Formation of ultracold, highly polar $X^1\Sigma^+$ NaCs molecules*, New J. Phys. **11**, 055042 (2009).

[Hal06] J. L. Hall, *Nobel Lecture: Defining and measuring optical frequencies*, Rev. Mod. Phys. **78**, 1279 (2006).

[Hal09] E. Haller, M. Gustavsson, M. J. Mark, J. G. Danzl, R. Hart, G. Pupillo, and H. C. Nägerl, *Realization of an excited, strongly correlated quantum gas phase*, Science **325**, 1224 (2009).

[Hal10] E. Haller, *One dimensional systems with tunable interactions*, Ph.D. thesis, University of Innsbruck (2010).

[Hän06] T. W. Hänsch, *Nobel Lecture: Passion for precision*, Rev. Mod. Phys. **78**, 1297 (2006).

[Has88] T. Haslwanter, H. Ritsch, J. Cooper, and P. Zoller, *Laser-noise-induced population fluctuations in two- and three-level systems*, Phys. Rev. A **38**, 5652 (1988).

[Her03] J. Herbig, T. Kraemer, M. Mark, T. Weber, C. Chin, H.-C. Nägerl, and R. Grimm, *Preparation of a pure molecular quantum gas*, Science **301**, 1510 (2003).

[Her05] J. Herbig, *Quantum-degenerate cesium: Atoms and molecules*, Ph.D. thesis, University of Innsbruck (2005).

[Hor97] P. Horak, G. Hechenblaikner, K. M. Gheri, H. Stecher, and H. Ritsch, *Cavity-induced atom cooling in the strong coupling regime*, Phys. Rev. Lett. **79**, 4974 (1997).

[Hud02] J. J. Hudson, B. E. Sauer, M. R. Tarbutt, and E. A. Hinds, *Measurement of the electron electric dipole moment using YbF molecules*, Phys. Rev. Lett. **89**, 023003 (2002).

[Hud08] E. R. Hudson, N. B. Gilfoy, S. Kotochigova, J. M. Sage, and D. DeMille, *Inelastic collisions of ultracold heteronuclear molecules in an optical trap*, Phys. Rev. Lett. **100**, 203201 (2008).

[Hut06] J. Hutson and P. Soldán, *Molecule formation in ultracold atomic gases*, Int. Rev. Phys. Chem. **25**, 497 (2006).

[Hut08] J. M. Hutson, E. Tiesinga, and P. S. Julienne, *Avoided crossings between bound states of ultracold cesium dimers*, Phys. Rev. A **78**, 052703 (2008).

[Hut09] J. M. Hutson, private communication (2009).

[Idz09] Z. Idziaszek and P. S. Julienne, *Universal rate constants for reactive collisions of ultracold molecules* (2009), preprint available at arXiv:0912.0370v1.

[IM86] G. Igel-Mann, U. Wedig, P. Fuentealba, and H. Stoll, *Ground-state properties of alkali dimers XY (X, Y=Li to Cs)*, J. Chem. Phys. **84**, 5007 (1986).

[Ing08] M. Inguscio, W. Ketterle, and C. Salomon (Eds.), *Ultra-cold Fermi gases*, IOS Press, Amsterdam, 2008, Proceedings of the international school of physics "Enrico Fermi", Course CLXIV, Varenna, 20-30 June 2006.

[Ino98] S. Inouye, M. R. Andrews, J. Stenger, H.-J. Miesner, D. M. Stamper-Kurn, and W. Ketterle, *Observation of Feshbach resonances in a Bose-Einstein condensate*, Nature **392**, 151 (1998).

[Jak98] D. Jaksch, C. Bruder, J. I. Cirac, C. W. Gardiner, and P. Zoller, *Cold bosonic atoms in optical lattices*, Phys. Rev. Lett. **81**, 3108 (1998).

[Jak02] D. Jaksch, V. Venturi, J. I. Cirac, C. J. Williams, and P. Zoller, *Creation of a molecular condensate by dynamically melting a Mott insulator*, Phys. Rev. Lett. **89**, 040402 (2002).

[Joc03] S. Jochim, M. Bartenstein, A. Altmeyer, G. Hendl, S. Riedl, C. Chin, J. Hecker Denschlag, and R. Grimm, *Bose-Einstein condensation of molecules*, Science **302**, 2101 (2003).

[Jon06] K. M. Jones, E. Tiesinga, P. D. Lett, and P. S. Julienne, *Ultracold photoassociation spectroscopy: Long-range molecules and atomic scattering*, Rev. Mod. Phys. **78**, 483 (2006).

[Jul09] P. Julienne, private communication (2009).

[Jun04a] T. Junglen, T. Rieger, S. Rangwala, P. Pinkse, and G. Rempe, *Slow ammonia molecules in an electrostatic quadrupole guide*, Eur. Phys. J. D **31**, 365 (2004).

[Jun04b] T. Junglen, T. Rieger, S. A. Rangwala, P. W. H. Pinkse, and G. Rempe, *Two-dimensional trapping of dipolar molecules in time-varying electric fields*, Phys. Rev. Lett. **92**, 223001 (2004).

[Jun08] M. Junker, D. Dries, C. Welford, J. Hitchcock, Y. P. Chen, and R. G. Hulet, *Photoassociation of a Bose-Einstein condensate near a Feshbach resonance*, Phys. Rev. Lett. **101**, 060406 (2008).

[Kat89] H. Katô, M. Otani, and M. Baba, *Hyperfine structure of the Na_2 $b\,{}^3\Pi_u$ state*, J. Chem. Phys. **91**, 5124 (1989).

[Ket99] W. Ketterle, D. Durfee, and D. Stamper-Kurn, *Making, probing and understanding Bose-Einstein condensates*, in: M. Inguscio, S. Stringari, and C. Wieman (Eds.), *Bose-Einstein condensation in atomic gases*, vol. CXL of *Proceedings of the international school of physics "Enrico Fermi"*, 67–176, IOS Press, Amsterdam, 1999.

[Kle07] J. Klein, F. Beil, and T. Halfmann, *Robust population transfer by stimulated Raman adiabatic passage in a Pr^{3+} : Y_2SiO_5 crystal*, Phys. Rev. Lett. **99**, 113003 (2007).

[Kno08] S. Knoop, M. Mark, F. Ferlaino, J. G. Danzl, T. Kraemer, H.-C. Nägerl, and R. Grimm, *Metastable Feshbach molecules in high rotational states*, Phys. Rev. Lett. **100**, 083002 (2008).

[Kno09] S. Knoop, F. Ferlaino, M. Mark, M. Berninger, H. Schöbel, H.-C. Nägerl, and R. Grimm, *Observation of an Efimov-like trimer resonance in ultracold atom-dimer scattering*, Nature Phys. **5**, 227 (2009).

[Kno10] S. Knoop, F. Ferlaino, M. Berninger, M. Mark, H.-C. Nägerl, R. Grimm, J. P. D'Incao, and B. D. Esry, *Magnetically controlled exchange process in an ultracold atom-dimer mixture*, Phys. Rev. Lett. **104**, 053201 (2010).

[Koc04] C. P. Koch, J. P. Palao, R. Kosloff, and F. Masnou-Seeuws, *Stabilization of ultracold molecules using optimal control theory*, Phys. Rev. A **70**, 013402 (2004).

[Koc08] T. Koch, T. Lahaye, J. Metz, B. Fröhlich, A. Griesmaier, and T. Pfau, *Stabilization of a purely dipolar quantum gas against collapse*, Nature Phys. **4**, 218 (2008).

[Köh06] T. Köhler, K. Góral, and P. S. Julienne, *Production of cold molecules via magnetically tunable Feshbach resonances*, Rev. Mod. Phys. **78** (2006).

[Kok01] S. J. J. M. F. Kokkelmans, H. M. J. Vissers, and B. J. Verhaar, *Formation of a Bose condensate of stable molecules via a Feshbach resonance*, Phys. Rev. A **63**, 031601 (2001).

[Kot05] S. Kotochigova and E. Tiesinga, *Ab initio relativistic calculation of the RbCs molecule*, J. Chem. Phys. **123**, 174304 (2005).

[Kow07] M. Kowalewski, G. Morigi, P. Pinkse, and R. de Vivie-Riedle, *Cavity cooling of translational and ro-vibrational motion of molecules: ab initio-based simulations for OH and NO*, Appl. Phys. B **89**, 459 (2007).

[Kra06a] T. Kraemer, *Few-body interactions in an ultracold gas of cesium atoms*, Ph.D. thesis, University of Innsbruck (2006).

[Kra06b] T. Kraemer, M. Mark, P. Waldburger, J. G. Danzl, C. Chin, B. Engeser, A. D. Lange, K. Pilch, A. Jaakkola, H.-C. Nägerl, and R. Grimm, *Evidence for Efimov quantum states in an ultracold gas of caesium atoms*, Nature **440**, 315 (2006).

[Krá07] P. Král, I. Thanopulos, and M. Shapiro, *Colloquium: Coherently controlled adiabatic passage*, Rev. Mod. Phys. **79**, 53 (2007).

[Kre08] R. Krems, *Cold controlled chemistry*, Phys. Chem. Chem. Phys. **10**, 4079 (2008).

[Kuz08] E. Kuznetsova, P. Pellegrini, R. Côté, M. D. Lukin, and S. F. Yelin, *Formation of deeply bound molecules via chainwise adiabatic passage*, Phys. Rev. A **78**, 021402 (2008).

[Kuz09] E. Kuznetsova, M. Gacesa, P. Pellegrini, S. F. Yelin, and R. Côté, *Efficient formation of ground-state ultracold molecules via STIRAP from the continuum at a Feshbach resonance*, New J. Phys. **11**, 055028 (2009).

[Lah07] T. Lahaye, T. Koch, B. Fröhlich, M. Fattori, J. Metz, A. Griesmaier, S. Giovanazzi, and T. Pfau, *Strong dipolar effects in a quantum ferrofluid*, Nature **448**, 672 (2007).

[Lah09] T. Lahaye, C. Menotti, L. Santos, M. Lewenstein, and T. Pfau, *The physics of dipolar bosonic quantum gases*, Rep. Prog. Phys. **72**, 126401 (2009).

[Lan08a] F. Lang, P. v. d. Straten, B. Brandstätter, G. Thalhammer, K. Winkler, P. S. Julienne, R. Grimm, and J. Hecker Denschlag, *Cruising through molecular bound-state manifolds with radiofrequency*, Nature Phys. **4**, 223 (2008).

[Lan08b] F. Lang, K. Winkler, C. Strauss, R. Grimm, and J. Hecker Denschlag, *Ultracold triplet molecules in the rovibrational ground state*, Phys. Rev. Lett. **101**, 133005 (2008).

[Lan09a] F. Lang, *Coherent transfer of ultracold molecules: From weakly to deeply bound*, Ph.D. thesis, University of Innsbruck (2009).

[Lan09b] F. Lang, C. Strauss, K. Winkler, T. Takekoshi, R. Grimm, and J. H. Denschlag, *Dark state experiments with ultracold, deeply-bound triplet molecules*, Faraday Discuss. **142**, 271 (2009).

[Leo00] P. J. Leo, C. J. Williams, and P. S. Julienne, *Collision properties of ultracold ^{133}Cs atoms*, Phys. Rev. Lett. **85**, 2721 (2000).

[Lev08] B. L. Lev, A. Vukics, E. R. Hudson, B. C. Sawyer, P. Domokos, H. Ritsch, and J. Ye, *Prospects for the cavity-assisted laser cooling of molecules*, Phys. Rev. A **77**, 023402 (2008).

[Li08] Z. Li, S. V. Alyabyshev, and R. V. Krems, *Ultracold inelastic collisions in two dimensions*, Phys. Rev. Lett. **100**, 073202 (2008).

[Lie63] E. H. Lieb and W. Liniger, *Exact analysis of an interacting Bose gas. I. The general solution and the ground state*, Phys. Rev. **130**, 1605 (1963).

[Lon09] B. E. Londoño, J. E. Mahecha, E. Luc-Koenig, and A. Crubellier, *Resonant coupling effects on the photoassociation of ultracold Rb and Cs atoms*, Phys. Rev. A **80**, 032511 (2009).

[Lu09] M. Lu, S. H. Youn, and B. L. Lev, *Trapping ultracold dysprosium: a highly magnetic gas for dipolar physics* (2009), preprint available at arXiv:0912.0050v3.

[Mal97] V. S. Malinovsky and D. J. Tannor, *Simple and robust extension of the stimulated Raman adiabatic passage technique to N-level systems*, Phys. Rev. A **56**, 4929 (1997).

[Mar95] J. Martin, B. W. Shore, and K. Bergmann, *Coherent population transfer in multilevel systems with magnetic sublevels. II. Algebraic analysis*, Phys. Rev. A **52**, 583 (1995).

[Mar96] J. Martin, B. W. Shore, and K. Bergmann, *Coherent population transfer in multilevel systems with magnetic sublevels. III. Experimental results*, Phys. Rev. A **54**, 1556 (1996).

[Mar03] M. Mark, *Bose-Einstein-Kondensation von Cäsium*, Diploma thesis, University of Innsbruck (2003).

[Mar07a] M. Mark, F. Ferlaino, S. Knoop, J. G. Danzl, T. Kraemer, C. Chin, H.-C. Nägerl, and R. Grimm, *Spectroscopy of ultracold trapped cesium Feshbach molecules*, Phys. Rev. A **76**, 042514 (2007).

[Mar07b] M. Mark, T. Kraemer, P. Waldburger, J. Herbig, C. Chin, H.-C. Nägerl, and R. Grimm, *Stückelberg interferometry with ultracold molecules*, Phys. Rev. Lett. **99** (2007).

[Mar07c] M. J. Mark, *Wechselwirkungseffekte eines Cäsium-BEC in eindimensionalen Gittern*, Diploma thesis, University of Innsbruck (2007).

[Mau04] P. Maunz, T. Puppe, I. Schuster, N. Syassen, P. W. H. Pinkse, and G. Rempe, *Cavity cooling of a single atom*, Nature **428**, 50 (2004).

[McC06] J. J. McClelland and J. L. Hanssen, *Laser cooling without repumping: A magneto-optical trap for erbium atoms*, Phys. Rev. Lett. **96**, 143005 (2006).

[McF06] J. J. McFerran, W. C. Swann, B. R. Washburn, and N. R. Newbury, *Elimination of pump-induced frequency jitter on fiber-laser frequency combs*, Opt. Lett. **31**, 1997 (2006).

[Mee05] S. Y. T. van de Meerakker, P. H. M. Smeets, N. Vanhaecke, R. T. Jongma, and G. Meijer, *Deceleration and electrostatic trapping of OH radicals*, Phys. Rev. Lett. **94**, 023004 (2005).

[Mee09] S. A. Meek, H. Conrad, and G. Meijer, *Trapping molecules on a chip*, Science **324**, 1699 (2009).

[Men07] C. Menotti, C. Trefzger, and M. Lewenstein, *Metastable states of a gas of dipolar bosons in a 2D optical lattice*, Phys. Rev. Lett. **98**, 235301 (2007).

[Mic06] A. Micheli, G. K. Brennen, and P. Zoller, *A toolbox for lattice-spin models with polar molecules*, Nature Phys. **2**, 341 (2006).

[Mic07] A. Micheli, G. Pupillo, H. P. Büchler, and P. Zoller, *Cold polar molecules in two-dimensional traps: Tailoring interactions with external fields for novel quantum phases*, Phys. Rev. A **76**, 043604 (2007).

[Mil93] J. D. Miller, R. A. Cline, and D. J. Heinzen, *Photoassociation spectrum of ultracold Rb atoms*, Phys. Rev. Lett. **71**, 2204 (1993).

[Mil07] P. Milman, A. Keller, E. Charron, and O. Atabek, *Bell-type inequalities for cold heteronuclear molecules*, Phys. Rev. Lett. **99**, 130405 (2007).

[Mor06] O. Morsch and M. Oberthaler, *Dynamics of Bose-Einstein condensates in optical lattices*, Rev. Mod. Phys. **78**, 179 (2006).

[Mor07] G. Morigi, P. W. H. Pinkse, M. Kowalewski, and R. de Vivie-Riedle, *Cavity cooling of internal molecular motion*, Phys. Rev. Lett. **99**, 073001 (2007).

[Nar08a] E. Narevicius, A. Libson, C. G. Parthey, I. Chavez, J. Narevicius, U. Even, and M. G. Raizen, *Stopping supersonic beams with a series of pulsed electromagnetic coils: An atomic coilgun*, Phys. Rev. Lett. **100**, 093003 (2008).

[Nar08b] E. Narevicius, A. Libson, C. G. Parthey, I. Chavez, J. Narevicius, U. Even, and M. G. Raizen, *Stopping supersonic oxygen with a series of pulsed electromagnetic coils: A molecular coilgun*, Phys. Rev. A **77**, 051401 (2008).

[New09] *Focus issue on cold and ultracold molecules*, New. J. Phys. **11** (2009).

[Ni08] K.-K. Ni, S. Ospelkaus, M. H. G. de Miranda, A. Pe'er, B. Neyenhuis, J. J. Zirbel, S. Kotochigova, P. S. Julienne, D. S. Jin, and J. Ye, *A high phase-space-density gas of polar molecules*, Science **322**, 231 (2008).

[Ni10] K. K. Ni, S. Ospelkaus, D. Wang, G. Quemener, B. Neyenhuis, M. H. G. de Miranda, J. L. Bohn, J. Ye, and D. S. Jin, *Dipolar collisions of polar molecules in the quantum regime* (2010), preprint available at arXiv:1001.2809.

[Nik00] A. N. Nikolov, J. R. Ensher, E. E. Eyler, H. Wang, W. C. Stwalley, and P. L. Gould, *Efficient production of ground-state potassium molecules at sub-mK temperatures by two-step photoassociation*, Phys. Rev. Lett. **84**, 246 (2000).

[Ols98] M. Olshanii, *Atomic scattering in the presence of an external confinement and a gas of impenetrable bosons*, Phys. Rev. Lett. **81**, 938 (1998).

[Ore84] J. Oreg, F. T. Hioe, and J. H. Eberly, *Adiabatic following in multilevel systems*, Phys. Rev. A **29**, 690 (1984).

[Ort09] M. Ortner, A. Micheli, G. Pupillo, and P. Zoller, *Quantum simulations of extended Hubbard models with dipolar crystals*, New J. Phys. **11**, 055045 (2009).

[Osp06] C. Ospelkaus, S. Ospelkaus, L. Humbert, P. Ernst, K. Sengstock, and K. Bongs, *Ultracold heteronuclear molecules in a 3D optical lattice*, Phys. Rev. Lett. **97** (2006).

[Osp08] S. Ospelkaus, A. Pe'er, K. K. Ni, J. J. Zirbel, B. Neyenhuis, S. Kotochigova, P. S. Julienne, J. Ye, and D. S. Jin, *Efficient state transfer in an ultracold dense gas of heteronuclear molecules*, Nature Phys. **4**, 622 (2008).

[Osp10a] S. Ospelkaus, K.-K. Ni, G. Quéméner, B. Neyenhuis, D. Wang, M. H. G. de Miranda, J. L. Bohn, J. Ye, and D. S. Jin, *Controlling the hyperfine state of rovibronic ground-state polar molecules*, Phys. Rev. Lett. **104**, 030402 (2010).

[Osp10b] S. Ospelkaus, K.-K. Ni, D. Wang, M. H. G. de Miranda, B. Neyenhuis, G. Quemener, P. S. Julienne, J. L. Bohn, D. S. Jin, and J. Ye, *Quantum-state controlled chemical reactions of ultracold potassium-rubidium molecules*, Science **327**, 853 (2010).

[Par05] G. B. Partridge, K. E. Strecker, R. I. Kamar, M. W. Jack, and R. G. Hulet, *Molecular probe of pairing in the BEC-BCS crossover*, Phys. Rev. Lett. **95**, 020404 (2005).

[Pas07] A. Pashov, O. Docenko, M. Tamanis, R. Ferber, H. Knöckel, and E. Tiemann, *Coupling of the $X^1\Sigma^+$ and $a^3\Sigma^+$ states of KRb*, Phys. Rev. A **76**, 022511 (2007).

[Pel08] P. Pellegrini, M. Gacesa, and R. Côté, *Giant formation rates of ultracold molecules via Feshbach-optimized photoassociation*, Phys. Rev. Lett. **101**, 053201 (2008).

[Pet02] C. J. Pethick and H. Smith, *Bose-Einstein condensation in dilute gases*, Cambridge University Press, 2002.

[Pil09] K. Pilch, A. D. Lange, A. Prantner, G. Kerner, F. Ferlaino, H.-C. Nägerl, and R. Grimm, *Observation of interspecies Feshbach resonances in an ultracold Rb-Cs mixture*, Phys. Rev. A **79**, 042718 (2009).

[Pit03] L. Pitaevskii and S. Stringari, *Bose-Einstein condensation*, Oxford University Press, 2003.

[Pol09] S. E. Pollack, D. Dries, and R. G. Hulet, *Universality in three- and four-body bound states of ultracold atoms*, Science **326**, 1683 (2009).

[Pup08] G. Pupillo, A. Griessner, A. Micheli, M. Ortner, D.-W. Wang, and P. Zoller, *Cold atoms and molecules in self-assembled dipolar lattices*, Phys. Rev. Lett. **100**, 050402 (2008).

[Pup09] G. Pupillo, A. Micheli, H. P. Büchler, and P. Zoller, *Condensed Matter Physics with Cold Polar Molecules*, in: R. V. Krems, W. C. Stwalley, and B. Friedrich (Eds.), *Cold molecules: Theory, expriment, applications*, CRC Press, Boca Raton, 2009, preprint available at arXiv:0805.1896v1.

[Rab07] P. Rabl and P. Zoller, *Molecular dipolar crystals as high-fidelity quantum memory for hybrid quantum computing*, Phys. Rev. A **76**, 042308 (2007).

[Reg03] C. A. Regal, C. Ticknor, J. L. Bohn, and D. S. Jin, *Creation of ultracold molecules from a Fermi gas of atoms*, Nature **424**, 47 (2003).

[Rei99] J. Reichert, R. Holzwarth, T. Udem, and T. W. Hänsch, *Measuring the frequency of light with mode-locked lasers*, Opt. Commun. **172**, 59 (1999).

[Rie05] T. Rieger, T. Junglen, S. A. Rangwala, P. W. H. Pinkse, and G. Rempe, *Continuous loading of an electrostatic trap for polar molecules*, Phys. Rev. Lett. **95**, 173002 (2005).

[Roj07] G. Rojas Kopeinig, *A tunable Bose-Einstein condensate in a three-dimensional optical lattice potential*, Diploma thesis, University of Innsbruck (2007).

[Rom04] T. Rom, T. Best, O. Mandel, A. Widera, M. Greiner, T. W. Hänsch, and I. Bloch, *State selective production of molecules in optical lattices*, Phys. Rev. Lett. **93**, 073002 (2004).

[Ros08] T. Rosenband, D. B. Hume, P. O. Schmidt, C. W. Chou, A. Brusch, L. Lorini, W. H. Oskay, R. E. Drullinger, T. M. Fortier, J. E. Stalnaker, S. A. Diddams, W. C. Swann, N. R. Newbury, W. M. Itano, D. J. Wineland, and J. C. Bergquist, *Frequency ratio of Al+ and Hg+ single-ion optical clocks; Metrology at the 17th decimal place*, Science **319**, 1808 (2008).

[Ryu05] C. Ryu, X. Du, E. Yesilada, A. M. Dudarev, S. Wan, Q. Niu, and D. Heinzen, *Raman-induced oscillation between an atomic and a molecular quantum gas* (2005), preprint available at arXiv:cond-mat/0508201v1.

[Sag05] J. M. Sage, S. Sainis, T. Bergeman, and D. DeMille, *Optical production of ultracold polar molecules*, Phys. Rev. Lett. **94**, 203001 (2005).

[San00] L. Santos, G. V. Shlyapnikov, P. Zoller, and M. Lewenstein, *Bose-Einstein condensation in trapped dipolar gases*, Phys. Rev. Lett. **85**, 1791 (2000).

[Saw07] B. C. Sawyer, B. L. Lev, E. R. Hudson, B. K. Stuhl, M. Lara, J. L. Bohn, and J. Ye, *Magnetoelectrostatic trapping of ground state OH molecules*, Phys. Rev. Lett. **98**, 253002 (2007).

[Sch99] U. Schünemann, H. Engler, R. Grimm, M. Weidemüller, and M. Zielonkowski, *Simple scheme for tunable frequency offset locking of two lasers*, Rev. Sci. Instrum. **70**, 242 (1999).

[Sch07] H. Schöbel, *Ultrakalte Cs_2-Moleküle in einer optischen Dipolfalle mit kontrollierbarer Elliptizität*, Diploma thesis, University of Innsbruck (2007).

[Sch08] T. R. Schibli, I. Hartl, D. C. Yost, M. J. Martin, A. Marcinkevičius, M. E. Fermann, and J. Ye, *Optical frequency comb with submillihertz linewidth and more than 10 W average power*, Nature Phot. **2**, 355 (2008).

[Sch09] M. Schnell and G. Meijer, *Cold Molecules: Preparation, applications, and challenges*, Angew. Chem. Int. Ed. **48**, 6010 (2009).

[Sch10] T. Schneider, B. Roth, H. Duncker, I. Ernsting, and S. Schiller, *All-optical preparation of molecular ions in the rovibrational ground state*, Nature Phys. (2010), advance online publication 7 March 2010, DOI: 10.1038/nphys1605.

[Set00] J. Y. Seto, R. J. L. Roy, J. Vergès, and C. Amiot, *Direct potential fit analysis of the $X^1\Sigma_g^+$ state of Rb_2: Nothing else will do!*, J. Chem. Phys. **113**, 3067 (2000).

[Sha08] E. A. Shapiro, A. Pe'er, J. Ye, and M. Shapiro, *Piecewise adiabatic population transfer in a molecule via a wave packet*, Phys. Rev. Lett. **101**, 023601 (2008).

[Sho91] B. W. Shore, K. Bergmann, J. Oreg, and S. Rosenwaks, *Multilevel adiabatic population transfer*, Phys. Rev. A **44**, 7442 (1991).

[Sho95] B. W. Shore, J. Martin, M. P. Fewell, and K. Bergmann, *Coherent population transfer in multilevel systems with magnetic sublevels. I. Numerical studies*, Phys. Rev. A **52**, 566 (1995).

[Shu09] E. S. Shuman, J. F. Barry, D. R. Glenn, and D. DeMille, *Radiative force from optical cycling on a diatomic molecule*, Phys. Rev. Lett. **103**, 223001 (2009).

[Sol10] P. Soldán, private communicationp (2010).

[Sta06] P. Staanum, S. D. Kraft, J. Lange, R. Wester, and M. Weidemüller, *Experimental investigation of ultracold atom-molecule collisions*, Phys. Rev. Lett. **96**, 023201 (2006).

[Sta10] P. F. Staanum, K. Højbjerre, P. S. Skyt, A. K. Hansen, and M. Drewsen, *Rotational laser cooling of vibrationally and translationally cold molecular ions*, Nature Phys. (2010), advance online publication 7 March 2010, DOI: 10.1038/nphys1604.

[Ste02] J. Stenger, H. Schnatz, C. Tamm, and H. R. Telle, *Ultraprecise measurement of optical frequency ratios*, Phys. Rev. Lett. **88**, 073601 (2002).

[Stö06] T. Stöferle, H. Moritz, K. Günter, M. Köhl, and T. Esslinger, *Molecules of fermionic atoms in an optical lattice*, Phys. Rev. Lett. **96** (2006).

[Str03] K. E. Strecker, G. B. Partridge, and R. G. Hulet, *Conversion of an atomic Fermi gas to a long-lived molecular Bose gas*, Phys. Rev. Lett. **91**, 080406 (2003).

[Stu05] J. Stuhler, A. Griesmaier, T. Koch, M. Fattori, T. Pfau, S. Giovanazzi, P. Pedri, and L. Santos, *Observation of dipole-dipole interaction in a degenerate quantum gas*, Phys. Rev. Lett. **95**, 150406 (2005).

[Stu08] B. K. Stuhl, B. C. Sawyer, D. Wang, and J. Ye, *Magneto-optical trap for polar molecules*, Phys. Rev. Lett. **101**, 243002 (2008).

[Stw04] W. C. Stwalley, *Efficient conversion of ultracold Feshbach-resonance-related polar molecules into ultracold ground state ($X\,^1\Sigma^+ v = 0, J = 0$) molecules*, Eur. Phys. J. D **31**, 221 (2004).

[Swa06] W. C. Swann, J. J. McFerran, I. Coddington, N. R. Newbury, I. Hartl, M. E. Fermann, P. S. Westbrook, J. W. Nicholson, K. S. Feder, C. Langrock, and M. M. Fejer, *Fiber-laser frequency combs with subhertz relative linewidths*, Opt. Lett. **31**, 3046 (2006).

[Tak98] T. Takekoshi, B. M. Patterson, and R. J. Knize, *Observation of optically trapped cold cesium molecules*, Phys. Rev. Lett. **81**, 5105 (1998).

[Tak05] M. Takamoto, F.-L. Hong, R. Higashi, and H. Katori, *An optical lattice clock*, Nature **435**, 321 (2005).

[Tar09] M. R. Tarbutt, J. J. Hudson, B. E. Sauer, and E. A. Hinds, *Preparation and manipulation of molecules for fundamental physics tests*, in: R. V. Krems, W. C. Stwalley, and B. Friedrich (Eds.), *Cold molecules: Theory, expriment, applications*, CRC Press, Boca Raton, 2009, preprint available at arXiv:0803.0967.

[Tel02] H. Telle, B. Lipphardt, and J. Stenger, *Kerr-lens, mode-locked lasers as transfer oscillators for optical frequency measurements*, Appl. Phys. B **74**, 1 (2002).

[Tha06] G. Thalhammer, K. Winkler, F. Lang, S. Schmid, R. Grimm, and J. Hecker Denschlag, *Long-lived Feshbach molecules in a three-dimensional optical lattice*, Phys. Rev. Lett. **96** (2006).

[Tha07] G. Thalhammer, *Ultrakalte gepaarte Atome in kohärenten Lichtfeldern*, Ph.D. thesis, University of Innsbruck (2007).

[Tic08] C. Ticknor, *Collisional control of ground state polar molecules and universal dipolar scattering*, Phys. Rev. Lett. **100**, 133202 (2008).

[Tie93] E. Tiesinga, B. J. Verhaar, and H. T. C. Stoof, *Threshold and resonance phenomena in ultracold ground-state collisions*, Phys. Rev. A **47**, 4114 (1993).

[Tol03] B. L. Tolra, N. Hoang, B. T'Jampens, N. Vanhaecke, C. Drag, A. Crubellier, D. Comparat, and P. Pillet, *Controlling the formation of cold molecules via a Feshbach resonance*, Euophys. Lett. **64**, 171 (2003).

[Tre09] C. Trefzger, C. Menotti, and M. Lewenstein, *Pair-supersolid phase in a bilayer system of dipolar lattice bosons*, Phys. Rev. Lett. **103**, 035304 (2009).

[Tsa97] C. C. Tsai, R. S. Freeland, J. M. Vogels, H. M. J. M. Boesten, B. J. Verhaar, and D. J. Heinzen, *Two-color photoassociation spectroscopy of ground state* Rb_2, Phys. Rev. Lett. **79**, 1245 (1997).

[Ude02] T. Udem, R. Holzwarth, and T. W. Hänsch, *Optical frequency metrology*, Nature **416**, 233 (2002).

[Unt05] P. Unterwaditzer, *Aufbau eines vollständigen Diodenlasersystems zur Laserkühlung und Detektion von gespeicherten Cs-Atomen*, Master's thesis, University of Innsbruck (2005).

[Van04] N. Vanhaecke, C. Lisdat, B. T'Jampens, D. Comparat, A. Crubellier, and P. Pillet, *Accurate asymptotic ground state potential curves of* Cs_2 *from two-colour photoassociation*, Eur. Phys. J. D **28**, 351 (2004).

[Van07] N. Vanhaecke, U. Meier, M. Andrist, B. H. Meier, and F. Merkt, *Multistage Zeeman deceleration of hydrogen atoms*, Phys. Rev. A **75**, 031402 (2007).

[van08] S. van de Meerakker, T. Bethlem, and G. Meijer, *Taming molecular beams*, Nature Physics **4**, 595 (2008).

[Vit97] N. V. Vitanov and S. Stenholm, *Population transfer via a decaying state*, Phys. Rev. A **56**, 1463 (1997).

[Vit98] N. Vitanov, B. Shore, and K. Bergmann, *Adiabatic population transfer in multistate chains via dressed intermediate states*, Eur. Phys. J. D **4**, 15 (1998).

[Vit08] M. Viteau, A. Chotia, M. Allegrini, N. Bouloufa, O. Dulieu, D. Comparat, and P. Pillet, *Optical pumping and vibrational cooling of molecules*, Science **321**, 232 (2008).

[Vog04] I. S. Vogelius, L. B. Madsen, and M. Drewsen, *Rotational cooling of heteronuclear molecular ions with $^1\Sigma$, $^2\Sigma$, $^3\Sigma$, and $^2\Pi$ electronic ground states*, Phys. Rev. A **70**, 053412 (2004).

[Vol06] T. Volz, N. Syassen, D. Bauer, E. Hansis, S. Dürr, and G. Rempe, *Preparation of a quantum state with one molecule at each site of an optical lattice*, Nature Phys. **2**, 692 (2006).

[Vul99] V. Vuletić, A. J. Kerman, C. Chin, and S. Chu, *Observation of low-field Feshbach resonances in collisions of cesium atoms*, Phys. Rev. Lett. **82**, 1406 (1999).

[Vul00] V. Vuletić and S. Chu, *Laser cooling of atoms, ions, or molecules by coherent scattering*, Phys. Rev. Lett. **84**, 3787 (2000).

[Wan06] D.-W. Wang, M. D. Lukin, and E. Demler, *Quantum fluids of self-assembled chains of polar molecules*, Phys. Rev. Lett. **97**, 180413 (2006).

[Wan07] D. Wang, J. T. Kim, C. Ashbaugh, E. E. Eyler, P. L. Gould, and W. C. Stwalley, *Rotationally resolved depletion spectroscopy of ultracold KRb molecules*, Phys. Rev. A **75**, 032511 (2007).

[Web03] T. Weber, *Bose-Einstein condensation of optically trapped cesium*, Ph.D. thesis, University of Innsbruck (2003).

[Wei85] W. Weickenmeier, U. Diemer, M. Wahl, M. Raab, W. Demtröder, and W. Müller, *Accurate ground state potential of Cs_2 up to the dissociation limit*, J. Chem. Phys. **82**, 5354 (1985).

[Wei98] J. D. Weinstein, R. deCarvalho, T. Guillet, B. Friedrich, and J. M. Doyle, *Magnetic trapping of calcium monohydride molecules at millikelvin temperatures*, Nature **395**, 148 (1998).

[Wei99] J. Weiner, V. S. Bagnato, S. Zilio, and P. S. Julienne, *Experiments and theory in cold and ultracold collisions*, Rev. Mod. Phys. **71**, 1 (1999).

[Win07a] K. Winkler, *Ultracold molecules and atom pairs in optical lattice potentials*, Ph.D. thesis, University of Innsbruck (2007).

[Win07b] K. Winkler, F. Lang, G. Thalhammer, P. v. d. Straten, R. Grimm, and J. Hecker Denschlag, *Coherent optical transfer of Feshbach molecules to a lower vibrational state*, Phys. Rev. Lett. **98** (2007).

[Wyn00] R. Wynar, R. S. Freeland, D. J. Han, C. Ryu, and D. J. Heinzen, *Molecules in a Bose-Einstein condensate*, Science **287**, 1016 (2000).

[Xu03] K. Xu, T. Mukaiyama, J. R. Abo-Shaeer, J. K. Chin, D. E. Miller, and W. Ketterle, *Formation of quantum-degenerate sodium molecules*, Phys. Rev. Lett. **91** (2003).

[Ye05] J. Ye and S. Cundiff (Eds.), *Femtosecond optical frequency comb: Principle, operation and applications*, Springer, New York, 2005.

[Ye08] J. Ye, H. J. Kimble, and H. Katori, *Quantum state engineering and precision metrology using state-insensitive light traps*, Science **320**, 1734 (2008).

[Ye09] J. Ye, private communication (2009).

[Yel06] S. F. Yelin, K. Kirby, and R. Côté, *Schemes for robust quantum computation with polar molecules*, Phys. Rev. A **74**, 050301(R) (2006).

[Yi07] S. Yi, T. Li, and C. P. Sun, *Novel quantum phases of dipolar Bose gases in optical lattices*, Phys. Rev. Lett. **98**, 260405 (2007).

[Zac09] M. Zaccanti, B. Deissler, C. D' Errico, M. Fattori, M. Jona-Lasinio, S. Müller, G. Roati, M. Inguscio, and G. Modugno, *Observation of an Efimov spectrum in an atomic system*, Nature Phys. **5**, 586 (2009).

[Zah06] N. Zahzam, T. Vogt, M. Mudrich, D. Comparat, and P. Pillet, *Atom-molecule collisions in an optically trapped gas*, Phys. Rev. Lett. **96**, 023202 (2006).

[Zam09] M. Asad-uz Zaman and D. Blume, *Aligned dipolar Bose-Einstein condensate in a double-well potential: From cigar shaped to pancake shaped*, Phys. Rev. A **80**, 053622 (2009).

[Zel08] T. Zelevinsky, S. Kotochigova, and J. Ye, *Precision test of mass-ratio variations with lattice-confined ultracold molecules*, Phys. Rev. Lett. **100**, 043201 (2008).

[Zep09] M. Zeppenfeld, M. Motsch, P. W. H. Pinkse, and G. Rempe, *Optoelectrical cooling of polar molecules*, Phys. Rev. A **80**, 041401 (2009).

[Zir08] J. J. Zirbel, K.-K. Ni, S. Ospelkaus, J. P. D'Incao, C. E. Wieman, J. Ye, and D. S. Jin, *Collisional stability of fermionic Feshbach molecules*, Phys. Rev. Lett. **100**, 143201 (2008).

[Żuc10] P. S. Żuchowski and J. M. Hutson, *Reactions of ultracold alkali metal dimers* (2010), preprint available at arXiv:1003.1418.

[Zwi03] M. W. Zwierlein, C. A. Stan, C. H. Schunck, S. M. F. Raupach, S. Gupta, Z. Hadzibabic, and W. Ketterle, *Observation of Bose-Einstein condensation of molecules*, Phys. Rev. Lett. **91**, 250401 (2003).

Acknowledgments

I would like to express my sincere gratitude to all those people who have contributed to making things work out.

First, I would like to thank Hanns-Christoph Nägerl for providing me with the opportunity for such an exciting project. He had the idea of starting a second line of research on the Cs BEC lattice apparatus in addition to the tunable quantum gas experiments that were already being performed, thus creating a very efficient experimental environment. He is a very encouraging mentor who fosters creative freedom and at the same time is always available for discussions both on scientific and technical issues and it was fun to develop the strategy for the ground-state experiments together with him. Due to his positive personality, it has been very enjoyable to work with him.

Rudi Grimm has generously supported our experiment and made a great contribution by constantly promoting a very lively and open atmosphere in ultracold physics in Innsbruck, which is gratefully acknowledged. The Grimm group and the whole quantum physics community in Innsbruck are an intellectually stimulating and at the same time very collaborative environment with a lot of accumulated technical and scientific expertise that is willingly shared. I would like to thank the whole Grimm group for scientific exchange and an enjoyable time.

I joined a fully functional BEC apparatus when I took over the molecules project. There, I could build up the STIRAP setup in the little remaining space in the lab. I therefore owe my gratitude to those people who built the BEC experiment and who made it a very flexible machine that is joyful to work on. These are the PhD students Mattias Gustavsson and Elmar Haller and the diploma students Peter Unterwaditzer, Anton Flir, and Gabriel Rojas Kopeinig.

Mattias was the first PhD student on this experiment and did a great job in building it. He was very helpful when it came to interfacing the spectroscopy setup with the main experiment. As in sports, he enjoyed little competitions and so a competition between him and me who of us could find the most molecular transitions in the initial spectroscopy on the Feshbach molecules made this tedious search much more entertaining.

Elmar Haller joined the experiment as a PhD student after Mattias and contributed a lot to the buildup phase of the experiment. Elmar is the lattice expert in our team and his work focuses on low dimensional systems with tunable interactions. I owe many thanks to him because of his contributions to keeping the machine running and improving it, his input on many technical and scientific issues and the fact that we could coordinate the lattice experiments and the molecules experiments in a very relaxed, friendly, and productive atmosphere.

Manfred Mark was a diploma student on the experiment when I joined, preparing a setup for Bragg spectroscopy on atoms, and later came back as PhD student. Manfred has contributed a lot to both the molecules project and the low-dimensional systems with his constant drive to improve the experiment. This includes the gradual exchange of electronics by more advanced designs. Manfred has worked a lot on the BEC appa-

ratus to keep it alive and running. In the ground-state experiments, I am very grateful to him for supporting me during many of the measurements and bringing in his ideas and his technical expertise.

Russell Hart joined as a postdoc in the past two years. His main focus has been on the low-dimensional systems but he was always happy to discuss about molecules. With his background in Cs atomic clocks, he has enriched the spectrum of ideas and approaches, which is gratefully acknowledged.

Three diploma students have helped with various technical aspects of the spectroscopy setup. Andreas Klinger, while he was still busy with coursework, helped in the early stages of the buildup and now has joined our team as diploma student. Lukas Reichsöllner and Oliver Kriegelsteiner have supported me with building electronics. The contributions of all three of them are appreciated.

The production of rovibronic ground-state molecules would not have been possible without excellent theory support. These are great collaborations that I highly appreciate. Nadia Bouloufa and Olivier Dulieu adopted me early on in terms of molecular physics and provided all the *ab initio* calculations and Franck-Condon factors that we used to plan our four-photon scheme. Ever since, they have been available to clarify molecular physics questions and provided us with more data pertinent to different aspects of the project. I would like to thank Helmut Ritsch a lot for his significant contributions on the quantum optics side when it came to simulating our STIRAP transitions and extracting more quantitative information such as transition strengths from our measurements. Tom Bergeman has shared his spectroscopic knowledge about the 0_u^+ states with us. This made an important difference in the spectroscopy on excited state levels and we are very grateful for this input. Houssam Salami did many of the calculations at Stony Brook. I enjoyed the interesting discussions with both of them on my visit to Stony Brook. Tom has been very helpful for developing the STIRAP transfer scheme in RbCs. Jesus Aldegunde and Jeremy Hutson calculated the hyperfine structure of the rovibronic ground state and provided conceptual input. With that, they have made a very significant contribution to the understanding and control of hyperfine structure for rovibronic ground-state molecules and other aspects of our work. Discussions on molecular structure with Eberhard Tiemann and Paul Julienne and discussions about coherent state transfer with Klaas Bergmann as well as discussions about lattice loading with Stefan Dürr are gratefully acknowledged. On the technical side, I am grateful for discussions and know-how about frequency combs early on in the project to Piet Schmidt, Michael Chwalla, Florian Tauser, Marco Prevedelli and Harald Schnatz. Harald Telle, Harald Schatz, Burghard Lipphardt, Janis Alnis, and Scott Diddams were very helpful for setting up the new locking scheme for the STIRAP lasers that will be used in future measurements.

I would also like to thank the team of Johannes Hecker Denschlag who did the STIRAP work on Rb_2 molecules in Innsbruck. Especially the discussions with Klaus Winkler and Gregor Thalhammer in the early stages of the experiments were very helpful.

Our experiments rely heavily on the support from the electronic and mechanical workshops. In the mechanical workshop, Anton Schönherr, Helmut Jordan, Armin Sailer, Andreas Reinalter, and Matthias Szabados and on the electronics side Arthur Wander, Gerhard Hendl and lately Michael Hofer have always been willing to help. In the early stages of the project, Josef Dummer and Manuel Kluibenschädl have also been very supportive. I would like to thank all of them for the nice and productive interaction.

Christine Götsch-Obmascher, Karin Köhle, Ingeborg Kaindl, Nicole Jorda, Patricia Moser and Sabine Hofer keep the institute running in terms of administrative tasks. Their help and uncomplicated approach to administration is greatly appreciated.

I conclude by noting my enormous gratitude to my family who have supported me in every possible way and to my wonderful girlfriend Barbara.